# Impact of leaky barriers and hydrokinetic turbines on channel hydrodynamics and fish movement

**A thesis submitted in partial fulfilment**

**of the requirement for the degree of Doctor of Philosophy**

# Stephanie Müller

CARDIFF UNIVERSITY

PRIFYSGOL CAERDYDD

**December 2021**

# Cardiff University
# School of Engineering

# Abstract

Rivers have been subject to the construction of numerous small and large-scale anthropogenic structures, causing the alteration and fragmentation of aquatic habitats. Despite the tremendous impact of these structures on fish movement and the aquatic environment, more obstructions are added to riverine systems, mainly for flood mitigation or harnessing renewable energy. As little is known about the ecological impacts of these structures, further research is required to minimise the risk of these obstructions presenting a barrier to fish movement. By the means of two case studies, this thesis aims to quantify the effects of two emerging in-stream obstructions, namely leaky barriers used for natural flood management (Chapter 2) and vertical axis hydrokinetic turbines (Chapter 3). Using scaled laboratory experiments, changes in channel hydrodynamics and fish movement were determined for each of the two barriers.

Leaky barrier hydrodynamics were characterised by flow diversion upstream of all structures, the formation of a modified wall jet underneath the barrier, and a structure-dependent upper wake. Juvenile Atlantic salmon (*Salmo salar*) and rainbow trout (*Oncorhynchus mykiss*) movement was not prevented by barrier presence but resulted in decreased upstream passage and proportion of time spent upstream.

The wake of a vertical axis turbine was asymmetric about the turbine's centreline and shifted towards the upstroke side. Due to this wake asymmetry, the individual wakes of twin-turbines either moved alongside each other, converged, or diverged depending on the turbine rotational direction. Juvenile rainbow trout avoided the near turbine region

and remained in the free-stream area under unconfined conditions. Small groups of fish were more explorative compared to individuals.

This thesis expands our current knowledge on these two emerging barriers, supporting their delivery as environmental-friendly, anthropogenic in-stream obstructions while ensuring flood mitigation, sustainable energy generation, and habitat connectivity.

# Acknowledgements

Cath, who patiently listed during our moaning-dish washing sessions. A special thanks also to my colleagues and friends from the School of Biosciences, Rhi, Numair, and Scott, and many more I was able to get to know. I very much appreciate the insights you provided me in the field of fish biology and statistics.

This Ph.D. thesis would not have been possible without the support of the technical staff of the IT, electrical and structural workshop. I am very grateful for their technical help realising our experimental setups, diagnosing and fixing countless faulty or assumed faulty devices, and driving many fish and me between places. I am also grateful for the company during the uncountable hours I spent in the lab. It was always a pleasure to chat and a safe feeling to know someone kept an eye on me.

Furthermore, I would also like to thank my former supervisors, Stefan and Olivier. Both provided me an insight into the world of academia with all its possibilities. The many opportunities to engage in academic activities during my undergrad and graduate studies and the countless gentle nudges inspired me and provided me with the courage to undertake a Ph.D. in a different country.

Not to forget, a special thanks to all the fish which participated in my experimental studies. Working with life fish has been an invaluable experience which I would not like to miss. Just by watching every fish swim, I have learned a lot about their behaviour and habitat requirements.

Finally, I would like to thank my dear partner, Jonte. He was always there for me when I needed a sympathetic ear, guidance, and support to overcome some deep points during my Ph.D. journey. I am grateful for his encouragement to do this course and explore life in a foreign country, even when it meant being apart.

Cardiff 2021                                                                                 Stephanie Müller

# List of publications and conferences

The following publications and conference presentations arose from this thesis:

## Journal publications

- **Müller, S.**, Muhawenimana, V., Wilson C. A. M. E., Ouro P. (2021) Experimental investigation of the wake characteristics behind twin vertical axis turbines, Energy Management and Conversion, 247: 114768, doi: 10.1016/j.enconman.2021.114768

- **Müller, S.**, Wilson C. A. M. E., Ouro P., Cable J. (2021) Experimental investigation of physical leaky barrier design implications on juvenile rainbow trout (*Oncorhynchus mykiss*) movement, Water Resources Research, 57, e2021WR030111, doi: 10.1029/2021WR030111

- **Müller, S.**, Wilson C. A. M. E., Ouro P., Cable J. (2021) Leaky barriers: leaky enough for fish to pass?, Journal of the Royal Society Open Science, 8: 201843, doi: 10.1098/rsos.201843

- **Müller, S.**, Follett, E. M., Ouro P., Wilson C. A. M. E. (under review) Influence of engineered logjam structures on channel hydrodynamics, submitted to Water Resources Research

## Conference publications

- **Müller, S.**, Muhawenimana, V., Ouro P., Cable J., Wilson C. A. M. E. (2020) Tracking fish swimming behaviour in response to a vertical axis turbine, Proceedings of

the 1st IAHR Young Professionals Congress, International Association for Hydro-Environment Engineering and Research, ISBN: 978-90-82484-6-63

## Conference presentations

- **Müller, S.**, Muhawenimana, V., Ouro, P., Wilson, C. A. M. E., Cable, J. (2021) Fish swimming behaviour and kinematics in the wake of a vertical axis turbine, 9th International Symposium on Environmental Hydraulics, Seoul, South Korea, online

- **Müller, S.**, Muhawenimana, V., Ouro, P., Wilson, C. A. M. E., Cable, J. (2020) Tracking fish swimming behaviour in the vicinity of a hydrokinetic turbine, International workshop for PhD and post-doctoral fellows on Salmonid research (NoWPas), online

- **Müller, S.**, Muhawenimana, V., Ouro P., Cable J., Wilson C. A. M. E. (2020) Tracking fish swimming behaviour in response to a vertical axis turbine, 1st IAHR Young Professionals Congress, International Association for Hydro-Environment Engineering and Research, online

- Muhawenimana, V., **Müller, S.**, Ouro, P. and Wilson, C. A. M. E (2020) Hydrodynamics of two closely spaced vertical axis turbine wakes, poster presentation, 7th PRIMaRE Conference, online

- **Müller, S.**, Ouro, P., Wilson, C. A. M. E., Cable, J. (2020) Impact of anthropogenic structures on fish swimming kinematics and passage, International workshop for PhD and post-doctoral fellows on Salmonid research (NoWPas), Laugarvatn, Iceland

- **Müller, S.**, Follett, E., Wilson, C. A. M. E., Ouro, P., Cable, J. (2019) Impact of hydrodynamics of porous and non-porous structures on upstream fish passage performance, 72nd Annual Meeting of the American Physics Society Division of Fluid Dynamics, Seattle, Washington, US

- Wilson, C. A. M. E., Muhawenimana, V., **Müller, S.**, Ouro, P., Benavides, A., Duque, C. (2019) Wake dynamics behind two closely spaced vertical axis turbines, 72nd Annual Meeting of the American Physics Society Division of Fluid Dynamics, Seattle, Washington, US

# Data accessibility

Data underpinning the results presented in this thesis can be accessed by contacting:

Dr Catherine Wilson (wilsonca@cardiff.ac.uk)

Dr Pablo Ouro (pablo.ouro@manchester.ac.uk)

Data already published are available in the Cardiff University data catalogue, with the repository link provided in the journal publications (see list of publications).

# Contents

# List of Figures

# List of Tables

# Nomenclature

## Abbreviation

| | |
|---|---|
| ADV | acoustic Doppler velocimetry |
| ARRIVE | animal research: reporting of in vivo experiments |
| COR | correlation |
| CRB | counter-rotating backwards |
| CRF | counter-rotating forward |
| GLM | general linear model |
| HAT | horizontal axis turbine |
| ISO | International Organization for Standardization |
| LB | leaky barrier |
| LED | light-emitting diode |
| LES | large eddy simulation |
| LWD | large woody debris |
| LWM | large woody material |
| MS | tricaine methane sulfonate |
| NACA | National Advisory Committee for Aeronautics |
| NFM | natural flood management |
| PIV | particle image velocimetry |
| PIT | passive integrated transponder |

| | |
|---|---|
| RAS | recirculating aquatic system |
| S | structure |
| S.d. | standard deviation |
| SNR | signal-to-noise ratio |
| SR | same rotation |
| TKE | turbulent kinetic energy |
| TSR | tip speed ratio |
| VAT | vertical axis turbine |
| UK | United Kingdom |

# Dimensionless parameters

| | |
|---|---|
| $Fr$ | Froude number |
| $F_0$ | jet Froude number |
| $Re$ | Reynolds number |
| $Re_d$ | Reynolds number based on dowel diameter |
| $Re_D$ | Reynolds number based on turbine diameter |
| | |
| $\lambda$ | tip speed ratio |
| $\lambda_s$ | scaling parameter |
| $\sigma$ | geometric solidity |

# Greek symbols

| | |
|---|---|
| $\nu$ | kinematic viscosity |
| $\Omega$ | rotational speed |
| $\Phi$ | logjam void ratio |

# Roman symbols

| | |
|---|---|
| $A$ | cross-sectional area |
| $A_p$ | frontal projected area |
| $A_{rv}$ | relative channel void area |
| $b$ | inter-cylinder gap height |
| $b_0$ | vertical gap height between flume bed and leaky barrier |
| $B_{flume}$ | flume width |
| $B_{fp}$ | floodplain width |
| $B_{mc}$ | main channel width |
| $c$ | chord length |
| $C_{wj}$ | jet decay coefficient |
| $d$ | dowel diameter |
| $D$ | turbine diameter |
| $g$ | gravitational constant |
| $H$ | flow depth |
| $H_{flume}$ | flume height |
| $H_{mc}$ | main channel height |
| $H_s$ | leaky barrier height |
| $H_{turbine}$ | turbine height |
| $\overline{H_1}$ | mean upstream flow depth |
| $\overline{H_2}$ | mean downstream flow depth |
| $\Delta H$ | backwater rise |
| $L_{flume}$ | flume length |
| $L_{fish}$ | fish standard length |
| $L_{fish,group}$ | mean group standrad length |
| $L_{fish,total}$ | fish total length |
| $L_s$ | leaky barrier longitudinal length |
| $m$ | fish mass |

| | |
|---|---|
| $n$ | number of dowels |
| $N_b$ | number of blades |
| $N_{excluded}$ | number of fish excluded from the analysis |
| $N_{tested}$ | number of tested fish |
| $N_{analysis}$ | number of fish included into the analysis |
| $Q$ | discharge |
| $Q_1, Q_2, Q_3, Q_4$ | Quadrant one to four |
| $Q_{bf}$ | bankfull discharge |
| $Q_{field}$ | discharge under field conditions |
| $Q_{lab}$ | discharge under lab conditions |
| $S_y$ | shaft-to-shaft/intra-turbine spacing |
| $tke$ | turbulent kinetic energy |
| $t_{spent}$ | percentage time spent |
| $T$ | analysis time |
| $u$ | streamwise velocity component |
| $\overline{u}$ | mean streamwise velocity |
| $\overline{u}_{max}$ | maximum mean streamwise velocity |
| $< \overline{u} >$ | depth-average mean streamwise velocity |
| $< \overline{u}_{b_0} >$ | depth-average initial jet velocity |
| $\Delta\overline{u}$ | mean streamwise velocity deficit |
| $u'$ | streamwise velocity fluctuation |
| $\sqrt{u'^2}$ | root mean square velocity fluctuation |
| $\overline{u'v'}$ | horizontal Reynolds shear stress |
| $\overline{u'w'}$ | vertical Reynolds shear stress |
| $U_0$ | bulk velocity |
| $U_{field}$ | bulk velocity under field conditions |
| $U_{lab}$ | bulk velocity under lab conditions |
| $v$ | lateral velocity component |
| $\overline{v}$ | mean lateral velocity |

| | |
|---|---|
| $v'$ | lateral fluctuation velocity |
| $V_{void}$ | pore volume |
| $V_{control}$ | volume occupied by non-porous logjam |
| $V_{solid}$ | volume occupied by solid logjam |
| $w$ | vertical velocity component |
| $\overline{w}$ | mean vertical velocity |
| $w'$ | vertical fluctuation velocity |
| $x$ | longitudinal direction |
| $y$ | lateral direction |
| $z$ | vertical direction |

*Chapter 1*

# Introduction

## 1.1  State of the world's rivers

Since 1970, an average decline of 83 % in freshwater species is reported, corresponding to a decline of approximately 4 % per year [246]. Amongst the 29,500 monitored freshwater-dependent species, to date, 27 % are listed as threatened with extinction, with 28 % of them being fish species [221]. This means that fish have had the highest extinction rate amongst all vertebrates [246]. Just considering migratory fish species (245 monitored), a decrease of 76 % was reported between 1970 and 2016, equivalent to a decline of approximately 3 % per year [55].

A wide range of threats cause this tremendous decline in freshwater fish and biodiversity, including overexploitation, invasive species, water pollution, flow modification, and habitat degradation [60], with ongoing climate and socio-economic changes, intensifying the already existing threats and causing the development of new, emerging threats such as climate change, e-commerce, infectious diseases, harmful algal blooms, expanding hydropower, emerging contaminants (e.g., microplastics, light, noise), engineered nanomaterial, freshwater salination, declining calcium as well as a combination of multiple stressors [184]. Despite the variety of potential causes, 40 % of the threats are represented by the degradation and alteration of the aquatic ecosystem worldwide (Figure 1.1 (a), [55]). Amongst the listed regions in Figure 1.1 (b), Europe's rivers have undergone particularly serious habitat changes, corresponding to

more than 60 % of the present threats [55].
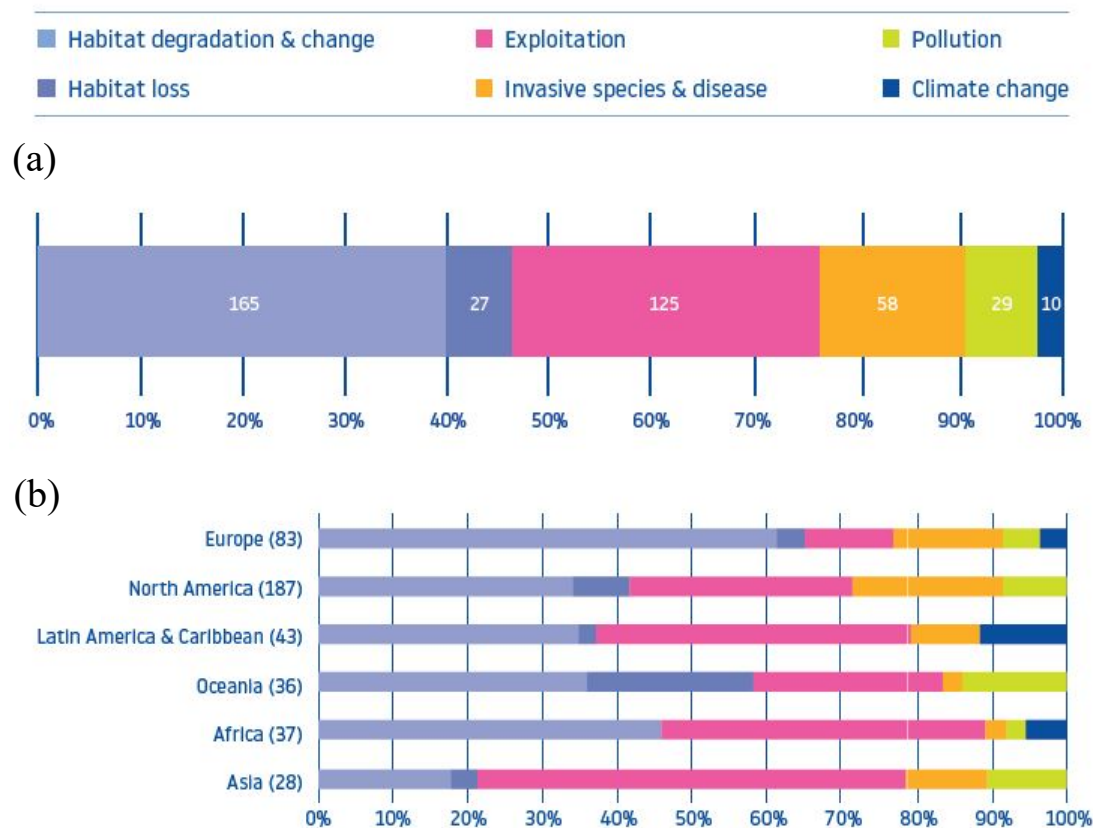


**Figure 1.1:** Global (a) and regional (b) based percentage of threats monitored for 116 migratory fish species, with the number inside the bars of the global distribution indicating the frequency a threat was recorded. Figure adapted from [55].

Habitat degradation describes the process of modifying, fragmenting, removing and or reducing the quality of a species' habitat [246]. Widespread degradation and loss of aquatic habitats has been observed worldwide but particularly in Europe as a result of the continuous expansion in infrastructure, agriculture, residential and commercial development, mining and energy generation [55]. The rising demand in energy, drinking water, food supply and flood mitigation schemes is accompanied by an increasing need for hydraulic engineering structures such as dams, levees, water in- and out-takes, hydraulic control structures, water diversion structures and hydropower schemes [85].

To date, 63 % of the world's rivers longer than 1000 km are considered to no longer be free-flowing [84], with free-flowing rivers being largely unaffected by anthropogenic alterations and characterised through high longitudinal, lateral, temporal, and vertical connectivity [85]. In particular, rivers longer than 500 km are rare in most parts of the world as indicated in Figure 1.2, with approximately 50 % of all rivers worldwide being characterised by reduced river connectivity [85]. Source-to-sea connectivity is impeded in 77 % and 54 % of the world's rivers longer than 1000 km and 500 km, respectively [85], limiting the exchange of water, nutrients and sediment as well as species movement [60, 14, 85]. Only remote regions such as the Arctic, Amazon basin, Alaska, north Russia and to a certain extent the Congo basin still have large connected rivers [152, 85]. Nevertheless, it will only be a matter of time until these regions are considered for construction projects, for instance, to extract energy (e.g., Amazon basin [14, 46]).
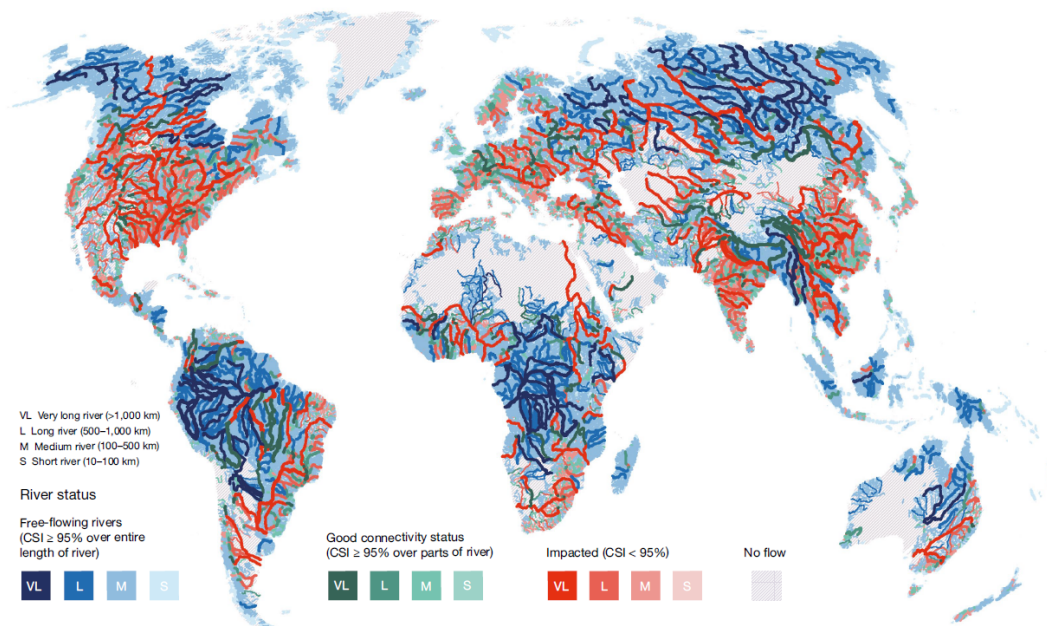


**Figure 1.2:** Map depicting (a) the world's free flowing rivers (blue colours), (b) rivers with good connectivity status (green colours) and (c) rivers with reduced connectivity (red colours), distinguished in very long (VL), long (L), medium (M) and short (S) river. Figure taken from [85].

As part of the "Adaptive Management of Barriers in European Rivers" (AMBER) project, a study was conducted assessing the number of barriers present in the UK's rivers [100]. In this study, a total of 23,618 in-stream barriers with a mean barrier height of approximately 3.46 m was recorded, including 19053, 2128 and 2437 artificial barriers in England, Scotland, and Wales, respectively. The large number of barriers resulted in a mean barrier density of 0.27 barriers/km (Figure 1.3 (a)). A comparison between field survey data and existing data (e.g. provided by local authorities), however, highlighted that 68 % of the barriers present were missing in the existing records. By correcting the large underestimation of barriers, a mean barrier density of one barrier per 1.5 km river stretch was calculated (Figure 1.3 (b)). These estimations indicate that only 3.3 % of the total river network in the UK is fully connected (Figure 1.3 (c)). Although 80 % of
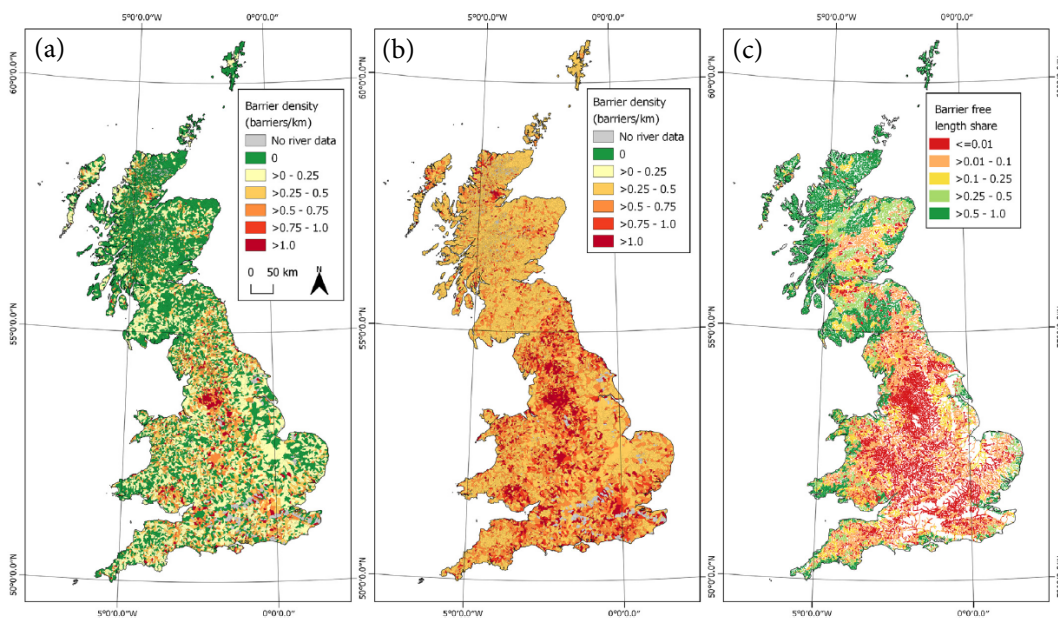


**Figure 1.3:** (a) Existing barrier density in barriers/km; (b) estimated barrier density in barriers/km based on data correction from field survey data; and (c) river length without barriers as proportion of total river network length in the UK, with barrier being defined as all man-made structures that interrupt the ecological process of a river as described by Vannote (1980) [224] (e.g., dams (excluding high-head dams), weirs, culverts, fords, ramped beds) [100]. Figure adapted form [100].

these structures are small-scale, only 1 % of the UK's rivers remain free-flowing [100].

Allowing rivers to flow freely is particularly important to maintain habitat and migratory corridors for aquatic organisms and ensure the transport of matter and energy along the river [201]. River connectivity is not only important for migratory fish species but also for resident species due to the different kinds of movement undertaken during their lifetime [57]. These movements can be distinguished into (i) resource-directed or home range movements, (ii) movements not under the control of the organisms, and (iii) movements not related to immediate resources or home range, i.e., migration [57]. Resource-directed movements include maintaining station within home range, foraging activities, habitat exploration or defensive behaviour [57]. Movements not under control of the organisms can be caused through accidental displacements, for example, by extreme weather events [57]. Finally, various fish species undertake migrations, mainly with the purpose of feeding or reproduction. Independent of the movement type, habitat connectivity is integral for the life cycle of fish, and hence, the diversity of drivers for movement should be considered when planning the construction of new in-stream obstructions. In the following, an overview of the implications of in-stream structures on fish movement and their habitat is presented.

## 1.2    River barriers and impact on fish movement

Fish are exposed to a wide range of riverine in-stream obstacles occurring either naturally (e.g., rocks, waterfalls, vegetation, and in-stream wood) or through the construction of anthropogenic hydraulic structures and hydropower schemes (e.g., weirs [11], sluice gates, culverts [79, 232], turbines [42], cylinder-like structures such as bridge piers or leaky barriers [144, 6, 129]). Anthropogenic in-stream obstructions may present physical, behavioural, and hydraulic barriers to fish [205]. In general, riverine barriers are considered to be in-stream obstacles that interrupt the ecological processes of the river continuum concept [100] described by Vannote (1980) [224]. This concept

classifies the physical parameters of the different river sections (e.g., width, flow depth, velocity, temperature) and its indicator species, starting at the river's source working towards the river's mouth [224]. Failing to navigate an in-stream barrier can prevent or slow down fish movement, potentially delaying fish migration [40]. The increased energy expenditure required to overcome or bypass these barriers may cause premature fatigue, potentially reducing the fish's ability to reproduce successfully or reach their spawning grounds in time [41].

## 1.2.1  Physical barriers

Physical, anthropogenic barriers can prevent fish movement along the river and therefore create isolated fish populations and limit essential nursing, spawning, and refuge sites [34, 39]. This, in turn, can affect species composition and community structure and reduces the genetic flow between populations [39].

## 1.2.2  Behavioural barriers

In-stream barriers may also act as behavioural barriers to fish movement [109]. Behaviour choice experiments, for instance, analysing fish preference towards dark or illuminated regions have shown that fish responses largely depend on the species' diel activity pattern [109]. Understanding fish preference towards light intensity presents one factor when designing culverts that may prevent them from becoming a behaviour barrier. Similarly, artificial light pollution at night has become an increasing threat to fish due to the rise in global light emission, which is known to alter behavioural activities [178]. Under light pollution conditions, rockfish, for example, showed an increase in oxygen consumption and movement activity during the night and the suspension of their natural activity cycle [178].

### 1.2.3 Flow barriers

In-stream barriers may also limit and prevent fish movement by generating a velocity or flow barrier. Such flow barriers may result from insufficient flow properties (e.g., streamwise velocities, turbulence levels), flow depths and the presence of turbulent structures [164], and may cause the linear or angular translation of the fish's body (i.e., displacement) or even the deformation of the fish's body (i.e., changes in swimming motion) [128]. Hence, only fish with certain swimming capabilities or life stages may be able to successfully navigate these barriers and therefore, to move between upstream and downstream reaches. Insufficient flow depths, for instance, occasionally found in block ramps in mountain streams, may limit fish movement to certain fish sizes or even create ecological traps for fish [172]. In contrast to the natural occurring low water periods, insufficient flow depth may also be caused by the abstraction and diversion of water for energy generation in hydropower plants. Regulations, however, are in place to control the amount of water abstracted to ensure sufficient flow depth, for example, over weirs and in fish passes, to maintain longitudinal connectivity. A fish pass or fishway, here, describes a man-made structure, constructed to enable upstream or downstream movement of target species past an obstacle [205]. In contrast, under high flow conditions, the flow confinements within crevices of these block ramps can generate regions of high streamwise velocity, creating challenging conditions for smaller individuals and or weaker swimmers [172]. Similarly, the flow confinement and smooth surface found in culverts used for road and rail crossings exposes fish abruptly to high streamwise velocities [232]. Sluice gates used to control and maintain water levels, as another example, have a backwater effect and increase upstream water levels. Depending on gate height, flow confinement may lead to overflow, high streamwise velocities beneath the structure and the formation of a recirculation zone or hydraulic jump. A study of a sluice gate near a hydropower facility showed an increase in fish passage rate with increasing gate depth [41]. It was unclear, however, whether this effect was caused by avoidance of the overflow or attraction to the higher velocities found beneath

the gate [41]. Additionally, an increase in turbine passage was observed when the gate was lowered, potentially a result of the overflow attracting fish towards to the hydro-electric facility [41]. Moreover, hydraulic jumps generated downstream of weirs can distract fish from overcoming these barriers due to their attraction to turbulence [77].

An increase in turbulence associated with in-stream obstructions leads to an increase in swimming cost [62], potentially restricting movement if fish fail to negotiate these obstacles [236]. In general, fish avoided regions of high turbulence intensity and Reynolds shear stress associated with hydraulic structures [144, 93, 236, 222, 50]. Extremely elevated levels of Reynolds shear stress, for example, can cause disorientation and damage to the fish's body (e.g., descaling, deformation, loss of mucus layer) [176], often observed in relation to conventional hydropower schemes [156, 97, 176]. Turbulence, however, has also been found to be a measure of habitat complexity and fish abundance of certain species [207]. This relationship is described by the so-called "turbulence attraction and avoidance hypothesis" developed by Smith et al. (2014) [207]. This hypothesis states that fish use elevated levels of turbulence to sense roughness elements (e.g., cover, woody debris) (attraction) using their "sensory" lateral line but deliberately choose positions away from these elements with reduced turbulence levels (avoidance) [207].

Similarly, predictable flows around hydraulic structures can attract fish due to their advantageous flow regions, which can be exploited by fish [128]. Flow alterations in relation to vertical-oriented cylinders, for instance, can benefit fish by reducing their swimming energy costs when capturing energy from vortices. Therefore, fish alter their locomotion by synchronising their swimming gait with the vortex street to maintain station within the associated vortex street (e.g. [129, 128, 218]; Figure 1.4 (a)). This specific locomotion is termed "Kármán gaiting" whereby fish tune their body wavelength, lateral translation and tailbeat frequency to the vortex shedding frequency [6] to utilise the energy of the vortices to station hold or propel forward in the velocity deficit of the wake [130, 132]. Kármán gaiting has been shown to be energetically

advantageous for fish by maximising their swimming efficiency [218]. In the case of carangiform swimmers (were movement is concentrated predominantly at the rear of the fish's body and tail, e.g. rainbow trout), this locomotion can be expressed using a travelling wave equation of form: $y = f_1(x,t)sin(f_2(x,t))$ where y is the displacement of the centreline, x is the position along the fish axis, $f_1(x,t)$ denotes the instantaneous amplitude and $f_2(x,t)$ is the instantaneous phase [228, 6]. Likewise, fish swimming in a reverse von Kármán Street are expected to experience similar hydrodynamic and energetic advantages as fish swimming in a regular von Kármán street [237, 92]. In contrast, vortices shed by horizontal axis cylinders (Figure 1.4 (b)) can negatively impact fish swimming stability [146, 236, 222], for example, leading to the eventual loss of swimming stability in regions of high downward-acting Reynolds shear stress caused by eddies featuring clockwise rotation [146] due to the fish's limited vertical flexibility [207]. Besides the rotational axis of the vortices, vortex length scale is thought to play an important role in fish swimming stability [128]. Vortices exceeding approximately two third [133] or 76 % [222] of the fish's body length can detrimentally affect balance due to an increase in torque acting on the body [133, 222]. Vortices more than an order of magnitude smaller than the fish's body length, however, are assumed to not affect fish as they can steadily swim through them [128].

Besides the previously discussed primary effects of in-stream barriers on fish movement, secondary effects may occur through changes of the geomorphological characteristics of the river, such as channel geometry and substrate distribution. Channel adaptations may impact habitat quality and availability, and therefore, fish movement due to habitat and water quality preferences. For instance, the construction of weirs results in a greater flow depth and lower velocities upstream of the weir, causing a reduction in sediment transport, with coarser gravel to be trapped upstream [167]. This, in turn, may cause changes in nutrient and energy fluxes, thermal regimes, and contaminant distribution. The downstream flow, on the other hand, is characterised by high-momentum flow, creating local scours [190]. Changes in flow depth, velocity, and sediment transport through the installation of weirs have been found to reduce the

(a) Von Kármán vortex street (vertical cyliner)

(b) Von Kármán vortex street (horizontal cylinder)
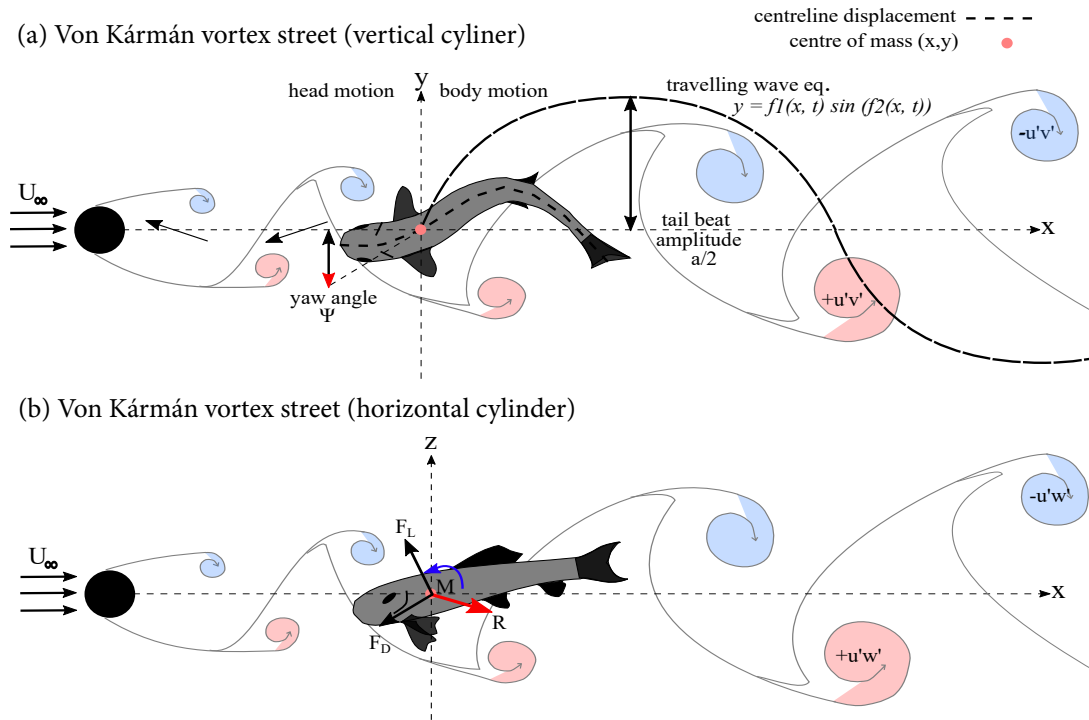
**Figure 1.4:** (a) Top-view of a fish swimming in the wake of a vertical cylinder periodically shedding vortices, also known as von Kármán vortex street. This specific swimming behaviour is termed Kármán gaiting, referring to fish using the vorticed to propel themselves forward. (b) Side-view of a fish swimming in the wake of a horizontal cylinder, experiencing destabilising vortices rotating around a horizontal axis.

proportion of riffles, pools, and gravel substrate within the channel, negatively affecting the spawning habitat of fish like trout [190]. Furthermore, the construction of an in-stream structure may reduce lateral habitat connectivity. The associated disconnection of the river from its floodplain may prevent fish from accessing floodplain habitat, potentially resulting in recruitment failure, the reduction of nursing habitat, as well as areas for refuge, particularly during high flow periods.

## 1.2.4   Selective fragmentation

Although in-stream barriers are generally undesirable and often require bypass solutions, they are also used for intentional river fragmentation (also known as selective fragmentation or isolation management), which might restrict the spread of non-native invasive species (INNS) which present another major threat to freshwater biodiversity [60, 180, 184, 101]. Since the 1950s, barriers have been used to limit the spread of a wide range of INNS, with an increasing interest in their use recognised since 2005 [101]. INNS can negatively impact the aquatic ecosystem by increasing predation pressure and competition for food and habitat, degrading habitat, leading to hybridisation and disease transmission, potentially causing the extirpation of native species [101].

Selective fragmentation might restrict the ranging and migration of INNS into adjacent habitats while simultaneously allowing passage of desired native species [180]. The concept of intentional fragmentation is based on a range of ecological filters, including biogeographic barriers (e.g., waterfalls), physiological barriers (e.g., discharge, flow depth, water temperature), biotic barriers (e.g., predators) and physical anthropogenic barriers (e.g., culverts, weirs, dams) [180]. Selective barriers are semi-permeable, allowing a subset of fish species to pass. To strengthen the effect of selectivity, further ecological filters can be applied based on physiological (e.g., swimming, jumping and climbing ability), morphological (body shape), sensory (e.g., electrical, acoustic, visual, olfactory, magnetic and carbon dioxide), phenological (e.g., migration and diel pattern), and or behavioural attributes (e.g., depth orientation, schooling) [180]. Barriers, such as anthropogenic hydraulic structures, for instance, can act as filters to fish movement by either: (a) preventing the movement of all species (e.g., dams); (b) allowing movement of all species (e.g., nature fishways); (c) allowing movement of the majority of desired fish species while reducing undesired fish species; or, ideally, (d) allowing movement of only desired species [180]. As physical barriers can be expensive to build and require frequent maintenance, traps, exclusion screens and non-physical solutions have gained in popularity to conserve and guide fish around water in-

and out-takes, as well as turbines, including for instance bubble curtains, pressure and light deterrents, electric fields and carbon dioxide barriers [112, 101]. To specifically use barriers for intentional river fragmentation, it is essential to not only understand structural, environmental, and hydrodynamic changes associated with these obstructions [11, 172, 206] but also to understand species-specific differences to prevent the passage of INNS. Furthermore, implications on resident fish undertaking small movements within their home range (e.g., to forage, spawn, seeks refuge and shelter) and other aquatic species such as crustaceans, amphibians and reptiles must be considered to maintain habitat connectivity [101].

## 1.3    Barrier mitigation strategies

Due to the vast number of large-scale and particularly small-scale barriers, mitigation strategies to restore longitudinal river connectivity have been developed. One option is complete or partial removal of obsolete barriers. Barrier removal can often be a cheaper solution than repairing or retrofitting these structures, or to install fish passage solutions [28, 64]. The decision of whether to remove a barrier, however, can be based on various reasons such as safety and security concerns, economic and environmental value, as well as existing legislations. The removal of obsolete barriers contributes to the European Water Framework Directive and Habitat Directive by improving ecological status and maintaining and restoring natural habitat. The project "Dam removal Europe" has been a driving force in restoring European rivers of high natural and cultural importance through the removal of unused dams and weirs [64]. The removal of six weirs on the River Villestrup, Denmark, for instance, has resulted in significant improvements in smolt output [26]. Removal of these weirs has also increased spawning success, fry survival and recruitment as well as smolt migration success [26]. Similarly, a study on the River Tees, north-east England, reported an increase in fish density and habitat diversity [216]. The changes observed in the upstream fish community at this river were linked to increased recruitment and dispersal of European eels [216].

Also, the partial removal of small-scale water supply dam in Alberta, Canada, showed an increase in movement activity between upstream and downstream reaches, with fish using the nature-like fishway to migrate, forage or hold station [214].

Nevertheless, the removal of existing barriers is often not possible due to various biological, or socio-economic reasons. In this case, the use of diversion schemes, retrofitting of existing barriers or the construction of fish passes may be used to mitigate the impact of the barrier and restore longitudinal river connectivity. Great effort has been undertaken in retrofitting existing barriers which cannot be removed or replaced with natural solutions. Typical examples for such barriers include hydraulic structures such as weirs (e.g., [77, 11]) and culverts (e.g., [79]) as well as hydrokinetic turbines (e.g., [211, 147]). Culverts, for instance, can act as hydraulic barriers to fish movement. Due to the flow confinement and smooth surfaces created, fish are abruptly exposed to high streamwise velocities [232, 79]. Physical adaptations, such as an increase in channel roughness, can generate secondary current cells, assisting smaller fish to overcome the barrier [232]. Weirs, as another example, may act as movement barriers depending on fish-species, season and site [11]. A study examining ramp length and slope under various discharges for a low-head ramped weir showed that attraction efficiency increased with ramp length and slope while passage efficiency decreased with ramp length but increased for lower discharges [11]. Moreover, a study considering fish passage over a broad-crested weir, identified waterfall height, plunge pool depth and discharge as key parameters influencing upstream passage [10]. Various combinations of these parameters, however, did not result in increased passage efficiency, highlighting the importance of the hydraulic environment generated in the moment of the passage attempt [10]. Furthermore, the development of hydropower turbines which safely facilitate downstream or combined upstream and downstream passage has been the subject of research and development (e.g. [38, 200, 171]). Novel turbine designs are being investigated, for example, for hydrokinetic turbines. These turbines do not require a difference in hydraulic head and hence, a hydraulic structure. Due to their open design and often low rotational speed, they are intended to permit fish to move

through the turbine (e.g., [104, 87, 42]). Archimedes screws, as another example, have been explored as an alternative to transport fish into the upstream region [171].

As fish are often able to migrate downstream by, for instance, either passing through the turbine or above weirs, upstream passage is often not possible without additional support structures such as fish passes. Great effort has been undertaken in restoring longitudinal river connectivity through the construction of fish ways. Depending on the structural design of the fishway and the target species, fish passes can be distinguished into (i) technical fish passes, (ii) nature-like fish passes, and (iii) special-purpose fish passes [65]. Nature-like fish passes mimic as much as possible the natural conditions of a river and are constructed from natural materials, allowing a wider range of species to pass. Examples include bottom ramps and slopes, bypass channel and fish ramps [65]. Due to the large space required for their construction, however, these fish passes are not suitable for urban areas. In such cases, technical and species-specific fish passes may present a more suitable solution. A wide range of technical fish pass solutions has been developed, including, for instance, pool passes, vertical slot passes, Denil passes, fish locks and fish lifts [65]. These passes must be chosen carefully, considering the swimming capabilities of the species present in the river (e.g., coarse fish versus game fish). In the presence of eel and lampreys, species-specific passes exist, providing climbing structures specifically designed for their elongated body.

As fish passage solutions, however, may fail due to unfavourable hydraulic conditions [172], they are still subject to design adjustments, including, for instance, the optimisation of structure geometry (e.g. height, ramp length and slope, orifice arrangement and shape [206, 11] and discharge [172]. In order to increase passage performance and minimise passage delay, fish passages need to (i) offer a suitable attraction flow, guiding fish toward the entrance of the fish pass, (ii) support fish to enter the structure, and (iii) provide flow conditions according to their biological need and swimming capabilities depending on species and life stage [206, 77, 10, 79, 205]. To assess the performance of a fishway, the following parameters may be assessed: barrier passage time

(e.g., conditional passage and failure time, approach time, internal passage time, transit time), barrier passage rate (e.g., conditional passage and failure rates), and percentage passage (e.g., proportional discovery, percentage entry, internal per cent passage, percentage passage) [205]. Furthermore, to increase passage efficiency and prevent fish, for example, from entering into hydropower plants or water in- and out-takes, exclusion screens (e.g., [217]) and visual cues, such as stroboscope lights and bubble curtains, can be used to modify fish movement [168].

Despite the wide range of fish passage solutions and diversion schemes, the construction of "transparent" barriers (i.e., barriers that do not cause changes in fish movement when compared to a free-flow, no barrier scenario) should be the desired aim which means that fish movement within obstructed parts of the rivers would not differ significantly from movement within a free-flowing river [39]. To achieve transparency, behavioural processes, movement frequency and timing, habitat use (e.g., cover, feeding), and susceptibility to predators should be considered, and an increase in energetic cost and migration delay should be avoided [39]. While this concept mainly relates to the construction of fish passes, it may also be transferred to any obstruction constructed in the river. To do so, an interdisciplinary approach will be required to fully understand the relationship between flow conditions, biomechanics, fish swimming behaviour, and movement requirements (e.g., movement direction, purpose, time, and environmental requirements) [39, 205].

## 1.4 Problem statement and thesis outline

Rivers have been subject to the construction of numerous small-scale, low-to-zero head anthropogenic obstructions, causing alteration and fragmentation of aquatic habitats by presenting physical, behavioural, and flow barriers to fish movement. Despite the tremendous impact of these structures on fish movement, more anthropogenic structures are added to riverine systems. They have mainly the purpose of mitigating flooding or

harnessing renewable energy. Often little is known about these emerging structures, requiring further research to quantify the impact on the aquatic ecosystem to minimise the risk of being a barrier to fish movement or causing detrimental alterations of the aquatic habitat.

The implications of two emerging in-stream barriers, namely leaky barriers used for natural flood management (Chapter 2 - Case study 1) and vertical axis hydrokinetic turbines (Chapter 3 - Case study 2) are studied in this thesis by means of two case studies. Using laboratory experiments conducted at the hydraulic facilities at the Hydro-Environmental Research Centre at Cardiff University, UK, this thesis aims to

1. quantify upstream and downstream channel hydrodynamics to identify characteristic flow alterations associated with the investigated emerging barriers and understand whether the identified flow alterations may present a flow barrier to fish movement; and

2. quantify how fish movement and passage behaviour changes with barrier presence, physical design, positioning, and operation to understand whether these structures may present a behaviour or physical barrier to fish movement and which of the tested solutions impacts least on fish movement

Following both case studies, Chapter 4 discusses the importance of considering primary and secondary impacts of such in-stream obstructions on the riverine environment, highlights opportunities and limitations of the use of ecohydraulic flumes, and raises considerations when planning the installation of in-stream structures. Hereafter, Chapter 5 summarises the main findings of this thesis.

The knowledge gained in through the analysis of channel hydrodynamics and fish movement in relation to both emerging in-stream structures and the consideration of potential secondary impacts of the aquatic environment will support the systematic advancement of these structures with focus on low environmental impact and will help managers make decisions in terms of operation, location and physical design.

In the following a short summary of both case studies is provided. Current knowledge and associated research gaps are outlined within each chapter.

### 1.4.1 Case study 1 - Leaky barriers

Rainfall intensity and frequency are expected to increase globally as global warming intensifies the hydrological cycle. Between 1981 and 2010, the number of record-breaking rainfall events has already increased by 12% worldwide. Enhanced rainfall causes the redistribution of water between surface and ground as soil storage capacity decreases and runoff increases, leading to a rise in regional flooding and an increase in future flood risk [98]. In Europe, for instance, flooding has been identified as a prime natural hazard which led to more than 165 floods during the last decade [191, 5, 63].

In recent decades, there has been a move from defences against flooding to an integrated flood risk management approach supporting, for instance, the application of natural flood management (NFM) measures alongside traditional flood defences [5]. NFM strategies use natural processes and local materials in the river corridor and catchment to provide environmentally, sustainable and cost-effective alternatives to traditional flood prevention. These strategies aim to slow down the surface flow, increase groundwater infiltrations, reduce the flood peak, and attenuate the flow reaching downstream communities. They include leaky barriers, also known as woody debris dams or engineered logjams, consisting of logs and branches arranged to span the entire width of the channel and positioned at intervals along the river corridor. Little, however, is known about their impact on river hydrodynamics and fish movement.

The first case study (Chapter 2) addresses the impact of physical leaky barrier design on channel hydrodynamics and fish spatial and passage behaviour. Using laboratory, small-scale flume experiments, upstream and downstream hydrodynamics are measured for five model leaky barrier designs, varying in length, porosity, and colour. Furthermore, juvenile rainbow trout (*Oncorhynchus mykiss*) and Atlantic salmon (*Salmo*

*salar*) movement behaviour is monitored under bankfull and near-bankfull flow conditions for a range of these barrier designs. These experiments aim to quantify leaky barrier-specific flow characteristics and potentially associated fish response to identify suitable design solutions which may provide guidelines for future field applications.

### 1.4.2   Case study 2 - Hydrokinetic vertical axis turbines

To date, 789 million people lack access to affordable, reliable, sustainable energy supply, resulting in social-economic inequality [149]. Until 2030 the UN Agenda for Sustainable Development aims to reduce this injustice by ensuring universal access to clean energy through increasing the renewable energy share [149]. A particular focus is on developing countries, small islands, and land-locked countries, often consisting of numerous remote communities. These countries often feature high biodiversity worth protecting and conserving. Hence, energy solutions need to be chosen with care to prevent habitat loss, degradation, and changes. Hydropower presents one renewable energy source, yet its full potential is unused. Initially deemed environmentally friendly, the tremendous environmental impacts of traditional, large-scale hydropower plants resulted in a greater focus on small-scale alternatives such as hydrokinetic vertical axis turbines (VATs).

VAT arrays present an innovative solution to harness energy from free-flowing rivers and estuaries, supplying coastal and inland communities with energy. They do not require hydraulic structures or large land areas, minimising impacts on the ecosystem. The relatively simple design allows VATs to be transported as single units, assembled, and maintained by local communities. Despite the economic, technical, and environmental advantages of VAT compared to traditional hydropower schemes, the main drawback remains in their low standalone performance [113]; however, this can be overcome by clustering multiple VATs in close proximities [213]. Yet, little is known of the impact of wake alterations associated with standalone and twin-VAT turbine setups on the spatial and swimming behaviour of individual fish and fish shoals.

The second case study (Chapter 3) addresses the impact of VATs on wake hydrodynamics and fish movement using laboratory, small-scale experiments. While wake hydrodynamics are quantified for a single and three twin-VAT configurations, individual juvenile rainbow trout movement is studied for a single VAT under confined and unconfined flow conditions for two discharges and two turbine operation states. Furthermore, single fish movement is compared to shoals swimming in the wake of a single VAT under unconfined spatial conditions. These experiments aim to inform how fish behave within proximity of such turbines and whether the turbine's wake influences fish movement. Overall, this chapter investigates if VATs can be used as low-environmental energy solutions.

*Chapter 2*

# Emerging migration barriers - part I: Leak barrier hydrodynamics and impact on fish movement

## 2.1 Introduction

The management and understanding of wood in rivers has undergone major transformations over the last four centuries [242, 243]. While initially wood was removed to enhance flow conveyance, navigation, and log transport, the resulting detrimental effect on ecosystem biodiversity and inability to recover from natural disturbance initiated the reintroduction of wood as part of river and floodplain management [183, 244, 243]. Since this change, the hydraulic, hydrological, geomorphological, and ecological effects of wood in rivers and streams have been extensively discussed, highlighting the importance of in-stream wood to control flow and create complex habitats through geomorphological and flow alterations (e.g., [2, 82, 243]). In addition to the use of in-stream wood and woodland planting in river restoration schemes [183, 27], the use of wood accumulations in rivers and streams as nature-based solution to flood risk management has received much attention over the last 10 years [71, 58, 35] as a result of the increasing number of major floods. In Europe, for instance, approximately 140 major floods were recorded between 1900 and 2005, with a flood being considered as a major

flood when exceptional economic losses are reached, hundreds of thousands of people have lost their homes and thousands of people have lost their life [20]. In contrast, during 2003 and 2013 more than 165 floods occurred [191], highlighting the tremendous increase in number of floods. Flooding causes significant socio-economic effects [191] and is likely to increase with more frequent, higher intensity rainfall events due to climate change [98, 123]. Climate projection models, solely considering the effects of climate change, anticipate an increase of the socio-economic impact of river floods in Europe by approximately 200 % [9]. Therefore, there is an urgent need to find sustainable solutions to attenuate the impact of flooding, shifting from traditional flood defences to an integrated catchment-wide approach based on flood risk management [5]. Particularly with the continued growth in population and the resulting expansion of cities and towns causing increased economic pressure to build on floodplains [239], a wide range of mitigation measures is required to reduce the impact of floods. The use of natural flood management, for example, presents one sustainable approach which can be applied alongside traditional flood defence schemes.

### 2.1.1   Natural flood management

Natural flood management (NFM), also known under the term "working with natural processes" and "nature-based solutions", describes the application of a wide range of techniques, aiming to reduce the impact of flooding by working with natural processes and materials, and therefore, to store and or slow down flood water [35]. NFM measures can be subdivided into four categories: woodland, runoff, coastal and estuary, and river and floodplain management, with examples for each category listed in Figure 2.1 (a) and their location within the catchment depicted in Figure 2.1 (b) [35]. The latter category, for instance, involves river and floodplain restoration, offline storage areas, and the use of wood from surrounding areas to form leaky barriers [35], otherwise known as woody debris dams [58] or engineered logjams [244]. The listed examples are by no means a complete list of all measures available, but they do include the meas-

ures thought to have the greatest potential to minimise flood and erosion risk according to Burgess-Gamble et al. (2018) [35]. Furthermore, many NFM measures are often employed in combination rather than separately.
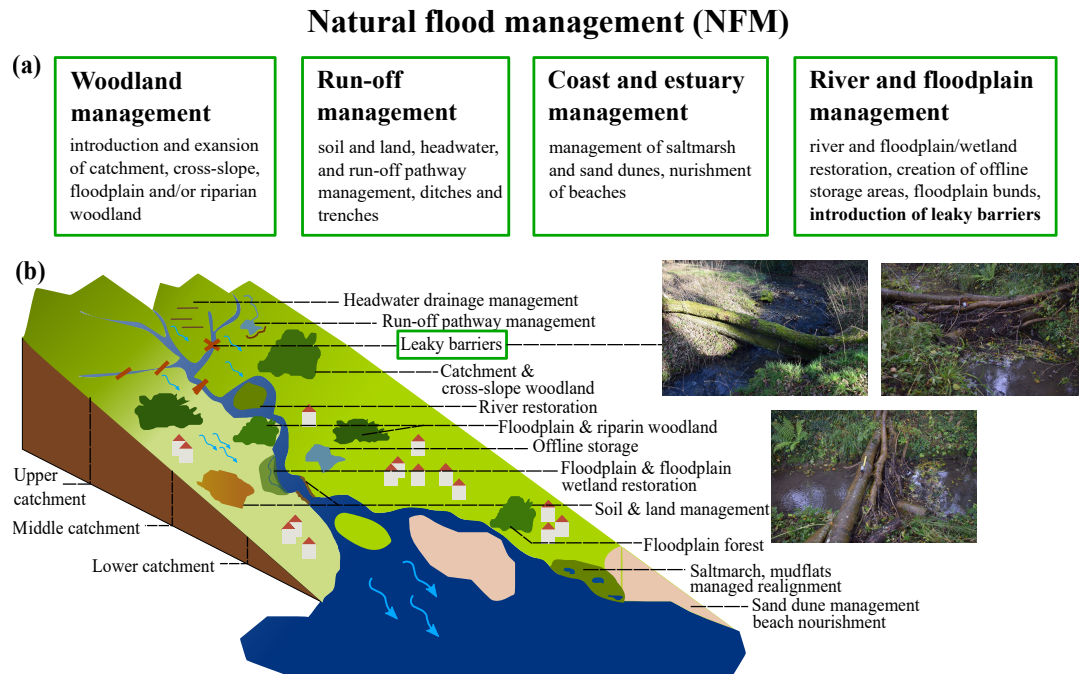


**Figure 2.1:** Natural flood management can be categorised into woodland, run-off, coast and estuary, and river and floodplain management. Example measures for each category are provided in (a) and visualised in the catchment schematic in (b). Content and schematic adapted from [35], Photo credit: E. Follett.

## 2.1.2   Leaky barriers

Over the last two decades, the use of leaky barriers (Figure 2.1 (b), right) has gained in popularity worldwide [210, 183], but particularly in the UK [35, 58, 96, 142] where a wide range of leaky barrier structures have already been installed (e.g., Pickering, North East England; Holnicote, South West England; Shropshire, West England; Stroud, South West England; Great Triley Wood, South East Wales and Peeblesshire, South Scotland) [35, 71, 96]. In these natural flood management schemes, leaky barriers are

installed in groups of 100 plus units, used on selected tributaries in the river network, sometimes with the key aim of desynchronising the tributary peak flows from the main river.

Although leaky barriers may also occur naturally, for instance, through trees falling into the watercourse and beavers constructing woody debris dams, this chapter focuses on the use of engineered leaky barriers. Leaky barriers, artificially introduced in the mid to upper catchments (i.e., where channel width is smaller than key debris length [131]), are formed from wooden logs, fallen trees, and branches (Figure 2.1 (b)), often sourced from the adjacent floodplains. Installed perpendicular to the flow, leaky barriers span the complete width of the river channel, allowing unhindered base flow and fish movement through a vertical gap ($b_0$) between the bottom of the structure and the riverbed, as depicted in Figure 2.2 for an idealised non-porous (a) and porous (b) leaky barrier. Under high flow conditions, these structures aim to reconnect rivers with their floodplains by partially blocking the flow in the upper water column. The resulting upstream backwater rise causes the water to spill onto the upstream floodplain, using this area for water storage and to enhance infiltration into the ground [108]. Combined with the hydraulic roughness provided by floodplain vegetation and forest [170], leaky barriers slow down the movement of the water throughout the catchment and attenuate flow downstream [63, 59, 71, 145].

### 2.1.2.1 Hydraulic and hydrodynamic alterations associated with leaky barrier structures

As the lower channel remains unobstructed, a reasonable proportion of the flow passes beneath the leaky barriers ($b_0$), while the remaining flow overtops or passes through the barrier. The idealised non-porous leaky barrier shown in Figure 2.2 (a) mimics the natural accumulation of sediment, leaf material, and woody debris, causing the flow to diverge around the barrier. Flow around a non-porous leaky barrier is analogous to flows passing a bluff body, such as a sluice, weir, and tidal gate, creating a zone

of elevated pressure upstream of the barrier, which causes the flow to diverge around the structure and leads to an increase in streamwise mean velocity beneath it. While a recirculation region is expected to form immediately downstream of the leaky barrier at height of the upper channel, the high velocity region exiting the barrier's gap ($b_0$) acts like a modified wall jet (Figure 2.2 (a), [61]). This jet maintains its maximum jet velocity until a downstream distance of $x/b_0 = (4U_0/U_{jet,max})^2$ before commencing a rapid decay [61, 25].
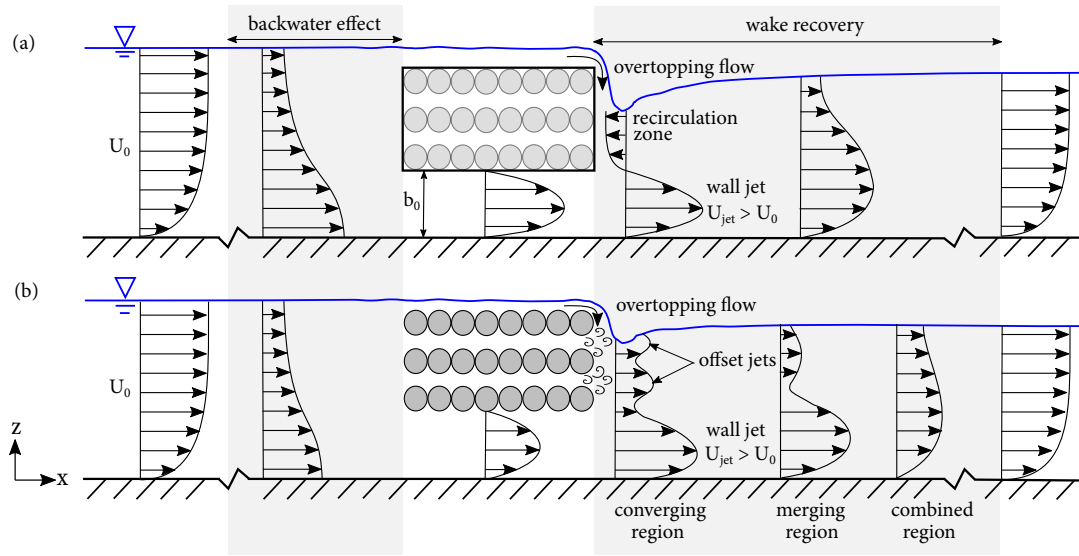


**Figure 2.2:** Typical streamwise mean velocity profiles upstream and downstream of an idealised (a) non-porous and (b) porous leaky barrier with vertical gap $b_0$. Upstream of the leaky barriers, logarithmic velocity distribution of bulk velocity $U_0$ starts to divert with decreasing proximity to the barrier, forming a modified wall jet $U_{jet}$, with $U_{jet} > U_0$. While a recirculation zone forms immediately downstream of the non-porous leaky barrier, smaller offset jets generated by the flow through the barrier gaps are present for the porous configuration which merge and diminish with increasing downstream distance. The cross-sectional blockage provided by the barrier causes a rise in backwater and the flow to overtop the structure.

In the case of the porous structure (Figure 2.2 (b)), this jet is anticipated to decrease in strength due to the increased proportion of flow passing through the barrier. Depending on the leaky barrier's physical design and log arrangement, this "through-flow" creates smaller and weaker offset jets, like a multiple jet configuration. The interaction

between a wall jet and an offset jet, or between two or more parallel jets, is character-ised by three distinct regions [76, 233, 54]. Within the converging region the parallel jets start to bend towards each other and create a recirculation zone in between the jets. In the merging region, both jets gradually merge with increasing downstream distance until finally reaching the combined region in which both jets behave like one [233]. Depending on the offset ratio between the jets, the near field is characterised by the shedding of Kármán-like vortices in the inner shear layer, causing interaction between jets [234]. In contrast, the free shear layer of a single jet, either offset or wall jet, is characterised by Kelvin-Helmholtz roll-ups [234].

The flow around porous leaky barrier structures exhibits similarities to the flow around horizontal cylinder configurations, which have been of specific interest due to their wide engineering application. While single horizontal cylinders have been studied ex-perimentally [105, 146] and numerically [153, 124, 161], only a few studies examine the flow field around multiple horizontal cylinders, with those studies focusing on four in-line square [121, 254, 235, e.g.] and staggered configurations [120, 122, 255]. Des-pite the useful insights of these studies, with the exception of the Lam and Zou (2009) study [122], which was conducted for Reynolds numbers ($Re$) based on dowel dia-meter ($d$) of 11,000<$Re_d$<20,000 (i.e., turbulent flow), the majority of these studies have only been conducted for low Reynolds numbers ($Re_d$<2100; i.e., laminar flow), which limits the applicability of these studies to the understanding of the hydrodynam-ics of full scale engineered leaky barriers in fully turbulent flows.

### 2.1.2.2   Ecological value of leaky barriers

Although leaky barriers are predominantly used to mitigate the impact of flooding, the introduction of in-channel large woody material (LWM) or debris (LWD) has multiple benefits for the aquatic ecosystem. It creates a diverse aquatic habitat by altering up-stream and downstream flow, enhancing and creating habitat complexity, and trapping sediment from floodplain run off and improving water quality [35]. Wooden struc-

tures, for instance, create overhead cover [150, 158, 59] as well as refugia for fish [150, 192, 59]. Small fish, in particular, can be attracted to coarse, branchy, complex wooden structures to seek shelter from predators, decreasing predator foraging success due to visual interference and prevention of entry [192]. Juvenile salmon particularly show increased survival when coarse, woody debris is present [192]. Nevertheless, fish responses to natural or the artificial introduction of wooden logs as in the case of leaky barriers may vary depending on fish species and decomposition of the wood as well as other habitat characteristics [16]. In addition, wooden materials provide food for the entire food chain [23]. Organic material, such as leaves and small sticks trapped within wooden accumulations and algae growing on the log's surface, provide food for macroinvertebrates, which, in turn, provide food for a diverse fish population [23].

By connecting the main channel with surrounding floodplains, wood accumulations like leaky barriers can also create seasonal wetlands [249], supporting lateral habitat connectivity [189] and providing fish spawning and nursery grounds [203], as well as low velocity areas protecting fish from downstream displacement during high flows [131, 73]. During flooding events, these structures are partially or completely submerged, altering the flow field by creating low and high velocity zones which enhance habitat complexity and therefore, provide diverse habitat for a wide range of species and life stages [131].

The complex habitat created through leaky barriers is often accompanied by varying velocities and turbulence levels. Immediately upstream of large wood accumulations, streamwise velocities decrease and flow depth increases, resulting in increased backwater. In contrast, downstream flow may consist of a combination of overtopping flow exiting the top of the LWM, flow through the gaps between branches potentially creating smaller off-set jets and turbulent structures, and flow exiting underneath the LWM, creating a stream of high momentum due to the blockage provided (Figure 2.2). In general, fish avoid regions of high vorticity, turbulence intensity and Reynolds shear stress associated with hydraulic structures [50, 222, 236, 93, 144]. Flow alterations in rela-

tion to vertical-oriented cylinders can benefit fish by reducing their swimming energy costs when capturing energy from vortices by altering their body kinematics to maintain station within the associated vortex street (Figure 1.4 (a); e.g., [129, 128, 218]). In contrast, vortices shed by horizontal axis cylinders can negatively impact fish swimming stability (Figure 1.4 (b); e.g., [222, 236, 146], for example leading to the eventual loss of swimming stability in regions of high downward-acting Reynolds shear stress caused by eddies featuring clockwise rotation [146] as described in Chapter 1.

The complex flow field created through leaky barriers can also alter the river morphology upstream and downstream of these structures, creating localised scour and scour pools, deposition mounds and banks as well as undercut banks [67, 131]. These, in turn, can provide additional shelter, cover and resting areas. In addition, smaller gravel is loosened and deposited downstream, supporting substrate rejuvenation [94] and hyporheic flows [33], supporting the creation of suitable spawning habitat.

### 2.1.3 Problem statement and chapter outline

Perceived as environmental-friendly hydraulic structures, engineered leaky barriers used for natural flood management are introduced in rivers, potentially creating movement barriers for fish. Yet, little is known about the physical design implications on the aquatic environment. Current physical design guidelines only focus on leaky barrier width, recommending the use of a minimum log length of the main channel to prevent downstream transport and damage to infrastructure [131]. Further existing guidelines, consider key parameters, namely the vertical gap underneath and within the porous structures, and total structure height [58], not taking into account porosity, longitudinal barrier length, and implications on flow alterations and free fish movement. These guidelines are based on existing knowledge about fish movement and habitat usage but lack empirical evidence of free fish movement and velocity measurements.

Through scaled laboratory experiments, five idealised model barrier designs composed

of arrays of horizontal, wooden cylinders were examined under 80 % and 100 % bank-full flow conditions in an open channel flume at the Hydro-Environmental Research Centre's hydraulic laboratory at Cardiff University. To mimic the natural characteristics of the leaky barriers as realistically as possible, the barrier's height, log diameter, vertical gap between the leaky barrier and the bed were scaled from those installed in Wilde Brook, Corvedale, Shropshire, UK, as part of the Natural Flood Management project "Shropshire Slow the Flow - Severn Tributaries" project [70].

For the chosen leaky barrier structures, this chapter explores

1. the impact of barrier length, dowel arrangement, and void fraction on first and second-order turbulence statistics as well as jet development and decay were analysed;

2. scaling effects for one leaky barrier configuration using two flumes at different scales;

3. whether barrier presence and design, including longitudinal length and barrier porosity, influences fish movement and upstream passage;

4. whether fish spend more time underneath longer barrier compared to the shorter barriers due to the provision of overhead cover; and

5. whether visual cues, here tested through barrier coloration, increase upstream passage.

Based on the knowledge gained through the outlined research questions, this chapter contributes to the existing knowledge by identifying characteristic hydrodynamic alterations upstream and downstream of a range of leaky barrier structures and discussing the potential of these flow alterations becoming a velocity barrier to fish movement; presenting whether leaky barriers with a vertical gap present a physical barrier fish movement and how their physical design may altered to prevent the spread of INNS; and raising considerations when installing engineered leaky barriers in the field.

Section 2.2 provides an overview of the leaky barrier designs tested, hydrodynamic measurement, and fish behaviour methods applied. Subsequently, hydrodynamic and fish behaviour results are depicted in Section 2.3 and are discussed in Section 2.4, considering potential primary and secondary implications on the aquatic ecosystem. Furthermore, this section outlines study limitations and highlights management requirements and remaining research questions. Section 2.5 summarises the identified physical design implications of leaky barriers on channel hydrodynamics and fish movement.

## 2.2 Methodology

Upstream and downstream hydrodynamics, and fish behaviour was investigated for five physical leaky barrier designs at the Hydro-Environmental Research Centre's hydraulics laboratory at Cardiff University. The following sections provide an overview of the general flume setup, flow conditions and leaky barrier structures used for hydrodynamic and fish behaviour experiments.

### 2.2.1 Flume setup

Experiments were conducted in a recirculating open channel flume (hereafter denoted as Flume 1) of length ($L_{flume}$) 10 m, width ($B_{flume}$) 1.2 m and depth ($H_{flume}$) 0.3 m, set to a bed slope of 1 in 1000 (Figure 2.3 (a) and (b)). The flume had a symmetrical compound channel section, with a rectangular main channel of width 0.6 m ($B_{m}c$) and total floodplain width of 0.6 m ($2B_{fp}$). The main channel had a bankfull depth of 0.15 m ($H_{mc}$). Prior to the installation of the barriers, uniform, subcritical flow conditions were established for bankfull (100 % $Q_{bf}$) and 80 % bankfull (80 % $Q_{bf}$) flow conditions, relating to a discharge of 0.028 m³/s and 0.022 m³/s as well as a flow depth ($H$) of 0.15 m and 0.13 m, respectively. These bare flume conditions represent

the control treatment (denoted as "C"). A detailed breakdown of the hydraulic test conditions is presented in Table 2.1.

Bankfull flow condition refers to the maximum discharge capacity of the main channel and, therefore, the greatest flow rate contained within the main channel before flow inundates onto floodplains. Hence, 80 % bankfull flow condition refers to 80 % of the maximum discharge capacity of the main channel. Both discharges were chosen to maximise the impact of the leaky barriers on the upstream water level. This is because for higher overbank flows, when the leaky barrier is fully submerged, leaky barriers no longer act as a control structure (i.e., causing a backwater effect) and act as hydrodynamic drag or "roughness". Therefore most practitioners suggest that leaky barriers will have the greatest impact on lower (more frequent) flows compared to the higher flows. The flow condition was achieved by controlling the water surface profile using a tailgate weir located at the downstream end. The discharge and tailgate weir height remained fixed for the subsequent leaky barrier experiments. The installation of the leaky barrier resulted in a change in water surface profile, generating gradually varied flow conditions. Flow depth was measured using a Vernier pointer gauge with an accuracy of $\pm 0.1$ mm and an ultrasonic flowmeter (TecFluid Nixon CU100) measured the discharge to a precision of $\pm 1.5$ %.

To examine the scale effects, a 1:2 scale replica test for one leaky barrier configuration (see Table 2.1; LB6; details given below) was carried out in a larger flume (hereafter denoted as Flume 2). The flume was 17 m long, 1.2 m wide and 1.0 m deep, with a rectangular cross-section and no lateral floodplains (Figure 2.3 (c)). The Froude scaling law was used, and the bulk velocity was scaled to maintain a Froude number ($Fr = U_0/\sqrt{(gh)}$) equal to 0.25 between comparative tests, corresponding to a discharge of $Q$=0.157 m³/s and flow depth of $H$=0.3 m. Froude number scaling was used to allow the barrier design to be adapted and scaled from those constructed in a field site on Wilde Brook (Corve catchment, Shropshire).

For both flumes, the flow direction was defined as the positive in $x$ direction, with $y$

(a)



(b)  (c) 
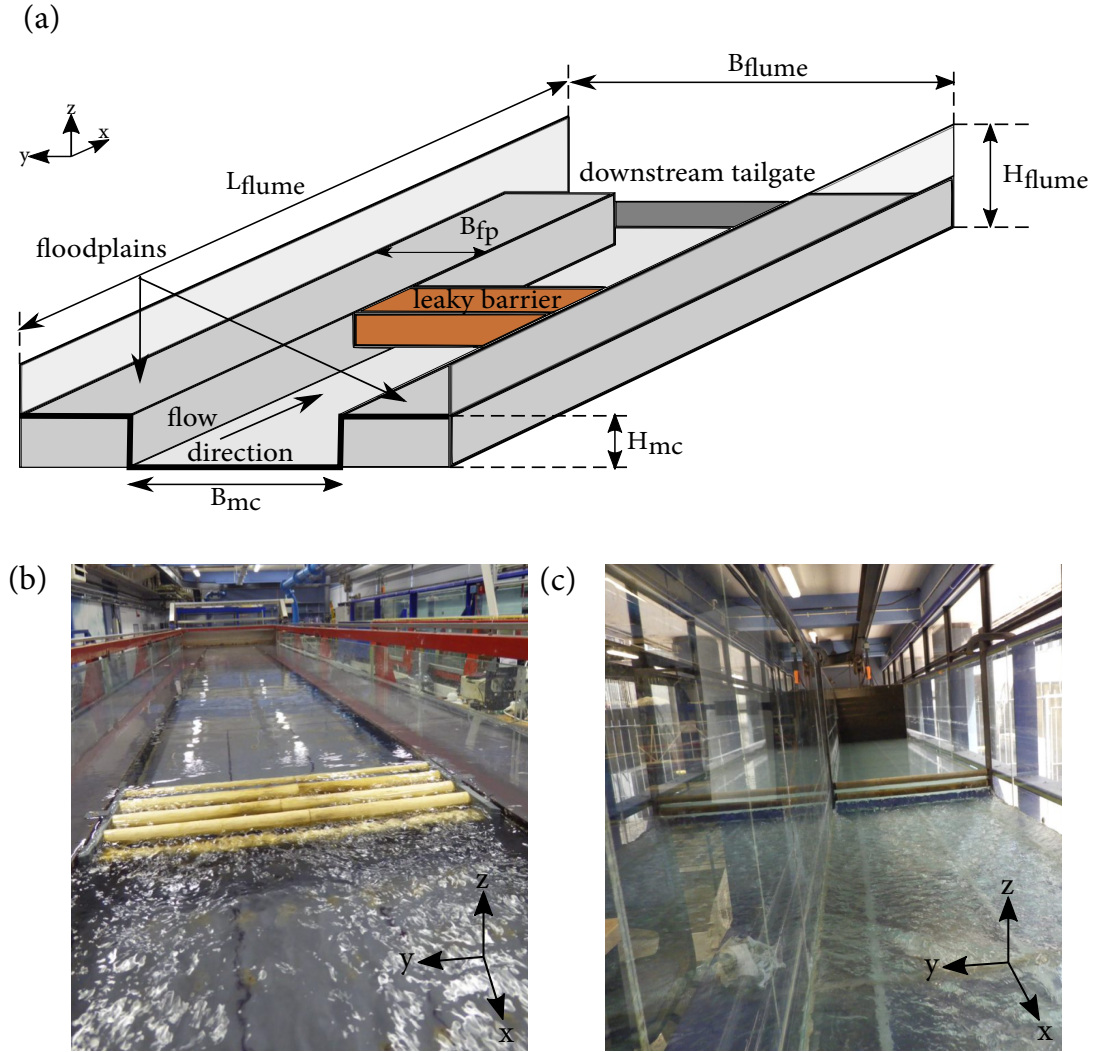
**Figure 2.3:** (a) Schematic of the experimental setup of Flume 1 ($L_{flume}$ x $B_{flume}$ x $H_{flume}$), comprising of a straight compound channel of width $B_{mc}$ and height $H_{mc}$ with symmetrical floodplains of width $B_{fp}$ on either side of the main channel. Photograph of the recirculating open channel flume showing the experimental setup for the five leaky barrier configurations LB1-5 tested in Flume 1 (b), and the scaled leaky barrier configuration LB6 tested in Flume 2 (c).

and $z$ being the lateral and vertical coordinates, respectively, as indicated in Figure 2.3. For the data analysis, the upstream and downstream edges of the barrier were defined as $x$=0 for $x$<0 and $x$>0, respectively, as indicated in Figure 2.4 (b).

The bulk velocities and flow rates selected for the experiments are in the correct range to comply with Froude similarity. For Froude similarity, discharge and velocity scale using the following relationships: $U_{field} = U_{lab}\sqrt{\lambda_s}$ and $Q_{field} = Q_{lab}\lambda_s^{5/2}$, respectively, where $\lambda_s$=6.7. At Wilde Brook, Corvedale (Shropshire, UK) no measurement of the discharge were available at the leaky barrier locations and the selected lab discharge correspond to field scale discharges of 2.55 and 3.25 m$^3$/s, for the 80 % $Q_{bf}$ and 100 % $Q_{bf}$ conditions, respectively, which is in keeping with the field channel scale (bankfull flow area = 4 m$^2$). The lab bulk velocity of 0.32 m/s for bankfull conditions relates to a field-scale velocity of 0.85 m/s, which corresponds to the approximate magnitude for a stream flowing at full bankfull capacity before inundating the floodplains.

### 2.2.2 Leaky barrier structures

In total, six leaky barrier structures were analysed with their main characteristics presented in Figure 2.4 and their experimental details given in Table 2.1, including frontal projected area ($A_p = B_{mc}H_s$ and $A_p = B_{mc}3d$ for LB1,4 and LB2,3,5,6, respectively), leaky barrier void ratio ($\Phi = V_{void}/V_{control}$) calculated from the ratio of the pore volume ($V_{void} = V_{control} - V_{solid}$), with $V_{solid}$ being the volume occupied by the solid barrier ($\Pi(d/2)^2 n B_{mc}$) and $V_{control} = B_{mc}H_s L_s$ (no leaky barrier present), and relative channel void area $A_{rv} = 1 - A_p/(B_{mc}H_{mc})$, calculated from the bankfull channel area $B_{mc}H_{mc}$ relative to leaky barrier projected area $A_p$. Table 2.1 also provides details about the flow conditions for each test, including flow discharge ($Q$), mean upstream flow depth ($\overline{H}_1$) and the difference between mean upstream ($\overline{H}_1$) and downstream ($\overline{H}_2$) flow depths ($\Delta H$), with $\overline{H}_1$ and $\overline{H}_2$ being calculated from the average of all water elevation measurements upstream and downstream, respectively. Upstream bulk velocity was computed as $U_0 = Q/(\overline{H}_1 B_{mc})$ or in case of overbank flow as $U_0 = Q/(H_{mc}B_{mc} + B_{flume}(\overline{H}_1 - H_{mc}))$. The Reynolds number was calculated based on the log diameter ($Re_d = U_0 d/\nu$).

Leaky barrier structures LB1-5 were constructed from wooden dowels of diameter ($d$)
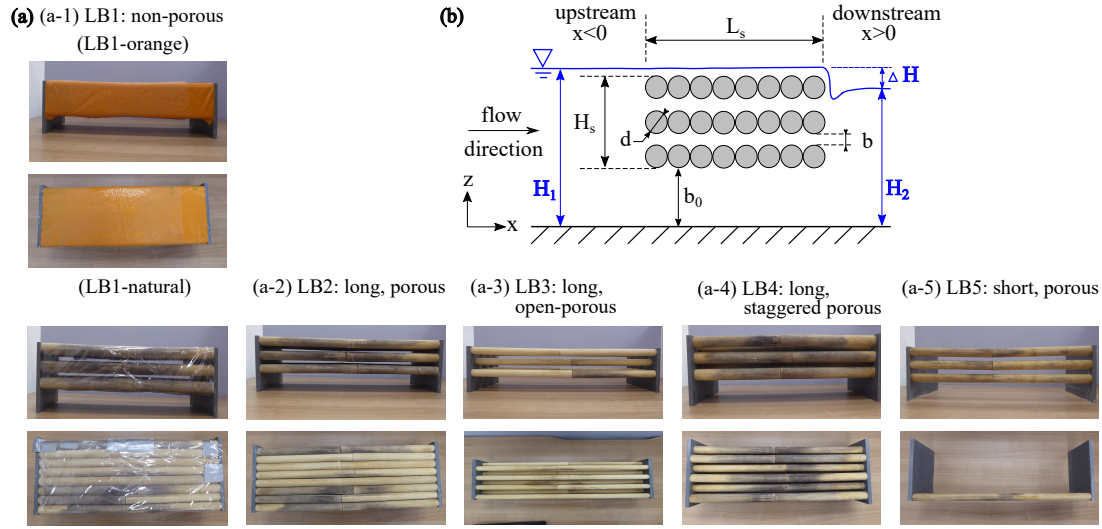
**Figure 2.4:** (a) Frontal (top) and top (bottom) view photographs of all leaky barrier structures (LB1-5), and (b) schematic diagram depicting an idealised leaky barrier of height $H_s$ and longitudinal length $L_s$ with vertical inter-cylinder gaps ($b$) and a vertical gap between the structure and the channel bed ($b_0$). The structure is composed of horizontal logs of diameter ($d$) aligned parallel to the channel bed and normal to the flow direction. Upstream ($H_1$) and downstream ($H_2$) flow depth is indicated in blue, with $\Delta H$ marking the difference between upstream, and downstream flow depth.

25 mm and had a structure height ($H_s$) of 100 mm, while structure LB6 was a 1:2 scale replica of LB5, constructed using dowels of diameter ($d$) 50 mm, spanning a vertical height ($H_s$) of 200 mm. Each dowel was aligned perpendicular to the main flow direction spanning the complete width of the main channel, i.e. $B_{mc}$=0.6 m for case LB1 to LB5, and $B_{mc}=B_{flume}$=1.2 m for case LB6. A vertical gap of $b_0$=50 and 100 mm (for LB1-5 and LB6, respectively) was created between the flume bed and the lowest dowel, remaining fixed for all configurations.

The six leaky barriers comprised of a non-porous structure LB1 (Figure 2.4 (a-1)), analogous to a bluff body, of length $L_s$=8 $d$ for which the structure was wrapped in polyethylene to ensure its impermeability; a porous structure LB2 (Figure 2.4 (a-2)) with three dowel rows, length $L_s$=8 $d$ and void ratio ($\Phi$=41.1 %); LB3 (Figure 2.4 (a-

**Table 2.1:** Leaky barrier structural characteristics and flow conditions for the six leaky barrier structures (LB1-6) and control conditions, including number of dowels ($n$), longitudinal barrier length ($L_s$), leaky barrier height ($H_s$), vertical gap ($b_0$), frontal projected area ($A_p$), barrier void ratio ($\Phi$), relative channel void area ($A_{rv}$), discharge ($Q$), mean upstream flow depth ($\overline{H}_1$), backwater rise ($\Delta H$), upstream bulk velocity ($U_0$) and Reynolds number ($Re_d$). (*Flow depth was not measured for the scaled leaky barrier LB6.)

| | $Q$ | n | $L_s$ | $H_s$ | $b_0$ | $A_p$ | $\Phi$ | $A_{rv}$ | $\overline{H}_1$ | $\Delta H$ | $U_0$ | $Re_d$ |
|---|---|---|---|---|---|---|---|---|---|---|---|---|
| | [m³/s] | [-] | [mm] | [mm] | [mm] | [m²] | [%] | [-] | [mm] | [mm] | [m/s] | [-] |
| Control (C) | 0.022 | - | - | - | - | - | - | - | 132.3 | - | 0.32 | - |
| LB1 | 0.022 | 24 | 200 | 100 | 50 | 0.06 | 0 | 0.33 | 157.5 | 33.3 | 0.22 | 5500 |
| LB2 | 0.022 | 24 | 200 | 100 | 50 | 0.05 | 41.1 | 0.43 | 140.5 | 9.5 | 0.26 | 6500 |
| Control (C) | 0.028 | - | - | - | - | - | - | - | 145.9 | - | 0.32 | - |
| LB1 | 0.028 | 24 | 200 | 100 | 50 | 0.06 | 0 | 0.33 | 172.3 | 32.7 | 0.24 | 6000 |
| LB2 | 0.028 | 24 | 200 | 100 | 50 | 0.05 | 41.1 | 0.43 | 158.4 | 16.0 | 0.28 | 7000 |
| LB3 | 0.028 | 12 | 200 | 100 | 50 | 0.05 | 70.5 | 0.43 | 160.3 | 15.7 | 0.27 | 6750 |
| LB4 | 0.028 | 15 | 175 | 100 | 50 | 0.06 | 55.0 | 0.33 | 161.9 | 27.6 | 0.27 | 6750 |
| LB5 | 0.028 | 3 | 25 | 100 | 50 | 0.05 | 41.1 | 0.43 | 155.1 | 9.6 | 0.29 | 7250 |
| LB6 | 0.157 | 3 | 50 | 200 | 100 | 0.18 | 41.1 | 0.5 | * | * | 0.44 | 22000 |

3)) is a staggered configuration with a greater inter-dowel gap and higher void ratio ($\Phi$=70.5 %); LB4 (Figure 2.4 (a-4)) is another staggered leaky barrier with a closer inter-log gap and lower void ratio than LB3 ($\Phi$=55 %); and LB5 (Figure 2.4 (a-5)) and LB6 are short length structures ($L_s$=1 $d$) composed of three horizontal dowels vertically-aligned.

River and barrier model designs were based on the geometric scaling of four length scales, which characterise the physical properties of the stream and leaky barriers at Wilde Brook, Corvedale (Shropshire, UK) [70]. The model to prototype scale was

approximately 1:7 (1:6.7) and based on geometric scaling of the (i) channel width
($b_{mc,field}/b_{mc,lab}$=4 m/0.6 m); (ii) bankfull depth ($h_{mc,field}/h_{mc,lab}$=1 m/0.15 m); (iii)
vertical gap underneath a leaky barrier ($b_{0,field}/b_{0,lab}$=0.33 m/0.05 m) and; (iv) log dia-
meter ($d_{field}/d_{lab}$=0.17 m/0.025 m). For Wilde Brook the channel's $b_{mc}/h_{mc}$ ratio var-
ies in the range 1.66$\leq b_{mc}/h_{mc} \leq$4.8, based on 10 selected cross-sections out of a set
of 105 observations. The $b_{mc}/h_{mc}$ ratio of 4 was chosen for this study and previous
studies on bed erosion [70] as this typifies the channel and this ratio was maintained in
our lab model. At Wilde Brook, the leaky barriers have a vertical gap to bankfull height
ratio ($b_0/h_{mc}$) in the range of 0.33$\leq b_0/h_{mc} \leq$0.5, which is typical of many leaky bar-
riers in the field and a $b_0/h_{mc}$ of 0.33 was maintained for our laboratory model. Geo-
metric scaling was applied for both barrier model designs using a dowel diameter, $d$, of
25 mm, which represents a typical field log diameter in the range 0.17$\leq d_{field} \leq$0.33 m
which is in keeping with the leaky barriers at Wilde Brook and other sites of this scale.

### 2.2.3 Hydrodynamic measurements

#### 2.2.3.1 ADV measurements

The upstream flow diversion and downstream wake hydrodynamics were examined by
measuring the three components of velocity using a sideways-looking acoustic Doppler
velocimetry (ADV, Nortek Vectrino, [154]).

The acoustic Doppler velocimeter measures the velocity of the water by the principle
of the Doppler shift [165]. Therefore, an acoustic transmitter sends out a beam of
acoustic waves at a fixed frequency, which will reflect off the particles transported in
the water [165]. Here, Sphericel®110P8 hollow glass spheres with a mean particle
size of 11.7 $\mu$m and a specific gravity of 1.10 g/cc (Potters Industries LLC) were added
to the water, enhancing the ADV signal. The change in frequency of the returning
acoustic waves is then received by the three acoustic receivers and used to calculate
the velocity of the water in the streamwise, lateral and vertical directions [165]. A

schematic of the working principle of the ADV is presented in Figure 2.5.

Measurements were carried out at a sampling rate of 200 Hz for 300-1800 s, depending on the data quality. The sufficiency of the sampling period length was checked by analysing the cumulative time average of the measurements and the root mean square velocity fluctuations ($\sqrt{u'^2}$) over the sampling period. In the near wake region immediately downstream of the leaky barrier, the sampling duration needed to be increased significantly up to 1200 s and 1800 s for LB1-5 and LB6, respectively, to capture a representative sample of the high-frequency turbulent fluctuations and obtain data of sufficient quality. Measurement data were filtered and post-processed using Matlab 2018b. In a first pre-filtering step, velocity



**Figure 2.5:** Schematic representing the operation principal of an acoustic Doppler velocimeter (ADV). Figure adapted from [154].

data with thresholds below 15 dB and 70 % for Flume 1 and 10 dB and 70 % for Flume 2 for SNR and Correlation [154, 43], respectively, were removed. In a second step, an open-source toolbox was implemented to despike the data [141, 140], using a despiking algorithm based on the three-dimensional phase space method introduced by Goring & Nikora (2002) [81] and modified by Wahl (2003) [230]. The velocity records were decomposed into time-averaged and fluctuating components ($u = \overline{u} + u'$), respectively, denoted by an overbar and prime operation. Reynolds shear stresses ($\overline{u'w'}$) were calculated by multiplying and subsequently time-averaging the velocity fluctuations in the vertical and longitudinal directions. Turbulent kinetic energy was calculated as $tke = 1/2(\overline{u'^2} + \overline{v'^2} + \overline{w'^2})$.

For LB1-5, 26 velocity profiles, including 14 profiles upstream and 12 profiles downstream, were measured along the channel centreline, starting at -0.8 $b_0$ and 1 $b_0$ up-

stream and downstream of the leaky barrier, respectively (Figure 2.6 (a)). Until approximately $4\,b_0$ upstream and downstream of the leaky barrier, velocity profiles were equally spaced by 20 mm ($0.4\,b_0$) in the longitudinal direction. As the distance away from the barrier increased, this longitudinal resolution increased to 60 mm ($1.2\,b_0$), 100 mm ($2\,b_0$), 250 mm ($5\,b_0$), 500 mm ($10\,b_0$) and 1000 mm ($20\,b_0$) between velocity profiles. In the vertical direction, up to 26 points were measured, equally spaced by 5 mm, and starting at between 10-15 mm from the flume bed until approximately 30 mm below the water surface, due to physical constraints of the ADV.
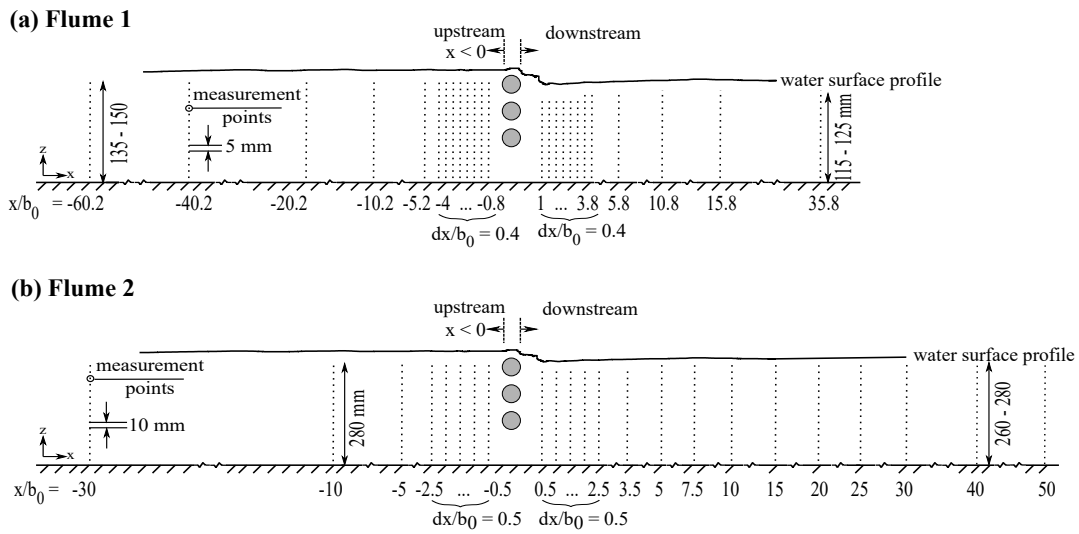


**Figure 2.6:** Schematic depicting the longitudinal ADV measurement locations along the main channel's centreline upstream and downstream of all leaky barriers for (a) Flume 1 and (b) Flume 2.

For the larger scale model (LB6; Figure 2.6 (b)), eight upstream profiles and 15 downstream profiles were measured starting at 20 mm above the flume bed until approximately 30 mm below the water surface with a vertical spatial resolution of 10 mm. Measurements started $30\,b_0$ upstream and finished $50\,b_0$ downstream of LB6, with velocity profiles equispaced by 50 mm ($0.5\,b_0$) between 0.5-2.5 $b_0$ upstream and downstream of the leaky barrier. With increasing distance away from the barrier, longitudinal spacing between velocity profiles increased to 100 mm ($1\,b_0$), 150 mm ($1.5\,b_0$), 250 mm

(2.5 $b_0$), 500 mm (5 $b_0$), 1000 mm (10 $b_0$) and 2000 mm (20 $b_0$). In addition, two velocity profiles were taken upstream ($x/b_0$=-10.4 and -1.4) and downstream ($x/b_0$=0.8 and 10.6) under near-bankfull discharge for LB1 and LB2. For the control treatment (i.e., no barrier), velocity measurements were conducted over a single vertical profile at $x/b_0$=0.8 for 80 % and 100 % bankfull discharge. Similarly, to the measurements under bankfull discharge, the velocity profiles consisted of 20-26 point measurements with a vertical resolution of 5 mm.

#### 2.2.3.2 Flow visualisation

The flow patterns and turbulence structure of the near wake field were visualized for each leaky barrier configuration. Fluorescent Fwt red and Flt yellow with green dye (Cole-Parmer Instrument Company Ltd) was injected along the centreline at the upstream edge of the barrier at multiple elevations. A GoPro Hero 5 underwater camera was positioned on the left-hand side of the main channel wall of Flume 1 looking towards the right-hand side of the flume and a Nikon D3300 camera was mounted outside on the glass flume sidewall of Flume 2.

### 2.2.4 Fish behaviour

All fish behaviour experiments were performed after the hydrodynamic measurements and extensive cleaning of the flume so it was free of ADV seeding material, and were approved by Cardiff University Animal Ethics Committee and conducted under Home Office License PPL 303424 following ARRIVE (**A**nimal **R**esearch: **R**eporting of **In Vivo E**xperiments) guidelines [111].

#### 2.2.4.1 Fish maintenance and holding facilities

Fish were maintained within a Recirculating Aquaculture System (RAS) at the Cardiff University Aquarium in 60-80 l tanks of 30-40 fish each. This system, enclosed within

a temperature-controlled room and maintained at 14±0.5 °C on a 12h:12h dark-light cycle (7 am - 7 pm), has integrated bag and drum filters (Pall Cooperation) alongside a plastic bio media in the sump tank and UV sterilization system. Water temperature and oxygen level are constantly monitored, and nitrite levels are tested weekly (Nutrafin). Every morning, fish were fed commercial trout pellets.

Prior to the experiments, fish were transported to a temporary holding tank, adjacent to the flume, and given at least one day recovery from the 20 min transport. This recirculating holding tank holds 500 l dechlorinated water (Seachem Prime Concentrated Conditioner, Tetra AquaSafe), constantly chilled to 14±1 °C (D-D The Aquarium Solution, DC 750) with an external filter (Aquamanta, EXF 600) and aerated by an external air pump (Tetratec Aps 400). Depending on the experiment and number of fish, fish were maintained either free-swimming within the tank, or in floating cages constructed from plastic mesh (hole size 5×5 mm) in small groups of 5-10, depending on number and size of fish tested.

All tanks were equipped with environmental enrichment to provide refugia (e.g. plant pots) to reduce stress, and care was taken to minimise stress caused by fish handling and transportation between facilities and tanks.

### 2.2.4.2 Experimental setup and procedure

The experimental test section used for the fish behaviour experiments is presented in Figure 2.7 and was 1.6 m long. The test section was bounded by plastic mesh with gap size 5×5 mm, spanning the full flume width, at approximately 0.7 m ($14\,b_0$) up- and downstream of the structure. The test section was divided into three spatial zones (indicated by the different colours in Figure 2.7): upstream (0.7 m; green area), downstream (0.7 m or 0.875 m for LB5; purple area) and barrier region ($L_s$; light blue area). Hence, when comparing control versus LB5 (short, porous design), the difference in area needs to be considered as LB5 only covers one eighth of the control "barrier" area. A GoPro Hero 5 underwater camera was positioned at the centre of the upstream end
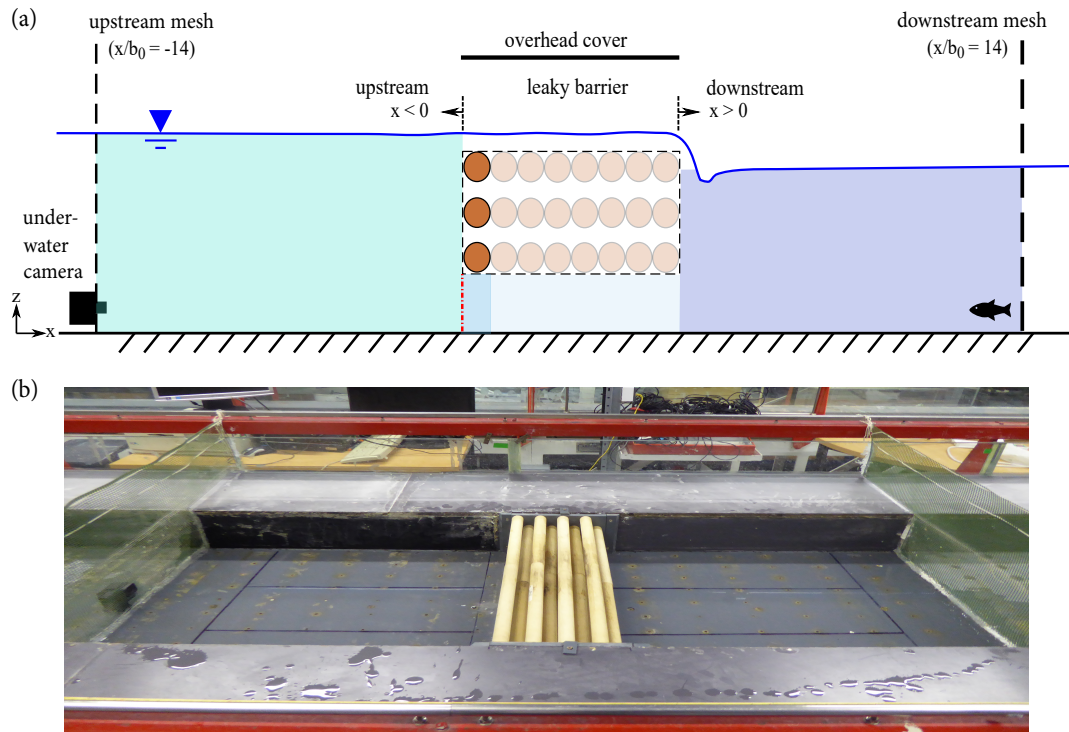
**Figure 2.7:** (a) Schematic and (b) photograph of the test section used for fish behaviour experiment. The test section was bounded by upstream and downstream mesh and divided into three regions, including upstream (green), beneath the leaky barrier (light blue) and downstream (purple). An underwater camera was positioned at the upstream end of the test section whilst fish were released at the downstream end. The red dotted line indicates the cut-off point for passes from the downstream and barrier region into the upstream region.

of the control section, immediately upstream of the mesh, pointing in the flow direction and was used to record fish spatial usage and passage behaviour. These recordings were used in addition to manual recordings using stop watches to ensure manually obtained results could be checked for accuracy. The water in the flume was dechlorinated (Seachem Prime Concentrated Conditioner) and chilled to 14 °C (D-D The Aquarium Solution, DC 2000).

On the test day, fish were individually introduced into the flume and given a 15 min acclimatisation period. Fish were released in the centre of the furthest downstream

section and allowed to explore the whole of the test section, experiencing a 2 min incremental increase in discharge over the first 10 min up to the test discharge level, followed by a 5 min acclimatisation at the test discharge. At all times, the downstream tailgate weir remained fixed at a pre-determined height set for the uniform flow condition. Each trial lasted 10 min in which individual fish were released at the most downstream end of the test section at the centreline of the main channel. Experiments were conducted under ambient light conditions comprising of LED lights mounted on the room ceiling and natural light supplied through the windows. During the tests, the following parameters were recorded and analysed for each barrier design:

(i) **Percentage of time spent** in each zone (upstream, barrier and downstream) with time starting as soon as fish entered one of the regions defined in Figure 2.7 (a);

(ii) **Number of upstream passes per fish** with passes defined as crossing from beneath the barrier region into the upstream region (cut-off point indicated by the red dotted line in Figure 2.7 (a)), representing the frequency of fish passing into the upstream region; and

(iii) **Percentage of upstream passing fish**, representing the number of fish passing from underneath the barrier into the upstream region

For simplification purposes, the number of upstream passes per fish and percentage of upstream passes per fish were summarised under the term "passage behaviour". All parameters were recorded using JWatcher v.1.0.

After completion of the test (10 min), fish were returned to the holding tank. After completion of the experiment fish were transported back to the RAS at the Cardiff University Aquarium.

### 2.2.4.3 Statistical data analysis

Following the conduction of the experiments, the recorded parameters were investigated for statistical significance using R v.3.6.3 statistical software. A range of general and generalised linear models (both known as GLM) was applied to investigate whether a dependent variable (e.g., recorded parameters) can be explained by one or more independent variable (e.g., treatments). General linear models assume a linear relationship between the dependent and independent variables and are the basis for a range of statistical tests such as the t-test, regression analysis and the analysis of variance (ANOVA) [179]. In contrast, generalised linear models are a generalisation of the general linear model, also allowing non-linear relationships between the dependent and independent variable [179].

In its simplest form, a GLM can be expressed in R as: model ⟵ glm(dependent variable ∼ independent variables, family, link), modelling mean and variance separately [179]. The family function represents the error distribution (i.e., scatter around the fitted relationship) and models the change in variance of the dependent variable. The choice of error distribution depends on the nature of the dependent variable, i.e., whether data are continuous or non-continuous [179]. General linear models are applied in the case of continuous data, modelling the errors as Gaussian (normal) distribution, while the error in generalised linear model is amended through other data distributions (e.g., Poisson, binominal) in the case of a non-continuous dependent variable [179]. The link function, in contrast, models the change in mean of the dependent variable. Amending the link function may help to establish a linear relationship between dependent and independent variables in the case of non-normal distributed data, with the default link function only being used for normal-distributed data. For each family, a range of link functions exists to transform the data, with an overview provided in Table 2.2 [179].

The choice of model family and link function strongly impacts how well the model represents the data. Model fit was assessed by checking whether (1) the residuals (i.e.,

scatter of data around modelled relationship) are normally distributed; (2) the variance of the residuals is homogenous (i.e., residuals should be uniformly distributed across the fitted values of the dependent variable); and (3) the model is not biased by unduly influential observations (i.e., observations which have a large influence on the model parameter estimates). Additional model evaluation criteria are provided for error families for discrete dependent variables (e.g., poisson GLMs) [179]. For these model families, model fit, for instance, was also assessed by checking for overdispersion (i.e., variance exceeds expectations for standardised poisson and binominal error distribution). Here, overdispersion was likely caused by zero-inflation (i.e., too many zeros included in the data) [179]. Large over-dispersion statistics (i.e., $> 2$), may be prevented by changing from a passion to a quasi-poisson, negative binominal or zero-inflated model error family [179]. A range of family-link function combinations was tested and assessed based on these criteria.

During the test of the different models, the p-value was noted as a measure of the estim-

**Table 2.2:** Overview of families and link functions for general and generalised linear models available in R. Table extracted from [179].

| Error families | Link functions |
|---|---|
| **Continuous dependent variable** | |
| Gaussian | *identity*, log, sqrt, inverse |
| inverse Gaussian | $1/mu^2$, inverse, identity, log |
| gamma | identity, log, sqrt, *inverse* |
| beta | *logit*, probit, cloglog, cauchit, log, loglog |
| **Discrete dependent variable** | |
| Poisson | *log*, identity, sqrt |
| quasipoisson | *log*, identity, logit, probit, cloglog |
| negative binominal | *log*, identity, sqrt |
| binominal | *logit*, probit, cauchit, log, cloglog |
| quasibinominal | *logit*, identity, probit, log, cloglog |

ated probability that the null-hypothesis is true (i.e., there is no association between the dependent and independent variables). P-value significance was taken at 0.05 [179]. Hence, a p-value $< 0.05$ indicates a high probability of a significant statistical pattern (i.e., $< 5\%$ probability that the null-hypothesis is true) while a p-value $> 0.05$ indicates the absence of a significant statistical pattern (i.e., $> 5\%$ probability that the null-hypothesis is true). As multiple independent variables may be included in a single model, non-significant variables were stepwise removed from the statistical analysis of the model.

For each experiment, the model best fitting the data, including error family and link function, is reported (Section 2.2.4.4.1 and 2.2.4.4.2) and final p-value highlighting statistical significance is presented in the results section (Section 2.3.2).

### 2.2.4.4 Experimental studies

In total, two fish behaviour experiments were conducted using juvenile Atlantic Salmon (*Salmo salar*, Linnaeus 1758; Section 2.2.4.4.1) and rainbow trout (*Oncorhynchus mykiss*, Walbaum 1792; Section 2.2.4.4.2). These studies investigated the impact of physical leaky barrier design on fish movement under near-bankfull and bankfull flow conditions using scaled, laboratory flume experiments.

### 2.2.4.4.1 Experiment (a): Impact of porosity and flow condition on juvenile Atlantic salmon movement

In this study, the effect of an idealised porous (LB2, Figure 2.4 (a-2)) and non-porous (LB1, Figure 2.4 (a-1, top)) leaky barrier model structures was investigated under two flow conditions, representing bankfull ($100\% \ Q_{bf}$) and near bankfull flow ($80\% \ Q_{bf}$), on free fish movement.

Fish passage behaviour tests were conducted between 21 January and 1 February 2019 between 7.30 am and 10 pm. Juvenile Atlantic salmon (mean $\pm$ s.d. mass, 12.3$\pm$5.4 g

and mean $\pm$ s.d. standard length ($L_{fish}$ (i.e., length from tip of mouth to end of the ver-
tebral column), 93.3$\pm$13.6 mm), sourced from Kielder Salmon Centre were maintained
within the Cardiff University Aquarium at 14$\pm$1 °C (Section 2.2.4.1). Atlantic salmon
is a target species of conservational concern due to the dramatic decline in Atlantic
salmon stocks [95] caused, among other things, by the construction of in-stream struc-
tures. Therefore, this species was chosen to better understand their spatial and passage
behaviour response to this emerging in-stream barrier to prevent leaky barrier from
being a physical, flow, or behavioural barrier to their movement. In general, Atlantic
salmon are anadromous, they hatch in rivers and streams, migrate to the sea to mature,
and then migrate back to their birthplace to spawn. Growing up in fast-flowing, clean,
and well-oxygenated freshwater, these fish demonstrate positive rheotaxis, orientating
themselves against the flow direction (Kalleberg (1958) in [220]). It should be noted
that at the time of the experiment, fish were at their parr-early smolt stage, which do not
show migratory behaviour. This study focuses on the free movement of these fish in
the vicinity of a porous and non-porous structure. Swimming tests, conducted by Pal-
stra et al. (2020), with juveniles (mean $\pm$ s.d. mass, 29.9$\pm$0.9 g and standard length,
123$\pm$16 mm) of similar length scale to our model fish, determined a critical swimming
speed at 0.959$\pm$0.103 m/s; however, it should be noted that swimming performance is
strongly dependent upon fish size [166].

Using the experimental setup and following the experimental procedure as explained
in Section 2.2.4.2, $N_{tested}$=16 fish were tested for the porous leaky barrier (LB2) under
80 % bankfull discharge while $N_{tested}$=14 fish were tested for all other treatments (con-
trol (C) and non-porous leaky barrier (LB1) for 80 % bankfull discharge, and control
(C), porous (LB2), non-porous leaky barrier (LB1) for 100 % bankfull discharge).

Treatment order could not be randomised in this study because of the construction
method of the installed barriers (barriers were glued into the compound channel us-
ing silicon adhesive). The porous structure was tested first, followed by non-porous
structure and control condition. For each treatment, 80 % bankfull discharge was

tested prior to 100 % bankfull flow condition. Human intervention took place only in cases where fish remained stationary in the furthest downstream transect and refused to swim. In this case, fish were gently nudged with the handle of the net, and in the 35 cases this occurred this stimulus worked for 26 of the fish. The nine non-responding fish were excluded from the analysis (included in analyses: $N_{analysed}$=10 for control 80 % $Q_{bf}$, $N_{analysed}$=12 for control 100 % $Q_{bf}$, $N_{analysed}$=13 for porous 80 % $Q_{bf}$, otherwise $N_{analysed}$=14). During each test, time spent in each zone (upstream, downstream or underneath barrier) and number of upstream passes as a measure of movement activity was recorded manually using stopwatches and the underwater camera (Section 2.2.4.2).

Spatial preference was analysed for statistical significance using a separate General Linear Model (GLM) with Gaussian distribution and identity link for each spatial zone, to investigate the difference in mean between time spent upstream, downstream, and underneath the structure (time proportion as dependent variable) and barrier treatment as well as flow condition (independent variables). Association between number of upstream passes per fish (dependent variable) and leaky barrier, as well as flow condition (independent variable), were tested using a GLM with Poisson distribution and identity as link function. A binomial GLM with logit link function was conducted to analyse potential associations between flow condition, as well as barrier and upstream passed fish and flood plain usage, which are reported as categorical variables (passed/not passed or used/not used).

### 2.2.4.4.2 Experiment (b): Impact of physical leaky barrier design on fish movement

In this study, the effect of four conceptual physical engineered leaky barrier model designs (LB1-3, LB5; Figure 2.4 (a-1, a-2, a-3, 5)) varying in porosity, longitudinal length and colour (orange versus natural; Figure 2.4 (a-1; top versus bottom)) on juvenile rainbow trout (*Oncorhynchus mykiss*) movement was investigated, including

spatial usage and upstream passage.

Fish passage behaviour tests were conducted using juvenile rainbow trout as model species, sourced from the Bibury Trout Farm. Rainbow trout, belonging to the salmonid family, are native to the Pacific Ocean in North America and Asia. However, rainbow trout have spread worldwide [51] as a result of stocking for angling purposes and farm escapees and although, non-native to the UK, can now be found in many UK rivers [66]. INNS, such as rainbow trout, may threaten native species and their diversity by competing for food sources, introducing new diseases, foraging with native species leading to hybridisation, or acting as a predator to native species. Therefore, understanding their swimming behaviour and passage responses to anthropogenic structures may support the identification of methods to limit or prevent their spread, contributing to the conservation of native species.

In total, three types of experiments were conducted, each with separate batches of fish ($N_{tested}$=136). Details in terms of the fish batch and experimental type (i), (ii) and (iii) are given below:

**(i) Leaky barrier length and porosity experiment:**

Fish response to four leaky barrier designs (LB1-3,5) were conducted under the bankfull flow condition between 21 March and 3 April 2019 between 7 am and 8 pm. Prior to the experiment, $N_{tested}$=30 rainbow trout (mean $\pm$ s.d. mass, 15.$\pm$11.1 g and mean $\pm$ s.d. standard length, 91.0$\pm$21.3 mm) were anaesthetised using 0.02 % MS-222 and tagged with 7.5 mm PIT-tags (ISO 11784 certified, Loligo Systems, Denmark), followed by covering the injection site with protective powder (Oraheasive powder) and allowing at least three weeks for recovery. Each fish was individually tested for each leaky barrier design and control treatment, i.e. without leaky barrier, in a random treatment order, with one day rest in between trials. PIT-tags were used to identify individuals to ensure each fish completed all treatments. These 7.5 mm tags were inserted into the lateral flanks with the fish under anaesthesia one to two weeks before the start of trials and were read using a handheld PIT-tag reader (Agrident, APR500

E).

**(ii) Cover experiment:**

Fish response to overhead cover was examined using $N_{tested}$=20 rainbow trout (mean $\pm$ s.d. mass, 11.5$\pm$3.8 g and mean $\pm$ s.d. standard length, 85.5$\pm$9.2 mm). Overhead cover was provided by a board of 0.01 m thickness and longitudinal length of 0.2 m, spanning the full width of the flume, and positioned at a vertical distance of 0.32 m above the flume bed and 5 m downstream of the flume inlet, matching the longitudinal leaky barrier position as indicated in Figure 2.7; no barrier was placed within the test section during these trials. The overhead cover presence was compared against the flume without an overhead cover to investigate fish preference for cover provided by different barrier designs. Similar to experiment (i), fish were anaesthetised and PIT-tagged prior to the experiment to allow identification of individuals. To ensure treatment randomization, 10 fish were tested first with overhead cover, while the remaining 10 fish were tested without overhead cover first. Subsequently, treatment order was reversed; hence, the fish tested without overhead cover were then tested with cover whilst fish first tested with cover were tested without. The trial took place on 29 March and 1 April 2019 between 9 am and 7.30 pm, allowing two days recovery between tests.

**(iii) Colour experiment:**

Fish response to the non-porous barrier (LB1) colour was tested between 12 March and 18 March 2020 between 7 am and 7.30 pm. Two barrier colours, including an orange non-transparent barrier (LB1-orange) and barrier with colourless and transparent wrapping (LB1-natural) mimicking a more natural non-porous design, were examined using $N_{tested}$=86 rainbow trout (mean $\pm$ s.d. standard length, 123.2$\pm$14.5 mm). It should be noted that fish used in this experiment were significantly larger compared those employed in experiments (i) and (ii) (GLM, $p$<0.0010) as this experiment was conducted at a later stage. Therefore, fish behaviour for the control case (without a leaky barrier) was monitored again to ensure there were no significant changes in behaviour between the fish used in this experiment and the control case in experiment (i). No significant

differences were found regarding spatial preference (GLM, $p$>0.0010) and percentage of upstream passing fish (GLM, $p$=0.3792) but number of upstream passes per fish was significantly lower in experiment (iii) (GLM, $p$<0.0010). Each fish was tested individually and only once. Fish remaining stationary at the furthest downstream end of the test section or impinging the downstream mesh were excluded from the analysis, resulting in the following numbers of tested individuals per treatment: $N_{analysed}$=32, 30 and 24 for LB1-natural (three fish excluded from analysis), LB1-orange and control (two fish excluded from analysis), respectively.

For all three experiments, spatial preference (upstream, downstream, beneath the barrier), percentage of upstream passing fish and number of upstream passes were analysed as key parameters for statistical significance. Passage behaviour was used to quantify fish swimming activity and interaction between the different velocity regions. Spatial preference was analysed using separate GLMs with Gaussian distribution and identity link for each of the spatial regions (upstream, barrier, and downstream), which allowed investigation of the differences in mean time proportion and leaky barriers as well as fish length. Differences in means between percentage of upstream passing fish and fish length as well as leaky barrier design were tested using a binomial GLM with logit link function. A negative binomial GLM with squared (experiments (i) and (ii)) and a quasi-Poisson GLM with identity (experiment (iii)) link function was conducted using the R library MASS to analyse potential differences in means between the number of upstream passes per fish, fish length, time upstream and leaky barrier design. Similar statistical tests were used to compare spatial preference and percentage of upstream passing fish between the control groups in experiments (i) and (iii) but using a negative binominal GLM with identity link to compare number of upstream passes per fish. Differences in fish length amongst the different experiment and test groups were analysed using a Gaussian GLM with link function identity. Treatment randomisation was taken into account for experiments (i) and (ii) by assigning an individual treatment order to each fish. Learning-based effects were assessed by analysing the percentage of upstream passing fish per test day using a binominal GLM with logit link function

in case of experiment (i).

## 2.3 Results

### 2.3.1 Hydrodynamics

Upstream and downstream channel hydrodynamics were measured under bankfull discharge along the main channel centreline for LB1-6 using ADV. In this results section, uniform flow conditions under 80 % and 100 % bankfull discharge (Section 2.3.1.1) as well as upstream and downstream hydrodynamics under bankfull flow condition (Section 2.3.1.2 and 2.3.1.3) are presented. In addition, Section 2.3.1.4 compares the 80 % and 100 % bankfull flow conditions.

#### 2.3.1.1 Uniform flow conditions

Normalised time-averaged longitudinal velocity ($\overline{u}/U_0$) results for the main channel hydrodynamics measured for the control situation, i.e. without leaky barrier present, at $x/b_0$=0.8 (Figure 2.6) are presented in Figure 2.8. The measured velocity profiles for the control scenario represent typical open-channel flow conditions following a logarithmic distribution. Slightly higher normalised mean longitudinal velocities were found for 80 % bankfull discharge, indicating higher distribution of momentum in the centre of the channel. This is caused by sidewall effects and the associated hydrodynamics redistributing momentum towards the channel centre under the 80 % bankfull discharge.

#### 2.3.1.2 Upstream hydrodynamics

Leaky barrier presence caused a change in water surface profile and increase in water depth, or backwater rise ($\Delta H$), upstream of the structure, which was highest for LB1
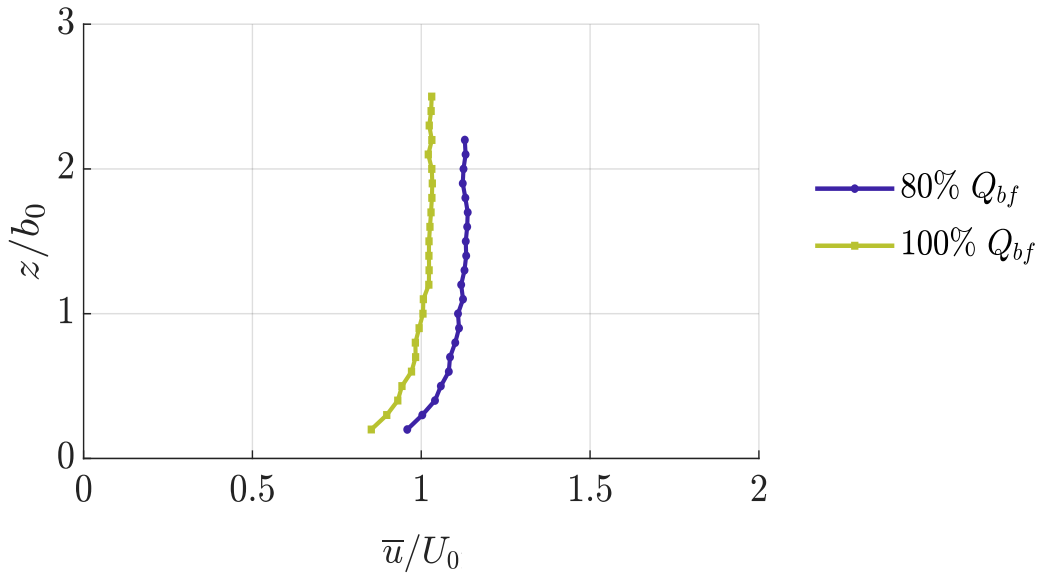
**Figure 2.8:** Mean longitudinal velocity profiles normalised by bulk velocity ($\overline{u}/U_0$) obtained under 80 % (blue) and 100 % (green) bankfull flow condition for the control case, i.e. no barrier present.

and LB4, i.e. proportional to the leaky barrier's void ratio ($\Phi$) as shown in Table 2.1. Upstream flow depth increased with proximity to the leaky barrier and caused the flow to spill onto the floodplains, with larger floodplain inundation observed for leaky barriers with higher cross-sectional blockage, i.e. at $x/H_s$=-0.4 the free surface elevation difference between the upstream value and that along the main channel ($H_1 - H_{mc}$) for each leaky barrier design is 23.0 mm (LB1), 10.0 mm (LB2), 11.5 mm (LB3), 11.5 mm (LB4), and 8 mm (LB5). Hence, floodplain inundation for the non-porous design (LB1) was approximately 2-2.3 times greater compared the long, porous logjams (LB3-4). Despite the decrease in logjam length in the case of LB5, floodplain inundation was only 20 % lower compared to its long counterpart (LB2).

To characterise the upstream flow, mean streamwise velocity profiles ($\overline{u}$) normalised by the bulk velocity $U_0$ (Table 2.1) are presented in Figure 2.9 (a-f) for all leaky barrier structures (LB1-6), respectively. Flow diversion towards the gap underneath the struc-

ture ($0 \leq z/b_0 \leq 1$) occurred with increasing proximity to all leaky barriers, showing an increase in mean streamwise velocities at heights coinciding with the location of the barriers' lower gap ($z/b_0 < 1$). At the height of the lowest dowel ($z/b_0 \approx 1$-1.5) an inflection point was observed, followed by a decrease in $\overline{u}/U_0$ with increasing proximity to the water surface. For all leaky barriers, onset of significant longitudinal flow diversion ($\max(\overline{u}/\langle \overline{u} \rangle) > 10\%$) occurred at approx. $-x/H_s > 0.6$ ($x/b_0 \approx$-1.2), with the largest velocity value obtained for those leaky barriers with largest blockage, i.e. lowest void ratio, LB1 and LB4. Furthermore, the profile just upstream of the LB1 indicates there is a notable velocity reduction before impinging the structure as this design is non-porous and, unlike the other designs, flow cannot penetrate through it.

Profiles of normalised vertical velocities ($\overline{w}/U_0$) upstream of the barriers are presented in Figure 2.10 (a-f) for all leaky barriers, showing a vertical acceleration of the flow when approaching the barrier, with maximum $\overline{w}/U_0$ observed near the height of the lowest dowel ($0.9 \leq z/b_0 \leq 1.5$). Largest $\overline{w}/U_0$ were obtained for the non-porous barrier LB1 ($\overline{w}/U_0$=-0.63), while values of $\overline{w}/U_0$ were 35.5%, 95.1%, 97.6%, 89.4% and 93.7% lower all porous logjams LB2-6, respectively.
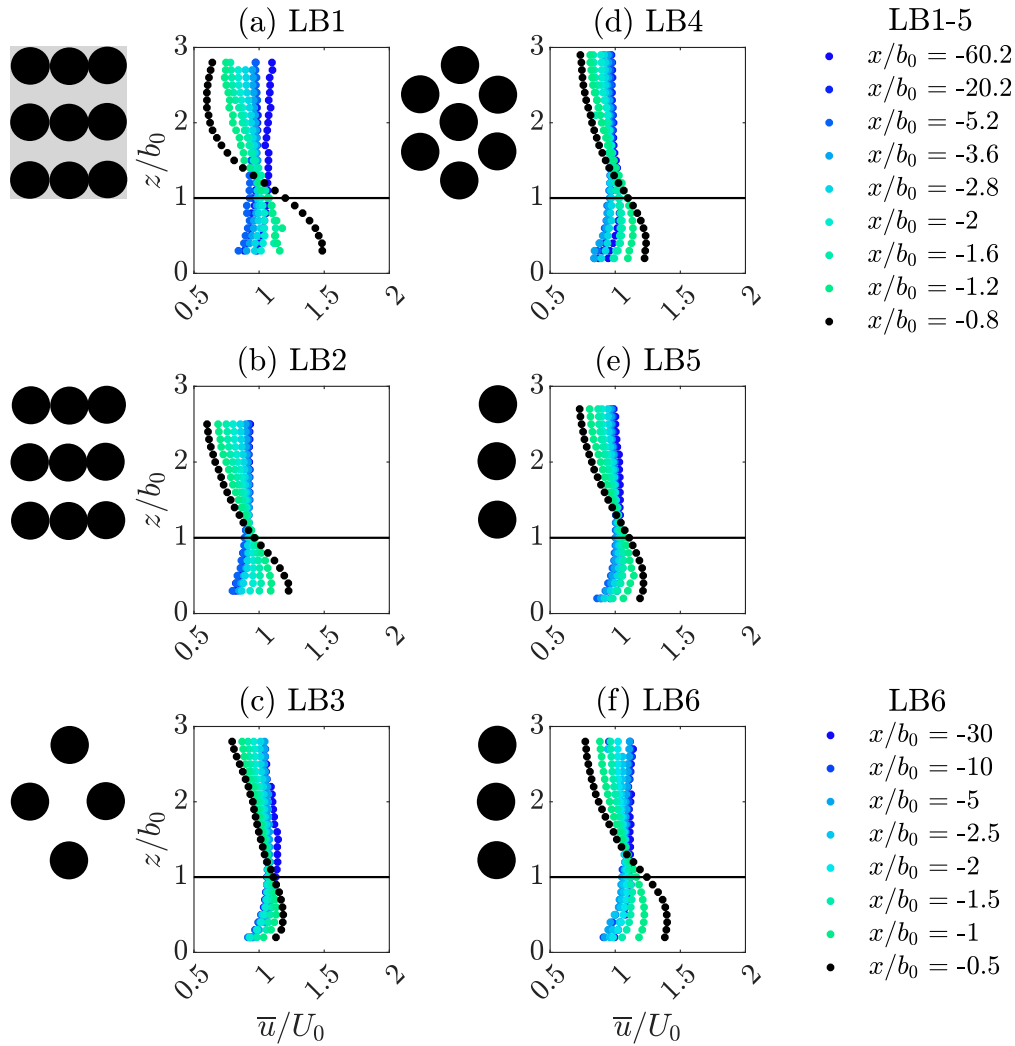
**Figure 2.9:** Progression of upstream mean streamwise velocity profiles ($\overline{u}$) normalised by the bulk velocity ($U_0$), depicting selected profiles measured between the furthest upstream profile (LB1-5: $x/H_s$=-30.1; LB6: $x/H_s$=-15) and the profile measured closed to the leaky barrier's upstream edge (LB1-5: $x/H_s$=-0.4; LB6: $x/H_s$=-0.25). Longitudinal velocity profile location ($x$) was normalised by the barrier height ($H_s$) of 100 mm for LB1-5 and 200 mm for LB6. Only the half of the leaky barrier structures LB1 to LB4 are shown on the left-hand side of the contour plot to indicate their vertical location. An increase in streamwise velocity was observed below the structure bottom edge ($z/b_0$=1, black horizontal line) due to flow diversion underneath structures. Vertical extent of recorded velocity profiles may vary due to longitudinal change in upstream flow depth.
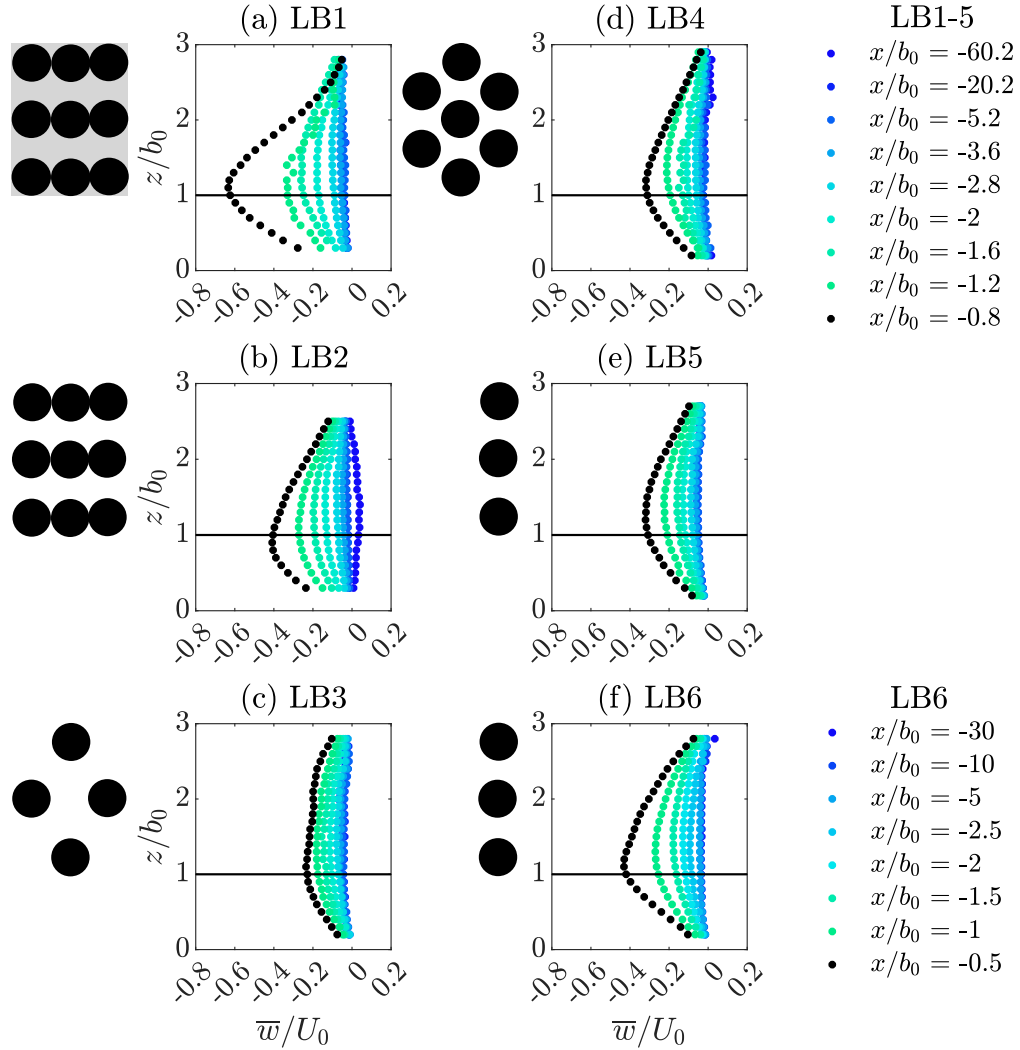
**Figure 2.10:** Progression of upstream mean vertical velocity profiles ($\overline{w}$) normalised by the bulk velocity ($U_0$), depicting selected profiles measured between the furthest upstream profile (LB1-5: $x/H_s$=-30.1; LB6: $x/H_s$=-15) and the profile measured closest to the barriers' upstream edge (LB1-5: $x/H_s$=-0.4; LB6: $x/H_s$=-0.25). Longitudinal velocity profile location ($x$) was normalised by the barrier height ($H_s$) of 100 mm for LB1-5 and 200 mm for LB6. Only the half of the leaky barrier structures LB1 to LB4 are shown on the left-hand side of the contour plot to indicate their vertical location. An increase in vertical velocity was observed at height of the lowest barrier edge ($z/b_0$=1, black horizontal line) due to flow diversion underneath structures. Vertical extent of recorded velocity profiles may vary due to longitudinal change in upstream flow depth.

### 2.3.1.3   Downstream hydrodynamics

To observe the instantaneous flow field immediately downstream of all leaky barriers, flow visualisation was used, with rhodamine dye injected at the barrier's upper edge midway through the barrier's longitudinal extent. Differences in near wake characteristics are shown in Figure 2.11 for the non-porous leaky barrier LB1 (a) and four porous barriers LB2 (b), LB3 (c), LB4 (d) and LB5 (e). The downstream wake of all barriers was characterised by the formation of a fast jet exiting the main gap between the bed ($z$=0) and structure lower edge ($z/b_0$=1), and a structure-dependent upper wake region ($z/b_0$>1). The interface between the primary jet and upper wake regions is shown by Figure 2.11 (a-c).
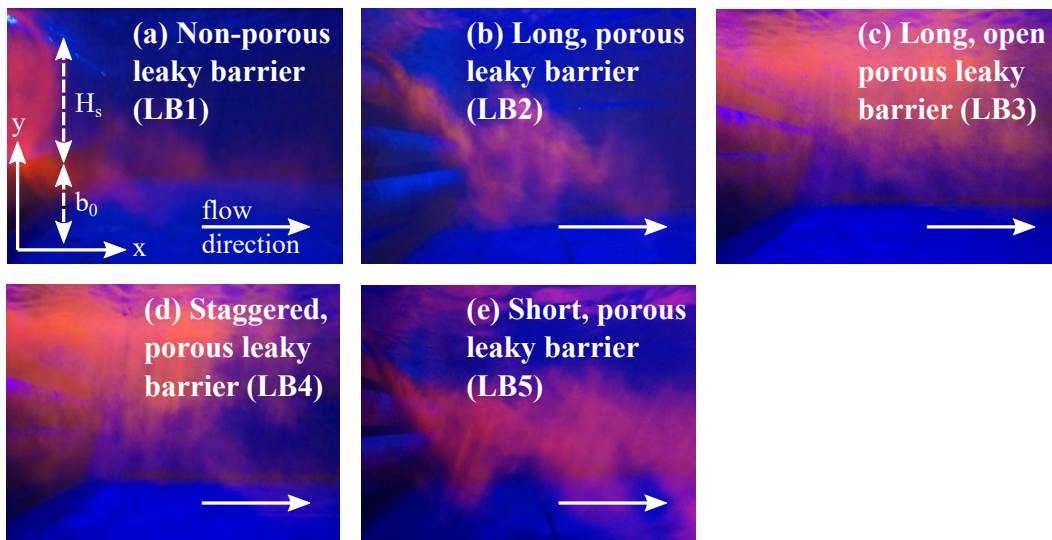


**Figure 2.11:** Pathways of water exiting the upper part of the leaky barrier shown with rhodamine dye injected upstream at the upper edge of non-porous (LB1, (a)), three long, porous (LB2, (b); LB3, (c); LB4, (d)) and one short, porous (LB5, (e)) leaky barriers. Strong plunging overtopping flow was observed for LB1; flow exiting the porous structures show the influence of flow progressing through the structure and dowel-scale turbulent mixing (LB2 and LB5, similar for LB6). The downstream edge of all leaky barriers is located at the left-hand side of the pictures and flow is from left to right.

In the case of the non-porous leaky barrier (LB1), the large cross-sectional blockage resulted in an increased upstream flow depth and water progressing over the upper surface of the leaky barrier (Figure 2.11 (a)). Upon exiting the structure, this over-flow stream plunged downwards along the barrier trailing edge until encountering the primary jet, shown by a pronounced line between lower and upper wake (Figure 2.11 (a)). In contrast, all porous barriers (LB2-6) were characterised by a lower cross-sectional blockage area due to the provision of inter-dowel gaps (Table 2.1). This resulted in reduced backwater rise and flow exiting the barrier over the upper wake vertical extent ($z/b_0 \geq 1$), strongly impacting the wake structure within the upper region. All porous leaky barriers lacked strong plunging overflow (Figure 2.11 (b-c)). The flow exiting above barriers with distinct flow through paths (LB2, LB5-6) was carried in the downstream and downward direction by flow exiting the structures as shown in the case of LB2 (Figure 2.11 (b)). On the other hand, flow exiting above the staggered (LB4) and the open, porous barrier (LB3) was predominantly transported in downstream direction and only slowly mixed with the flow through the structure, which progressed slower in downstream direction due to dowel mixing as shown in the case of LB4 (Figure 2.11 (c)).

#### 2.3.1.3.1 Near wake region

**First and second order statistics**

The implications of physical leaky barrier design on the lower ($z/b_0 < 1$) and upper ($z/b_0 > 1$) wake regions, as observed in Figure 2.11, are presented in greater detail in Figures 2.12 and 2.13, showing contours of normalised mean streamwise ($\overline{u}/U_0$) and vertical ($\overline{w}/U_0$) velocities, turbulent kinetic energy ($tke/U_0^2$) and vertical Reynolds shear stress ($\overline{u'w'}/U_0^2$), respectively.

The lower wake of all leaky barriers is characterised by the formation of a primary jet exiting the region underneath the structure ($z/b_0 \leq 1$), consisting of high stream-wise velocities, which dominated over the vertical velocity components, with values

for $\langle \overline{u} \rangle / U_0$ being 79.9 %, 104.4 %, 102.9 %, 101.1 %, 105.2 % and 102.5 % for higher compared to $\langle \overline{w} \rangle / U_0$ for LB1-6, respectively (i.e. $u \gg w$, $x/b_0$=1, Figure 2.12 (a, c, e, g, i, k)). This high momentum flow extends between the flume bed and lower barrier edge, and the magnitude of diverted flow varied with structure physical characteristics. Immediately downstream of the leaky barrier ($x/b_0$=1), the highest $\overline{u}/U_0$ was found for the non-porous barrier LB1, while maximum velocity magnitude were 35.4 %, 25.1 %, 18.3 % and 34.4 % lower for the porous leaky barriers LB2-5, respectively [($z/b_0((\overline{u}/U_0)_{max})$, $(\overline{u}/U_0)_{max}$); LB1: (0.3, 3.11); LB2: (0.2, 2.01); LB3: (0.2, 2.33); LB4: (0.3, 2.54); LB5: (0.4, 2.04); LB6: (0.8, 2.30)]. Scaling the short, porous jam (LB5) resulted in a 11.3 % higher maximum velocity magnitude for LB6. Streamwise velocities decreased vertically, with minimum $\overline{u}/U_0$ found at the highest measurement point, shown by the blue-green contours in Figure 2.12 (a, c, e, g, i, k).

Immediately downstream of all porous barriers (LB2-4) at $x/b_0$=1, the value of $d\overline{u}/dz$ at the vertical location of the shear layer ($z/b_0 \approx 1$; Figure 2.13 (d, f, h)) was -0.01, -0.01 and -0.02 for LB2-4, respectively (Figure 2.12 (c, e, g)). The strength of shear at this vertical elevation is reflected in the mixing between the slower flow exiting the barrier upper wake region and flow exiting the lower gap ($b_0$) for barriers LB2-4, shown by the vertical location of peak magnitude of $tke/U_0^2$ [Figure 2.13 (c, e, g); ($z/b_0((tke/U_0^2)_{max})$, $(tke/U_0^2)_{max}$); LB2: (0.8, 0.26); LB3: (0.9, 0.19); LB4: (0.9, 0.18)], $\overline{u'w'}/U_0^2$ [Figure 2.11 (d, f, h); ($z/b_0((\overline{u'w'}/U_0^2)_{max})$, $(\overline{u'w'}/U_0^2)_{max}$); LB2: (0.8, 0.10); LB3: (0.9, 0.06); LB4: (0.9, 0.06)] and a change in sign of $\overline{w}/U_0$ (Figure 2.12 (d, f, h)) immediately downstream of the barrier ($x/b_0$=1). The upper wake region of these leaky barriers (LB2-4) was characterised by low values of $\overline{u}/U_0$ and $tke/U_0^2$ as indicated by the blue contour colours.

The upper wake region of the short porous barriers (LB5-6) was characterised by the presence and decay of the secondary jets and the flow diversion between individual dowels, which is shown by the large values of $\overline{u}/U_0$ [Figure 2.12 (i, k); ($z/b_0((\overline{u}/U_0)_{max})$, $(\overline{u}/U_0)_{max}$); LB5: (1.7, 1.38); LB6: (1.6, 2.24)], $tke/U_0^2$ [Figure
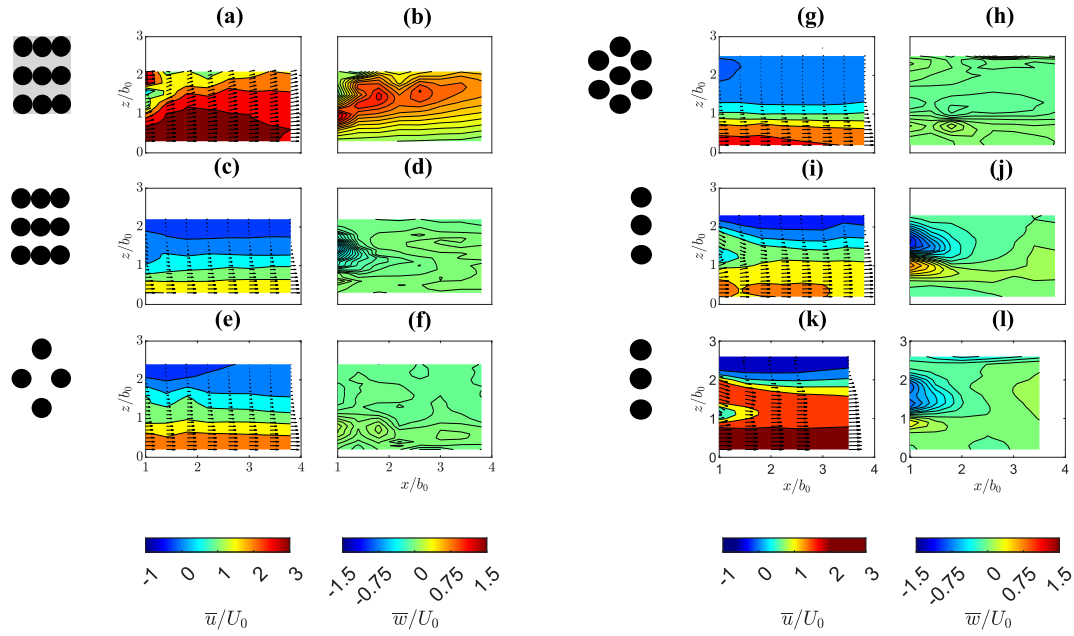
**Figure 2.12:** Contours of mean streamwise ($\overline{u}/U_0$) and vertical ($\overline{w}/U_0$) velocity normalised by bulk velocity $U_0$ along the main channel centreline (x-z plane) downstream of all barriers; LB1 [a, b], LB2 [c, d], LB3 [e, f], LB4 [g, h], LB5 [i, j] and LB6 [k, l]. Only the half of the leaky barrier structures LB1 to LB4 are shown on the left-hand side of the contour plot to indicate their vertical location.

2.13 (i, k); $(z/b_0((tke/U_0^2)_{max}), (tke/U_0^2)_{max})$; LB5: (1.3, 0.54), LB6: (1.5, 0.40)], and $\overline{u'w'}/U_0^2$ [Figure 2.12 (j, l); $(z/b_0((\overline{u'w'}/U_0^2)_{max}), (\overline{u'w'}/U_0^2)_{max})$; LB5: (1.4, -0.2), LB6: (1.5, -0.21)] at height of the lowest inter-dowel gap (1.5$\leq$ $z/b_0$ $\leq$1.75) at $x/b_0$=1; similar to flow around a cylinder [241, 161]. In comparison to LB5, values of $\overline{u}/U_0$ were 1.6 times higher while maximum $tke/U_0^2$ was 0.74 times lower for the scaled leaky barrier LB6 at height of the lowest inter-dowel gap. A less distinct secondary jet of lower $\overline{u}/U_0$ was observed for LB2 following the lowest dowel gap [$x/b_0$=1; $z/b_0$=1.5; $\overline{u}/U_0$=0.5] associated with the increase in streamwise structure length ($L_{s,LB5}$=1/8 $L_{s,LB2}$).

In case of the non-porous leaky barrier (LB1), the rapid vertical expansion of the lower jet into the upper wake region ($z/b_0$>1; $\overline{w}/U_0$ $\gg$0, Figure 2.12 (b)) was associated with
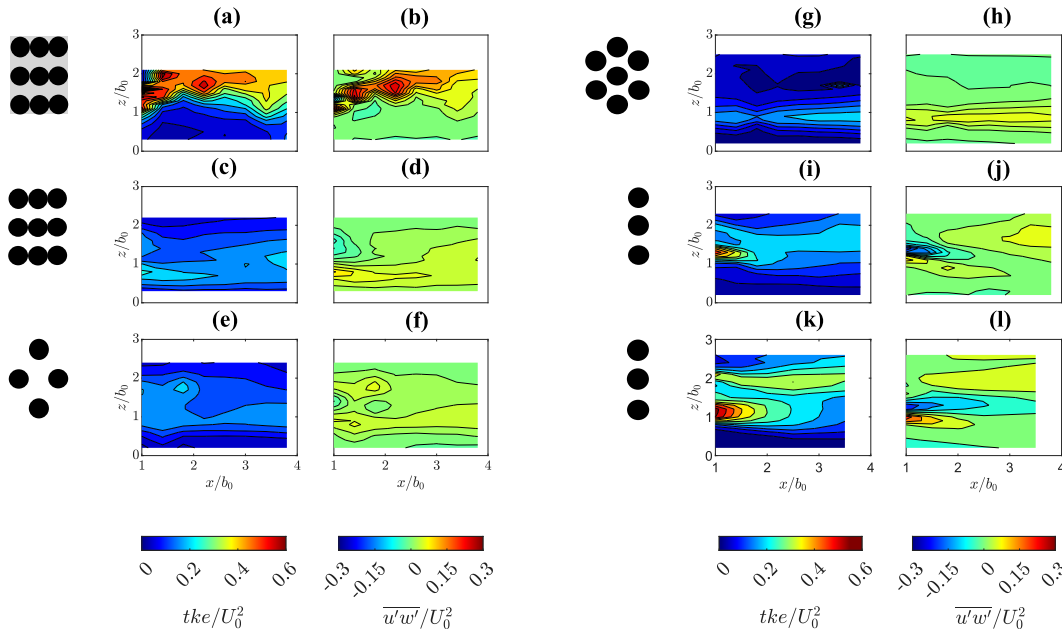
**Figure 2.13:** Contours showing turbulent kinetic energy ($tke/U_0$) and vertical Reynolds shear stress ($\overline{u'w'}/U_0^2$) normalised by bulk velocity squared $U_0^2$ along the main channel centreline (x-z plane) downstream of all leaky barriers; LB1 [a, b], LB2 [c, d], LB3 [e, f], LB4 [g, h], LB5 [i, j] and LB6 [k, l]. Only the half of the leaky barrier structures LB1 to LB4 are shown on the left hand side of the contour plot to indicate their vertical location.

a larger gradient of velocities in the vertical direction that triggered shear stresses in the near wake. This region started at height of the lowest barrier edge ($z/b_0 \approx 1$), showing highest values in $\overline{u'w'}/U_0^2$ and $tke/U_0^2$ ($x/b_0$=1; $z/b_0$=1.1, $(\overline{u'w'}/U_0^2)_{max}$=0.28; $z/b_0$=1.4, $(tke/U_0^2)_{max}$=0.61; Figure 2.13 (a-b)) and progressed upward with increasing streamwise distance from the leaky barrier.

**Quadrant analysis**

To investigate the impact of physical leaky barrier design on turbulence in the near-wake region, quadrant analysis was used to examine the relationship between the temporal fluctuations of streamwise and vertical velocity components, their distribution between the four quadrants and contribution to the vertical Reynolds shear stress, $\hat{S}_Q$

[182]. Quadrant 1 ($Q_1$) represents $u'$>0 and $w'$>0 (inward interaction), quadrant 2 ($Q_2$) corresponds to $u'$<0 and $w'$>0 (ejection-like events), quadrant 3 ($Q_3$) represents $u'$<0 and $w'$<0 (outward interaction), and quadrant 4 ($Q_4$) with $u'$>0 and $w'$<0 (sweep-like events) ($\sum_1^4 \hat{S}_{Qi} = \overline{u'w'}$). Stress contributions $\hat{S}_Q$ from each quadrant were calculated using the methodology presented in Raupach (1981) [182] and are shown in Figure 2.14 for $x/b_0$=1 downstream of all leaky barrier designs.

In the vicinity of the lower edge ($z/b_0 \approx$1), the peak magnitude and fractional contribution of $Q_1$ and $Q_3$ to the shear stress was more pronounced for the non-porous barrier (LB1) and short porous barriers LB5 and LB6. For these leaky barrier designs, the maximum contribution of turbulent events corresponding to $Q_1$ and $Q_3$ to the total sum of all four quadrants was between 86-89 % [($z/b_0, (\hat{S}_{Q_1} + \hat{S}_{Q_3})/ \sum_1^4 abs(\hat{S}_{Qi})$)); LB1, (1.1, 89 %); LB5, $Q_{1/3}$: (1.1, 86 %); LB6: (0.9, 89 %)]. Peak magnitude of such events was slightly less pronounced for the long porous barriers (LB2-4) due to reduced flow diversion underneath the structure and flow adjustment over the barrier length whereby phenomena from $Q_1$ and $Q_3$ contributed to more than 79-84% of the turbulent events [($z/b_0, (\hat{S}_{Q_1} + \hat{S}_{Q_3})/ \sum_1^4 abs(\hat{S}_{Qi})$)); LB2, (0.8, 84 %); LB3, (0.9, 79 %); LB4, (0.8, 81 %)].

Above the structure lower edge ($z/b_0$>1), the nature of the events contributing to the vertical Reynolds shear stress was strongly impacted by physical barrier characteristics and in some cases flow over the structure. In case of the staggered long porous leaky barrier LB4, the absence of direct flow paths within the structure prevented the generation of secondary jets and regions of shear stress within the upper wake region, also shown by consistently low values in mean streamwise velocity (Figure 2.12 (g)), and turbulence quantities (Figure 2.13 (g) and (h)). Therefore, turbulent momentum transport, in this case, is solely associated with the expansion of the primary jet into the upper region. In contrast, leaky barriers with distinct flow paths allowing flow through the structure (i.e., LB2-3, LB5-6) featured peaks in the contribution of events from $Q_2$ and $Q_4$ caused by ejections and sweeps that increased Reynolds shear stresses at bar-
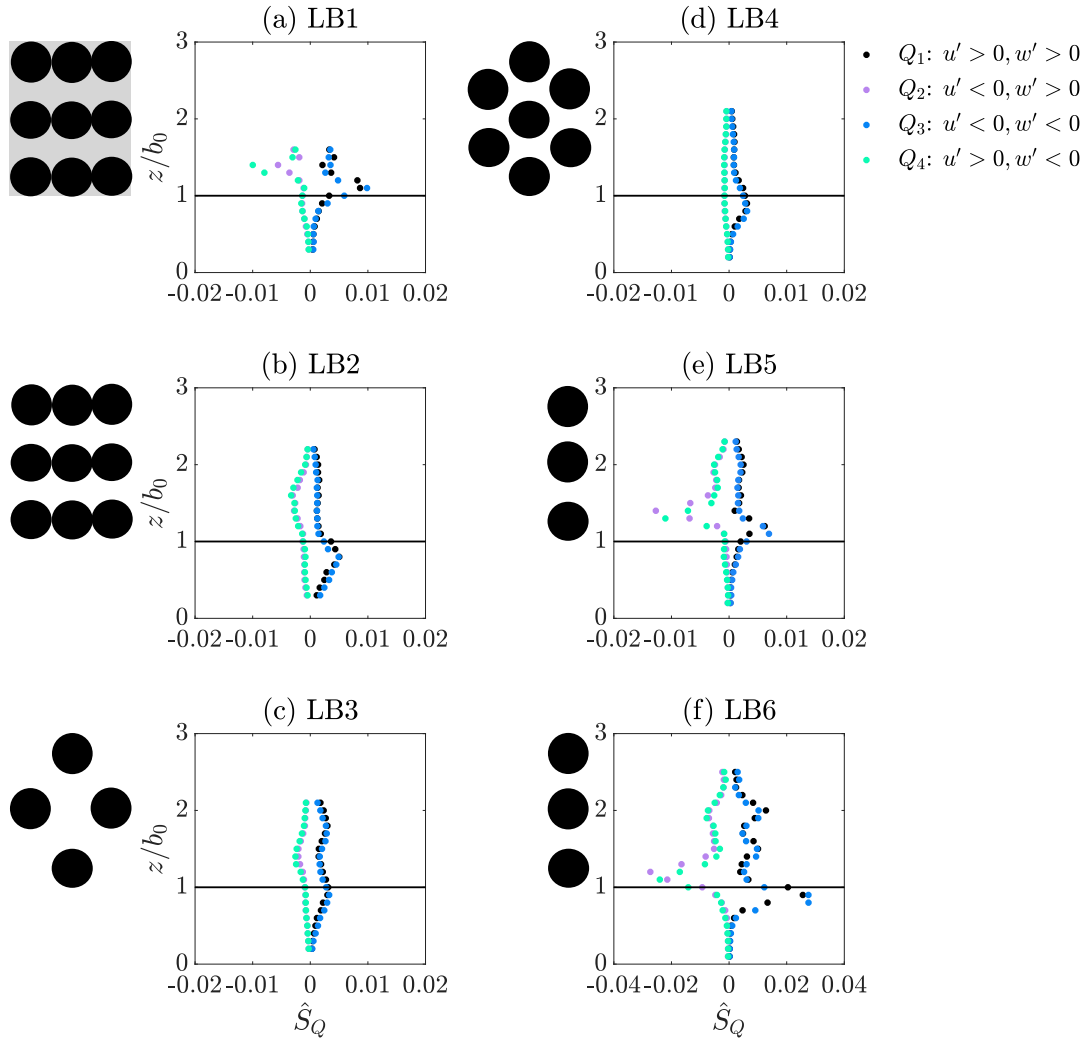
**Figure 2.14:** Vertical Reynolds shear stress contributions ($\hat{S}_Q$) for all leaky barrier configurations at $x/b_0$=1, divided into four quadrants: quadrant 1 ($Q_1$): $u'$>0, $w'$>0, quadrant 2 ($Q_2$): $u'$<0, $w'$>0, quadrant 3 ($Q_3$): $u'$<0, $w'$<0, and quadrant 4 ($Q_4$): $u'$>0, $w'$<0.

rier height (Figure 2.13 (d-f) and (j-l)). This peak was located above the primary peak from contributions of $Q_1$ and $Q_3$ and at height of the lowest dowel and inter-dowel gap ($z/b_0$=1.2-1.6). This flow diversion through the gaps between the lowest and middle row causes a faster stream to form, i.e. secondary jet (Figures 2.12 and 2.13), which

then mixes with the surrounding flow in the upper wake region above and below this jet.

Conversely, for the non-porous structure LB1, an increase in frequency of $Q_2$ and $Q_4$ events was also observed ($z/b_0$=1.4, $Q_2$: -0.006 $m^2/s^2$, $Q_4$: -0.01 $m^2/s^2$). This upper wake region was associated with mixing of plunging flow that had progressed over the top of the structure (Figure 2.11) rather than flow through an inter-dowel gap. Hence, momentum is predominantly transported downward ($w'$<0), a result of the strong overtopping flow observed only for LB1 (Figure 2.11), caused by its high blockage and impermeable design (Table 2.1).

Interestingly, similar secondary peaks in values for $Q_2$ and $Q_4$ events as well as those in $Q_1$ and $Q_3$ were observed for both short leaky barriers (LB5-6). These are a result of the flow separation observed around individual dowels likely arising in vortex shedding phenomena, contributing to the mixing of the secondary flow streams with the upper wake region and enhancing the wake recovery. In case of the short leaky barriers (LB5-6), a secondary peak in $Q_2$ and $Q_4$ was found at height of the middle dowel [$(z/b_0, \hat{S}_{Qi})$; LB5, $Q_2$: (2.0, -0.003 $m^2/s^2$), $Q_4$: (1.9, -0.003 $m^2/s^2$); LB6, $Q_2$: (2.0, -0.007 $m^2/s^2$), $Q_4$: (2.0, -0.008 $m^2/s^2$)], which was less pronounced in comparison to the peak observed at lowest dowel height ($z/b_0$=1.2-1.6). This peak was accompanied by a secondary peak in $Q_1$ and $Q_3$ at a similar vertical elevation and peak magnitude for LB5 [$(z/b_0, \hat{S}_{Qi})$; $Q_1$: (2.0, 0.003 $m^2/s^2$), $Q_3$: (1.9, 0.002 $m^2/s^2$)] and two smaller peaks for the scaled barrier LB6 at height of the lowest inter-dowel gap ($z/b_0$=1.6, $Q_1$: 0.01 $m^2/s^2$, $Q_3$: 0.01 $m^2/s^2$) and near the middle dowel height ($z/b_0$=2.1, $Q_1$: 0.01 $m^2/s^2$, $Q_3$: 0.01 $m^2/s^2$). Similarly, in the case of the long, open porous barrier LB3, a slight increase in occurrence of $Q_1$ and $Q_3$ events was observed at the lower edge of the middle dowel [$(z/b_0, \hat{S}_{Qi})$; $Q_1$: (1.8, 0.003 $m^2/s^2$), $Q_3$: (1.7, 0.003 $m^2/s^2$)], indicating that momentum transport of similar strength as observed at the structure lower edge. These peaks are associated with flow diversion and wake recovery due to the secondary flow streams through the middle and upper inter-dowel

gap.

### 2.3.1.3.2   Far wake region

**Recovery of mean streamwise velocity**

To analyse the impact of physical leaky barrier design on wake recovery, the velocity deficit ($\Delta\overline{u}$) between furthest upstream (LB1-5: $x/b_0$=-60.2; LB6: $x/b_0$=-30) and selected downstream profiles was computed for all leaky barriers and is presented in Figure 2.15. Values of $\Delta\overline{u}$<0 indicate that the streamwise velocities measured downstream of the leaky barrier are smaller than the velocities measured at the farthest upstream profile, resulting in a velocity deficit, while values of $\Delta\overline{u}$>0 indicate that there are higher mean streamwise velocity values downstream of the barrier than at the unperturbed upstream profile and hence, a velocity surplus.

In the case of the non-porous leaky barrier (Figure 2.15 (a)), a velocity surplus ($\Delta\overline{u}$>0) was initially present immediately downstream of the barrier ($x/b_0$=1) over 0$\leq z/b_0 \leq$1 (Figure 2.15 (a), black solid circles) and was observed throughout the profile vertical extent for $x/b_0$>1.4, which was associated with the rapid vertical expansion of the primary jet and its mixing with the wake flow. Similarly, all porous leaky barriers (Figure 2.15 (b-f)) initially showed a positive velocity deficit within the main gap region (0$\leq z/b_0 \leq$1) as a result of the high-momentum flow exiting beneath the barriers. In the upper wake region ($z/b_0 \approx$1-2.5), however, a negative velocity deficit was observed as previously shown by the low streamwise mean velocities (Figure 2.12 (c, e, g, i, k)). Close to the barrier structure ($x/b_0$=1), both short porous leaky barriers (LB5-6) showed additional peaks of velocity surplus due to the flow diversion around the individual dowels at height of the lowest dowel gap (Figure 2.13 (e, f), black solid circles, $z/b_0 \approx$1.7 and 1.6 for LB5 and LB6, respectively). These secondary jets, however, diminished by approximately $x/b$>8 ($x/b_0$>2) for both leaky barriers as they were dissipated from mixing with the surrounding flow. The average velocity deficit $\Delta\overline{u}$ between the furthest upstream and downstream profiles (blue solid circles) was less
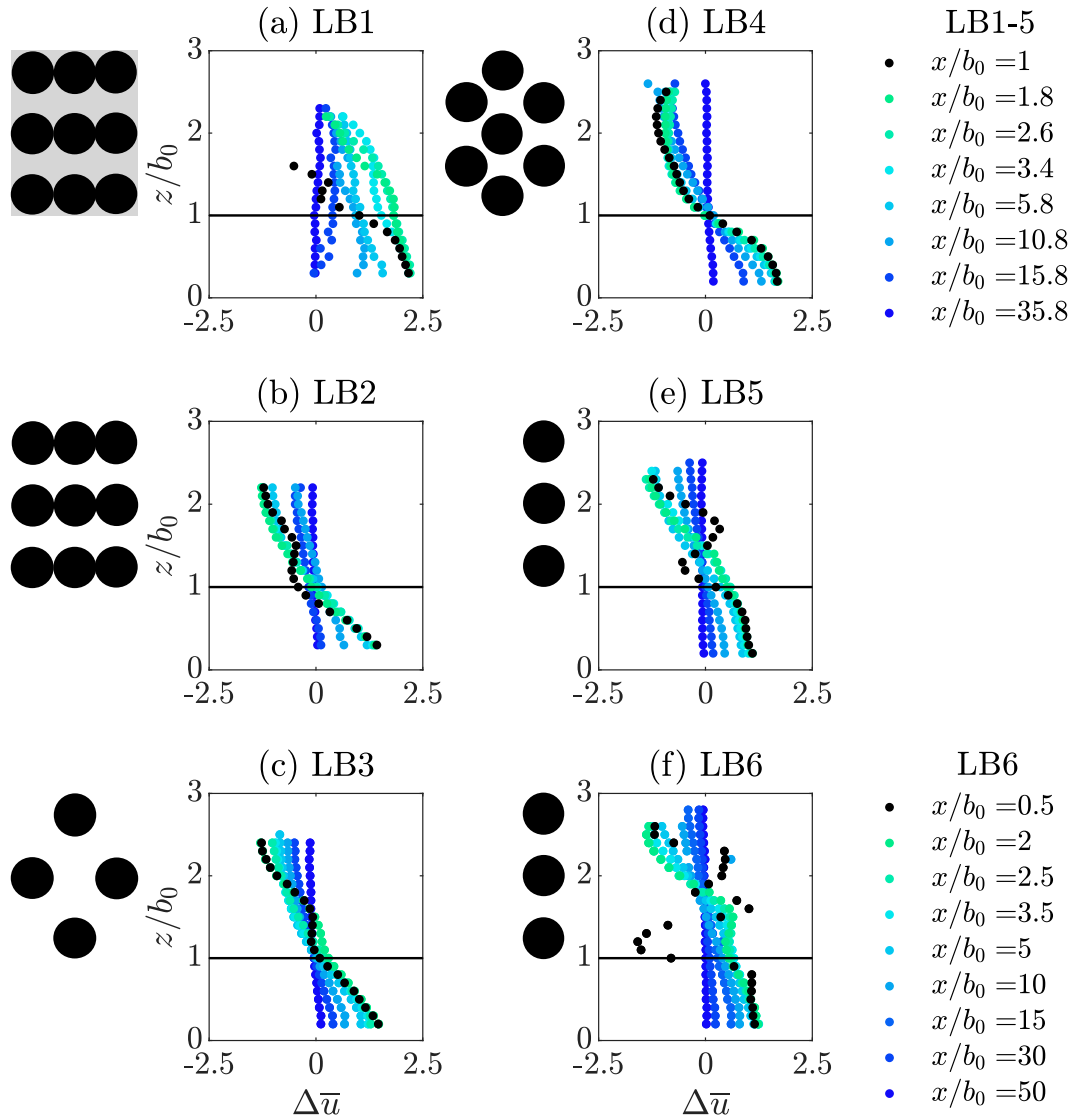
**Figure 2.15:** Progression of velocity deficit computed from the difference between furthest upstream profile (LB1-5: $x/b_0$=-60.2; LB6: $x/b_0$=-30) and selected downstream profiles $\left(\text{LB1-}\right.$

5: $\Delta \overline{u} = \dfrac{\overline{u} - \overline{u}_{x/b_0=-60.2}}{\overline{u}_{x/b_0=-60.2}}$, LB6: $\Delta \overline{u} = \overline{u} - \dfrac{\overline{u}_{x/b_0=-30}}{\overline{u}_{x/b_0=-30}}\left.\right)$. Vertical extent of recorded velocity profiles may vary due to longitudinal change in downstream flow depth.

than 10 % (4.3 %, 9.9 %, 9.3 %, 6.9 %, 7.7 %, 1.9 % for LB1-6) with maximum absolute magnitude of $\Delta \overline{u}$ less than 20 % (10.4 %, 9.5 %, 15.8 %, 18.5 %, 10.0 %, 6.1 %,

for LB1-6) for all structures. Increasing the scale of LB5 resulted in 1.4 times longer wake recovery for the larger-scale logjam LB6 which recovered by $x/b_0 \geq 50$.

**Decay of maximum jet velocity**

While the maximum streamwise velocity $\overline{u}_{max}$ and velocity profile $\overline{u}(z)$ of flow exiting the lower gap varied with physical leaky barrier design (Figure 2.16), $\overline{u}(z)$ decayed in a self-similar fashion with increasing longitudinal distance from all leaky barriers ($x/b_0$). Decay of local maximum velocity in the lower gap region ($0 < z/b_0 < 1$), $\overline{u}_{max}$, relative to depth-averaged velocity over the lower gap region at the initial downstream measurement point $\langle \overline{u}_{b_0} \rangle$ with increasing downstream longitudinal distance from the logjam $(x/b_0)^{-1/2}$ is shown in Figure 2.16. Maximum mean streamwise velocity downstream of all structures initially maintained an elevated value close to that obtained at the measurement point nearest to the logjam ($x/b_0$=1), which was reduced as the mixing region between the jet and surrounding flow reached the location of jet maximum velocity. $\overline{u}_{max}/\langle \overline{u}_{b_0} \rangle$ was within 1.05±1.18 for LB1 and LB3-6 (mean ± s.d.; 1.14±0.02, 1.63±0.03, 1.05±0.02, 1.16±0.03, 1.18±0.01, 1.10±0.02 for LB1 to LB6) within $0 \leq x/b_0 \leq 4$ and above this range for LB2 (1.63±0.03). For LB2, the magnitude of $\overline{u}_{max}$ was greater than the depth-average velocity in the gap region due to a pronounced linear shape of the downstream velocity profile, with maximum observed $\overline{u}/U_0$ located at the lowest measurement point, $z/b_0$=0.02.

Both the initial depth-averaged velocity in the lower gap region and the initial maximum jet velocity were increased for leaky barriers with lowest inverse of relative channel void area $A_{rv}^{-1}$ (Table 2.1). LB1 and LB4 had lower $A_{rv}^{-1}$=0.33 due to the higher projected area of these structures which occupied the full structure extent, in comparison to LB2, LB3, LB5, LB6 for which $A_{rv}^{-1}$ was increased ($A_{rv}^{-1}$=0.43-0.5, Table 2.1) due to the arrangement of gaps between the structure dowels. The average local maximum velocity over $0 \leq x/b_0 \leq 4$ relative to bulk velocity $\overline{u}_{max}/U_0$=2.9, 2.2, 2.0, 2.5, 1.9, 2.0 for LB1-6, respectively. Downstream of the potential core region ($x/b_0 > 4$), the local maximum jet velocity, $\overline{u}_{max}$, reduced from the initial value
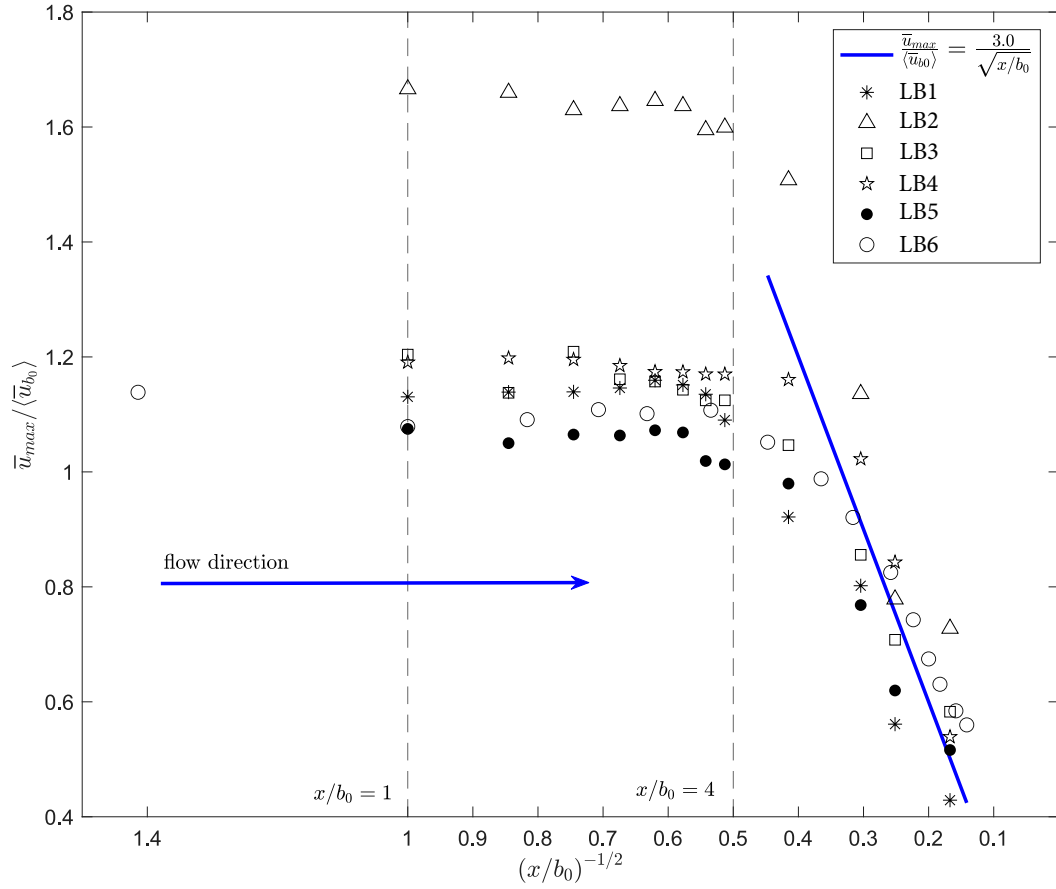
**Figure 2.16:** Decay of local maximum velocity $\overline{u}_{max}$ downstream of structures LB1-6 relative to depth-averaged initial jet velocity $\langle\overline{u}_{b_0}\rangle$ ($0\leq x/b_0 \leq 1$) with increasing longitudinal distance from the barrier $(x/b_0)^{(-1/2)}$, with measurements for LB1-6 respectively represented by black asterisks (LB1), open triangles (LB2), open squares (LB3), open stars (LB4), solid circles (LB5), and open circles (LB6). Dashed black line at $(x/b_0)^{(-1/2)}$=0.5 ($x/b_0$=4) denotes observed length of potential core region over which maximum jet velocity remained close to the initial measured value. Solid blue line indicates observed scaling of longitudinal decay $(\overline{u}_{max}/\langle\overline{u}_{b_0}\rangle) \sim C_{wj}(x/b_0)^{(-1/2)}$, with decay coefficient $C_{wj}$=3.0±0.5 fit to measurements for LB1-6 ($x/b_0$>4).

as it lost momentum due to mixing with surrounding flow. The decay of $\overline{u}_{max}/\langle\overline{u}_{b_0}\rangle$ in the region downstream of the potential core scaled with $(x/b_0)^{-1/2}$. Average $C_{wj}$

$(\overline{u}_{max}/\langle \overline{u}_{b_0} \rangle \approx C_{wj}(x/b_0)^{-1/2})$ across all leaky barriers for $x/b_0$ >4 was $C_{wj}$=3.0±0.5 (mean ± s.d. of six leaky barriers), with $C_{wj}$=2.4±0.2, 3.7±0.5, 2.6±0.3, 2.9±0.4, 3.2±0.3, 3.2±0.5 respectively for LB1-6 (Figure 2.16, solid blue line; $F_0$ ≈0.5-1).

### 2.3.1.4   Comparison between 80% and 100% bankfull discharge

In addition to the presented hydrodynamic measurement results shown for 100 % bankfull discharge, four more velocity profiles were recorded for near-bankfull flow conditions (80 % $Q_{bf}$) as described in Section 2.2.3.1. Upstream velocity profiles for the non-porous (LB1) and porous (LB2) barrier are shown on the left-hand side of Figure 2.17 (a) and (b), respectively.

Furthest upstream ($x/b_0$=-10.4) of the barriers, velocity profiles still follow a near-logarithmic distribution similar to that recorded under control conditions. Immediately upstream of the structure ($x/b_0$=-1.4) higher values of $\overline{u}/U_0$ occurred for the 80 % bankfull flow conditions regardless of the leaky barrier structure. For the non-porous design, however, there is higher momentum flow going through the bottom gap, changing the velocity distribution with the highest values occurring at mid-gap height ($0.5b_0$) and progressively decreasing towards the water surface. Such changes in the longitudinal velocity distribution for 80 % bankfull flow conditions are more subtle for LB2 as a result of a decreased flow blockage as this structure allows through flow. For LB1, due to its blocking-nature (Figure 2.17 (a)) there is a 20 % increase in upstream flow depth for both flow conditions compared with control conditions (Table 2.1). This resulted in overbank flows for both discharges, which led to lower in-channel mean longitudinal velocities upstream of the barriers. For the non-porous structure the main-channel flow depth exceeded bankfull flow depth by 15 % and 5 % for 100 % and 80% bankfull discharges, respectively, while for the porous structure this only increased by 8 % and 6 % for 100 % and 80 % bankfull discharge, respectively, with overbank flow only observed for bankfull flow conditions.

Downstream velocity profiles are shown on the right-hand side of Figure 2.17 (a) and
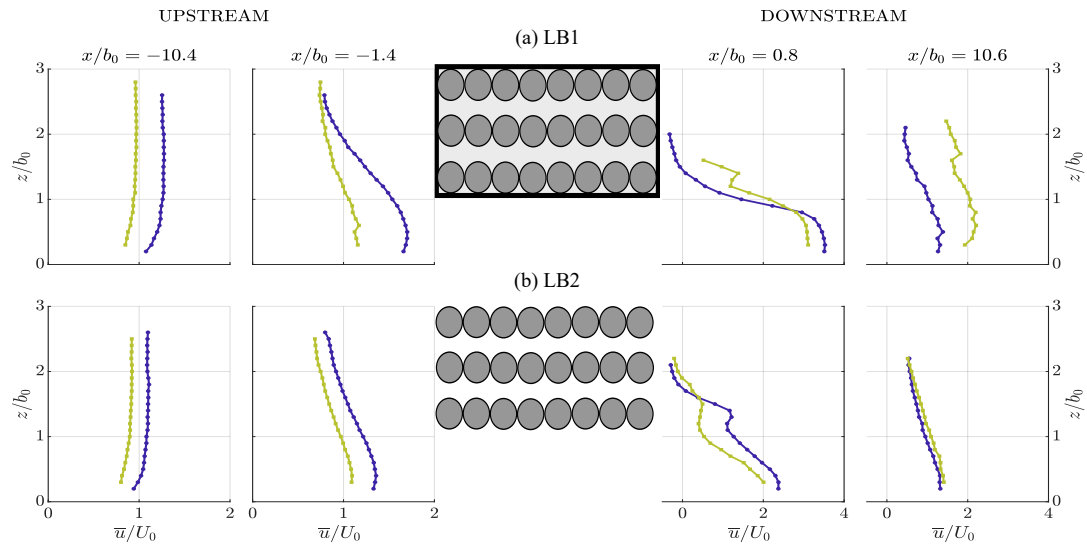
**Figure 2.17:** Mean longitudinal velocity profiles ($\overline{u}/U_0$) obtained under 80 % (blue) and 100 % (green) bankfull flow condition for the (a) non-porous (LB1) and (b) long, porous (LB2) leaky barrier.

(b) for LB1 and LB2, respectively. Immediately downstream of LB1 ($x/b_0$=0.8), the maximum $\overline{u}/U_0$ is found at approximately one third of the gap height ($0.33b_0$) and increased 2.7 and 2.0 times compared to values at $x/b_0$=-1.4 (Figure 2.17 (a)) for 100 % and 80 % bankfull flow, respectively. The maximum $\overline{u}/U_0$ was 10 % higher for the 80 % bankfull discharge than for bankfull conditions, as in the latter case, the upstream flow spills onto the floodplains and overtops the barrier, redistributing momentum from the main channel and more specifically, from the "under flow" region beneath the structure. In all cases, velocity profiles show a progressive decrease in $\overline{u}/U_0$ with increasing elevation in the water column. Immediately downstream of LB2, the maximum longitudinal velocity only increased by approximately 1.8 times compared to $x/b_0$=-1.4 for both flow conditions (Figure 2.17 (b)). Longitudinal mean velocities were still slightly higher for 80 % bankfull flow, likely due to the overbank flow observed under bankfull conditions, as well as the increased flow through the barrier. A notable feature in the wake of the leaky barrier is a second peak featuring a slight increase in longitudinal mean velocity at the lowest inter-dowel gap, i.e. $z/b_0$=1.5, as a result of flow going

through LB2. With increasing downstream distance, longitudinal velocities start to recover. Far downstream, at $x/b_0$=10.6, the difference in $\overline{u}/U_0$ between discharges was more pronounced for LB1, with higher longitudinal mean velocities under the bankfull flow. In contrast, velocity recovery was found to be independent of discharge for the porous barrier, likely due to the reduced overtopping flow.

### 2.3.2    Fish behaviour

Fish spatial and passage behaviour response was investigated for a range of non-porous and porous physical leaky barrier designs for juvenile Atlantic salmon (as described in Experiment (a) in Section 2.2.4.4.1, with results presented in Section 2.3.2.1) and juvenile rainbow trout (as described in Experiment (b) in Section 2.2.4.4.2, with results presented in Section 2.3.2.2).

#### 2.3.2.1    Leaky barrier impact on juvenile Atlantic salmon

Juvenile Atlantic salmon response was investigated for a non-porous (LB1) and porous (LB2) leaky barrier under 80 % and 100 % bankfull discharge conditions. Fish behaviour results were analysed in terms of time fish spent downstream, upstream and underneath the barrier as well as percentage of fish passing from the downstream into the upstream region, and mean number of upstream passes per fish recorded during the 10 min test period (Figure 2.18).

Mean proportion of time fish spent downstream, upstream and underneath the barrier after being released is shown in Figure 2.18 (a) for 80 % bankfull (left) and 100 % bankfull (right) flow conditions. Spatial preference was significantly more impacted by barrier porosity (GLM, all $p$<0.001) than by an increase in discharge (GLM, all $p$>0.001). Independent of the flow condition, fish spent more time downstream when no leaky barrier (control) was placed inside the test section (71 % and 77 % for 80 % and 100 % bankfull discharge, respectively). Time spent downstream significantly

differed between control condition and barriers present (GLM, LB2: $p<0.001$ and LB1: $p=0.0057$), but also among barriers (GLM, $p=0.0097$). In contrast, time spent upstream only significantly differed from the control case when the non-porous barrier (LB1) was present (GLM, $p=0.0239$). In case of the non-porous leaky barrier, fish spent similar time upstream (48 % and 41 %) and downstream (50 % and 44 %) for 80 % and 100 % bankfull flow conditions, respectively. Time spent underneath LB1 increased from 2 % to 15 % when increasing the discharge but did not differ significantly from the control condition (GLM, $p=0.341$). Conversely, in the presence of the porous barrier (LB2), fish spent most time underneath the barrier, demonstrated by 69 % and 70 % for 80 % bankfull and 100 % bankfull discharge, respectively, which significantly differed from the control condition (GLM, $p<0.001$) as well as from what was observed for the non-porous barrier (GLM, $p<0.001$). Similar to what was observed for the non-porous barrier, fish spent equal time upstream (15 %) and downstream (16 %) under 80 % bankfull flow conditions; however, under 100 % bankfull flow time spent downstream increased to 29 % while time spent upstream decreased to 1 %.

The percentage of fish passing at least once from the downstream into the upstream region for 80 % (blue) and 100 % bankfull (green) flow conditions is presented in Figure 2.18 (b). No significant association was found between flow condition and percentage of upstream passing fish (GLM, $p=0.9667$), however, a significant difference between control situation and the presence of the barriers was noted (GLM, $p=0.0026$). While in the absence of a barrier (control), 60 % and 50 % of the tested fish passed at least once into the upstream region under 80 % and 100 % bankfull flow, respectively, a higher percentage of fish passed upstream when a non-porous barrier was present (GLM, $p=0.0665$) and smaller percentage of fish passed upstream under the presence of the porous barrier LB2 (GLM, $p=0.1573$). The percentage of fish passing upstream was significantly different between LB2 and LB1 (GLM, $p=0.0012$).
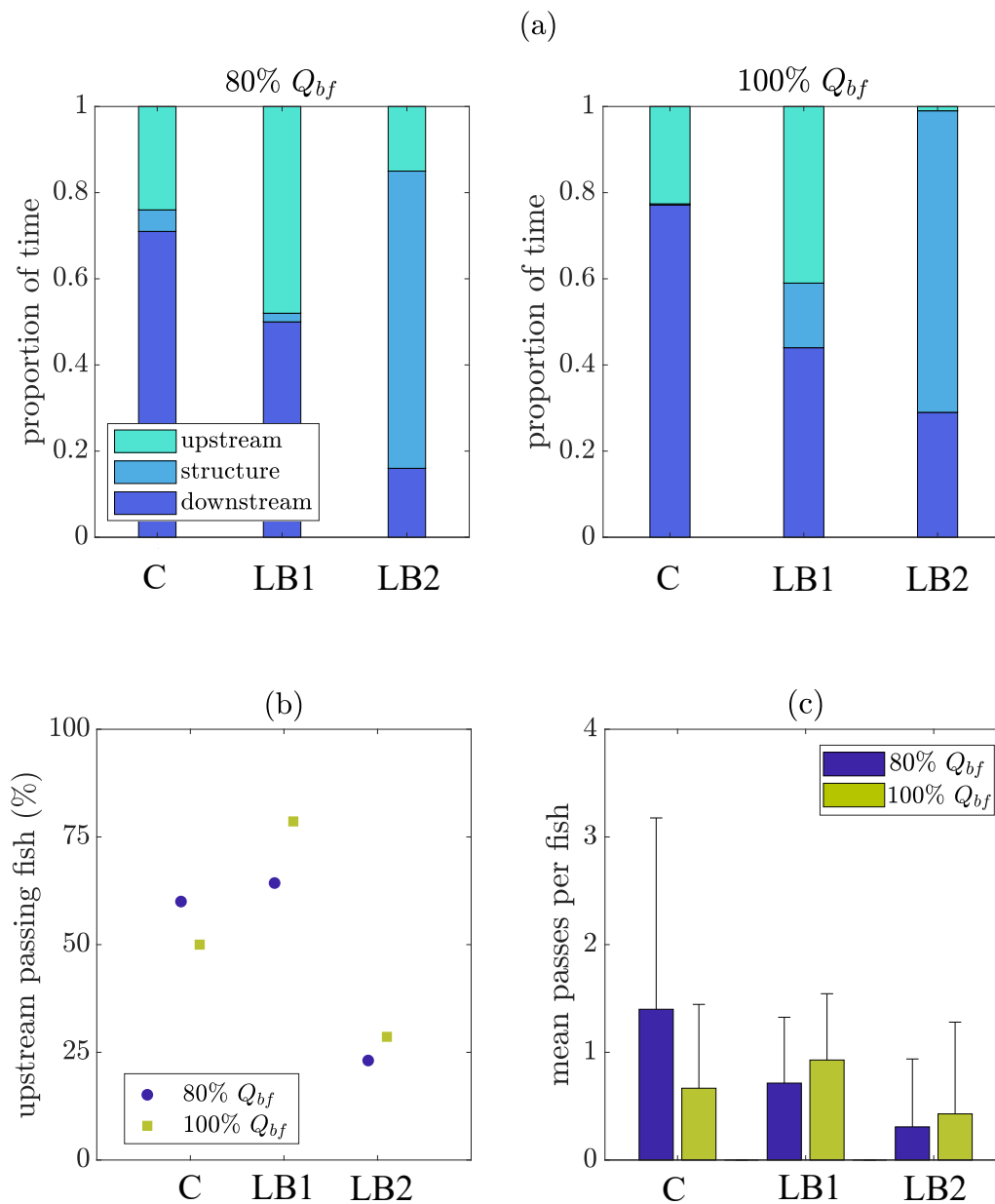
**Figure 2.18:** Summary of fish behavioural test showing (a) average time fish spent downstream (blue), beneath the structure (light blue) and upstream (green) under control (denoted as C), non-porous (LB1) and porous barrier (LB2) for 100 % (right) and 80 % (left) bankfull flow conditions. Percentage of fish passing from downstream area into upstream area is presented in (b) for 80 % (blue) and 100 % (green) bankfull flow conditions. Mean upstream passes per fish are shown in (c) with error bars representing standard deviation.

As every fish was able to pass multiple times from the downstream region into the upstream region, Figure 2.18 (c) presents the mean number of passes per fish. Despite no significant association between number of upstream passes per fish and flow condition (GLM, $p$=0.9963), the mean number of upstream passes per fish significantly differed when a barrier was present (GLM, $p$=0.0174). Under the control treatment, each fish passed on average 1.4 and 0.67 times from downstream to upstream under 80 % and 100 % bankfull discharge, respectively. This number decreased, not significantly, in the presence of a non-porous leaky barrier LB1 (0.71 and 0.93 times for 80 % and 100 % bankfull discharge; GLM, $p$=0.5138), but even more so when a porous barrier LB2 was present which led to a significant difference to the control condition (0.31 and 0.43 time for 80 % and 100 % bankfull discharge; GLM, $p$=0.0096). In addition, a significant difference in mean passes per fish was noted amongst both barriers (GLM, $p$=0.0297). Highest variation in mean passes per fish was found for the control treatment.

When increasing the discharge to 100 % bankfull flow or when increasing barrier blockage (i.e., non-porous structure LB1) conditions, upstream water level rose, inundating both floodplains on either sides of the main channel and therefore, opening potential, new habitat. Interestingly, under these conditions, a small, not significant, minority of fish (7 % for LB1, both discharges and 17 % for control, 100 % bankfull discharge) used the additional space by swimming onto the floodplains. Hence, no significant association was found between floodplain usage and discharge (GLM, $p$=0.3304) and leaky barriers presence (GLM, $p$=0.1621).

To analyse the impact of human interaction on fish behaviour, all tests were performed with and without nudged fish. Similar significant independent variables were calculated for the percentage of upstream passing fish, floodplain usage and time spent upstream, downstream and beneath the barrier. Only the dependent variable "passes per fish" resulted in a different result when prodded fish were excluded, showing that neither flow condition (GLM, $p$=0.8893) nor barrier (GLM, $p$=0.119) had a signific-

ant impact. In comparison, barrier was found to be significant factor influencing fish behaviour (GLM, $p$=0.0174) when nudged fish were included.

### 2.3.2.2   Leaky barrier impact on juvenile rainbow trout

In a second set of experiments, juvenile rainbow trout response was analysed for a range of leaky barrier designs under bankfull flow condition (as described in Section 2.2.4.4.2 (i), with results presented in Section 2.3.2.2.1), including a non-porous leaky barrier (LB1), a long, porous barrier (LB2), a long, staggered barrier (LB3) and a short, porous leaky barrier (LB5). Furthermore, fish response to overhead cover (as described in Section 2.2.4.4.2 (ii), with results presented in Section 2.3.2.2.2) and barrier colour (as described in Section 2.2.4.4.2 (iii), with results presented in Section 2.3.2.2.3) was investigated. Fish behaviour results were analysed in terms of time fish spent downstream, upstream and underneath the barrier as well as percentage of fish passing from the downstream into the upstream region, and mean number of upstream passes per fish.

### 2.3.2.2.1   Experiment (i): Fish response to leaky barrier length and porosity

Spatial behaviour, analysed in terms of time spent downstream, beneath the barrier, and upstream, showed that fish spent the least time beneath the barrier, and more time downstream than upstream (Figure 2.19 (a)). Hence, leaky barrier presence significantly impacted on the time fish spent within the different spatial regions (GLM, upstream and downstream $p$<0.0010, barrier region $p$=0.0060). Passage behaviour, including percentage of upstream passing fish (Figure 2.19 (b)) and number of passes per fish (Figure 2.19 (d)), was negatively affected by the barrier presence (GLM, $p$<0.0010), and resulted in less fish passing into the upstream region. Of all the leaky barrier designs examined, the short barrier (LB5) differed least from the control case in terms of percentage of upstream passing fish and number of passes per fish (GLM, $p$=0.1943 and $p$=0.0186, respectively). Although fish length did not impact spatial
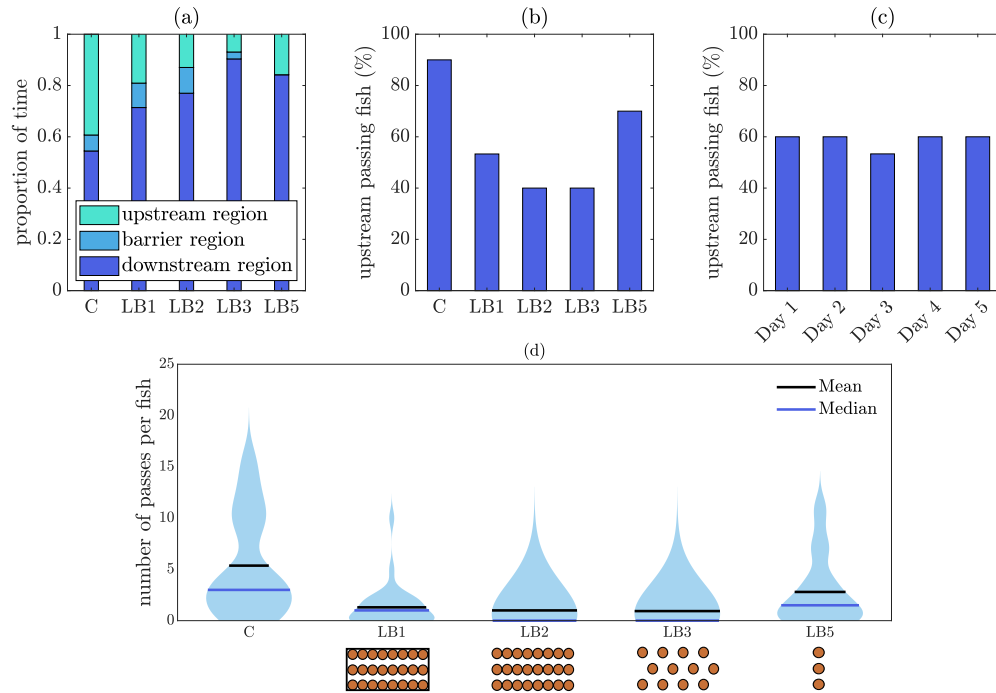
**Figure 2.19:** Impact of the tested leaky barrier structural design on fish behaviour. (a) Percentage time fish spent downstream, within the leaky barrier region and upstream, (b) percentage of upstream passing fish, (c) percentage of upstream passing fish per test day independent of treatment, and (d) number of passes per fish for the no-barrier control set-up (denoted as "C") and each of the analysed leaky barrier designs (LB1-3, LB5) with the width of the density distribution denoting frequency. Note, for simplicity, LB1-orange is denoted as LB1 in this figure.

usage nor upstream passes per fish (GLM, spatial usage: upstream $p$=0.0660, downstream $p$=0.0620, barrier $p$=0.7768; upstream passes per fish: $p$=0.1030), it affected number of upstream passing fish (GLM, $p$=0.0074), with larger fish being less likely to pass upstream.

The impact of leaky barrier porosity on fish behaviour was analysed by comparing the non-porous barrier (LB1) against the two porous barriers (LB2 and LB3). There was no significant difference between the three barrier porosities for the number of upstream passing fish (GLM, LB2: $p$=0.2874 and LB3: $p$=0.4257) and mean number of passes

per fish (GLM, LB2: $p$=0.7204 and LB3: $p$=0.5708). A non-significant decrease in time spent in the upstream area occurred with increased porosity (LB3<LB2<LB1; GLM, LB2: $p$=0.4369 and LB3: $p$=0.1191). Hence, time spent downstream increased with increasing porosity with only the long, open-porous leaky barrier (LB3) significantly differing from the non-porous LB1 (GLM, $p$=0.0167). Despite all three long barriers providing a similar overhead area of cover for the fish, time spent beneath them significantly varied amongst the long, open-porous (LB3) and the non-porous (LB1; GLM, $p$=0.0321) as well as long-porous barrier (LB2; GLM, $p$=0.0217), showing that fish spent less time beneath LB3 (3 %) and most time beneath LB1 and LB2 (10 %).

The impact of barrier length on fish behaviour was tested by comparing the long, porous barrier (LB2) with the short, porous barrier (LB5). Decreasing the length of the barrier led to an increase in the number of upstream passing fish from 40 % to 73 % (GLM, $p$=0.0090). Similarly, for the shorter design, mean passes per fish significantly increased 2.8 times (GLM, $p$=0.0346). In contrast, there was no significant difference between barrier length in terms of time spent downstream and upstream (GLM, $p$=0.3582 and $p$=0.5231, respectively), but a higher proportion of fish spent time beneath the longer leaky barrier (LB2; GLM, $p$=0.0018).

To avoid learning-based bias of the experimental results due to the repeated use of fish for each treatment, the treatment-independent percentage of upstream passing fish per test day was analysed (Figure 2.19 (c)), showing that on each test day 60 % of the fish passed into the upstream region, with the exception of day 3 (53 %). Hence, no significant difference was found between the number of upstream passing fish and test days (GLM, $p$=0.9794), suggesting learning effects were negligible.

### 2.3.2.2.2 Experiment (ii): Fish response to overhead cover

Reducing leaky barrier length may alter fish behaviour, potentially due to the shortened overhead cover offering a reduced shelter and refuge region. A second fish behaviour

experiment (Experiment (ii), Section 2.2.4.4.2) was conducted analysing the impact of overhead cover preference without a barrier (control condition), but spatial preference did not significantly differ amongst cover versus no-cover conditions (Figure 2.20 (a); GLM, upstream: $p$=0.3617, downstream: $p$=0.8090, barrier: $p$=0.0764), with almost equal time spent upstream (cover: 38 %, no-cover: 28 %) and downstream (cover: 61 %, no-cover: 64 %) of the cover region. Although the presence of overhead cover did not impact percentage of upstream passing fish (75 % and 85 % for overhead cover and no overhead cover, respectively) and number of passes per fish (mean: overhead cover 4.95 and no overhead cover: 2.65, median: 2) (Figure 2.20 (c); GLM, $p$=0.0582), fish length significantly impacted the percentage of upstream passing fish (GLM, $p$=0.0219), with larger fish being less likely to pass upstream. Fish length also impacted time spent up- and downstream (GLM, $p$=0.0106 and $p$=0.0240, respectively) with larger fish spending slightly less time upstream and more time downstream, but this did non-significantly impact time spent within the overhead cover region (GLM, $p$=0.6206).

### 2.3.2.2.3  Experiment (iii): Fish response to leaky barrier colour

The impact of leaky barrier colour on fish behaviour was investigated by comparing an orange non-porous barrier (LB1-orange) against a natural-looking non-porous leaky barrier (LB1-natural) as described in Experiment (iii) (Section 2.2.4.4.2).

A larger proportion of time was spent downstream (GLM, $p$=0.0344) and less time was spent upstream for LB1-natural case (GLM, $p$=0.0086) compared to the LB1-orange case (Figure 2.20 (b)). More fish were found to pass upstream (76 %) when LB1-orange was present, with this percentage being significantly lower in case of LB1-natural (23 %) (Figure 2.20d; GLM, $p$<0.001) (Figure 2.20 (d)). Similarly, the number of upstream passes per fish was significantly different amongst both leaky barrier colours (Figure 2.20 (d); median: LB1-orange: 1, LB1-natural: 0; GLM, $p$=0.0091). Fish length did not significantly impact the percentage of upstream passing fish, num-

ber of passes per fish nor the time spent underneath the barrier (GLM, $p$=0.1283 and $p$=0.7129, respectively) but did influence time spent upstream and downstream (GLM, $p$=0.0055 and $p$=0.0343, respectively).
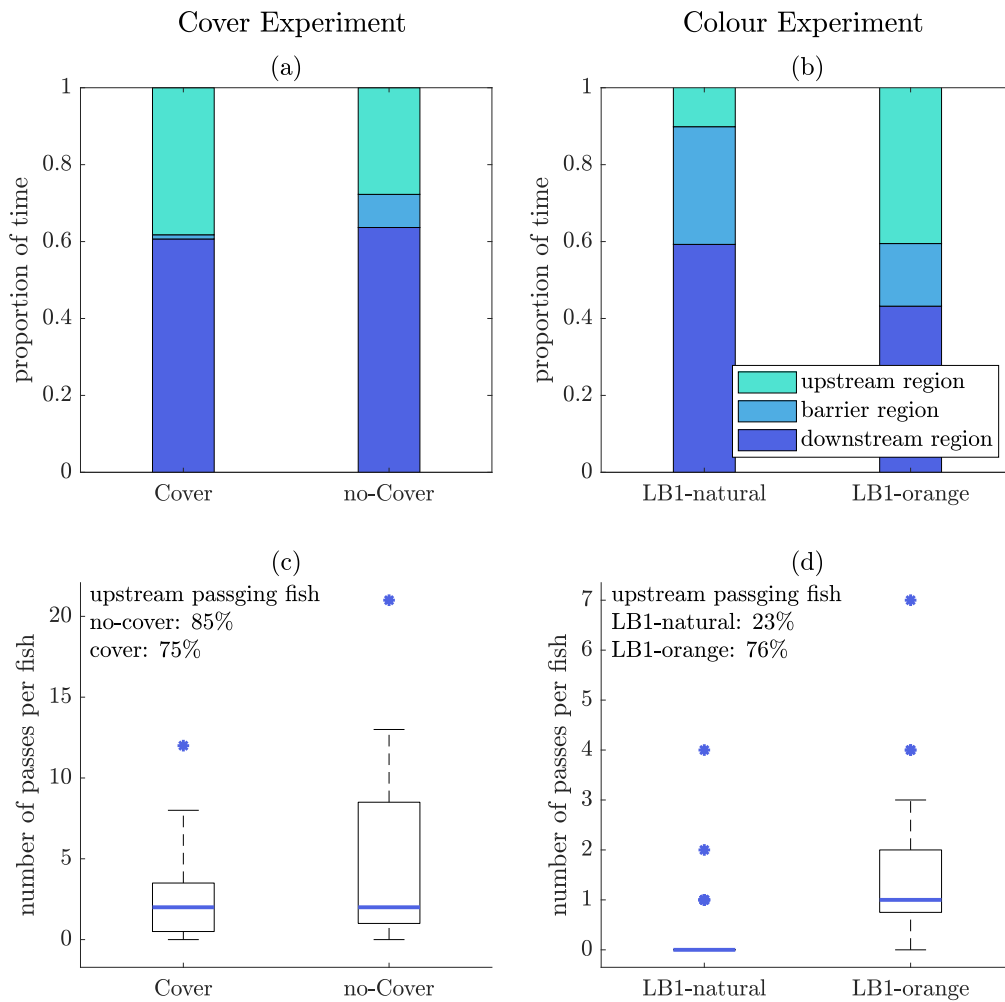


**Figure 2.20:** Fish behaviour experiments investigating the impact of overhead cover presence without barrier (a and c) and leaky barrier colour (b and d) on average time fish spent downstream, beneath the leaky barrier and upstream (a and b), and percentage of upstream passing fish and distribution of passes per fish (c and d). Note, for simplification, LB1-orange was previously denoted as LB1.

## 2.4   Discussion

Flooding is likely to increase with more frequent, higher intensity rainfall events due to climate change [98, 123]. Therefore, there is an urgent need to find sustainable solutions to attenuate the impact of flooding such as natural flood management, including the use of channel-spanning engineered leaky barriers [35]. Despite the increasing interest in these structures, little is known about how the physical design of these structures influences channel hydrodynamics and subsequently channel geomorphology, fish habitat and movement. Therefore, the impact of six engineered leaky barrier structures on channel hydrodynamics and fish movement was investigated here.

Leaky barrier hydrodynamics were characterised by flow diversion upstream of all structures due to the increased cross-sectional blockage provided by these barrier and the formation of a primary jet underneath the barrier. Downstream wake hydrodynamics were characterised by high-momentum flow exiting the barrier main gap and a structure-dependent upper wake, influencing near wake decay. Far wake decay, on the other hand, was self-similar. Wake recovery was design-independent, with velocities recovered within $\pm 10\,\%$ by the farthest downstream measurement profile.

Importantly, all tested leaky barrier designs did not block juvenile Atlantic salmon and rainbow trout movement, but they did impact spatial usage and upstream passage when compared with a no barrier free-flow scenario. The difference in discharge was not the decisive component impacting fish behaviour, instead the physical design of the barrier was more important. Two barrier designs, namely the non-porous (LB1) and short-porous (LB5) barrier, impacted least on spatial usage and fish movement compared to their long-porous counterparts (LB2-3). While the high-momentum flow did not prevent fish from passing into the upstream region, barrier colour had the greatest impact on upstream passage.

In the following, the impact of physical leaky barrier design on channel hydrodynamic (Section 2.4.1), fish movement (Section 2.4.2, and expected channel alterations (Sec-

tion 2.4.3) is discussed. Moreover, study limitations (Section 2.4.4) and research gaps (Section 2.4.5) are outlined.

## 2.4.1   Impact of leaky barrier physical design on channel hydrodynamics

### 2.4.1.1   Impact of leaky barrier physical design on channel hydrodynamics and hydraulics

Upstream of all leaky barriers, a change in water surface profile and increase in backwater rise ($\Delta H$) was observed, which was proportional to the barrier's void ratio ($\Phi$, Table 2.1). Upstream flow depth increased with proximity to the leaky barrier, causing the flow to spill onto the floodplains, with larger floodplain inundation observed for leaky barriers with higher cross-sectional blockage [145]. The relationship between barrier cross-sectional area and floodplain water depth is a key feature when using channel-spanning engineered leaky barriers to mitigate flood risk. The subsequent reconnection of the main channel with its adjacent floodplains enhances infiltration into the ground and therefore, contributes to the slowing down of flow [53, 35]. Hence, an increase in channel obstruction (e.g., through an increase in cross-sectional blockage) will improve flood attenuation [53, 35, 145]. Besides the cross-sectional blockage area of leaky barriers, the backwater rise of large wood accumulations without a vertical gap is dependent on the approach flow Froude number, the compactness of the structure and the percentage of organic fine material, such as branches and leaves [196], and can be predicted from the unobstructed flow depth, the unit discharge and a dimensionless structural parameter including jam length, frontal area density, drag coefficient, and solid volume fraction [68]. Experiments investigating leaky barriers featuring a vertical gap, as in this chapter, showed that the backwater rise increased with barrier resistance and a decrease of the gap height ($b_0$), and can be predicted using a combination of a sluice gate model and incorporating the hydrodynamic drag generated by the

barrier [69].

Upstream of all tested leaky barriers, streamwise mean velocities increased near $x/H_s \approx 1$, marking the onset of longitudinal flow diversion. In line with our observation, the onset of longitudinal flow diversion for the flow around porous structures, such as submerged vegetated canopy, often represented by vertical wooden dowels, was found at a similar streamwise location [188, 47].

Following the flow diversion upstream of all leaky barriers at the height of the main gap ($z/b_0 \leq 1$), a high-momentum jet formed underneath all barriers, similar to a modified wall jet [61] or the flow beneath a wooden log or logjam [21]. The initial local maximum jet velocity was maintained over a potential core region extending from $0 \leq x/b_0 \leq 4$ (Figure 2.16, dashed black line at $x/b_0=4$ associated with change in curvature for all data series), similar to values previously observed for offset jets with an initial uniform velocity on a rough bed and free jets ($x=4b_0$, [25]) but reduced from plane wall jets ($x=8b_0$, [8]). For classic jet flows with an initial near-uniform velocity, the initial local maximum velocity is equal to the uniform jet velocity ($\overline{u}_{max}/\langle\overline{u}_{b_0}\rangle=1$). Results showed values of $\overline{u}_{max}/\langle\overline{u}_{b_0}\rangle >1$, due to non-uniformity of the initial jet shape and discrete measurement locations. This high-momentum flow presents a key feature for the physical leaky barrier design to prevent blockage of the barrier main gap by brush and leaves, allowing constant base flow and fish movement.

In contrast, the upper wake ($z/b_0 \leq 1$) was strongly dependent on dowel arrangement and longitudinal barrier length. For instance, the upper wake of all long, porous leaky barriers (LB2-4) was characterised by low values of $\overline{u}/U_0$ and $tke/U_0^2$ because of the internal flow diversion slowing the flow through the structures. A similar reduction in mean streamwise velocity was observed for flow around patches of vertical wooden cylinders mimicking submerged vegetated canopies [253].

In comparison to the long, porous leaky barriers (LB2-4), the near wake of the short, porous leaky barriers (LB5-6) was characterised by the presence and decay of secondary jets due to the presence of distinct flow paths, indicated by the increase in $\overline{u}/U_0$ at

height of the inter-dowel gaps (b). For these barriers, regions of high vertical Reynolds shear stress were found downstream of the lowest dowel, with $\overline{u'w'}/U_0^2 > 0$, indicating turbulent momentum in the upward direction, and values of negative $\overline{u'w'}/U_0^2$ distributed mostly at the upper edge of the lowest dowel, indicating turbulent momentum transport downward. This pattern is similar to that in a cylinder wake with vortex shedding [241, 162], suggesting that this transient phenomenon also takes place for LB5 and LB6. In contrast, for the longer, porous jam LB2, less strong secondary jets were observed at height of the inter-dowel gaps, likely to be caused by the increase in longitudinal barrier length.

The upper wake of the non-porous leaky barrier (LB1), was characterised by the expansion of the high-momentum jet into the upper wake region, resulting in a large velocity gradient that causes an increase in Reynolds shear stress. Similar downstream flow alterations were observed for flow exiting an under-short sluice gate, not only showing the expansion of the high-momentum flow but indicating the existence of a recirculation zone at structure height [61]. Due to the physical limitations of the ADV, the existence of such a recirculation zone could not be proven.

Wake recovery was self-similar (Figure 9; [25]), independent of the physical logjam design, and scaled with $(x/b_0)^{-1/2}$, similar to previous observations for plane free jets ($\overline{u}_{max}/\langle \overline{u}_{b_0} \rangle \sim (x/b_0)^{-1/2}$, [181]) and plane wall jets ($\overline{u}_{max}/\langle \overline{u}_{b_0} \rangle \sim C_{wj}(x/b_0)^{-1/2}$, [245, 8, 25]). The decay occurred over an elongated length scale for wall jets relative to free jets due to reduced entrainment, with decay coefficient $C_{wj}$ observed to be related to jet Froude number, $F_0 = \langle \overline{u}_{b_0} \rangle / \sqrt{gb_0}$ ($C_{wj} \sim 3.5$, $F_0 = 3\text{-}9$ [245]; $C_{wj} \sim 2.7$, $F_0 \approx 1$, [8]). An average decay coefficient of $C_{wj} = 3.0 \pm 0.5$ was observed for all leaky barrier designs, with $F_0 = 0.78 \pm 0.16$. Wake decay was almost complete by $x/b_0 \geq 35$ for leaky barriers LB1-5 and by $x/b_0 = 50$ for LB6. The wake length decay scale is of interest when introducing multiple leaky barriers along a stream. For example, allowing the full decay distance between logjams allows decay of logjam-induced increases in maximum longitudinal velocity and turbulence, promoting suspended sediment cap-

ture.

### 2.4.1.2 Scaling impacts

Scaling impacts were examined through a generalized 1:2 scale test (LB6) of the short, porous logjam LB5. Comparability of the results presented for LB5 and LB6 are limited due to the absence of floodplains in the LB6 test case. Results showed that a similar near wake structure was generated by both structures, with a main secondary jet generated in the gap between the lower and middle dowels (Figure 2.12). For all structures including LB5 and LB6, the region over which maximum jet velocity remained close to the initial measured value extended four gap widths downstream (Figure 2.16; [4]. Although the difference was slight between all structures, Froude scaling of bulk velocity resulted in similar jet Froude numbers for both barriers ($F_0$=3.18, 3.21 for LB5 and LB6 respectively) and similar magnitude of wall jet coefficient, ($C_{wj}$=3.2$\pm$0.3, 3.2$\pm$0.5 for LB5 and LB6, respectively), which was previously observed to vary with jet Froude number [245, 8]. However, the long-distance recovery of the primary jet was found to require a slightly longer relative distance in the larger case LB6, for which the wake recovery distance, relative to gap width, was 1.4 times longer than the smaller case LB5 (Figure 2.15).

## 2.4.2 Impact of leaky barriers on fish movement and the aquatic environment

In the following, impacts of hydrodynamic and hydraulic changes as well as leaky barrier presence on the fish movement and channel geomorphology are discussed.

**2.4.2.1   Fish response to hydrodynamic and hydraulic alterations**

Under high flow conditions, leaky barriers aim to reconnect the main channel flow zone with the adjacent floodplain zone. By doing so, water backs up and spills onto the floodplains and inundates them, creating new habitat for aquatic organisms but also supporting upstream nutrient and sediment exchange [189]. Floodplains often contain wood in the form of logs, trees, branches and brush with high densities of macro-invertebrates and therefore, potentially provide additional food sources for fish [78]. Floodplain flow also creates seasonal wetlands [249], supporting lateral habitat connectivity [189], providing fish spawning and nursery grounds [203], as well as low velocity areas, protecting fish from downstream displacement during high flows [73]. Not all flow conditions, however, lead to the flow spilling onto the floodplains, and floodplain inundation strongly depends on the storm event flow magnitude, and conveyance capacity of the channel, as well as physical properties of the barrier. Although, fish explored the floodplain regions during the experiments conducted, this may not be the case in the field with increased in-stream and floodplain boundary roughness (e.g. mud, debris, and floodplain vegetation) and predators.

While the wide range of flow alterations observed are expected to enhance habitat complexity and therefore, result in an increase in fish habitat diversity [59, 231], certain flow alterations, such as the formation of the primary jet, may present velocity barriers to certain fish species and life stages but also provide cues for fish to pass. In the case of the non-porous barrier (LB1), a larger number of fish passed upstream, despite the higher streamwise mean velocities. This may indicate that higher momentum flow provides a clearer signal for fish of where to pass. While strong swimming species, such as the tested juvenile Atlantic Salmon and rainbow trout, were not prevented from passing into the upstream region (LB1-3, LB5), weaker swimming species (e.g., cyprinids) and younger individuals, however, may struggle to overcome the increase in streamwise velocity. The repeated exposure to regions of high-momentum flow due to the presence of multiple leaky barriers along a river stretch may result in an increase in

energy expenditure and a delay in fish movement or prevent fish from reaching certain habitats. Therefore, care should be taken when designing or choosing the physical design of leaky barriers to maintain habitat connectivity for all species present in the corresponding river.

Besides the impact of the primary jet on fish movement, the upper near wake ($z/b_0 \geq 1$) may also influence fish movement. The increased turbulence associated with the non-porous (LB1) and the short porous barrier (LB5) as well as along the shear layer between upper wake and primary jet, may act as a deterrent as fish have been found to avoid regions of high turbulent kinetic energy, Reynolds shear stresses, and coherent vortical structures [222, 93, 146]. In contrast, the reduced mean velocities and turbulence level in the case of the long, porous barriers (LB2-4) may provide resting and foraging areas for fish. In addition, flow around single and horizontal cylinder rows, similar to LB5-6, have highlighted an increase in spills, i.e. the loss of swimming stability, in regions of high downward-acting Reynolds shear stress caused by vortices featuring clockwise rotation due to the hydrodynamic forces acting on the fish causing the fish to become unbalanced [222, 146].

### 2.4.2.2 Fish response to leaky barrier design and presence

Besides the wide range of flow alterations caused by the leaky barrier designs and their indirect impacts on fish movement, barrier physical appearance may also influence the spatial preference and passage of fish.

Barrier complexity and length of the leaky barriers, for instance, may have presented one parameter influencing fish movement. Here, the short-porous (LB5) and non-porous (LB1) barriers were the least physically complex and allowed a higher percentage of upstream passing rainbow trout compared to the long-porous barriers (LB2 and LB3). The complexity of wooden structures is an important factor, providing a refuge for small fish against predators by causing visual interference and entry prevention [192]. However, when reducing barrier length to decrease complexity as in the

case of the short-porous design (LB5), the provision of overhead cover decreases. The results show no differences in spatial usage and passage behaviour of juvenile rainbow trout when overhead cover was present or removed. Conversely, juvenile Atlantic salmon spent most of their time underneath the long, porous, natural-looking leaky barrier, LB2. Atlantic salmon have been found previously to show a strong preference for overhead cover [90], unlike rainbow trout [36, 127], reflecting inter-species differences. Overhanging logs and complex accumulations of wood, or wooden cylinders as used in this chapter, are an important source of cover in rivers, which provides habitats for different species [59]. A study comparing a wooden against an acrylic, transparent velocity shelter, for example, showed an increase in the use of the wooden structure, which was assumed to be linked to visual stimuli caused by the shade [139].

Besides the physical complexity of leaky barriers and the provided overhead cover, colour was identified as another potential key parameter providing a visual cue to fish upstream passage. More juvenile rainbow trout moved upstream when comparing a coloured, orange barrier (LB1-orange) against a design sealed with colourless, transparent wrapping (LB1-natural), with the latter emulating a more natural design as the wooden dowels account for the barrier colour. Possibly the orange LB1 provides a clearer visual cue for fish passage or may not have been associated with shelter due to its unnatural colour. Depending on species, fish can differentiate colours and are attracted to different colours [102]. Salmonids, for instance, possess well-developed colour vision (Niwa and Tamura (1969) cited by [148]), but little is known about their attraction to colour and coloured objects. In contrast, bluegill sunfish and young carp react more towards red [102, 19] while Japanese marine fish species show greater preference for blues and greens [107]. Furthermore, Bermuda bream are only attracted to colour if the object is in motion rather than being stationary, with highest attraction shown to multi-coloured fabric as well as orange, corresponding to longer wavelengths [138]. For fish, hue is more important than contrast [107] as well as object shape and brightness [19], with colour perception thought to be species-specific and colour intensity and wavelength strongly dependent on water quality [126] and ambient light

conditions. It should be noted, that in all experiments, ambient light conditions varied throughout the experiment, which might have influenced fish perception of the barrier colour. However, randomisation of treatments and fish test order was used to account for variations in ambient light.

Treatment randomisation was also applied to minimize learning effects due to the repeated exposure to the test section, flow conditions, and similar barrier designs. This issue has previously been discussed by Mallen-Cooper (1994) [136]; they showed an increase in fish successfully negotiating the fishway indicating potential habituation to the repeated exposure to certain flow conditions and structures. Conversely, in this chapter, the repeated use of rainbow trout did not show an increase in upstream passing fish. This may be due to the variations in barrier design, creating individual wake patterns for each barrier design. However, this is an important aspect which should be further investigated as leaky barriers are often installed in large numbers (100 plus units) to desynchronise tributary flow from that of the main river. Due to the limited design guidelines of these barriers to date and their constant interaction with natural processes (e.g., natural accumulation of driftwood), fish are likely to encounter changing physical designs and different associated wake patterns. Hence, the porous leaky barriers (LB2-6) may become non-porous over time, creating a barrier similar to LB1. Frequent maintenance may be required to prevent the creation of a physical, solid barrier for fish movement. In addition, while a single barrier as in our study did not block fish movement, the cumulative effect of multiple leaky barriers may significantly impact fish movement.

### 2.4.3 Anticipated impacts on channel geomorphology

Upstream vertical flow diversion and the resulting high-momentum flow beneath all leaky barriers are presumed to elevate bed shear stress, and therefore, to increase the risk of pit formation and particle mobilisation if the maximum jet velocity underneath the barriers exceeds the critical Shields parameter. Scour formation is anticipated to

coincide with the onset of upstream flow diversion ($x/H_s \approx 1$) and to be largest within the region in which the initial jet core is being preserved ($x/b_0 \leq 4$) for all leaky barriers. Alongside engineered leaky barriers [70, 69], similar scour formations have been observed for flow underneath sluice gates [223], in-stream wood [231], accumulation of wooden pieces on retention racks [195, 7] and bridge piers [117]. Scour formation and extent was found to depend on discharge and structure properties. While Schalko et al. (2019) showed that scour depth increased with discharge for wood accumulations at vertical retention racks [195], Lagasse et al. (2010) identified size, shape and location of logjams as key parameters influencing scour associated with wood accumulations at bridge piers [117]. In contrast, logjam roughness and porosity did not significantly impact scour pattern and depth [117]. A study analysing wood accumulation at a vertical retention rack showed that wood accumulations forming near the water surface (i.e., triangular distribution shape), caused deep bed scour which extended in longitudinal direction but less downstream sediment deposition [7]. As leaky barriers used for natural flood management span the width of the channel, they are likely to accumulate organic material which reduces the barrier void ratio and therefore, increases scour formation and extent. Furthermore, scour was found to increase with increased cross-sectional blockage area due to the increase in flow diversion [21, 117]. These observations indicate that the largest scour may be expected for the non-porous barrier (LB1), which also showed highest primary jet velocity.

An increase in likelihood of bedload transport is expected due to increased velocity and bed shear stress in the primary jet, which increases the Shields parameter [103]. This, in turn, is likely to increase flushing of gravel and fine sediment underneath the structure, enhancing habitat quality through the creation of suitable spawning habitat [29]. In addition, an increase in Reynolds stress and turbulent kinetic energy was observed in the near wake region downstream of the non-porous (LB1) and short, porous (LB5-6) leaky barriers (Figure 2.13), which would increase the mixing of suspended sediment [103]. Moreover, the flushing of fine sediment from bed material may also promote hyporheic exchange and therefore to an increase in dissolved oxygen within

the hyporheic zone, beneficial for aquatic organisms (e.g., salmonids) [29].

The high-momentum flow observed for all leaky barriers may also result in bank erosion within the gap between barrier structure and bed, potentially influencing structural integrity. Flume studies examining partially channel-spanning, emerging side logs showed that a single log can increase the potential of bank erosion due to flow diversion toward the gap between log and bank, almost doubling near bank velocities [251], while the introduction of multiple logs in the longitudinal direction reduced erosion rates because of the wake interference between logs [252]. Gap width between log and bank was found to be a key parameter influencing near-bank velocities and therefore, bank erosion [251] which is comparable to our gap between flume bed and barrier structure. Hence, reducing $b_0$ may result in higher primary jet velocities and therefore, a greater risk of bank erosion. Besides bank erosion, floodplain erosion presents another risk associated with the overbank flow caused by the blockage provided by the barrier structures. A flume study investigating the impact of wood accumulation at a bridge demonstrated the rapid increase in floodplain velocity downstream of the bridge, highlighting the increased risk of floodplain erosion [157].

### 2.4.4 Experimental limitations

It should be noted, that transferability and comparability of the results presented in Section 2.3 to real-life leaky barriers is limited. First, leaky barriers installed in the field will not consist of idealised horizontal cylinders equally spaced and of identical size, but rather of non-uniform logs sourced from the adjacent floodplains, consisting of varying diameter, roughness, and curvature. Further experimental simplifications consist of a straight flume, strong lighting conditions, and clean water which, together with the idealised leaky barrier structures, may also influence fish response.

Secondly, leaky barriers in the field are subject to changes in shape, dowel arrangement and void ratio caused by the accumulation of fine organic material and associated de-

cay [196]. These changes result in continuous alterations of the near wake and hence, further research is required to quantify the impact of such changes on channel hydrodynamics. Despite the strong dependency of the wake pattern at barrier height on leaky barrier design, the creation of a region of high momentum flow ($z/b_0$<1) is still expected due to the preservation of the gap between the bed and the barrier.

Thirdly, all experiments were conducted using a fixed bed, similar to a bedrock channel [198]. While the smooth bed may have increased the streamwise mean velocities and therefore, influenced the results obtained, the use of a fixed bed also neglects the interaction between leaky barrier, flow, and sediment transport processes [198]. This is an important relationship which requires further experimental investigation [75] as, for instance, the use of a movable bed was found to decrease backwater rise associated with channel-spanning large wood accumulations [194].

Moreover, experiments were mostly conducted under 100 % bankfull flow conditions. While similar upstream and downstream hydrodynamic changes were observed under 80 % bankfull discharge, lower and higher flow depths may change turbulent structures and channel-floodplain interactions. Similarly, fish studies were only performed on two strong swimming fish species of a particular size category, sourced from hatcheries. The fish size used in our experiment might not be appropriately scaled to the experimental flow conditions.

Finally, the physical limitations of the ADV (i.e., submergence of the ADV head and required distance from the leaky barrier) prevented velocity measurements over the upper part of the water column and within approximately 50 mm upstream and downstream of the leaky barriers. The interaction between overtopping flow and near wake is an important aspect as an experimental study of a submerged log showed that overtopping flow can inhibit the formation of turbulent structures [198], and therefore, would significantly influence the near wake.

Despite limitations, the use of scaled eco-hydraulic flume experiments is useful for assessing geometric and physical modifications of key design parameters (e.g., barrier

length, colour, dowel arrangement, and porosity) of small in-stream hydraulic structures and corresponding hydrodynamic changes and fish response [11]. So far, design guidelines for leaky barriers are limited, and only a few studies have assessed the impact of leaky barriers on fish movement [58] but not channel hydrodynamics, with the assessment being predominantly based on existing knowledge rather than experimental evidence.

### 2.4.5 Scope for further research

Based on the findings discussed in Section 2.4.1, 2.4.2, 2.4.3 and the study limitations outlined in Section 2.4.4, the following research gaps were identified, providing scope for further research.

Firstly, a research gap remains in quantifying how a stepwise increase in leaky barrier complexity resembling more natural designs influences channel hydrodynamics and fish movement. Leaky barrier complexity may be achieved by using natural materials (e.g., twigs, logs) or 3D printed representations of wood can increase barrier complexity, mimicking more closely the characteristics of natural leaky barriers while maintaining controllability of barrier properties [75].

Secondly, a research gap remains to characterise the impact of overtopping flow on the near wake structure and turbulent structures generated immediately downstream of the leaky barrier which could not be measured due to the limitations of the ADV. High-fidelity simulations and advanced velocity measurement techniques (e.g., PIV) may be advantageous to unveil the instantaneous flow in such a region.

Another research gap remains in examining the impact of the high momentum primary jet influences weaker fish species (e.g., cyprinids) and younger life stages to prevent leaky barriers from becoming a flow barrier to fish movement. While fish may be capable to overcome one such high-momentum flow once, the repeated exposure to regions of high-momentum flow due to the presence of multiple leaky barriers along a

river stretch may result in an increase in energy expenditure and a delay in fish movement or prevent fish from reaching certain habitats. Consequently, further research is necessary, quantifying the cumulative impact of leaky barriers on fish movement and reach velocity to maintain habitat connectivity for all species present in the corresponding river. Moreover, a research gap remains in quantifying the interaction between primary jet and hyporheic exchange and the resulting impact on aquatic organisms and habitat. Besides the impact of the primary jet on fish movement, a research gap remains in quantifying the impact, if any, of the structure-dependent upper near wake ($z/b_0 \geq 1$) to better understand whether the upper wake may provide resting and nursing areas or presents a challenge for fish swimming stability.

Although leaky barriers are primarily used as a nature-based solutions for flood risk management, they could also serve as selective barriers to river longitudinal connectivity due to their impact on fish spatial usage and upstream passage. Hence, these barriers may limit the movement and spread of INNS, such as rainbow trout, while ensuring connectivity for desired, native species [180]. So far, rainbow trout have struggled to successfully establish populations in the majority of the UK rivers, although this may not continue to be the case with climate change [66]. Further research is needed to investigate the use of leaky barriers as selective barriers. This may include the understanding of species-specific differences and therefore, the deployment of specific barrier designs to allow selective passage; for example, the reduction of gap height to exclude larger species to create a physical barrier or decreasing barrier porosity to achieve a stronger primary jet velocity to create a velocity barrier.

Moreover, further research is required to quantify the observed floodplain flow, including inundation depth, infiltration, hydrodynamics, and transport processes associated with the overbank flow. While overbank flow may lead to floodplain erosion, bankside erosion may be a result of the primary jet generated beneath the leaky barriers. Further research, however, is required to examine the impact of the high-momentum flow on bankside erosion in relation to $b_0$. Bankside erosion, in turn, may influence

the structural integrity of the barrier. Downstream displacement of such structures may have detrimental impact when accumulating on retention racks or bridge pier, causing rather than preventing flooding [157]. Key barrier members, therefore, should be restrained using anchors and ballast [204] and a log length of minimum width of the channel [131] is recommended for the construction of leaky barriers. Further research investigating lift and drag forces acting on the barrier structure may be beneficial to estimate structural resistance under varying flow conditions as unsteady flow conditions were found to increase forces two to three times compared to steady flow conditions [204].

Finally, as logjam have been found to enhance habitat quality and diversity, a research gap remains in exploring the potential of engineered leaky barriers to contribute river restoration.

## 2.5   Conclusion

The impact of five idealised physical leaky barrier designs was investigated under bankfull and near-bankfull flow conditions using small-scale, laboratory experiments. Key design parameters investigated included barrier length, dowel arrangement, porosity, and barrier colour.

Upstream and downstream channel hydrodynamics were investigated for all leaky barriers through ADV measurements and dye visualization. The results show that upstream flow was diverted towards the lower gap ($b_0$) between the bed and barrier's lower edge, creating a primary jet whose strength varied with physical leaky barrier design. Jet local maximum velocities were maintained until a downstream distance of $4b_0$ before rapidly decaying with an average wake decay coefficient of $3.0\pm0.5$. The upper wake was structure-dependent, featuring smaller secondary jets for all porous leaky barriers with distinct flow paths (LB2-3, LB5-6), particularly pronounced for the short barrier structures (LB5-6) that resembled the flow around cylinders. Quad-

rant analysis of turbulence fluctuations immediately downstream of the leaky barriers revealed that inward-outward events dominated over the shear layer at the lower end of the structure, with its magnitude being lowest for the more porous design. In fact, increasing barrier void ratio led to more steady wakes with lower turbulence kinetic energy and shear stress levels. Therefore, near wake decay was dependent on physical design parameters while far wake decay was self-similar, resulting in almost full flow recovery at downstream distances of $35b_0$ and $50b_0$ for LB1-5 and LB6, respectively. A comparison between near-bankfull (80 %) and bankfull (100 %) flow conditions showed a lower maximum mean streamwise velocity downstream of the porous (LB2) and non-porous leaky barriers (LB1) under 100 % bankfull discharge due to the observed overbank flow in the this case. Hence, physical leaky barrier design strongly influences upstream and downstream hydrodynamics and therefore, for instance, floodplain inundation, sediment transport processes, bank erosion, structure stability, and fish movement behaviour. Therefore, the physical leaky barrier design should be chosen with care to maximise overbank flow and flood plain inundation to mitigate the risk of flooding while preventing adverse impacts on the aquatic habitat or becoming a flow barrier to fish movement. A flow barrier, for instance, may be prevented by increasing the vertical gap width or leaky barrier porosity, lowering the maximum primary jet velocity depending on species preference.

A preliminary experiment investigating the impact of a porous (LB2) and non-porous (LB1) leaky barrier structure on juvenile Atlantic salmon movement under bankfull and near-bankfull discharge showed that barrier porosity, rather than discharge, was the decisive component impacting fish movement and spatial preference. More fish underwent upstream passage for the non-porous design compared to its porous counterpart, highlighting the importance of physical leaky barrier design. In a second study, juvenile rainbow trout response to a larger range of leaky barrier designs was investigated under bankfull discharge, including a non-porous (LB1), two long-porous (LB2-3), and a short porous (LB5) leaky barrier structure. A decrease in porosity and longitudinal barrier length positively influenced the number of upstream passing fish and

the number of upstream passes per fish. Leaky barrier colour rather than wake hydrodynamics was the decisive parameter in terms of upstream passage in the case of the non-porous barrier, highlighting the use of colour as a visual cue. Spatial usage did not depend on leaky barrier design as in all cases fish spent more time downstream. Based on these results, leaky barrier presence is likely to reduce fish upstream passage and increase time spent downstream. Barrier presence, however, did not prevent fish from moving between downstream and upstream sections if a gap between the bed and barrier is maintained. Maintenance might be required to prevent the gap from blocking and gap size should be amended according to the largest fish species present. Leaky barrier length may be amended to increase or decrease shade and cover depending on species preferences. Colour, in contrast, might be used to increase upstream passage. Targeted modification of the physical design of leaky barriers, for instance, may not only mitigate flood risk but also be used as a tool to adapt habitat suitability depending on species present [198]. To prevent leaky barriers from becoming a physical barrier or flow barrier to fish movement, periodic maintenance and monitoring, especially during migration time is recommended.

Both hydrodynamic and fish behaviour results expand the current state of knowledge on engineered leaky barriers and support the delivery of leaky barriers as environmentally friendly hydraulic structures used for natural flood management. More specifically, the findings provide a better understanding of the impact of physical barrier designs on channel hydrodynamics. Furthermore, both fish studies highlight the importance of incorporating barrier porosity, longitudinal barrier length, and colouration into the design process. Using this knowledge, leaky barriers may also be modified to act as selective barriers to longitudinal river connectivity and thus, limit the spread of invasive non-native species. Both, hydrodynamic and fish studies, together with further research, may play an important role in the design and delivery of engineered leaky barriers as sustainable, green, eco-friendly hydraulic structures used for natural flood management while ensuring the mitigation of flooding, maintaining habitat, and enhancing habitat connectivity for aquatic organisms.

## 2.6 Chapter acknowledgement and contributions

Prior to the submission of this thesis, parts of this chapter have been published or submitted for publication. Details of the contributions of co-authors and persons involved in the experiments are outlined below:

The experimental investigation of upstream and downstream hydrodynamics has been submitted for publication to Water Resources Research as: **Müller S., Follett, E. M., Ouro P., Wilson C., Influence of engineered logjam structures on channel hydrodynamics**. Conceptualisation of this experiment was done by C. Wilson, E. Follett and S. Müller. Data were collected and curated by S. Müller (LB1-3, LB5) and E. Follett (LB4, LB6). Data were analysed and visualised by S. Müller, E. Follett (Figure 2.16 and corresponding text) and P. Ouro. The original draft was created by S. Müller and E. Follett (Section 2.3.1.3.2) and reviewed and edited by all authors.

The impact of 80 % and 100 % bankfull discharge presented in Section 2.3.1.4 was published as: **Müller S., Wilson C., Ouro P., Cable J. (2021) Leaky barriers: leaky enough for fish to pass?, R. Soc. Open Sci., 8: 201843, doi: 10.1098/rsos.201843**. The methodology for this section was done by S. Müller and C. Wilson, measurements and data visualisation was undertaken by S. Müller, with results interpreted by S. Müller, C. Wilson and P. Ouro. This section was originally drafted by S. Müller, and reviewed and edited by all authors.

Hydrodynamic measurements were also supported by Yin Lok Kwan and Ana Pinto Oliveira.

Fish behaviour studies analysing juvenile Atlantic salmon and juvenile rainbow trout response to leaky barrier design were published as: **Müller S., Wilson C., Ouro P., Cable J. (2021) Leaky barriers: leaky enough for fish to pass?, R. Soc. Open Sci., 8: 201843, doi: 10.1098/rsos.201843** and **Müller S., Wilson C., Ouro P., Cable J. (2021) Experimental investigation of physical leaky barrier design implications on**

*Chapter 3*

# Emerging migration barriers - part II: Vertical axis turbines wake hydrodynamics and impact on fish movement

## 3.1 Introduction

To date, almost 800 Million people lack access to affordable, reliable, sustainable energy supply, resulting in social-economic inequality [149]. By 2030 the UN Agenda for Sustainable Development aims to reduce this injustice by ensuring universal access to clean energy through increasing the renewable energy share [149]. A particular focus lies on low-middle income countries, small islands, and land-locked countries, often consisting of numerous remote communities, yet without access to clean energy, [149]. These countries often feature high biodiversity that needs protecting and conserving. Hence, clean energy solutions need to be chosen with care to prevent habitat loss and degradation. In 2019, the estimated share of global electricity production, however, still comprised of 73 % non-renewable electricity and only 27 % of renewable energy [185]. Amongst the renewable energy share, hydropower (not including ocean power) accounted for almost 16 % of global electricity generation [185]. Yet, the

full hydropower potential is untapped, likely caused by the ongoing conflict between the hydropower industry and conservationists.

### 3.1.1 Environmental impact of traditional and hydrokinetic hydropower schemes

#### 3.1.1.1 Environmental concerns associated with traditional, small and large-scale hydropower plants

Despite the long-reaching tradition of small and large-scale hydropower plants and their ability to cover the baseload (i.e., electricity constantly required) and balancing power (i.e., electricity to cover variations in energy demand), the concerns regarding their environmental impact have steadily been growing.

One concern associated with traditional hydropower plants is their impact on river continuity. Due to the requirement of a difference in head to convert potential energy into electrical energy [97], hydraulic structures such as weirs and dams are needed. These structures cause the interruption of the river continuum [1], not only influencing the movement of fish and other aquatic organisms but also interrupting the transport of material such as sediment, particulate matter, and nutrients [1, 13].

While river continuity can be reinstated through the construction of bypass channels and fish passes, further concerns are the reduction of flow between the abstraction and release point [1] and the rapid fluctuations in discharge and flow depth. These short-term fluctuations are referred to as hydropeaking [22] and can affect fish throughout all life stages [89]. Changes in flow availability tremendously influence habitat availability and quality [13]. Moreover, the rapid release in water increases the transport of suspended matter and enhances water turbidity, which may negatively impact fish spawning and other behaviour [1]. Besides the suspension of particulate matter, rapid water releases may also resuspend concentrated pollutants, which decreases water quality [1].

While in times of low water release river stretches may dry out (i.e., reducing habitat availability), periods of rapid water release (although increasing habitat availability) may cause bank erosion, further increasing suspended solids and widening rivers [1]. Alongside these described habitat alterations, alterations in flow availability associated with hydropower plants may also reduce resident and migratory species and replace native species with INNS [1]. Variations in flow may superimpose flow cues important for fish migration, delaying or even preventing them from completing their lifecycle [13]. Due to the increased understanding of these impacts, regulations have been put in place, ensuring a minimum requirement of flow [89]. Moreover, seasonal flow regulations have been suggested, for instance, including the relatively constant release of water during migration and spawning periods and the determination of a maximum discharge released to avoid the deterioration of spawning grounds during intra-gravel life stages [89].

Another concern associated with traditional hydropower schemes is the increase in fish mortality caused by fish entering the turbine [156, 97, 169]. Primary mechanisms identified to cause fish injury and mortality associated with conventional hydropower plants include, for instance, high levels of shear and turbulence, rapid pressure changes, cavitation, and the collision with the leading edge of turbine blades [97, 176]. Experiments analysing fish injuries associated with turbine passage at a small-scale hydropower plant in Germany, equipped with a Kaplan turbine, identified tears in fins and loss of scales to be the most frequent injuries observed [143]. Further injuries included haemorrhages, dermal lesions, partial amputation of fins, pigment anomalies, and bruises [143]. Less common were emboli in eyes and fins, amputation of body parts, and spinal deflections [143]. Depending on the severity, such injuries may only mildly impact fish or cause severe stress and even mortality. Differences in injuries are often related to fish body morphology, length, and life stage, and turbine type [176]. To reduce fish tests, the impact of hydropower turbines on various fish species have been quantified using a range of probabilistic, numerical, and empirical models (e.g., [187, 88]). Furthermore, innovative approaches to reduce animal testing include, for

instance, the use of autonomous sensors [56].

Due to the importance of traditional hydropower plants to meet the increasing energy demand, great effort has been undertaken in guiding fish away from turbine intakes [168], protecting them from entering the powerhouse using exclusion screens [217]. In addition, greater focus has been given to the development of innovative technologies, allowing fish to descend through the turbine (mainly applicable for low-head hydropower plants) [155, 147, 171], and hydrokinetic turbines due to their presumed lower environmental impact.

### 3.1.1.2   Environmental concerns associated with hydrokinetic turbines

Hydrokinetic turbines, in contrast to conventional hydropower schemes, do not require partial or channel-spanning hydraulic structures to divert flow and generate a head difference [97]. Extracting energy from the free-flowing flow offers the benefit of preserving longitudinal river continuity and allows fish to avoid these structures by swimming around them as they would with other riverine and marine obstructions (e.g., boats, piers) [97, 229]. Despite these advantages of hydrokinetic turbines over traditional hydropower plants, there are still concerns regarding their impact on the aquatic environment.

Due to the installation of hydrokinetic turbines within the free-stream, fish are not protected from encountering these structures, which increases the risk of aquatic animals colliding with the turbine's blades and structure or becoming entangled in underwater cables [37]. Strike risk and associated injuries, however, are presumed to be minor as a result of the comparable low rotational turbine speed and the possibility of fish to detect, evade, and avoid the turbine [97]. Scaled, laboratory studies of horizontal and vertical axis turbines confirmed a low risk of fish collision, having observed no or a low number of strikes, none of which caused injuries [24, 248].

Further concerns regarding the deployment of hydrokinetic turbines include the use of

paints, cleaning materials, hydraulic fluids, and chemicals to control biofouling and their potential toxicity to aquatic vegetation and animals [37]. Use of these materials requires further research, particularly focusing on suitable biodegradable products. Uncertainty also exists in connection with the emission of electromagnetic fields and whether these may attract, deter or even injure aquatic life [37]. Noise from the generator presents another potential stressor, influencing aquatic organisms [37, 48].

Another concern associated with hydrokinetic turbines is how fish behaviour might change in response to wake hydrodynamics [37]. Field studies of marine hydrokinetic turbines, for instance, reported the accumulation of certain fish species and marine mammals around such devices [229, 31, 74, 240]. Fraser et al. (2018), for example, highlighted an increase in the number of fish at the lower part of the water column, particularly under high flow conditions (i.e., flood phase), indicating that fish might benefit from the low-momentum regions downstream of such devices [74]. Besides hydrodynamic alterations associated with these structures, other environmental variables that might influence fish attraction include light conditions, water depth, flow direction, discharge, temperature, predator-prey availability, as well as the provision of spawning and nursing locations [31]. The attraction of fish to turbines and their support structures, in turn, is presumed to increase predation risk [74, 240] as well as fish collision risk due to potential flight responses [240].

### 3.1.2 Vertical axis hydrokinetic turbines

Based on the significant impact of traditional hydropower schemes on the aquatic environment and the advantages provided by hydrokinetic alternatives, there is increased interest to improve vertical axis turbines (VATs). A particular focus has been given to the enhancement of the rotor's efficiency and deploying VATs in multi-turbine arrangements (e.g., twin-VAT) to take advantage of flow acceleration due to blockage effects of closely located turbine rotors (e.g., [52, 114]). VATs offer a wide range of mechanical and hydrodynamic advantages compared to HATs. Their vertical rotational axis,

for instance, allows positioning of the generator and other heavy components on the ground or a floating platform, which diminishes their technical complexity compared to HATs and improves their suitability to river applications [110].

From an operational point of view, the relatively low rotational speed and rectangular cross-section that maximise the swept rotor area in constrained shallow waters make VATs particularly suitable for rivers and estuaries with low-to-medium flow velocities [110]. VATs operate independently of the flow direction, i.e., they are omnidirectional; hence, no yaw-angle correction and alignment with the flow direction are needed. Subsequently, these unique operational characteristics also have the advantage of potentially reducing the environmental impact by operating at lower rotational speeds than HATs.

### 3.1.2.1   Impact of VAT on fish behaviour

So far, only a few studies have examined the impact of VAT on fish, with the majority of these studies conducted under controlled, laboratory conditions [42, 137, 24] rather than in the field [87].

While most studies highlighted no or low risk of fish collision and mortality [87, 42], which may be associated with the low rotational speeds and open design of the turbine rotor, the presence of VATs influences fish movement. Benthic reef fish and larger predators, for instance, avoided moving closer than 0.3 m and 1.7 m away from the rotor, respectively, for a VAT turbine deployed in a confined marine environment [87]. Similarly, brown trout were less likely to pass around the turbine, subsequently showing avoidance behaviour and awareness of the turbine [24]. Like individual fish, fish change shoaling behaviour in the presence of a VAT [137]. For instance, fish spent approximately 46 % more time shoaling when the turbine was stationary rather than rotating [137]. Behavioural adaptations, however, are rarely investigated in the context of flow alterations. Only Berry et al. (2019) reported that fish preferred the high-momentum regions on either side of the turbine compared to the low-momentum area

of the turbine's wake [24]. Therefore, further research is required to understand the influence of the turbulent structures and wake characteristics on fish movement.

### 3.1.2.2  Wake alterations associate with single VAT and twin-VATs

The wake developed by a single VAT has been extensively studied through small-scale experimental testing in open channels (e.g., [15, 17, 32, 162, 209]), wind tunnels (e.g., [186, 219, 226]), and high-fidelity numerical simulations (e.g., [3, 118, 159, 175, 174, 202]), with only a handful of full-scale devices tested in field campaigns (e.g., [52, 113]).

Based on the observations from these studies, the primary regions developed in the wake of a VAT in an open-channel are depicted in the schematic presented in Figure 3.1, which outlines three distinct regions, namely the near-wake ($x/D \leq 2$), transition zone ($2 \leq x/D \leq 5$), and far-wake ($x/D \geq 5$) [162], with $x$ indicating the streamwise location and $D$ being the turbine diameter.
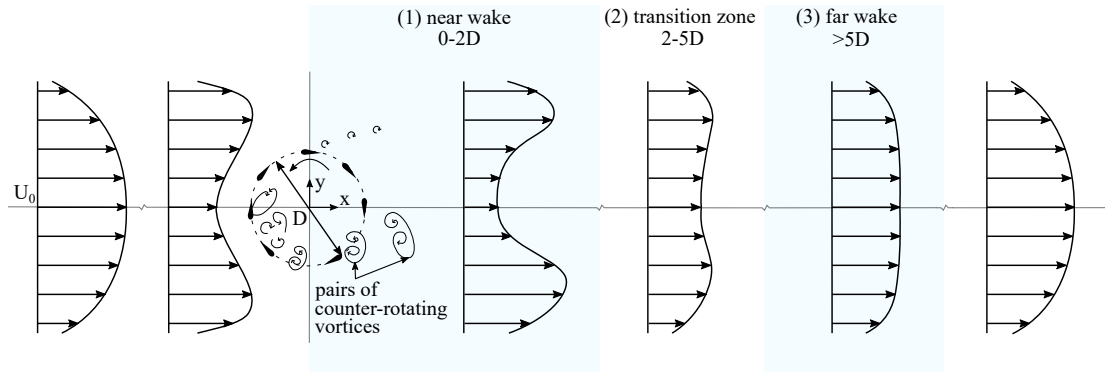


**Figure 3.1:** Wake evolution of a single, counter-clockwise rotating VAT of diameter $D$, consisting of three distinct regions [162]: (1) a near-wake region ($x/D \leq 2$), characterised by a low-momentum region laterally bounded by shear layers that result from the advection of two pairs of counter-rotating vortices over the downstroke side and smaller vortices over the upstroke side; (2) a transition zone ($2 \leq x/D \leq 5$); and (3) a far-wake region ($x/D \geq 5$) characterised by wake recovery. Flow from left to right. Figure adapted from [32].

The near-wake region is characterised by turbine-induced flow structures, such as two counter-rotating vortices shed by the blades when undergoing dynamic stall during the downstroke phase [32]. The coherent turbulent structures generate a shear layer that isolates the low-momentum region developed in the near-wake core from the high-velocity region outside the wake, thus limiting entrainment of the surrounding flow [162]. The blades experience lower flow separation over the upstroke rotation as their relative velocity is larger than during their downstroke motion, which also prevents deep dynamic stall [159]. The shedding pattern of these turbulent structures depends on the tip-speed ratio, i.e., the relative blade velocity to that of the approaching flow. This unevenly generated flow during the downstroke and upstroke motion of the rotor blades can render the near-wake asymmetric about its centreline (e.g., [32, 186, 202, 219]). Within the transition zone, the wake starts to vertically and laterally expand with a larger ambient turbulent flow entrainment that increases the turbulent fluxes and intensity, and momentum begins to recover at a faster rate [162]. In the far-wake region, the core momentum further recovers with increasing downstream distance until it eventually reaches a mean velocity value similar to that of the free stream flow at distances that vary with the turbine's aspect ratio and dynamic solidity (e.g., [15, 160]).

To unfold the full potential of VATs, there remains a need for a detailed understanding of wake hydrodynamics of multiple VATs to identify their optimal arrangement and thus, maximise the harnessed kinetic energy when deployed in arrays [212]. The pilot wind-energy project FLOWE [52, 113], for instance, showed that VATs could achieve a higher power density than HATs when deployed in twin-configurations. To date, VAT wake interactions have been studied mostly for side-by-side twin-turbine setups, mainly focusing on the turbines' rotational direction [173, 226] and less on the shaft-to-shaft lateral spacing and relative alignment to the incident flow direction [119, 226, 250].

Figure 3.2 depicts twin-VAT setups with devices co-rotating or counter-rotating forward and backward, corresponding to cases in which blades move with or against
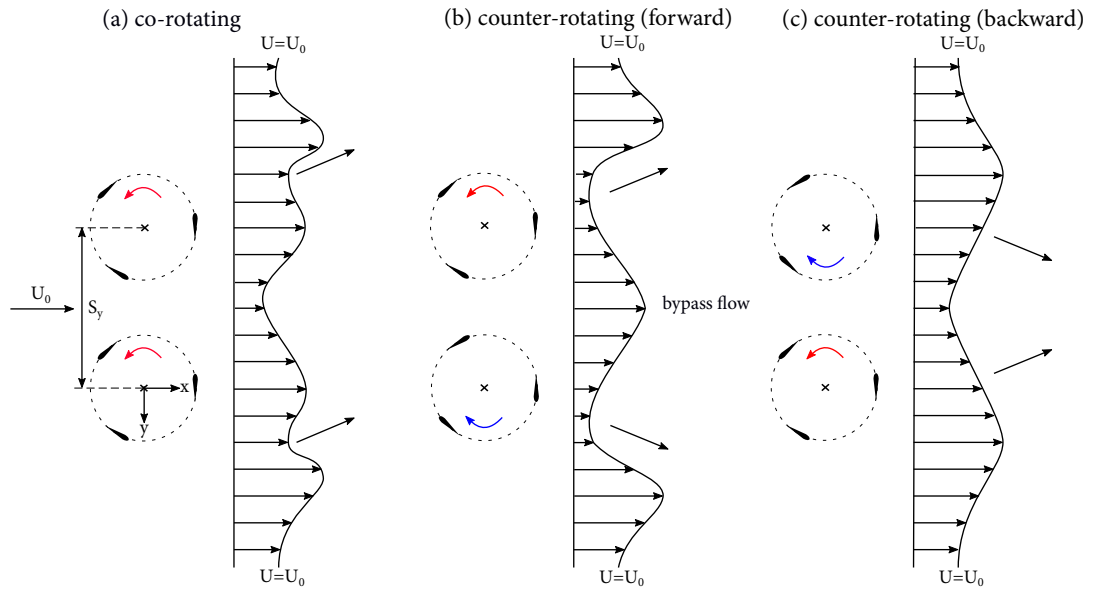
**Figure 3.2:** Wake interaction of three twin-VAT arrangements varying in rotational direction, laterally spaced by $S_y$, namely (a) co-rotating, (b) counter-rotating forwards, and (c) counter-rotating backwards.

the flow direction in the bypass region. Comparison of the wake evolution for these configurations shows that the individual wakes of co-rotating VATs (Figure 3.2 (a)) evolve independently in the downstream direction, with a reduced interference in the near-wake [119]. These wakes start to interact with each other and partially merge at a downstream distance that depends on the relative shaft-to-shaft separation ($S_y$) [173]. In contrast, the individual wakes of two turbines rotating in counter-rotating forward direction (Figure 3.2 (b)) spread outwards in an axisymmetric fashion, leading to laterally expanded wakes that progressively diverge with increasing downstream distance, creating a high momentum flow region between both turbines. Conversely, in the counter-rotating backward case (Figure 3.2 (c)), a prolonged combined wake is observed after the transition zone. Both individual wakes progressively move towards each other before merging and interacting [119]. This, in turn, results in a lower high-velocity bypass region [173] that varies with intra-turbine spacing, i.e. smaller

$S_y$ values result in a higher flow blockage within the bypass region that reduces the flow velocity in this area. The wake patterns observed for twin-VATs have been mostly characterised in the horizontal plane by two-dimensional simulations [99] with only limited experimental and numerical in-depth studies looking at the three-dimensional wake evolution for multi-turbine arrangements such as twin-VATs [119, 174, 226], providing scope for further experimental investigations.

### 3.1.3   Problem statement and chapter outline

The continuous increase in energy demand and current change in energy policy towards net-zero carbon economies is leading to the rapid expansion and development of new sustainable renewable energy technologies. To date, hydropower is one of the largest renewable energy sources [185] which has long been considered as an environmentally friendly and clean form of energy generation. The growing concern about the ecological impact of traditional hydropower projects [1], however, is propelling the development of innovative small-scale, low head solutions and hydrokinetic alternatives [18] such as vertical axis river turbines (VATs). While VATs provide a wide range of technical and environmental benefits compared to HATs, their main drawback remains a lower standalone performance. This, however, can be overcome by deploying two or more VAT rotors in close proximity [113]. Yet, there is still a lack of empirical evidence on the three-dimensional wake alterations associated with twin-turbines, and how turbine presence and the turbulent wake influences fish movement in order to increase the uptake of VAT as sustainable, environmental-friendly energy technology..

Through scaled laboratory experiments, a scaled single and a range of twin-VAT configurations were investigated in two open channel flumes at the Hydro-Environmental Research Centre's hydraulic laboratory at Cardiff University. This chapter explores

1. the impact of lateral spacing $(S_y)$ and rotational direction on the three-dimensional wake evolution of twin-VAT (Figure 3.2);

2. the impact of a single VAT on individual juvenile rainbow trout (*Oncorhynchus mykiss*) under confined spatial conditions for two discharges and two turbine operation states;

3. the impact of spatial confinement by comparing fish response to a single VAT in two flumes of different lateral spacing; and

4. individual fish swimming behaviour response to a single VAT in comparison to small shoals.

Based on the knowledge gained through the outlined research questions, this chapter contributes to the existing knowledge by expanding the understanding of the three-dimensional wake hydrodynamic, recovery and decay depending on rotational direction and lateral spacing; quantifying whether turbine presence and operation causes avoidance behaviour in fish; identifying whether spatial confinement on either side of the turbine may present a velocity or behaviour barrier preventing fish from passing the turbine; understanding whether individuals respond differently to turbine presence and operation compared to small groups of fish; and raising considerations when installing VAT in the field.

Section 3.2 provides an overview of the turbine configurations tested as well as the hydrodynamic measurement and fish behaviour methods applied. Subsequently, hydrodynamic and fish behaviour results are presented in Section 3.3. Results are then discussed in Section 3.4, considering potential primary and secondary implications on the aquatic ecosystem. Furthermore, this section outlines study limitations, management considerations, and highlights remaining research questions. Section 3.5 summarises the identified implications of vertical axis turbines on wake hydrodynamics and fish movement and places them into the context of using VAT as a sustainable energy solution and their ability to maintain longitudinal river connectivity.

## 3.2   Methodology

Downstream hydrodynamics and fish behaviour were investigated for a range of single and twin-vertical axis turbine configurations at the Hydro-Environmental Research Centre's hydraulics laboratory at Cardiff University. The following sections provide an overview of the turbines and experimental methods employed for the hydrodynamic and fish behaviour studies.

### 3.2.1   Model turbines

The adapted VATs used for the experiments, as shown in Figure 3.3, were manufactured with a rotor diameter $D$=0.12 m and height $H_{turbine}$=0.12 m, i.e. with an aspect ratio $H_{turbine}/D$ equal to unity. The rotor comprised three blades ($N_b$=3) that were 3D printed with laser-sintered PA 2200 material conforming to a NACA 0015 foil profile geometry with zero preset pitch angle, and 0.03 m chord length ($c$; i.e., length between leading and trailing edge), which yielded a geometric solidity $\sigma = N_b c/\pi D \approx$0.24. This non-dimensionless parameter ($\sigma$) may be used to ensure geometric similarity when comparing the experiments presented with other studies. DC motors (Nider DMN37K50G18A, DC 12V) were used in each turbine to impose a constant rotational speed ($\Omega$=58 rpm) for an optimum tip-speed ratio $\lambda$=1.9 [162]. Turbine design and optimum tip-speed ratio have been amended from previous experiments conducted at the Hydro-Environmental Research Center at Cardiff University [162].

Each blade was attached to a main circular shaft of 0.006 m diameter using two horizontal struts of 0.003 m diameter, attached at vertical positions 0.01 m away from the bottom and top tips of the blades; both components were made of stainless steel. The bottom end of the turbine shaft was connected to a bearing attached to the flume bed, leaving a clearance of 0.02 m to the bottom tip of the blades. The upper end of the shaft was connected to an encoder (Kübler, 5-30VDC, 100mA) that measured the rotational

speed.
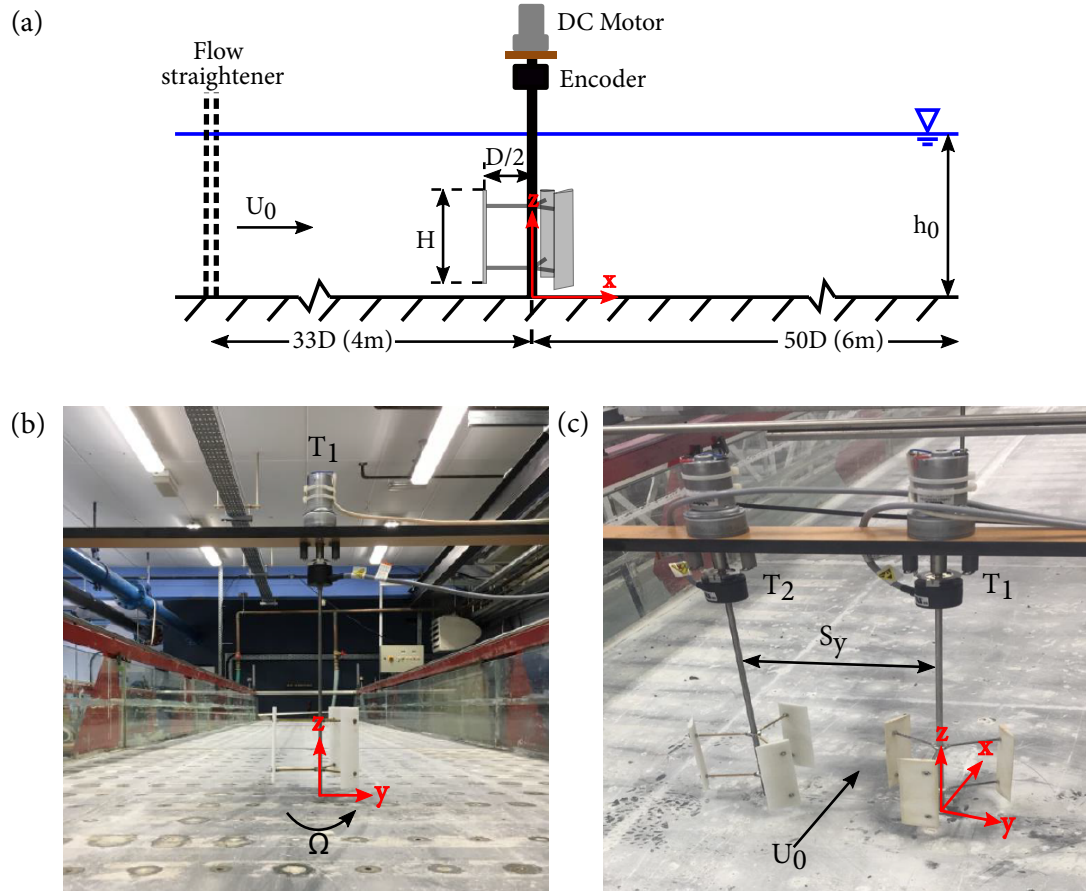


**Figure 3.3:** (a) Side-view schematic of the experimental setup, depicting the streamwise location of a single VAT of height $H_{turbine}$ and radius $D/2$, (b) cross-sectional photograph of the VAT $T_1$ located at the flume centre, $33D$ downstream of the flume inlet and rotating in counterclockwise direction, (c) cross-sectional photograph of twin-VAT setup comprising of VATs $T_1$ and $T_2$ laterally spaced by a distance of $S_y$. Photographs in (b) and (c) looking in downstream direction.

### 3.2.2 Hydrodynamic measurements

The three-dimensional wake hydrodynamics behind a single VAT and six twin-VAT setups varying in rotational direction and lateral turbine spacing were experimentally investigated using acoustic Doppler velocimetry measurements.

#### 3.2.2.1   Experimental setup

Hydrodynamic measurements were undertaken in a 10 m long, 1.2 m wide, and 0.3 m deep recirculating flume with a slope of 0.001 (denoted as Flume 1, as described in Section 2.2.1), with the experimental setup depicted in Figure 3.3. Flow depth and discharge were controlled by a pump and a tailgate weir which were located at the downstream end of the flume and kept constant throughout the experiment. Flow depth was measured using a Vernier pointer gauge with an accuracy of $\pm 0.1$ mm while discharge was measured with an ultrasonic flowmeter (TecFluid Nixon CU100) with a precision of $\pm 1.5\,\%$. Prior to the installation of the VAT, sub-critical uniform flow with a discharge of $Q$=0.053 m³/s and a flow depth of $H$=0.23 m were established. Further hydraulic parameters are presented in Table 3.1, including cross-section averaged bulk velocity ($U_0 = Q/A$), bulk Reynolds number ($Re = U_0 R_H / \nu$ with $\nu$ denoting the fluid kinetic viscosity and $R_H$ the hydraulic radius), Reynolds number based on turbine diameter $D$ ($Re_D = U_0 D / \nu$), and Froude number ($Fr = U_0 / \sqrt{gH}$).

**Table 3.1:** Details of hydraulic parameters adopted in the experiments, including flow discharge ($Q$), water depth ($H$), bulk velocity ($U_0$), bulk Reynolds number ($Re$), Reynolds number based on the turbine's rotor diameter ($Re_D$), and Froude number ($Fr$).

| Q | $H$ | $U_0$ | $Re$ | $Re_\mathrm{D}$ | Fr |
|---|---|---|---|---|---|
| [m³s⁻¹] | [m] | [ms⁻¹] | [-] | [-] | [-] |
| 0.0053 | 0.23 | 0.19 | $3.16 \cdot 10^4$ | $2.28 \cdot 10^4$ | 0.13 |

#### 3.2.2.2   Turbine set-ups

The seven investigated turbine setups are summarised in Table 3.2 and comprised one single VAT and six twin-VAT configurations, varying in rotational direction and intra-turbine spacing.

For the single turbine case (ST), a turbine, $T_1$, was placed 4 m downstream of the flume

inlet at the centre of the flume as shown in Figure 3.3 (b) and installed as described in Section 3.2.1. The position of $T_1$ was set as the coordinate origin, considering as positive $x$-coordinates the streamwise flow direction, the positive lateral ($y$) direction over the right-hand side of the flume, and the $z$-coordinates in the upward direction starting at the flume's bed. The ST case was conducted to characterise the individual wake of a VAT and used as a reference wake distribution for the comparison with the twin-turbine setups.

**Table 3.2:** Details of the single turbine test case (ST, $N_{turbine}$=1) and twin-turbine configurations ($N_{turbine}$=2), consisting of twin-turbines rotating in the same rotational direction (SR), counter-clockwise forward direction (CRF), and counter-clockwise backward direction (CRB), laterally spaced by $S_y/D$=1.5 or $S_y/D$=2.0. Turbines were tested for a discharge $Q$=0.053 m$^3$/s and flow depth $H$=0.23 m, and rotated at a constant rotational speed of $\Omega$=58 rpm.

| $N_{turbines}$ | $S_y/D$ | **Test case** | **Direction of rotation** | **Description** |
|---|---|---|---|---|
| 1 | - | ST | Counter-clockwise | $T_1$ anti-clockwise |
| 2 | 1.5 | SR–1.5 | Same rotational direction | $T_1$ and $T_2$ anti-clockwise |
| | | CRF–1.5 | Counter-rotating forward | $T_1$ clockwise and $T_2$ anti-clockwise |
| | | CRB–1.5 | Counter-rotating backward | $T_1$ anti-clockwise and $T_2$ clockwise |
| 2 | 2.0 | SR–2.0 | Same rotational direction | $T_1$ and $T_2$ anti-clockwise |
| | | CRF–2.0 | Counter-rotating forward | $T_1$ clockwise and $T_2$ anti-clockwise |
| | | CRB–2.0 | Counter-rotating backward | $T_1$ anti-clockwise and $T_2$ clockwise |

For the twin-turbine configurations, a second turbine, $T_2$, was placed at the same streamwise location as the first turbine with a lateral shaft-to-shaft separation of $S_y$, as indicated in Figure 3.3 (c). Two shaft-to-shaft intra-turbine spacings were analysed, including $S_y$=1.5$D$ and $S_y$=2.0$D$. For each lateral spacing, three turbine rotational

directions were tested as depicted in Figure 3.2, including:

(i) two turbines rotating in the same direction, hereinafter denoted as "same rotation" SR setup (Figure 3.2 (a));

(ii) two turbines rotating in counter rotating forward direction, i.e., in the bypass region, the blades of each turbine move in flow direction, hereinafter denoted as "counter-rotating forward" CRF setup (Figure 3.2 (b)); and

(iii) two turbines rotating in counter-clockwise backward direction, i.e., in the bypass region, the blades of each turbine move against the incoming flow, hereinafter denoted as "counter-rotating backward" CRB setup (Figure 3.2 (c))

### 3.2.2.3   ADV measurements

Hydrodynamic measurements were conducted using a side-looking Acoustic Doppler Velocimeter (ADV) (Nortek Vectrino). To ensure sufficient data quality and capture a representative sample of the high-frequency turbulence fluctuations characteristic for VAT wakes, sampling periods of 300 s (cross-sections at $x/D$=1.0, 1.5 and 2.0) and 180 s (cross-sections at $x/D$>2.0) were adopted with a frequency of 200 Hz. Signal quality was enhanced by seeding the water with spherical®110P8 hollow glass spheres (Potters Industries LLC) with a mean particle size 11.7 $\mu$m and specific gravity of 1.10 g/cc.

To characterise the approach flow conditions, one lateral cross-section was measured at 1 m upstream of the turbine (approx. 8 $D$). This cross-section comprised six vertical velocity profiles laterally spaced by 0.1 m, starting at $y/D$=0. Each velocity profile consisted of 20 measurement points vertically spaced by $\Delta z$=0.01 m (0.08 $D$), starting at 0.01 m above the flume bed until approximately 0.03 m below the water surface. Then, for each of the single and twin-turbine configurations, lateral cross-sections ($y - z$ planes) were measured at nine streamwise locations starting at 1$D$ and reaching until 10$D$ downstream of the turbine, as depicted in Figure 3.4 (a). Each cross-section

comprised 12 to 14 vertical velocity profiles in the lateral direction for the single and twin-turbine setups, respectively. Lateral spacing between vertical profiles was 0.05 m (0.42 $D$) (ST: -1.25$\leq y/D \leq$1.25, twin-VATs: -1.25$\leq y/D \leq$7.92), and increased to 0.1 m (0.83$D$) within the free-stream region, as shown in Figure 3.4 (b).
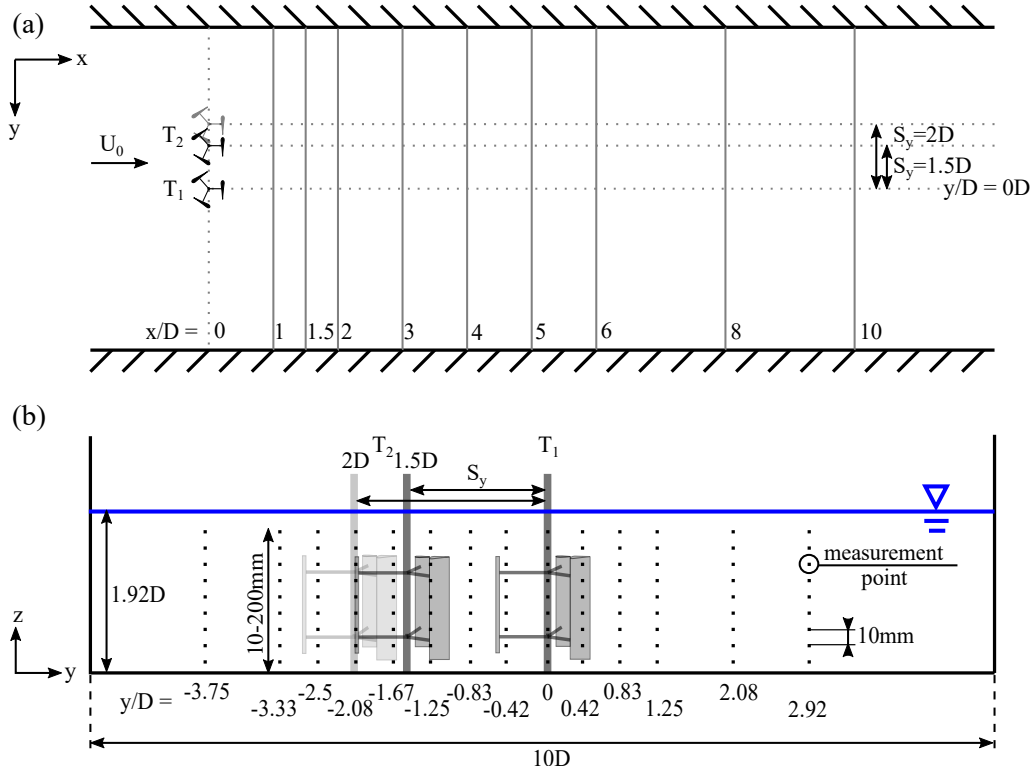


**Figure 3.4:** ADV wake measurement locations, showing (a) locations of cross-sections ($y - z$ plane) measured in streamwise direction, starting at 1$D$ and until 10$D$ downstream of the turbines, and (b) lateral distribution of the vertical measurement profiles over the flume section.

Velocity data were filtered and post-processed using Matlab (2019a). Data with SNR $\leq$15 % and COR $\leq$70 dB were removed from the data set, after which data were despiked using an open-source toolbox [141, 140]. The instantaneous filtered velocity vector $\boldsymbol{u} = (u, v, w)$ record was then divided using the Reynolds decomposition: $\boldsymbol{u}(t) = \overline{\boldsymbol{u}} + \boldsymbol{u}'(t)$, with the time-averaged operation denoted as $\overline{(\cdot)}$ and the fluctuating components represented as $(\cdot)'$. Normalised turbulence statistics were computed

in terms of streamwise turbulence intensity ($u'/U_0 = \sqrt{\overline{u'u'}}/U_0$), turbulent kinetic energy ($tke = 0.5(\overline{u'u'} + \overline{v'v'} + \overline{w'w'})/U_0^2$), and Reynolds shear stresses ($\overline{u'v'}/U_0^2$ and $\overline{u'w'}/U_0^2$). Cross-sectional plots are presented normal to the flow (y-z-plane) and looking in the downstream flow direction.

### 3.2.3   Fish behaviour

Fish swimming behaviour experiments were undertaken following completion of the hydrodynamic measurements and extensive cleaning of the flume to remove ADV seeding material. Fish behaviour studies were approved by Cardiff University Animal Ethics Committee and conducted under Home Office License PPL 303424 following ARRIVE guidelines [111].

#### 3.2.3.1   Fish maintenance and holding facilities

Before and after the experiments, fish were held in in 60-80 l tanks of approximately 40-50 fish each within a Recirculating Aquaculture System (RAS) at the Cardiff University Aquarium, enclosed within a temperature-controlled room maintained at $14\pm0.5$ °C on a 12h:12h dark-light cycle. This system has integrated bag and drum filters (Pall Cooperation) as well as a plastic bio media in the sump tank and an UV sterilization system. Water temperature and oxygen level were constantly monitored while nitrite levels were tested weekly, using a water quality test kit (Nutrafin). Fish were fed commercial trout pellets every morning.

Prior to the start of the experiments, fish were transported to a temporary holding tank at the hydraulic facilities at Cardiff University. At least one day recovery was provided from the approximately 20 min transport. This holding tank consists of 500 l dechlorinated water (Seachem Prime Concentrated Conditioner, Tetra AquaSafe), constantly recirculated and chilled to $13\pm1$ °C (D-D The Aquarium Solution, DC 750) with an external filter (Aquamanta, EXF 600). The tank was aerated by multiple external air

pumps (e.g., Tetratec Aps 400). Due to the manual operation of the ambient light, fish were maintained on a 14h:10h dark-light cycle. Depending on the experiment, fish were either maintained free swimming within the tank or in floating mesh cages.

All tanks and cages within the Cardiff University Aquarium and the hydraulic facilities were equipped with environmental enrichments to provide refugia (e.g., plant pots) and minimise stress. Particular care was taken to minimise stress when handling and transporting fish between facilities and tanks.

### 3.2.3.2    Experimental setup and procedure

A first set of experiments was conducted in a 10 m long, 0.3 m wide and deep recirculating flume with a longitudinal bed slope of 1/1000 (hereafter denoted as Flume 3 and referred to as "confined spatial condition"; Figure 3.5 (a)). A single VAT (Figure 3.5 (c)) of similar properties as described in Section 3.2.1 was placed approximately 4.4 m downstream of the flume inlet. To connect the shaft with the flume bed, a PVC board of approximately 10 mm thickness was attached to the flume bed, allowing the integration of a bearing to connect the turbine.

Additional experiments were conducted in a flume of 10 m length, 1.2 m width and 0.3 m depth, with same bed slope (hereafter denoted as Flume 1 [F1] and referred to as "unconfined spatial conditions"; Figure 3.5 (b)). As in Flume 3, a VAT of similar dimensions and rotational direction was placed approximately 4.4 m downstream of the flume inlet within the lateral centre of the flume. The Reynolds scaling law was used to scale the bulk velocity to allow comparability between tests and preserve the same turbulent wake structure as found in Flume 1.
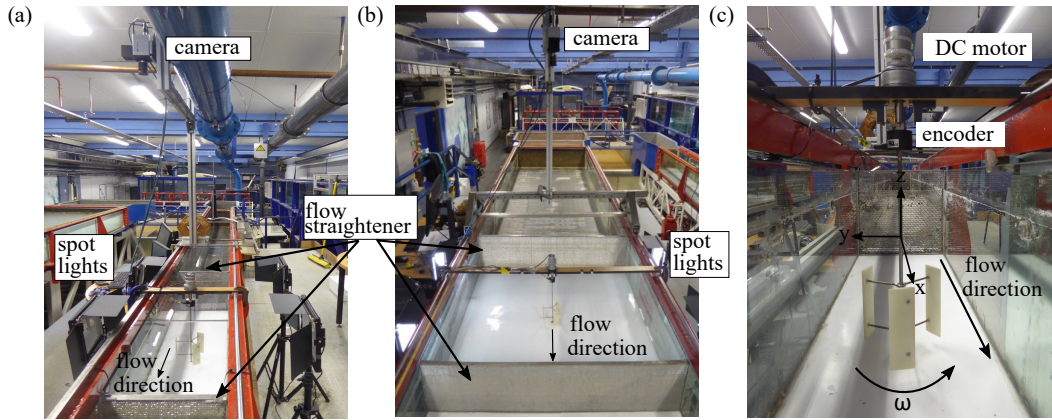
**Figure 3.5:** Photograph of the experimental setup in Flume 3 (a) and Flume 1 (b), depicting the streamwise location of a single vertical axis turbine of diameter $D$. The vertical axis turbine, shown in (c) was located within the lateral centre of the flume approximately 4.4 m downstream of the flume inlet, rotating in counter-clockwise direction; all photographs looking in upstream direction.

Experiments were conducted for two flow conditions: denoted as "mild" (**M**; $Q$=0.013 m$^3$/s; $H$=0.23 m) and "high" (**H**; 0.017 m$^3$/s; $h$=0.23 m), and two turbine operational states: denoted as "stationary" (**S**; 0 rpm) and "rotating" (**R**; 58 and 75 rpm for 0.013 and 0.017 m$^3$/s, respectively). For both flow conditions, the VAT operated at an optimum tip speed ratio of 1.9 [162]. Discharge ($Q$) and flow depth ($h$) were regulated by a pump with 0.03 m$^3$/s capacity, and a tailgate weir at the downstream end of the flume, respectively, and kept constant throughout the experiments. Flow depth was measured using a Vernier pointer gauge with an accuracy of $\pm$0.1 mm, and discharge was measured with an ultrasonic flow meter (TecFluid Nixon CU100) with $\pm$1.5 % precision.

To enhance the contrast between fish and flume bed, a white PVC plate was glued into both flumes using silicon adhesive. Both test sections were illuminated by two spotlights (Neewer Bi-Colour LED) positioned on either side of the test section, to minimise shaded areas and ensure equal light distributions. All experiments were conducted under ambient light conditions comprising of LED lights mounted on the room

ceiling.

To monitor fish swimming behaviour a camera (Baumer) was mounted above the flume, recording monochrome series of tif images of size 600x2352 pixel and 2048x2000 pixel at approximately 80 fps and 55 fps for Flume 3 and 1, respectively. A 10 mm thick clear, transparent perspex plate was mounted on top of the water surface to prevent reflections from the light. Additionally, a GoPro Hero camera (version 5, 7 and 9; 60 fps, 1080x1920 pixel), positioned on the left-hand side of the flume and mounted on a tripod, was used to simultaneously record the side view of the test section.

On the test day, fish were introduced into the flume at the centre of the furthest downstream end of the test section and given a 20 min acclimatisation period. During this time, fish were allowed to explore the whole of the test section, while experiencing a 5 min incremental increase in discharge over the first 10 min up to the test discharge level (mild=0.013 m³/s, high=0.017 m³/s), followed by a 10 min acclimatization at the test discharge. At all times, the downstream tailgate weir remained fixed at a predetermined height, set for the uniform flow condition. After the acclimatisation, fish were caught using a fishing net and the perspex plate was mounted on top of the water surface. Then, fish were re-released at the most downstream end of the test section at the centreline of the main channel. Each trial lasted 10 min and 30 s. The additional 30 s were added to the recording to account for the handling and release of the fish as well as the cleaning of the perspex plate at the beginning of each trial and were excluded from the analysis, resulting in a total analysis time of $T$=600 s.

During the tests, human intervention was avoided if possible and only took place when fish impinged the downstream flow straightener, which often happened immediately after the release and within the first 30s used to setup the trial. In this case, fish were carefully encouraged to swim or removed from the flow straightener by tapping against it. In the case of repeated impinging of the flow straightener, the experiment was terminated, and fish were removed from the test section and the analysis (indicted by

number of excluded fish $N_{excluded}$).

During the test, the following parameters were recorded and analysed:

**(i) Spatial usage**

To analyse the spatial usage of the test section, each image series was converted into a video which then was analysed using JWatcher v.1.0. The test section was divided into 30 and 70 quadrants for Flume 3 and 1, respectively. These quadrants were equally distributed between the upstream and downstream region, as depicted in Figure 3.6.
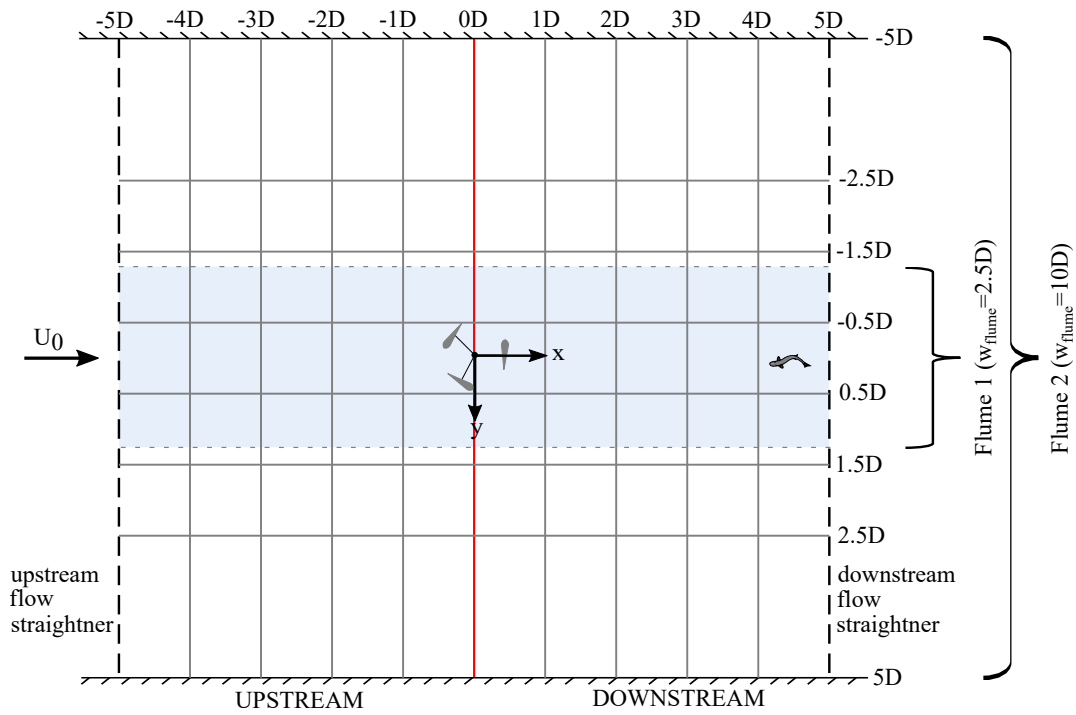


**Figure 3.6:** Subdivision of the test section in Flume 3 and Flume 1 used to analyse the spatial use. Flume 3, highlighted in light blue covers 1/4 of the lateral area of Flume 1 and consists of a longitudinal length of $10\,D$ and a lateral length of $2.5\,D$. In contrast the test section used in Flume 1 was $10\,D$ long and $10\,D$ wide. For the single fish tests, a turbine ($T_1$) was positioned in the centre of the test section and marks the point of origin for our coordinate system. For the group tests, a second turbine of similar characteristics was placed at a lateral spacing of $S_y$=$1.5\,D$ towards the left-hand side of the flume when looking into the downstream direction.

For each quadrant, the time spent ($t_{spent}$) was manually logged and the percentage of the total analysed time ($T = 600s$) was calculated.

Table 3.3 provides an overview of the parameters determined based on the percentages of time recorded, including percentage of time spent upstream and downstream of the turbine, in the centre, left and right-hand side of the downstream section, immediately upstream of the turbine (here termed bow-waking), and in and outside of the turbine's vicinity (here termed avoidance and attraction, respectively). It should be noted that the area over which the time spent near the turbine (attraction) and away from the turbine (avoidance) was calculated was scaled accordingly to account for the increase in lateral space in Flume 1.

**(ii) Distance and swimming velocities**

Fish position was extracted using Kinovea v0.8.15, a semi-automatic, open-source tracking software [45]. Due to the high susceptibility to errors (e.g., shaded areas, fish swimming close to flume walls, particles drifting through the test section), videos were created using a reduced frame rate of 2 fps and 1 fps for Flume 3 and 1, respectively, to reduce such errors through manual correction of the frames. For each frame, streamwise ($x$) and lateral ($y$) position of the fish was recorded and extracted from the software. Then, data were analysed using MS Excel and Matlab 2019a,b and 2020a. Prior to the analysis, the extracted fish positions were calibrated to account for image distortion. Based on the corrected coordinates, the total distance covered ($\overline{s}$) by each fish was estimated using the Pythagorean theorem. Similarly, the mean distance between fish and turbine ($\overline{s}_{turbine}$) was estimated over time.
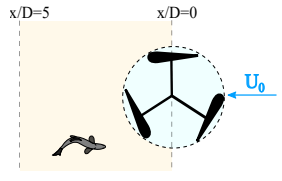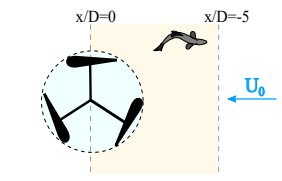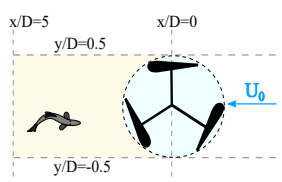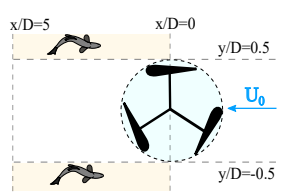
**(iii) Swimming velocities**

Swimming velocities were determined based on the distance covered (as described in (ii)) between frames and the corresponding time step ($v_{fish} = s/\Delta t$). This approach provides an estimate of the swimming velocities over time but neglects the direction of the fish (i.e., whether the fish actively swam or drifted downstream). Based on the
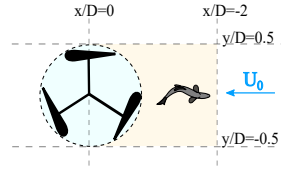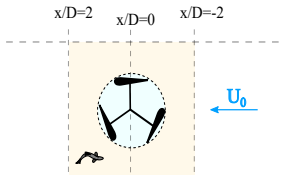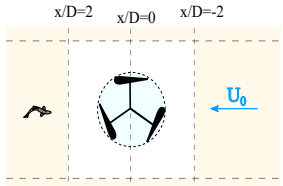
velocities calculated, the time spent at predefined velocity ranges was calculated.

**Table 3.3:** Quantification of the percentage of time spent swimming downstream and upstream of the turbine, within the downstream centre as well as on the left and right-hand side of the downstream part of the test section, bow-waking immediately upstream of the turbine, inside (attraction) and outside (avoidance) of the turbine's vicinity

| Percentage of time | Description | |
|---|---|---|
| **Downstream swimming** | fish swimming within the downstream section: $0 \le x/D \le 5$, Flume 3: $-1.25 \le y/D \le 1.25$ or Flume 1: $-5 \le y/D \le 5$ |  |
| **Upstream swimming** | fish swimming within the upstream section: $-5 \le x/D \le 0$, Flume 3: $-1.25 \le y/D \le 1.25$ or Flume 1: $-5 \le y/D \le 5$ |  |
| **Swimming in the downstream centre** | fish swimming immediately downstream of the turbine within the centre of the downstream section: $0 \le x/D \le 5$, $-0.5 \le y/D \le 0.5$ |  |
| **Swimming on the left and right-hand side of the downstream section** | fish swimming on the left hand-side of the downstream section: $0 \le x/D \le 5$, Flume 3: $-1.25 \le y/D \le -0.5$ or Flume 1: $-5 \le y/D \le -0.5$; fish swimming on the right-hand side of the downstream test section: $0 \le x/D \le 5$, Flume 3: $0.5 \le y/D \le 1.25$ or Flume 1: $0.5 \le y/D \le 5$ |  |

*Continued on next page*

Table 3.3 – *Continued from previous page*

| Percentage of time | Description | |
|---|---|---|
| **Bow-waking** | fish swimming immediately upstream of the turbine: -2$\leq x/D \leq$-0.5, -0.5$\leq y/D \leq$0.5 |  |
| **Attraction** | fish swimming within the vicinity of the turbine: -2$\leq x/D \leq$2, Flume 3: -1.25$\leq y/D \leq$1.25 or Flume 1: -2.5$\leq y/D \leq$2.5 |  |
| **Avoidance** | fish remaining at a greater distance from the turbine: -2$\leq x/D \geq$2, Flume 3: -1.25$\leq y/D \geq$1.25 or Flume 1: -2.5$\leq y/D \geq$2.5 |  |

## (iv) Group behaviour
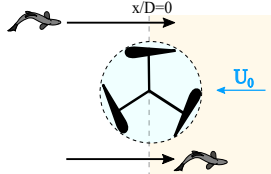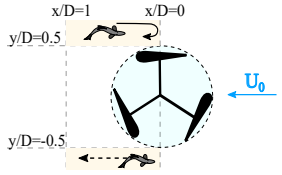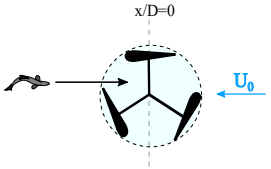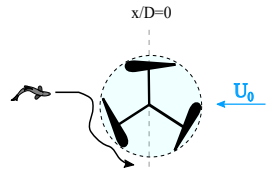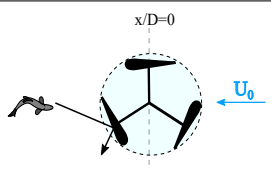
For the experiment examining small group behaviour, the percentage of time spent swimming as individuals, pair or shoal was calculated using the fish positions tracked over time as described in (i). Fish were considered to swim as a pair if their distance was <3 $L_{fish}$ [83]. Analogously, fish were considered to swim as a shoal when the distance between all fish was <3 $L_{fish}$, with a shoal comprising at least three fish.

## (v) Fish behaviour

A range of behaviours were defined and recorded while analysing the datasets, with an overview of these behaviours provided in Table 3.4 [248, 49]. Behaviours investigated included (1) **Passing**, the movement from the downstream section into the upstream section using $x/D$=0 as cut-off point (Figure 3.6, red line); (2) **Near-Pass**, swimming towards the cut-off line at $x/D$=0 followed by drifting or actively swimming downstream; (3) **Entering**, fish entering the turbine rotor area; (4) **Evasion**, sudden change

in swimming direction in close proximity of the turbine to actively avoid a direct contact with the turbine blades; and (5) **Strike**, fish potentially experiencing a contact with the turbine's blade. Each behaviour was derived from the count of an individual event and the percentage of fish showing this behaviour.

**Table 3.4:** Summary of behaviours recorded, including passing into the upstream section, attempting to pass, entering the rotor area, evading to prevent a contact with the turbine blade, and strikes [248, 49].

| Behaviour | Description | |
|---|---|---|
| **Passing** | fish moving from downstream into upstream region, crossing cut-off line: $x/D$=0 |  |
| **Near-Pass** | fish moving to the cut-off line ($x/D$=0) followed by actively swimming or drifting downstream |  |
| **Entering** | fish entering into turbine swept area (light blue circle): -0.5$\leq x/D \leq$0.5, -0.5$\leq y/D \leq$0.5 |  |
| **Evasion** | sudden change in swimming direction in close proximity to the turbine ($x/D \leq$1) to avoid a direct contact with the turbine |  |
| **Strike** | fish being in contact with the a blade of the turbine |  |

For simplification purposes, number of upstream passes per fish and percentage of upstream passes per fish were summarized under the term "passage behaviour". Sim-

ilarly, the term "movement behaviour" was also used, which refers to the distance covered and maintained from the turbine as well as the range of swimming velocities observed.

After completion of the test (10 min 30 s), fish were weighed and measured, and then returned to the holding tank. At the end of each test series fish were transported back to RAS at the Cardiff University Aquarium.

### 3.2.3.3   Statistical data analysis

Following the conduction of the experiments, the recorded parameters were investigated for statistical significance using R v.3.6.3 statistical software. A range of general and generalised linear models (both known as GLM) was applied to investigate whether a dependent variable (e.g., recorded parameters) can be explained by one or more independent variable (e.g., treatments). An explanation of the models used and the reasoning for their choice can be found in Section 2.2.4.3.

For each experiment, the model best fitting the data, including error family and link function, is reported in Section 3.2.3.4.1, 3.2.3.4.2 and 3.2.3.4.3, and final p-values highlighting statistical significance are presented in the results section (Section 3.3.2).

### 3.2.3.4   Experimental studies

In total, three experimental studies (a-c) were conducted, investigating the impact of a single VAT on individual and small groups of juvenile rainbow trout *Oncorhynchus mykiss*, Walbaum 1792), sourced from the Bibury Trout Farm, UK, and chosen as model species due to the increasing spread of rainbow trout and threat to native species as described in Section 2.2.4.4.2. These experiments examined (a) the impact of discharge and turbine operation state on fish movement under confined spatial conditions (Section 3.2.3.4.1), (b) the impact of spatial confinement on fish movement under mild

flow conditions for two turbine operation states (Section 3.2.3.4.2), and (c) the movement behaviour of shoals (Section 3.2.3.4.3). Specific details regarding number of fish tested and statistical analysis are provided below.

A summary of the experimental test conditions is provided in Table 3.5, including discharge ($Q$), cross-section averaged bulk velocity ($U_0 = Q/A$), bulk Reynolds number ($Re = U_0 R_H / \nu$ with $\nu$ denoting the fluid kinetic viscosity and $R_H$ the hydraulic radius), Reynolds number based on turbine diameter $D$ ($Re_D = U_0 D / \nu$), Froude number ($Fr = U_0 / \sqrt{gh_0}$), and turbine rotational speed ($\omega$).

**Table 3.5:** Experimental details for all four treatments (MS, HS, MR, HR) investigated in Flume 3 and both treatments analysed in Flume 1 (MS-F1, MR-F1), including flow discharge ($Q$), bulk velocity ($U_0$), bulk Reynolds number ($Re$), Reynolds number based on the turbine diameter ($Re_D$), Froude number ($Fr$), and turbine rotational speed ($\Omega$).

| Study | Flume | Treatment | | $Q$ $[m^3 s^{-1}]$ | $U_0$ $[ms^{-1}]$ | $Re$ $[-]$ | $Re_D$ $[-]$ | $Fr$ $[-]$ | $\Omega$ $[rpm]$ |
|---|---|---|---|---|---|---|---|---|---|
| (a) | F1 | mild-stationary | **MS** | 0.013 | 0.19 | 17,300 | 22,800 | 0.126 | 0 |
| | | mild-rotating | **MR** | 0.013 | 0.19 | 17,300 | 22,800 | 0.126 | 58 |
| | | high-stationary | **HS** | 0.017 | 0.25 | 22,700 | 30,000 | 0.167 | 0 |
| | | high-rotating | **HR** | 0.017 | 0.25 | 22,700 | 30,000 | 0.167 | 75 |
| (b) | F1 | mild-stationary | **MS-F1** | 0.053 | 0.19 | 17,300 | 22,800 | 0.126 | 0 |
| | | mild-rotating | **MR-F1** | 0.053 | 0.19 | 17,300 | 22,800 | 0.126 | 58 |
| (c) | F1 | mild-rotating | **-** | 0.053 | 0.19 | 17,300 | 22,800 | 0.126 | 58 |

### 3.2.3.4.1 Experiment (a): Impact of discharge and turbine operation state on individual fish movement

In this study, the effect of discharge and turbine operation state on fish movement was investigated by exposing individual fish to two discharges (mild: $Q$=0.013 m³/s and high: $Q$=0.017 m³/s) and two turbine operation states (rotating and stationary) under confined test condition in Flume 3. The range of test combinations resulted in the following four treatments: MS (mild-stationary), MR (mild-rotating), HS (high-stationary), and HR (high-rotating).

Fish passage behaviour tests were conducted between 23 November and 1 December 2020 between 8 am and 5 pm. For each treatment, $N_{tested}$=20 juvenile rainbow trout were tested, resulting in a total of 80 fish of mean standard length $\pm$ s.d., 57.0$\pm$5.9 mm, mean total length $\pm$ s.d., 66.8$\pm$6.9 mm, and mean mass $\pm$ s.d., 3.1$\pm$0.9 g. An overview of the number of fish tested ($N_{tested}$), excluded ($N_{excluded}$) and analysed ($N_{analysed}$) as well as mass ($m$), standard ($L_{fish}$) and total ($L_{fish,total}$) length is provided for each treatment in Table 3.6 (Flume 3). Fish tested for each treatment did not significantly differ in fish standard length (GLM, $p$=0.7904), total length (GLM, $p$=0.5691) and mass (GLM, $p$=0.1281).

Treatment order was not randomised as each fish was only tested once. The MS treatment was tested first, followed by MR, HS, and HR. For each test, the parameters presented in Section 3.2.3.2 were analysed using the image series obtained.

Time upstream and downstream was tested for significance using a Gaussian GLM with an identity and inverse link function respectively. Similarly, the proportions of time spent bow-waking, within the downstream centre as well as in the left and right-hand side of the downstream section were examined using Gaussian GLMs with an identity link function. Also, the time proportion within and outside the turbine's vicinity, and the proportions of time spent swimming at a range of different swimming speed were analysed using Gaussian GLMs with identity link. Similarly, attraction

**Table 3.6:** Fish behaviour experimental details comprising of number of tested fish ($N_{tested}$), excluded ($N_{excluded}$) and analysed ($N_{analysed}$) as well as their average mass ($m$), standard ($L_{fish}$) and total length ($L_{fish,total}$) $\pm$ s.d. for each treatment and experimental setup.

| Study | Flume | Treatment | | $N_{tested}$ | $N_{excluded}$ | $N_{analysed}$ | $m$ $\pm s.d.$ [g] | $L_{fish}$ $\pm s.d.$ [mm] | $L_{fish, total}$ $\pm s.d.$ [mm] |
|---|---|---|---|---|---|---|---|---|---|
| (a) | F1 | mild-stationary | **MS** | 20 | 0 | 20 | 3.4 $\pm$ 0.9 | 57.0 $\pm$ 5.7 | 67.9 $\pm$ 7.8 |
| | | mild-rotating | **MR** | 20 | 0 | 20 | 2.9 $\pm$ 0.7 | 56.2 $\pm$ 5.3 | 65.7 $\pm$ 5.8 |
| | | high-stationary | **HS** | 20 | 0 | 20 | 2.9 $\pm$ 0.8 | 56.6 $\pm$ 6.1 | 65.8 $\pm$ 6.7 |
| | | high-rotating | **HR** | 20 | 0 | 20 | 3.3 $\pm$ 0.9 | 58.0 $\pm$ 6.8 | 68.0 $\pm$ 7.4 |
| (b) | F1 | mild-stationary | **MS-F1** | 21 | 2 | 19 | 1.9 $\pm$ 0.3 | 49.2 $\pm$ 2.1 | 57.0 $\pm$ 3.3 |
| | | mild-rotating | **MR-F1** | 22 | 3 | 19 | 2.1 $\pm$ 0.4 | 50.7 $\pm$ 4.3 | 58.4 $\pm$ 3.1 |

and avoidance time were compared using a Gaussian GLM with identity link function. Likewise, the difference in distance swam and distance maintained from the turbine and the treatments were determined by Gaussian GLMs with identity function. Using a two-proportion z-test, significant difference between treatments were determined for the percentage of fish passing upstream, conducting near-passes, bow-waking, entering, showing evasion behaviour, or experiencing strikes. Differences in fish standard length, total length and mass amongst treatments was tested for significance using Gaussian GLMs with identity link. As these parameters did not significantly differ amongst treatments, fish standard length was not included as an independent parameter in the final models. Hence, treatment was the only independent variable.

### 3.2.3.4.2 Experiment (b): Impact of spatial confinement on individual fish movement under mild flow conditions

In this study, the impact of spatial confinement was tested by conducting a replica test in Flume 1. As described in Section 3.2.3.2, the test section in Flume 1 was created in a similar way as in Flume 3, with flow conditions scaled based on the Reynolds number. The test section in Flume 1, however, had four times the width compared to the test section in Flume 3. The impact of flow confinement was analysed for both turbine operation states (stationary and rotating) but only for the mild flow condition. These treatments are termed MS-F1 and MR-F1 as shown in Table 3.5 (Study (b)).

Fish behaviour experiments for this study were conducted between 29 March and 7 April 2021 between 8am and 5pm. In total, 21 and 22 fish were tested for MS-F1 and MR-F1, respectively. Due to technical difficulties (e.g., incomplete recordings) and fish impinging the downstream flow straightener, $N_{excluded}$=5 fish were excluded from the analyses, resulting in 19 fish per treatment and therefore, a total number of $N_{analysed}$=38 fish of mean standard length $\pm$ s.d., 50.0$\pm$3.4 mm, mean total length $\pm$ standard deviation, 57.7$\pm$3.2 mm, and mean mass, $\pm$ s.d., 2.0$\pm$ 0.4 g. An overview of the number of fish tested ($N_{tested}$), excluded ($N_{excluded}$) and analysed ($N_{analysed}$) as well as mass ($m$), standard ($L_{fish}$) and total ($L_{fish,total}$) length is provided for each treatment in Table 3.6 (Study (b)). Fish tested for each treatment did not significantly differ in fish standard length (GLM, $p$=0.1658), total length (GLM, $p$=0.1926), and mass (GLM, $p$=0.0642).

As in experiment (a), treatment order was not randomised as each fish was only tested once. The MS-F1 treatment was tested first, followed by MR-F1. For each test, the parameters presented in Section 3.2.3.2 were analysed using the image series obtained.

As the focus of this experiment was a comparison of confined and unconfined spatial conditions for fish movement, results from MS-F1 and MR-F1 were compared against the results obtained in experiment (a) for MS and MR. Due to the significant difference

in fish standard length (GLM, $p<0.001$), total length (GLM, $p<0.001$) and mass (GLM, $p<0.001$) between the fish used in experiment (a) and (b), fish standard length was included as an independent variable alongside treatment. Fish standard length of the fish used in experiment (b) was significantly smaller than the ones tested in experiment (a) (GLM, MR versus MR-F1: $p<0.001$, MS versus MS-F1: $p<0.001$). The difference in standard length, total length, and mass for MS-F1 and MR-F1, and for MS, MR, MS-F1 and MR-F1 were determined using a Gaussian GLM with identity link function. As in experiment (a), the significant impact of treatment and standard length on parameters based on the proportion of time spent (i.e., upstream, downstream, downstream-centre, left and right-hand side, in and outside the turbine's vicinity, swimming velocities) was examined using Gaussian GLMs with identity link function. Similarly, attraction and avoidance time were compared using a Gaussian GLM with identity link function. Distance covered during the test period and mean distance kept from the turbine were tested for significance using Gaussian GLMs with identity and inverse link function, respectively. A two-proportion z-test was used to compare the impact of spatial confinement depending on turbine operation state on the number of upstream passing fish, fish attempting to pass, bow-waking, entering the turbine, evading, and experiencing a strike.

### 3.2.3.4.3 Experiment (c): Impact of single vertical axis turbine on fish shoals

In this experiment, shoals consisting of three fish were investigated under similar test conditions as MR-F1 (experiment (b)) to examine the effect of shoaling on fish movement behaviour. Therefore, groups of three fish were tested in Flume 1 under mild flow conditions and were exposed to a single, rotating VAT.

Fish behaviour tests were conducted between 22 March and 22 April, 2021, between 8 am and 5 pm. Prior to the start of the experiments fish were size matched into groups of three and acclimatised in their groups for 16 days. As no information were available on the time required for rainbow trout to form a shoal, the familiarisation time of 12

days determined for guppies *Poecilia reticulata* [83] was used as lower limit. On the test day, groups of fish were acclimatised and tested as described in Section 3.2.3.2. In total, 20 groups were tested, with $N_{excluded}$=3 groups being excluded from the analyses due to premature termination of the trial, or fish being indistinguishable or undetectable during the data analysis (e.g., fish are overlapping or blending into the environment). The remaining 17 groups were of mean standard length $\pm$ s.d., 60.1$\pm$10.4 mm, mean total length $\pm$ s.d., 69.2$\pm$11.7 mm, and mean mass $\pm$ s.d., 3.8$\pm$2.0 g. For each group, mean group distance covered and distance kept from the turbine, mean percentage of time spent at a range of swimming velocities and percentage time spent as individuals, pair or shoal was determined as described in Section 3.2.3.2. These parameters were then compared against the results obtained in experiment (b).

It should be noted that this experiment is part of a larger data set in which shoals of fish were tested for a stationary and rotating, single VAT (control and ST-1.5, respectively) and three twin-turbine configurations comprising of twin-turbines rotating in the same rotational direction (SR-1.5), in counter-clockwise forward (CRF-1.5) and backward direction (CRB-1.5), laterally spaced by $S_y$=1.5 (see Table 3.2). The full data set has not been analysed yet and only preliminary results are presented in Section 3.3.2.3 for one treatment (ST-1.5). Treatments were randomised for each group, with fish being tested once per day for five consecutive days. Hence, fish analysed for experiment (c) might have experienced other treatments prior to the test which may influence the results presented in Section 3.3.2.3.

Prior to the comparison of the results obtained for experiment (c) and (b), the variation within groups and the impact of standard length was determined. Variations between groups and distance swam, and groups and mean distance kept from the turbine was analysed using a one-way analysis of variance (ANOVA). The impact of fish standard length on the distance swam, distance maintained from the turbine, percentage time fish swam at a range of swimming velocities and time spent as an individual, pair or shoal was tested for significance using a Gaussian GLM with identity link function.

Moreover, results obtained in experiment (c) were compared against the results of experiment (b). Besides treatment, fish standard length was included as an independent parameter as fish standard length significantly differed between experiments (GLM, $p$<0.001), with fish being smaller in experiment (b). The significant influence of fish standard length was determined using a Gaussian GLM with identity link function. Mean distance swam and the percentage of time spent at a range of swimming speeds, and as individuals, pair and shoal was also tested for significance using a Gaussian GLM with identity link function. In contrast, a Gaussian GLM with inverse link function was used to determine the significance level of the distance maintained from the turbine.

## 3.3    Results

### 3.3.1    Hydrodynamic measurements

In this section, the ADV measurement results characterising the approach flow and the wake behind the single and twin-turbine configurations (Table 3.2) are presented at a range of downstream y-z cross-sections and longitudinal locations.

#### 3.3.1.1    Approach flow

The vertical distribution of normalised streamwise mean velocity ($\overline{u}/U_0$), streamwise turbulence intensity ($u'/U_0$), and vertical Reynolds shear stresses ($\overline{u'w'}/U_0^2$) are presented in Figure 3.7 (a-c), respectively, for six lateral locations over the left-half (looking in downstream direction) of the cross-section (the approach flow is deemed symmetric). The mean velocity profiles show a power-law distribution over the flow depth, with a nearly constant turbulence intensity distribution, yielding a depth-averaged value of $u'/U_0$=0.14. There is some non-uniformity in the $u'w'$ distribution between lateral locations, especially at $y/D$=-3.3. This non-uniformity may be attributed to the flow
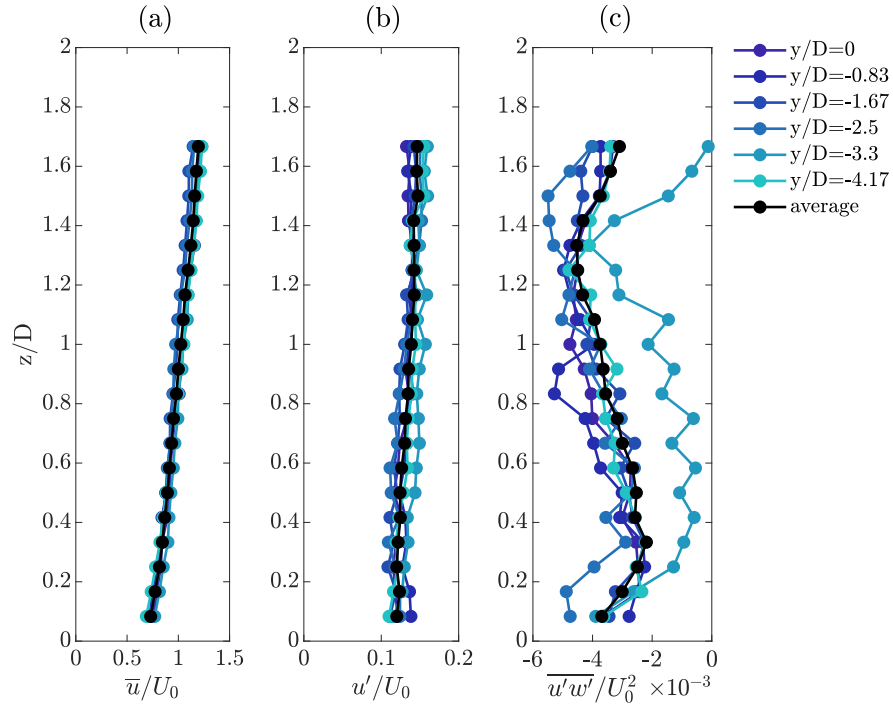
**Figure 3.7:** Upstream profiles measured at six lateral locations beginning at the flume centreline ($y/D$=0). (a) Time-averaged streamwise velocity $\overline{u}$ normalised by the bulk velocity $U_0$, (b) streamwise turbulence intensity $u'$ normalised by $U_0$, and (c) vertical Reynolds shear stress $\overline{u'w'}$ normalised by $U_0^2$. The black line and symbols correspond to the average value from the vertical measurements.

not being fully developed by this distance and the profile's proximity to the flume wall (located $0.83D$ away from the lateral wall), which can impact the distribution of turbulent fluxes [208].

### 3.3.1.2  Single turbine wake evolution

Before examining the dynamics of twin-turbine wakes, the wake characteristics of the single turbine (ST) are presented in $y - z$-planes at downstream distances from $x$=1 $D$ to 5 $D$ to identify the turbine's key characteristics and three-dimensional evolution. The black rectangular outline in the contour plots represents the projected area of the

turbine rotor and the flume's centreline is at $y/D$=0.

The distribution of the normalised mean streamwise velocity ($\overline{u}/U_0$) for the ST is shown in Figure 3.8. The near wake ($x/D \leq 2$) immediately downstream of the rotor was characterised by a region of large velocity deficit, which was particularly pronounced at the upstroke side ($y/D \leq 0$) of the blades' rotation, i.e., where the blades move against the flow and thus, generate the highest relative velocity. This caused the wake to be asymmetric relative to the rotor centreline. Until $x/D$=2, the areas near the top and bottom tips of the blades an the upstroke side appeared to attain minimum mean streamwise velocity values, likely arising from tip-vortices generated by the blades. In contrast, over the downstroke side ($y/D \geq 0$), mean streamwise velocity was larger, with the lowest values distributed over the mid-turbine height ($0.3 \leq z/D \leq 0.9$) rather than the tip location. Beyond $x/D$=3, the transitional-wake region was characterised by a vertical and lateral expansion of the low-velocity wake. In the far wake ($x/D \geq 6$, not shown here for brevity), most of the momentum was recovered, with velocities
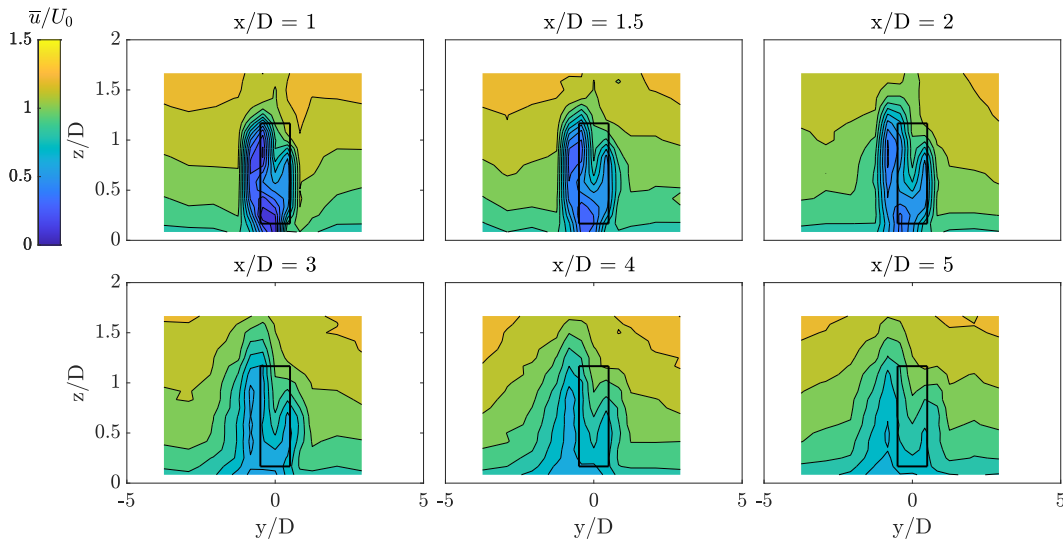


**Figure 3.8:** Contours of $\overline{u}/U_0$ at downstream cross sections located at $x/D$=1, 1.5, 2, 3, 4 and 5 (looking in downstream direction) for the case with the single turbine (ST) rotating with anti-clockwise motion.

yielding values close to the approach flow velocity, but remnants of the wake signature were still visible over the whole water column.

The distribution of turbulent kinetic energy ($tke$) is presented in Figure 3.9. Like the distribution of $\overline{u}/U_0$, the upstroke side featured highest values of $tke$ over the whole wake length due to the turbine blades moving into the flow and the shedding of energetic vortices. Over the downstroke side, turbulence levels were lower, likely linked to the reduced dynamic-stall vortices strength due to the experiment's Reynolds number.
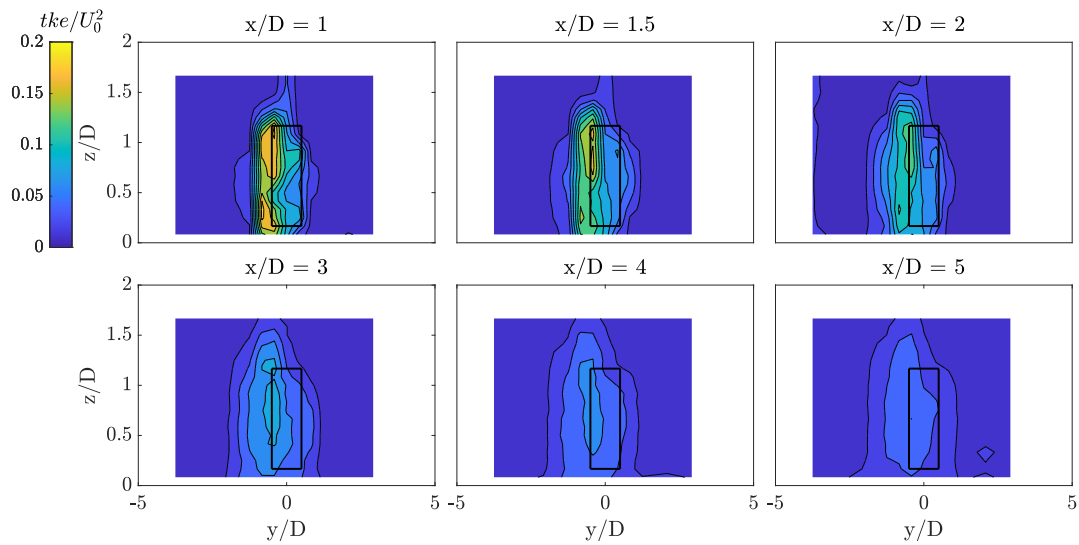


**Figure 3.9:** Contours of $tke/U_0^2$ at downstream cross sections located at $x/D$=1, 1.5, 2, 3, 4 and 5 (looking in downstream direction) for the ST case, with the VAT rotating anti-clockwise.

Turbulent momentum exchange is indicated by the horizontal (Figure 3.10) and vertical (Figure 3.11) components of the Reynolds shear stress, which show that regions of highest shear stresses were mostly found in the near wake. The high magnitudes observed for $\overline{u'v'}$, originated from the convection of dynamic-stall vortices and the interaction with the ambient flow. Both positive and negative values were found on the upstroke side ($y/D \leq 0$), with the latter being observed on the outside region of the rotor swept area and the former $\overline{u'v'}$ inside. This pattern was observed only over the near-wake region as the turbine-induced vortical structures lose their coherence due to
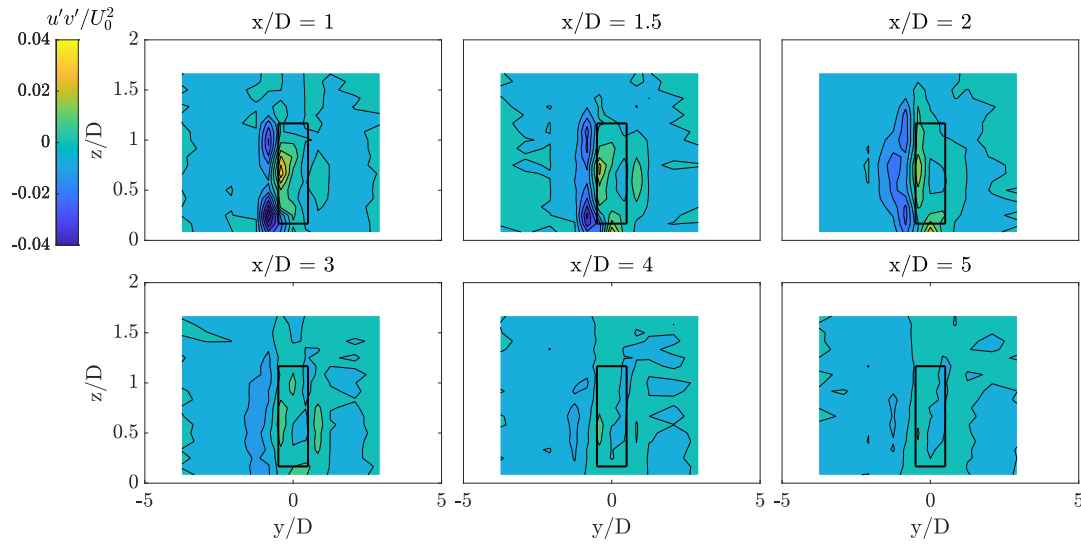
**Figure 3.10:** Contours of $\overline{u'v'}/U_0^2$ at downstream cross sections located at $x/D$=1, 1.5, 2, 3, 4 and 5 (looking in downstream direction) for the ST case, with the VAT rotating anti-clockwise.
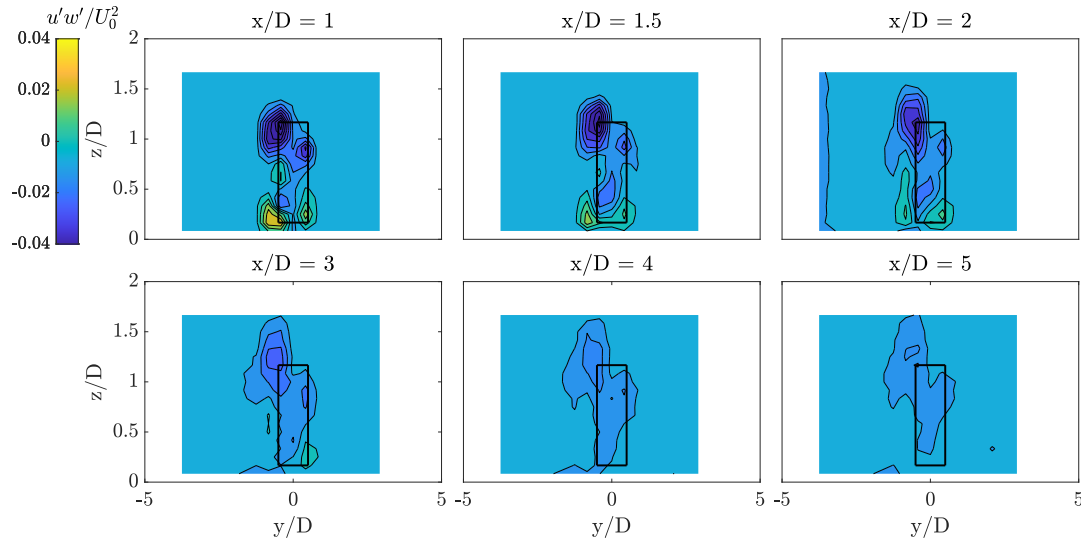


**Figure 3.11:** Cross section contours of $\overline{u'w'}/U_0^2$ at downstream locations of $x/D$=1, 1.5, 2, 3, 4 and 5 (looking in downstream direction) for the ST case, with the VAT rotating anti-clockwise.

the mixing with the ambient flow. Vertical Reynolds shear stresses ($\overline{u'w'}/U_0^2$) showed predominantly negative values on the upper half of the turbine ($z/D \geq 0.8$), due to the flow over-topping the turbine being transported downward into the wake. In the near wake ($x/D \leq 2$), positive $\overline{u'w'}$ values appeared on the lower half of the turbine

($z/D \leq$0.7), with particularly large values near the corners of the rotor's swept area, unveiling the interaction between the bottom tip vortices and the upward flow going through the bottom gap between the turbine's rotor and flume bed. Further downstream (i.e., after $x/D$=3), $\overline{u'w'}$ shear stresses strongly decayed due to the mixing of the wake with the ambient flow.

### 3.3.1.3 Twin-VAT wake results

In this section, the impact of rotational direction and lateral turbine spacing is elucidated for each of the twin-VAT cases (Table 3.2). The characteristics of the wakes developed downstream of the six twin-VAT setups, i.e., for three rotation combinations and two inter-turbine spacings: SR–1.5, CRF–1.5, CRB–1.5, SR–2.0, CRF–2.0, and CRB–2.0, were analysed using contour plots at cross-sections normal to the flow direction ($y - z$-planes) at several streamwise locations. Mean streamwise velocities are discussed for cases adopting the two inter-turbine separations of $S_y/D$=1.5 and 2.0 while higher-order statistics are discussed only for setups with $S_y/D$=1.5, as those with $S_y/D$=2.0 have a similar spatial distribution. The solid black rectangles represent the perimeter of the turbine's rotor and the flume's centreline is located at $y/D$=0.

Contours of $\overline{u}/U_0$ at $x/D$=1, 2, 3, 5 and 10 are presented in Figure 3.12 for SR–1.5, CRF–1.5, and CRB–1.5, and in Figure 3.13 for SR–2.0, CRF–2.0, and CRB–2.0. Similar wake characteristics to the ST case (Figure 3.8) were found for the individual wakes at $x/D$ =1.0 behind each of the turbines for the SR and CRF cases, with the lowest velocities found on the upstroke side of the blades rotation. For both cases, the wakes appeared asymmetric to the vertical axis between the turbines. In the CRB–1.5 case, however, both wakes already merged at $x/D$=1.0 where the low-momentum region of the individual wakes collapsed.

In the SR–1.5 and SR–2.0 case, the same rotational direction of both turbines caused the individual asymmetric wakes to progress alongside each other within the near-wake ($x/D \leq$2), better depicted from the setup with $S_y/D = 2.0$. In the transition

zone ($x/D \geq 2$), both wakes started to interact and merge into a single combined low-momentum region by $x/D$=5, as represented in Figure 3.2 (a). In the far-wake, the combined wake expanded vertically across the water column and laterally, especially to the left-hand side of $T_2$. In fact, widest wake extent was found at $x/D$=10.0 for this configuration.
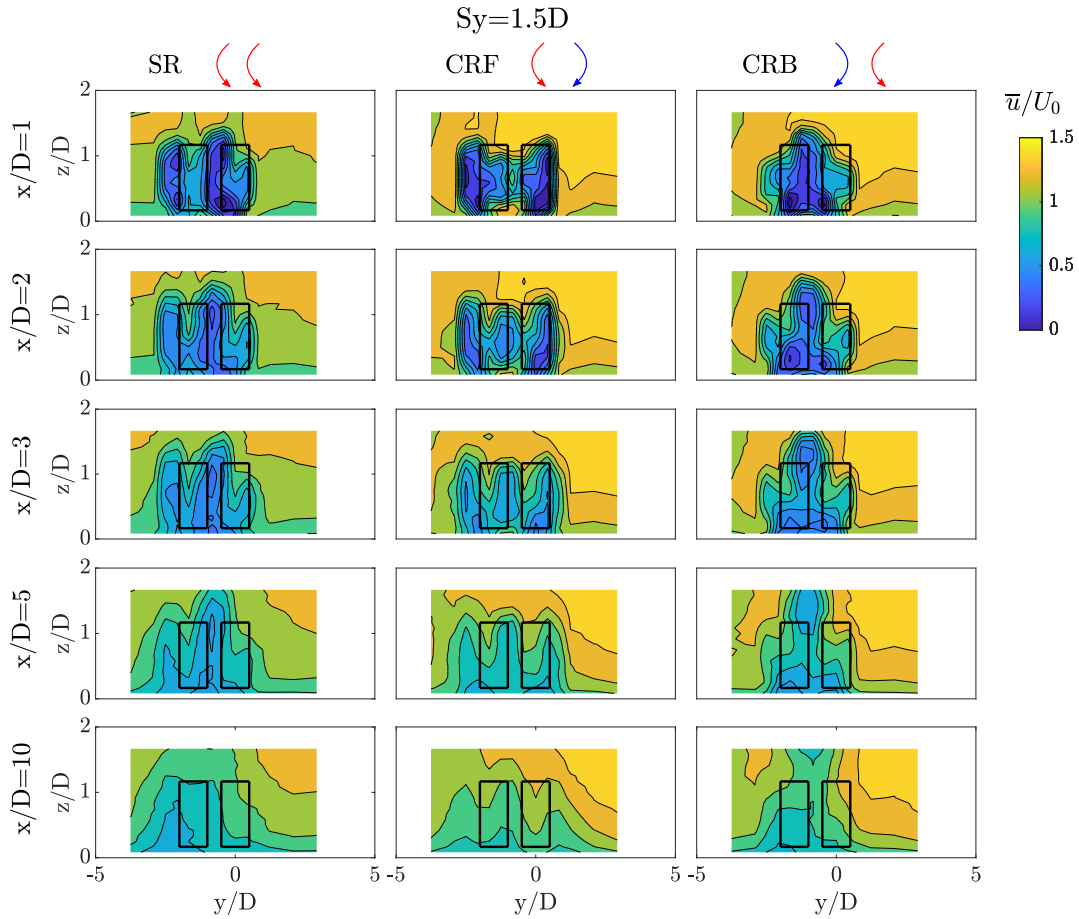


**Figure 3.12:** Cross section contours of $\overline{u}/U_0$ at downstream locations of $x/D$=1, 2, 3, 5 and 10 for the SR–1.5 (left), CRF–1.5 (middle), and CRB–1.5 (right) cases.

In contrast, the individual wakes in the CRF (counter-rotating forward) cases moved outwards in opposite directions. In this setup, the bypass flow enhanced by the down-stroke rotation of the blades which further separated both low-momentum wakes, especially for the CRF–2.0 setup (Figure 3.2 (b)). Both wakes remained separated by the
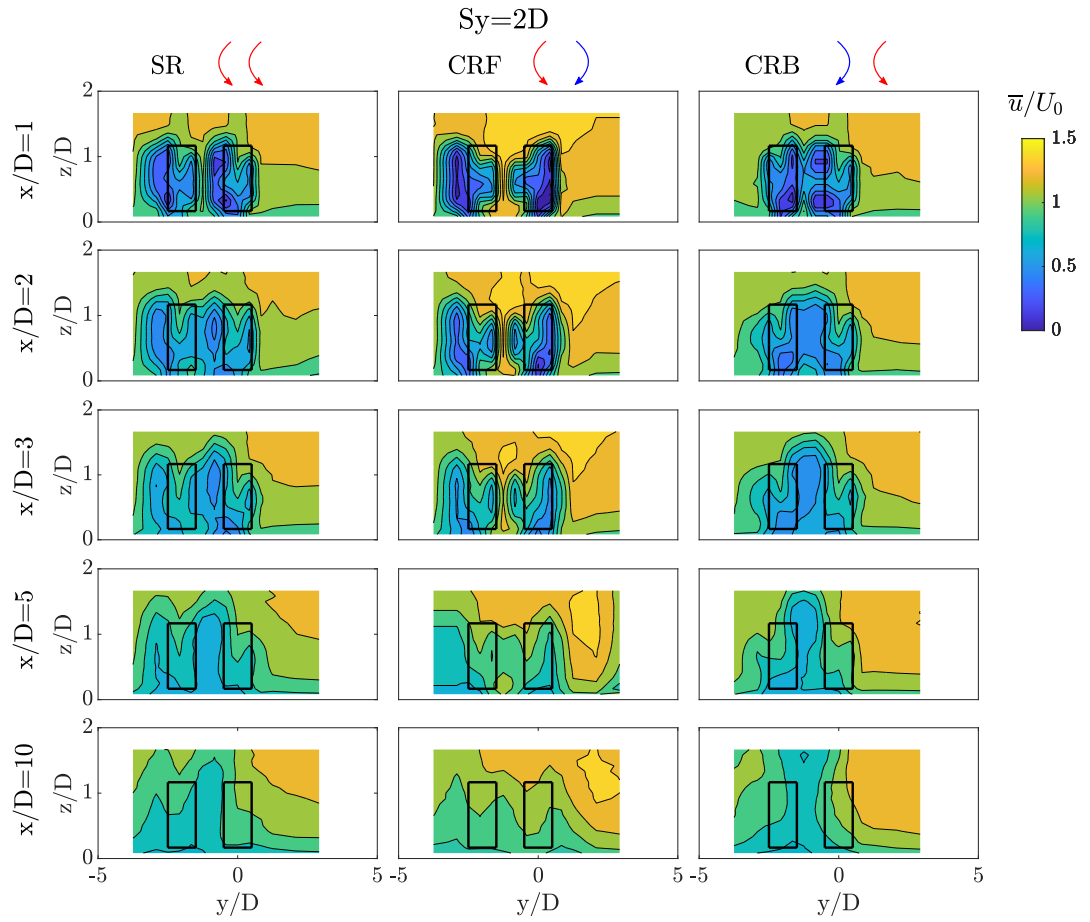
**Figure 3.13:** Cross section contours of $\overline{u}/U_0$ at downstream locations of $x/D$=1, 2, 3, 5 and 10 for the SR–2.0 (left), CRF–2.0 (middle), and CRB–2.0 (right) cases.

bypass flow until $x/D \approx$1.5 and mirrored each other relative to the centre of the gap between both turbines. For CRF–1.5, the wakes gradually merged with further increasing downstream distance ($x/D \geq$5). In contrast, for the CRF–2.0 case, the individual wakes appeared to be more independent, likely due to the blades' downstroke motion within the bypass region which further amplified the relative velocity of the flow (i.e., $\overline{u}/U_0 \geq$1) and thus, isolated both wakes and delayed their mixing. Compared to the SR and CRB cases, such limited wake interaction led to the wake having the highest streamwise velocities at the furthest measured location of $x/D$=10 as shown later in Section 3.3.1.4 in terms of spatially averaged velocity values.

In the CRB (counter-rotating backward) cases, individual turbine wakes interacted with one another shortly downstream of the rotors, collapsing into a single low-momentum region at $x/D$=1.0 and $x/D$=2.0 for the CRB–1.5 and CRB–2.0 case, respectively. After $x/D$=3.0, the combined wake occupied a narrower lateral extent compared to the SR and CRF cases, which extended notably in the vertical direction throughout most of the water column, and was nearly axisymmetric relative to the vertical axis at the centre of the combined swept area, i.e., $S_y/2$.

The distribution of $tke/U_0^2$ for each configurations and lateral spacing (Figure 3.14 and Figure 3.15 for $S_y/D$=1.5 and 2.0, respectively) was found to be similar to that
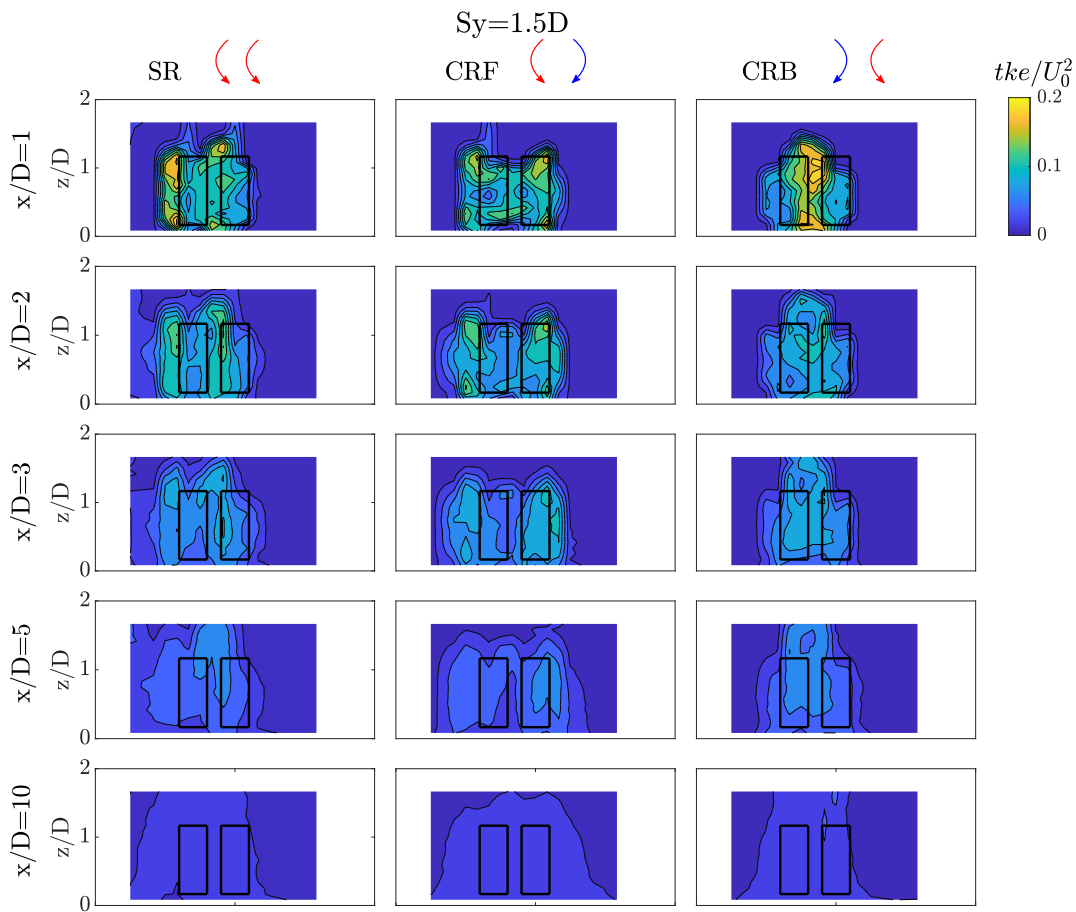


**Figure 3.14:** Cross section contours of $tke/U_0^2$ at downstream locations of $x/D$=1, 2, 3, 5 and 10 for the SR–1.5 (left), CRF–1.5 (middle), and CRB–1.5 (right) cases.
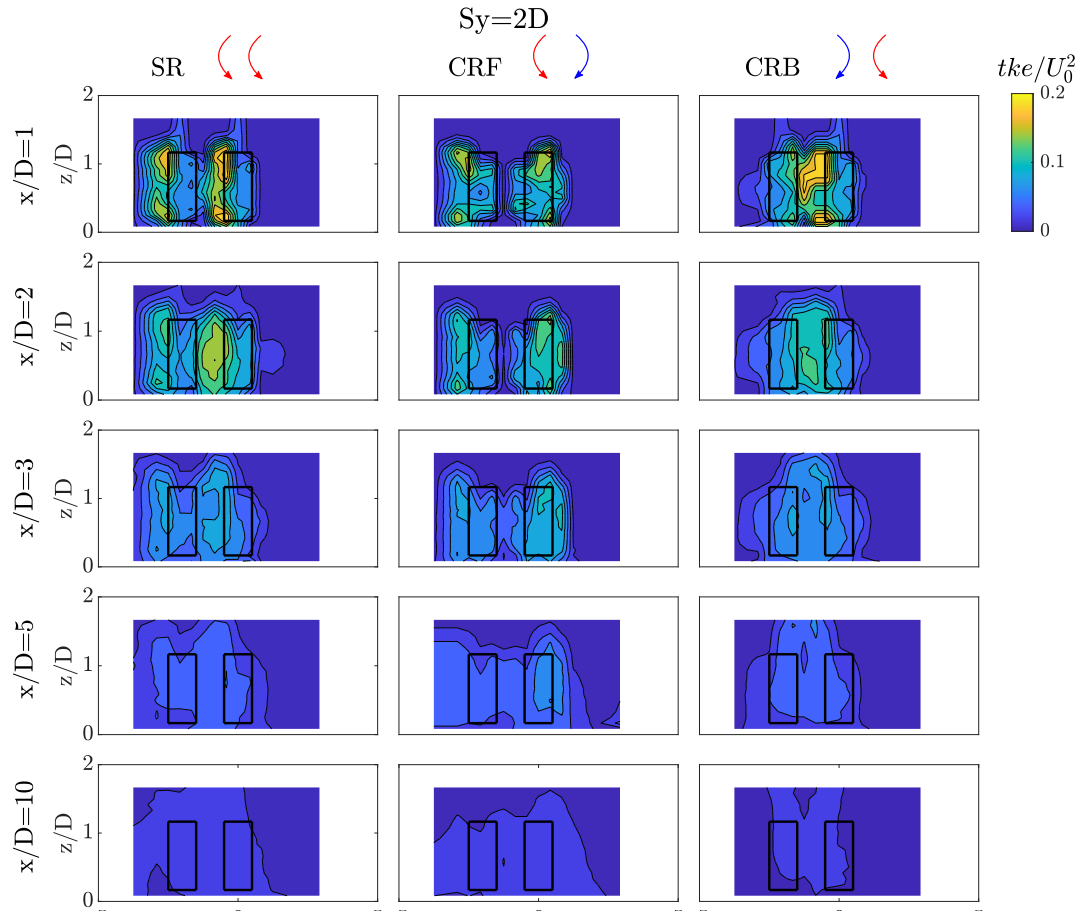
**Figure 3.15:** Cross section contours of $tke/U_0^2$ at downstream locations of $x/D$=1, 2, 3, 5 and 10 for the SR–2 (left), CRF–2 (middle), and CRB–2 (right) cases.

for the ST case (Figure 3.9), i.e. the areas with highest $tke$ pockets are those with the lowest velocity magnitude. During the upstroke movement, the blades shed vortical structures that increased turbulent mixing and triggered high levels of $tke/U_0^2$. Although both wakes in the SR–1.5 case evolve independently in the near-wake region, their interaction and merging in the transition zone ($x/D \geq 2$) resulted in a region of high turbulent kinetic energy behind the twin-turbine swept area, which enhanced the mixing of both wakes. Particularly high values of $tke/U_0^2$ were observed in the bypass region immediately downstream of the CRB–1.5 case due to the collapse of the wake regions generated from the upstroke motion of the blades. In this region, the $tke$ values

for CRF–1.5 were reduced, with maxima located on the outskirts of the wake. With increasing downstream distance, the turbulent kinetic energy decreased to approach the values of the upstream $tke$ levels at $x/D$=10.

Reynolds shear stresses, $\overline{u'v'}/U_0^2$ and $\overline{u'w'}/U_0^2$, are presented in Figures 3.16 and 3.18, respectively, for all $S_y/D$=1.5 twin-VAT cases and in Figures 3.17 and 3.19, respectively, for all configurations featuring a lateral spacing of $S_y/D$=2.0. Peak $\overline{u'v'}/U_0^2$ magnitudes were observed on the periphery of the swept areas of each turbine, indicative of turbulent momentum exchange and where vortices are generated. These are clearly observed for the CRF–1.5 case, even until a streamwise distance of $x/D$=5.0. Similar to the ST case, vertical Reynolds shear stresses $\overline{u'w'}/U_0^2$ were mostly negative
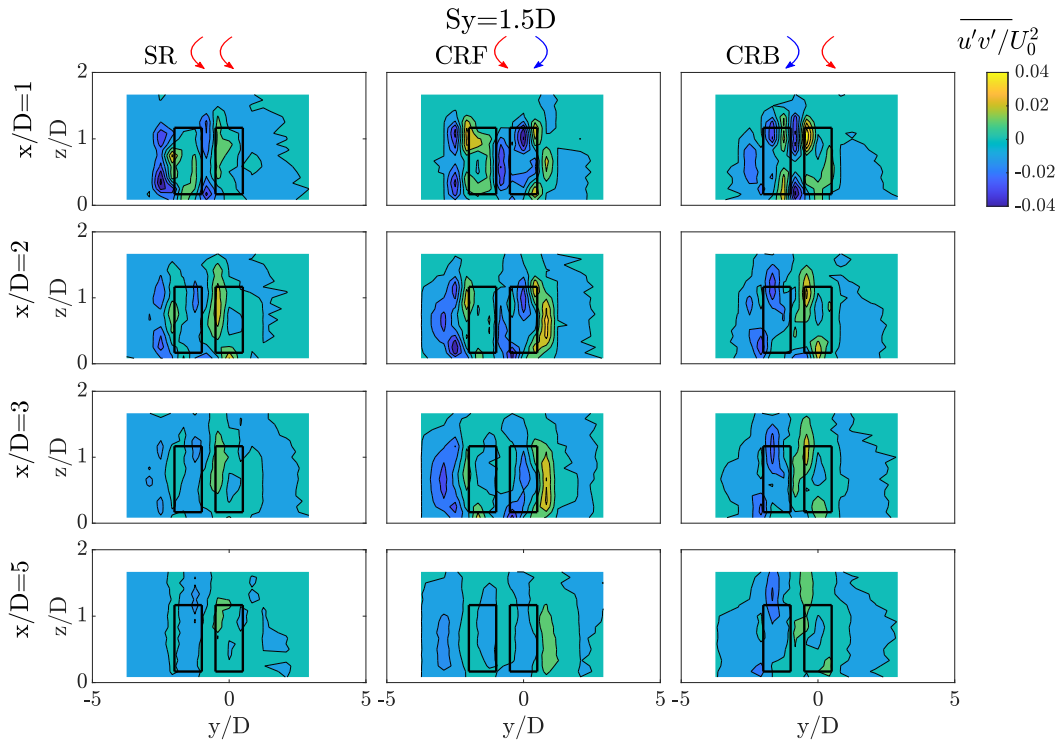


**Figure 3.16:** Cross section contours of $\overline{u'v'}/U_0^2$ at downstream locations of $x/D$=1, 2, 3, and 5 for the co-rotating (SR–1.5; left), counter-rotating forward (CRF–1.5; middle), and counter-rotating backward (CRB–1.5; right) with $S_y/D$=1.5.
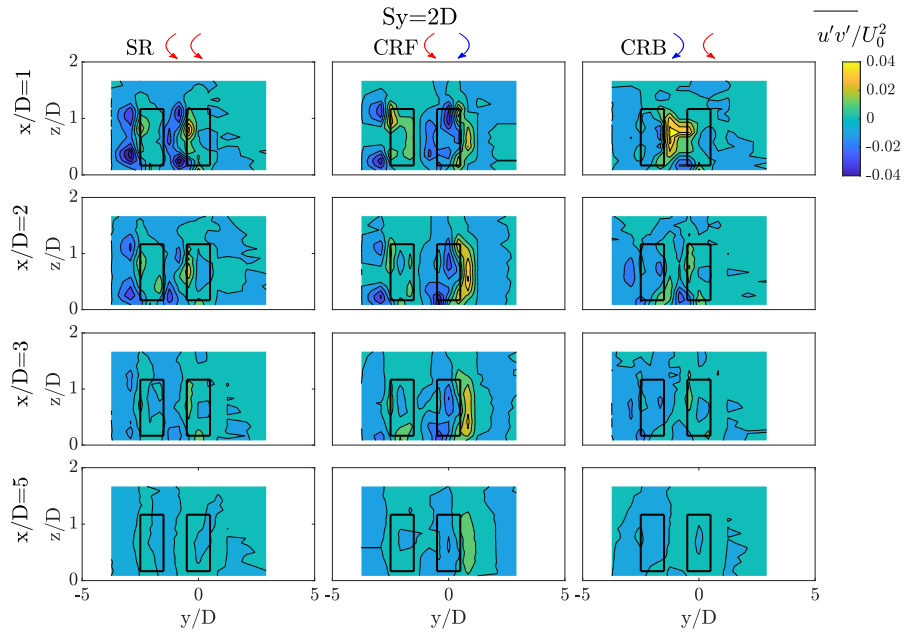
**Figure 3.17:** Cross section contours of $\overline{u'v'}/U_0^2$ at $x/D$ = 1, 2, 3, and 5 for the SR–2 (left), CRF–2 (middle), and CRB–2 (right) case.
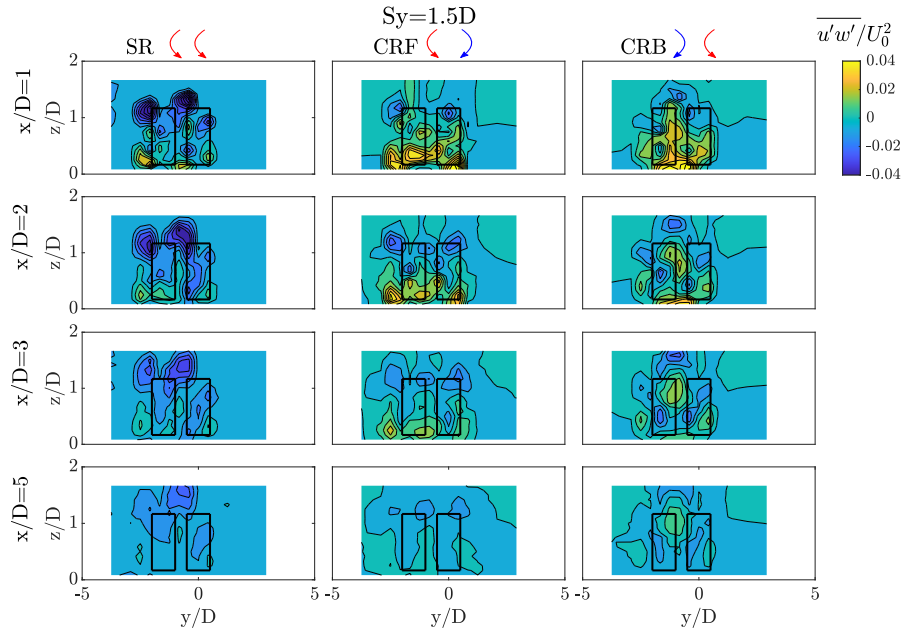


**Figure 3.18:** Cross section contours of $\overline{u'w'}/U_0^2$ at $x/D$=1, 2, 3, and 5 for the SR–1.5 (left), CRF–1.5 (middle), and CRB–1.5 (right) case.

on the upper half of the turbines as turbulent momentum entrained downwards into the wake region, and positive on the lower half; with the exception of CRB–1.5 in which the mixing of vortical structures from each of the turbine rotors showed a different pattern suggesting that the turbulent wake flow is more complex for this setup. Tip vortices were also present, triggering high shear stress levels around the top tips of the blades in the near wake ($x/D \leq 2$).
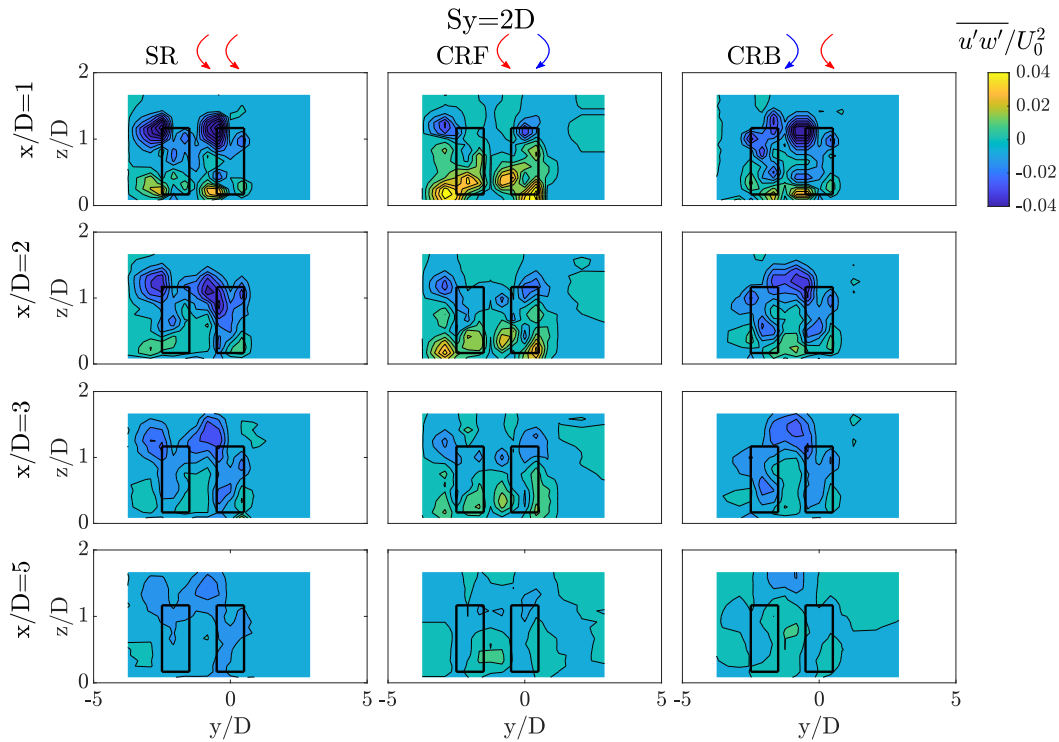


**Figure 3.19:** Cross section contours of $\overline{u'w'}/U_0^2$ at downstream locations of $x/D$=1, 2, 3, and 5 for the SR–2 (left), CRF–2 (middle), and CRB–2 (right) cases.

### 3.3.1.4   Wake recovery

The integral change of the wake in downstream direction was estimated in terms of the cross-sectional average of the streamwise velocity and turbulence intensity. These were approximated by integrating the measured quantities at the ADV locations within

the turbine area for ST case ($0.5 \leq y/D \leq 0.5$) and the region spanning both VATs for the twin-setups ($S_y/D$=1.5: $0.5 \leq y/D \leq 2$, $S_y/D$=2.0: $0.5 \leq y/D \leq 2.5$). In the vertical, only those points within the turbine area were considered. The spatial-averaging operation is denoted as $\langle \cdot \rangle$ and results of ($\langle \overline{u} \rangle / U_0$) and ($\langle u' \rangle / U_0$) are provided in Figures 3.20 and 3.21 for the ST and six twin-VAT cases, comparing rotational direction and lateral spacing, respectively.
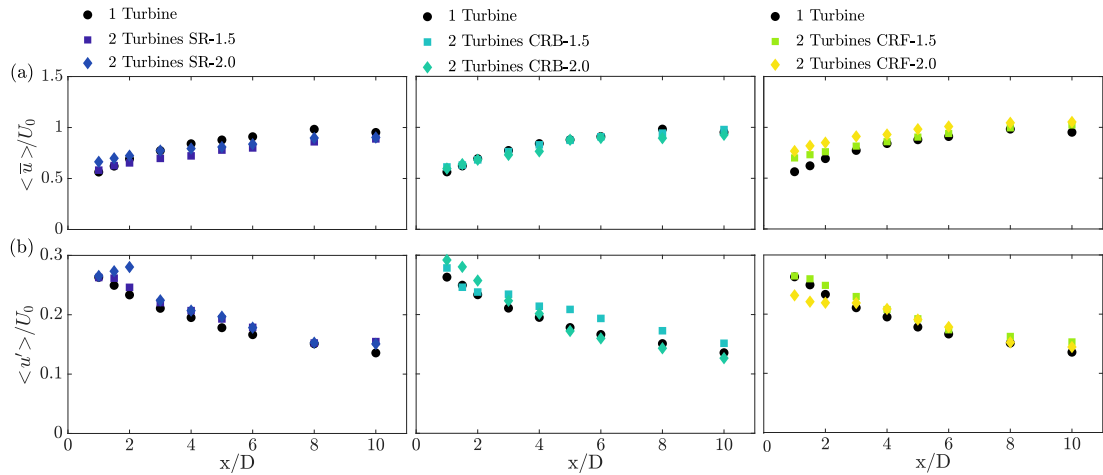


**Figure 3.20:** Comparison of the lateral spacing impact for the three rotational directions with values of spatially-averaged (a) mean streamwise velocity $\langle \overline{u} \rangle$, and (b) turbulent intensity $\langle u' \rangle$, normalised by $U_0$ at all measured locations in downstream direction.

Immediately downstream of the turbines ($x/D$=1), the cross-sectional mean velocity recovery was observed to exceed values of $\langle \overline{u} \rangle / U_0 \geq 50\%$ for all configurations, especially for the CRF (counter-rotating forward) configurations which attained the highest initial wake velocity. Larger intra-turbine spacing consistently enhanced wake recovery due to a higher momentum flowing through the bypass region. In the case of CRF–2.0, for instance, $\langle \overline{u} \rangle / U_0$ fully recovered to the bulk velocity value at $x/D$=5, while for CRF–1.5 this was at approximately $x/D$=8.

Figure 3.21 indicates that rotational direction plays a more important role than lateral spacing, shown in Figure 3.20. In comparison to the single turbine case, CRF configurations featured the largest kinetic energy in the wake region due to a higher initial
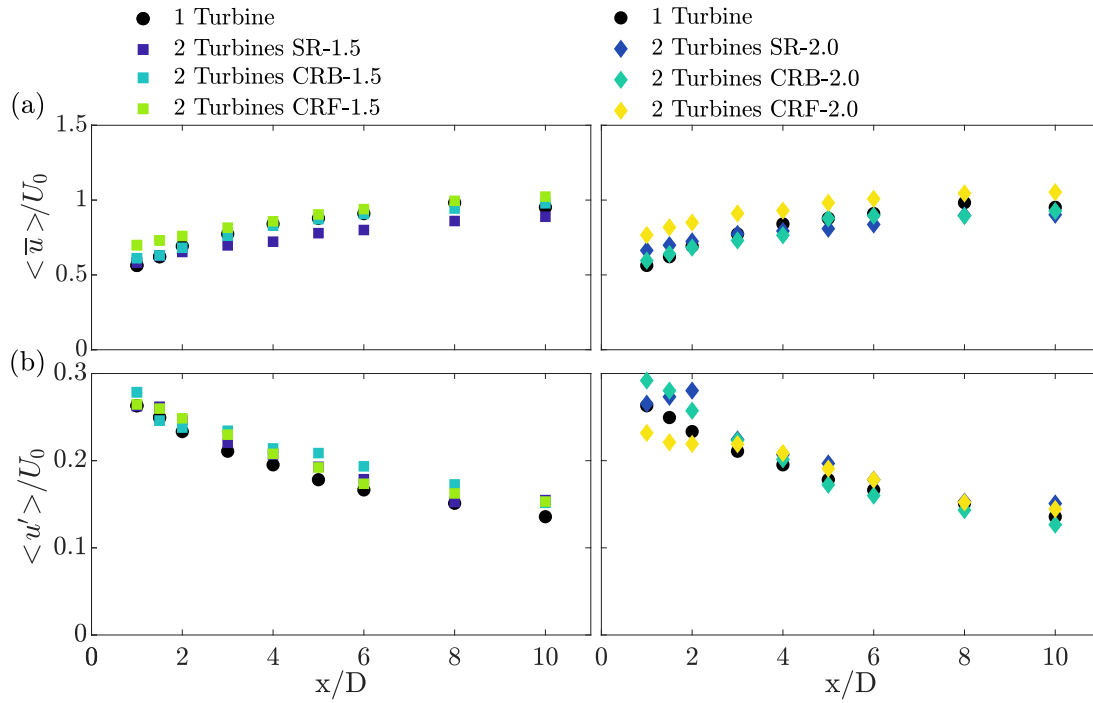
**Figure 3.21:** Comparison of the rotational direction for the two lateral spacing values with values of spatially-averaged (a) mean streamwise velocity $\langle \overline{u} \rangle$, and (b) turbulent intensity $\langle u' \rangle$, normalised by $U_0$ at all measured locations in downstream direction.

wake velocity, even exceeding the velocities from the single turbine wake. CRB setups followed a similar wake velocity evolution over the wake length as the single turbine, but with full wake recovery attained at 8 and 10 $D$ downstream for $S_y/D$=1.5 and 2.0, respectively. The slowest wake recovery was found for the SR cases that achieved velocities of $\langle \overline{u} \rangle/U_0 \geq 80\%$ at $x/D$=10 despite featuring a larger velocity than the ST case at $x/D$=1. In terms of wake unsteadiness, the highest turbulence intensity values ($\langle u' \rangle/U_0$) were found for both CRB cases as a consequence of the large interaction between both wakes at all downstream locations. In contrast, the lowest turbulence intensities were found in the case of CRF–2.0 due to the wider inter-turbine spacing, minimising the interplay between turbulent wakes. In all cases, free-stream values of $\langle u' \rangle/U_0$ were reached at approximately $x/D$=10.

The rate of wake recovery of the seven configurations is presented in Figure 3.22,

showing the spatially-averaged velocity deficit ($\Delta\langle\overline{u}\rangle$) and decay slopes of -1/3, -1/2 and -2/3. Classic shear-flow theory states that for self-similar axisymmetric and planar wakes the velocity deficit decay should be proportional to $x^{-2/3}$ and $x^{-1/2}$, respectively. While VAT wakes did not attain self-similarity within the measured range of $1\leq x/D \leq 10$, the decay rates appeared to be between -1/3 and -1/2 for all cases. The ST and both CRB cases followed a -1/2 slope over the measured wake length. In contrast, the SR cases showed an initial slope approximately equal to -1/3 until $x/D$=4–5 downstream, followed by a slope increase closer to a -1/2 decay. CRF setups featured the slowest decay rates of -1/3 over the wake length, despite showing the lowest velocity deficit at the wake onset.
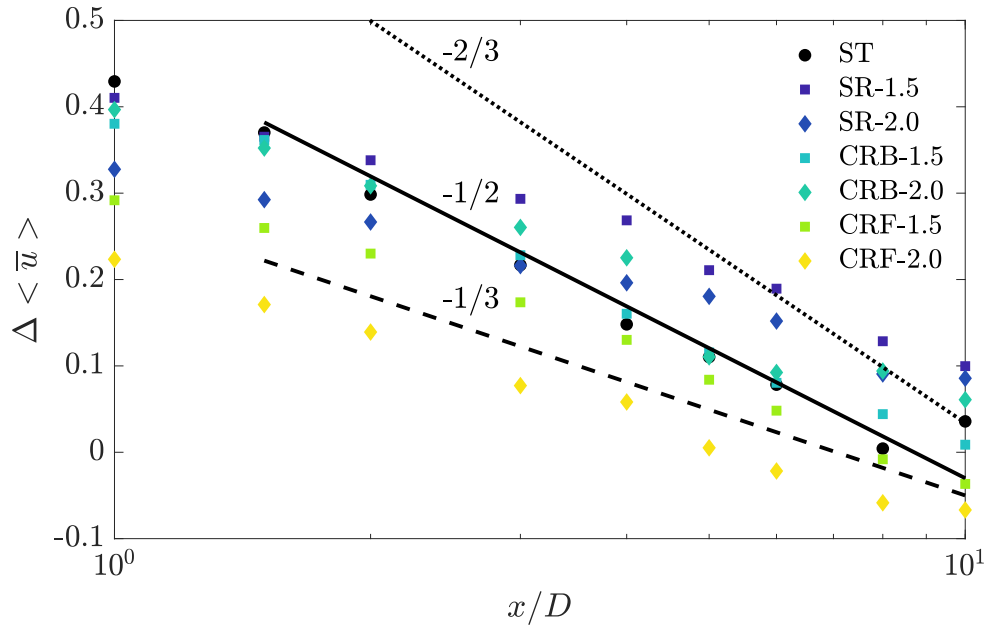


**Figure 3.22:** Wake recovery rate obtained from the spatially-averaged velocity deficit $\Delta\langle\overline{u}\rangle$ in semi-log scale for the seven cases. Straight, dashed and dotted lines represent the -1/2, -1/3 and -2/3 slopes.

### 3.3.2   Fish behaviour

To examine fish response to a single VAT, three experiments were conducted, invest-igating (a) the impact of discharge and turbine operation state under confined spatial conditions (Section 3.2.3.4.1), (b) the impact of spatial confinement (Section 3.2.3.4.2), and (c) the impact of VAT on shoaling behaviour (Section 3.2.3.4.3). Under confined conditions, fish behaviour was unaffected by discharge or turbine operation state. Fish, however, avoided the turbine by preferring to remain furthest downstream, outside the turbine wake. Under unconfined spatial conditions, fish remained at even greater dis-tances from the turbine, further reducing fish-turbine interactions. In comparison to individual fish, shoals covered greater swimming distances and moved closer to the turbine. In the following, results for each experiment are presented.

### 3.3.2.1   Experiment (a): Impact of flow condition and turbine operation state on fish movement

To quantify the impact of flow condition (mild versus high) and turbine operation state (stationary versus rotating) on fish movement, the following treatments were com-pared: MS, MR, HS, HR, as described in Section 3.2.3.4.1.

Independent of the flow condition and the turbine operation, fish spent most time down-stream (MS: 78 %, MR: 75 %, HS: 83 %, HR: 68 %; GLM, $p$=0.6395) and least up-stream (MS: 22 %, MR: 25 %, HS: 17 %, HR: 31 %; GLM, $p$=0.6395) as shown in Figure 3.24 (a) and indicated by an increase in scatter density in Figure 3.23. Within the downstream section, fish preferred to stay near the side walls but particularly fur-thest downstream within the corners of the test section as highlighted by the yellow colours in the density scatter plot marking the fish positions over time (Figure 3.23).

Fish spent slightly more time in the corner of the left-hand side of the test section (look-ing in downstream direction; MS: 46 %, MR: 28 %, HS: 45 %, HR: 25 %) compared
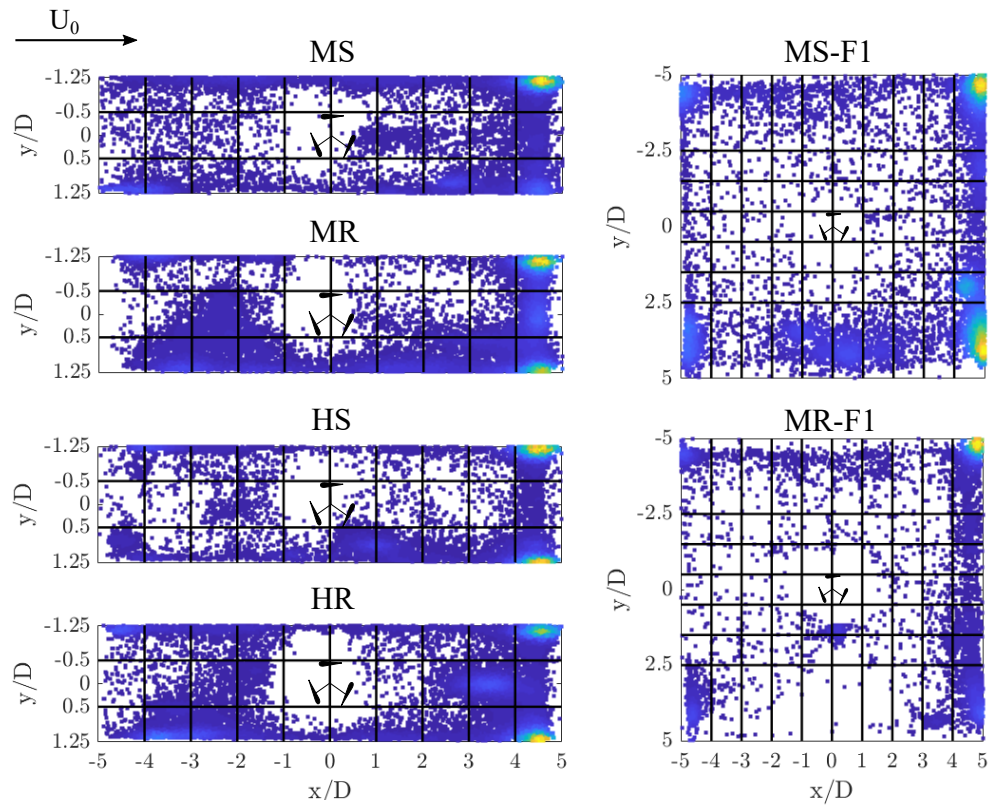
**Figure 3.23:** Scatter plot depicting the fish positions over the 10 min test time for all fish tested, contoured by the density of the scatter, with yellow colours marking the highest density of fish positions observed at a given location and blue colours showing lower densities. Results are presented for all four treatments analysed in the Flume 3 (MS, MR, HS, HR) and both treatments investigated in Flume 1 (MS-F1, MR-F1). Please note, MS-F1 and MR-F1 consists of less data point due to a reduced number of fish analysed and a lower frame rate used for the tracking analysis. Flow from left to right.

to the right-hand side (MS: 23 %, MR: 33 %, HS: 35 %, HR: 29 %). Neither observation, however, was influenced by treatment (GLM, $p$=0.2089 and $p$=0.7583 for left and right-hand side, respectively). Given that most time downstream was spent along the flume walls, fish were rarely observed swimming within the downstream centre (Figure 3.24 (c); MS: 8 %, MR: 14 %, HS: 3 %, HR: 15 %) which corresponds to the low-momentum region of the turbine's wake. Although treatment was not the decisive factor (GLM, $p$=0.195), time spent within the downstream centre increased when the

turbine rotated (Figure 3.23).
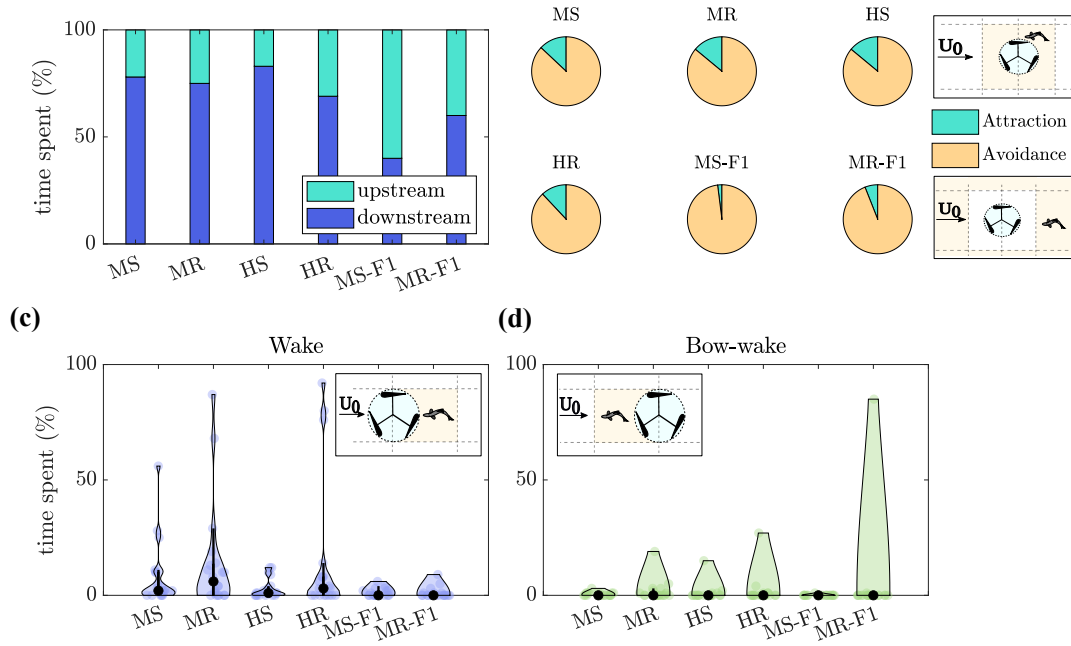


**Figure 3.24:** (a) Mean percentage of time spent upstream (green) and downstream (blue) of the turbine. (b) Percentage of time spent within the vicinity of the turbine (-2$\leq x/D \leq$2, and -1.25$\leq y/D \leq$1.25 and -2.5$\leq y/D \leq$2.5 for Flume 3 and 1, respectively, with the area used for the analysed being scaled to account for the difference in flume width), termed as "attraction", and outside this region, termed as "avoidance". (c) Scatter plots presenting the percentage of time spent within the wake (left; 0$\leq x/D \leq$5, -0.5$\leq y/D \leq$0.5) and (d) immediately upstream of the turbine within it's bow-wake (right; 0$\leq x/D \leq$-2, -0.5$\leq y/D \leq$0.5) for each fish tested. Results are presented for each treatment, including MS, MR, HS and HR for Flume 3 and MS-F1 and MR-F1 for Flume 1.

To analyse fish attraction and avoidance behaviour, the percentage time spent in and outside the turbine's vicinity was compared as shown in Figure 3.24 (b). Fish spent significantly more time avoiding the turbine (MS: 86 %, MR: 86 %, HS: 85 %, HR: 88 %; GLM, $p$<0.001) independent of turbine operation state and flow condition (GLM, attraction: $p$=0.1950, avoidance: $p$=0.9658), highlighting low attraction of the turbine. Although "attraction" time was influenced by the fish primarily using this region to

move between downstream and upstream region, they were also observed to swim near the turbine or within the turbine's bow-wake. During all treatments, however, only a few fish swam in the turbine's bow-wake (Figure 3.24 (d); MS: 1 %, MR: 4 %, HS: 5 %, HR: 7 %, z-test; MS versus MR: $p$=1.000, HS versus HR: $p$=1.000, MS versus HS: $p$=0.4788, MR versus HR: $p$=0.4996), with the time spent within this region being unaffected by treatment (GLM, $p$=0.6290).

In agreement with the large proportion of time spent avoiding the turbine and time spent within the downstream corners of the test section, mean distance from the turbine was approximately 8-9 $L_{fish}$ as shown in Figure 3.25 (b). Mean distance from the turbine was independent of discharge and turbine operation state (GLM,p=0.8932). Besides the distance maintained during the test period, fish movement was also quantified in terms of distance covered. Despite the large proportion of time spent within the downstream corners, fish moved through the entire test section as depicted in Figure 3.23. Distances covered were 257, 266, 185 and 331 $L_{fish}$ for MS, MR, HS and HR, respectively, as presented in Figure 3.25 (a). Overall, turbine operation state and discharge did not significantly influence distance swam (GLM, $p$=0.0734), although distance swam significantly differed between HS and HR (GLM, $p$=0.0090), with fish swimming approximately 1.8 times greater distances under the HR treatment.

Movement behaviour was also investigated in terms of swimming velocities, with the distribution of swimming velocities and the percentage of time spent swimming at the different velocities presented in Figure 3.25 (e) and (f), respectively. Independent of the treatment, fish swam most at velocities of 0-0.03 m/s (GLM, $p$=0.08227). While fish spent equal times swimming at this velocity range under mild flow conditions (MS and MR: 71 %), under high flow conditions, fish swam significantly more time at these velocities when the turbine was stationary (HS: 84 %, HR: 63 %; GLM, $p$=0.0114). In contrast, time spent swimming at velocities greater than 0.15 m/s was significantly influenced by the discharge and turbine operation state (GLM, $p$=0.0155). Specifically, a significant difference was found when comparing HS and HR (GLM, $p$=0.0068), and
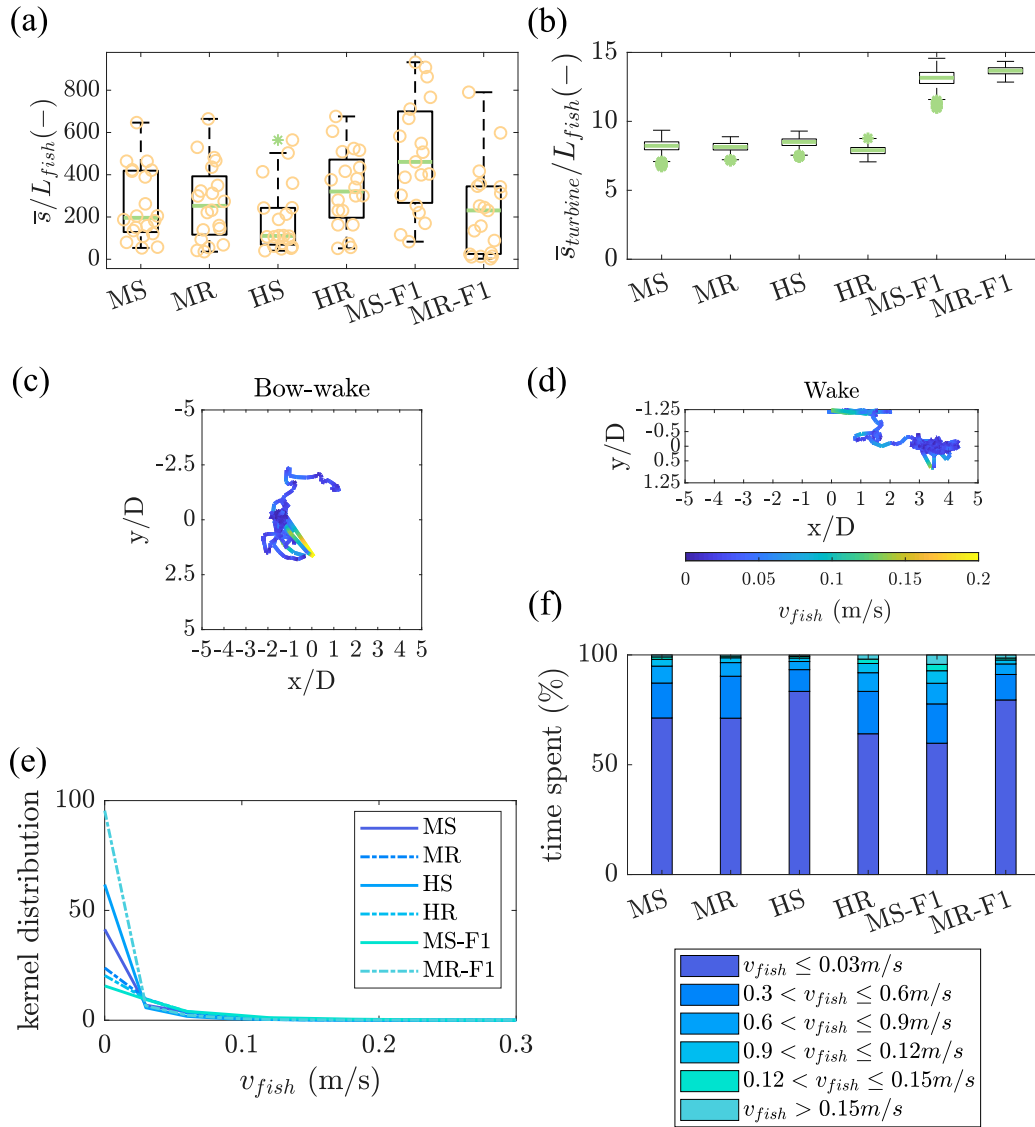
**Figure 3.25:** (a) Box plot showing the distribution of distances swam by each fish, with the green line marking the median distance covered, the yellow circles depicting the distance covered by each fish and the green stars showing outliers. (b) Box plot depicting of the mean distance kept to the turbine, with the green line marking the median and the green stars highlighting outliers. Example movement trajectories showing a fish swimming in (c) the turbine's bow-wake (MR-F1) and (d) the turbine's wake (HR). Colour of the line indicated the swimming velocity. (e) Distribution of swimming speeds observed over time and associated kernel distribution visualised as black line. Flow from left to right. (f) Mean proportion of time spent at each velocity bin, ranging from 0 m/s to >0.15 m/s. Results are presented for each treatment, including MS, MR, HS and HR for Flume 3, and MS-F1 and MR-F1 for Flume 1.

HR and MR (GLM, $p$=0.0045). In contrast, turbine operations state did not impact on time spent at velocities >0.15 m/s under mild flow condition (MR versus MS; GLM $p$=0.4928), and discharge was no influencing parameter when the turbine was stationary (MS versus HS; GLM, $p$=0.5910).
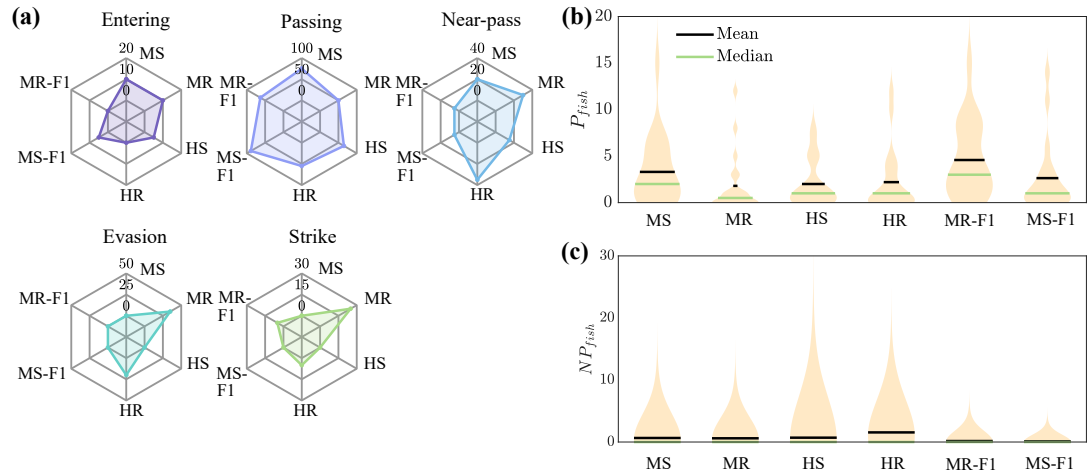


**Figure 3.26:** (a) Spyder plots depicting the percentage of fish observed to conduct the following behaviours: *Entering* into the turbine swept area; *Passing* from the downstream into the upstream section; *Near-pass*, i.e. attempting to pass into the upstream section but drifting or actively swimming downstream prior to passing $x/D$=0; *Evasion*, i.e. sudden movement to avoid a collision with the turbine's blade; and *Strike*, i.e. fish potentially colliding with the turbine's blade. (b) Distribution of upstream passes per fish ($P_{fish}$) and (c) near-passes per fish ($NP_{fish}$) presented as violin plot with the black and green line marking the mean and median of the distribution. Results are presented for all four treatments analysed in the Flume 3 (MS, MR, HS, HR) and both treatments investigated in Flume 1 (MS-F1, MR-F1).

Other fish behaviours analysed included entering into the rotor area, passing into the upstream region, attempting to pass (denoted as near-passes), actively evading a collision with the turbine and experiencing a strike from one of the turbine blades as described in Table 3.4 and depicted in Figure 3.26 (a). Fish entered the rotor area under all treatments except for the HR condition (MS: 10 %, MR: 10 %, HS: 5 %, HR: 0 %; z-test; MS versus MR, HS versus HR, and MS versus HS, $p$=1.000, MR versus

HR, $p$=0.4682). Similarly, treatment did not significantly impact the percentage of fish passing from the downstream into the upstream region (MS: 75 %, MR: 50 %, HS: 65 %, HR: 55 %; z-test, MS versus MR: $p$=0.1914, HS versus HR: $p$=0.7469, MS versus HS: $p$=0.7301, MR versus HR: $p$=1.000). In addition, the number of passes per fish ($P_{fish}$) were recorded as depicted in Figure 3.26 (b), showing similar $P_{fish}$ for all treatments (mean $\pm$ s.d.; MS: 3$\pm$4; MR, HS and HR: 2$\pm$3; GLM, $p$=0.5365). While a large number of fish successfully passed into the upstream section, others attempted to pass but drifted or actively swam downstream after reaching the cut-off line at $x/D$=0. Percentage of fish attempting to pass (MS: 20%, MR: 30%, HS: 15%, HR: 35%; z-test, MS versus MR: $p = 0.715$, HS versus HR: $p = 0.2733$, MS versus HS and MR versus HR: $p = 1.000$) and likewise, near-passes per fish ($NP_{fish}$; GLM, $p = 0.6189$; Figure 3.26 (c)) did not differ amongst treatments. Evasion moves were only observed when the turbine rotated (MS: 0 %, MR: 35 %, HS: 0 %, HR: 20 %), which were significantly higher under mild rather than high flow conditions (z-test, MS versus MR: $p$=0.0125, HS versus HR: $p$=0.1138, MR versus HR: $p$=0.4788). Likewise, potential collisions were only observed when the turbine rotated (MS: 0 %, MR: 25 %, HS: 0 %, HR: 5 %), with the percentage of fish potentially experiencing a strike being almost significantly affected by the discharge when the turbine rotated (MS versus MR: $p$=0.0558, HS versus HR: $p$=1.000, MR versus HR: $p$=0.184).

### 3.3.2.2    Experiment (b): Impact of spatial confinement on fish movement

The impact of spatial confinement was investigated by comparing fish swimming in Flume 3 (MS and MR) against fish swimming in Flume 1 (MS-F1 and MR-F1) under mild flow conditions and for both turbine rotation states (stationary (S) and rotating (R)) as described in Section 3.2.3.4.2. Here, the lateral length of the test section of Flume 1 was four times the width of Flume 3, hence providing more space for fish to pass around the turbine.

While fish spent most time downstream and least time upstream under confined flume

conditions (Flume 3), the increase in lateral space resulted in a higher percentage of time spent upstream independent of the turbine operation state (MS: 22 %, MR: 25 %, MS-F1: 60 %, MR-F1: 40 %) as shown in Figure 3.24 (a), highlighting a significant impact of the spatial conditions (GLM, percentage time upstream: $p$=0.0044, percentage time downstream: $p$=0.0045). Particularly when the turbine was stationary (MS and MS-F1), time spent upstream and downstream significantly differed between the two flumes (GLM, $p$=0.0012 and $p$=0.0012, respectively). Downstream of the turbine, fish spent most time along the flume walls independent of the spatial confinement as shown in Figure 3.23 (LHS: MS: 46%, MR: 28 %, MS-F1: 27 %, MR-F1: 48 %, GLM, $p$=0.1672; RHS: MS: 23 %, MR: 33 %, MS-F1: 12 %, MR-F1: 11 %, GLM, $p$=0.0591). Hence, fish spent less time within the downstream centre of the test section as depicted in Figure 3.24 (c) (MS: 8 %, MR: 14 %, MS-F1: 1 %, MR-F1: 1 %; GLM, $p$=0.2934) and Figure 3.23. Fish length did impact time spent within the wake of the turbine, with larger individuals spending more time within the low-momentum region (GLM, estimate: 1.1228, std error: 0.2671, $p$<0.001).

Interestingly, fish were also observed to swim immediately upstream of the turbine, i.e., within the turbine's bow-wake (MS: 35 %, MR: 40 %, MS-F1: 5 %, MR-F1: 11 %). Spatial confinement did not significantly impact the number of fish observed in the bow-wake when the turbine was stationary (MS versus MS-F1; z-test, $p$=0.0572) or when the turbine rotated (MR versus MR-F1; z-test, $p$=0.0818). While the time spent in the bow-wake strongly varied amongst individuals (Figure 3.24 (d)), percentage time spent was unaffected by fish standard length (GLM, $p$=0.6961) and treatment (GLM, $p$=0.5156). Analysis of fish attraction and avoidance behaviour (Figure 3.24 (c)) showed that fish spent significantly more time outside the turbine's vicinity (GLM, $p$<0.001) independent of the spatial condition (MS: 86 %, MR: 86 %, MS-F1: 98 %, MR-F1: 6 %; GLM, $p$=0.0942). Hence, least time was spent near the turbine independent of the treatment (MS: 14 %, MR: 14 %, MS-F1: 2 %, MR-F1: 6 %; GLM, $p$=0.0962). Only when the turbine was stationary, time spent near the turbine significantly differed amongst flumes (MS versus MS-F1; GLM, $p$=0.0424).

Fish movement behaviour was quantified in terms of distance covered during the test period, distance maintained from the turbine and swimming velocities as presented in Figure 3.25 (a)(b), (e) and (f), respectively. On average, a greater mean swimming distances was apparent for MS-F1, which was almost twice as far as for the other treatments (MS: 257 $L_{fish}$, MR: 266 $L_{fish}$, MS-F1: 489 $L_{fish}$, MR-F1: 230 $L_{fish}$), highlighting the significant impact of the spatial condition and turbine operation state (GLM, $p$<0.001). More specifically, under unconfined conditions, fish covered a greater distance when the turbine was stationary rather than rotating (MS-F1 versus MR-F1; GLM, $p$<0.001). In contrast, fish standard length did not significantly influence distance swam (GLM, $p$=0.75421). Due to the increase in lateral space in the case of Flume 1 and in agreement with the observations that fish spent most time within the downstream corners (Figure 3.23), mean distance maintained from the turbine increased to 13 and 14 $L_{fish}$ for MS-F1 and MR-F1, respectively, compared to $8 L_{fish}$ for MS and MR (Figure 3.25 (b)). Hence, more space resulted in significant greater distance maintained form the turbine (GLM, MR versus MR-F1: $p$<0.001 and MS versus MS-F1: $p$<0.001) independent of the turbine operation state (GLM, MR versus MS: $p$=0.6623 and MR-F1 versus MS-F1: $p$=0.1499). This was also influenced by fish standard length (GLM, $p$=0.0043).

As in Section 3.3.2.1 (Figure 3.25 (e) and (f)), swimming velocities were analysed by comparing the density distribution of the swimming velocities recorded and the percentage of time spent at these velocities. Fish swam most at swimming speeds of 0-0.03 m/s (MS: 71 %, MR: 71 %, MS-F1: 49 %, MR-F1: 51 %), unaffected by treatment (GLM, $p$=0.0992) and fish standard length (GLM, $p$=0.2397). While under confined condition, fish spent equal time swimming at these velocities (MS and MR: 71 %), under confined conditions, fish spent significantly less time at the lower velocities when the turbine was stationary (MR-F1 versus MS-F1; GLM, $p$=0.0134). In contrast, treatment significantly influenced the time spent at swimming velocities greater than 0.15 m/s (GLM, $p$<0.001) while fish standard length was a non-significant parameter (GLM, $p$=0.5291). A significantly larger proportion of time was spent at

higher velocities under unconfined conditions compared to confined conditions when the turbine was stationary (MS versus MS-F1; GLM, $p<0.001$) and when the turbine rotated (MS-F1 versus MR-F1; GLM, $p<0.001$).

Fish behaviour was also analysed in terms of the percentage of fish entering the turbine, exhibiting evasion behaviour, presumable colliding with the turbine's blade, attempting to pass ("near-pass") and passing from the downstream region into the upstream region (Figure 3.26 (a)). Fish entered the rotor area under all treatments except for the MR-F1 condition (MS: 10 %, MR: 10 %, MS-F1: 5 %, MR-F1: 0 %; z-test, MS versus MS-F1: $p=0.9793$ and MR and MR-F1: $p=0.4908$). Strikes, on the other hand, were only observed when the turbine rotated independent of the spatial confinement (MS: 0 %, MR: 25 %, MS-F1: 0 %, MR-F1: 5 %; z-test, MS versus MS-F1: $p=NA$ and MR versus MR-F1: $p=0.2064$). Likewise, evasion moves were only observed when the turbine rotated, with a significantly lower number of fish evading under unconfined spatial conditions (MR: 25 %, MR-F1: 5 %; z-test, MR versus MR-F1: $p=0.0151$).

Upstream passes and near-passes were the most frequent observed behaviours. Independent of the turbine operation state and spatial confinement, similar numbers of fish passed into the upstream section (MS: 75 %, MR: 50 %, MS-F1: 89 %, MR-F1: 63 %; z-test, MS versus MS-F1: $p=0.4473$ and MR versus MR-F1: $p=0.6134$) and attempted to pass upstream (MS: 20 %, MR: 30 %, MS-F1: 5 % and MR-F1: 5 %; z-test, MS versus MS-F1: $p=0.3698$ and MR versus MR-F1: $p=0.1108$). Additionally, the number of passes (Figure 3.26 (b)) and near-passes (Figure 3.26 (c)) per fish was determined. In agreement with the number of fish passing and attempting to pass, the number of passes per fish (MS: 20 %, MR: 30 %, MS-F1 and MR-F1: 5 %; GLM, $p=0.1325$) and number of near-passes per fish (mean $\pm$ s.d.; MS: $1\pm2$, MR: $1\pm1$, MS-F1: $0\pm1$, MR-F1: 0; GLM, $p=0.7544$) were unaffected by the treatment. Fish standard length, however, affected the number of near-passes per fish, with larger individuals being more likely to undergo passage attempts into the upstream region (GLM, estimate: 0.04049, std error: 0.01708, $p=0.0202$).

**3.3.2.3   Experiment (c): Impact of VAT on shoaling behaviour**

To examine the impact of a VAT on shoaling behaviour, small groups comprising of three fish were tested under mild flow conditions for a single, rotating turbine in Flume 1 as described in Section 3.2.3.4.3. Furthermore, results obtained were compared against individual fish swimming under similar test conditions (MR-F1). The preliminary results of the movement behaviour shown in Figure 3.27 were analysed in terms of distance covered during the test period (a), distance maintained from the turbine (b), time spent as individuals, in pairs or as a shoal (c-d), swimming velocities observed (e) and mean proportion of time spent at these velocities (f).

Swimming behaviour was analysed in terms of time spent as individual (i.e., not swimming together), swimming in pairs (i.e., two fish together and one fish swimming along) and shoaling (i.e., all fish together) as shown in Figure 3.27 (c) and (d). On average, fish spent almost equally time in pairs (45 %) and as individuals (44 %), and least time as a shoal (12 %), independent of mean group standard length (GLM, individual: $p$=0.3071, pair: $p$=0.7092, shoal: $p$=0.1164).

The analysis of the mean distance swam during the test period (Figure 3.27 (a)) showed that on average groups covered a distance of approximately $395\pm110\,L_{fish}$, with distance swam varying significantly between groups (ANOVA, $p$<0.001). Mean group standard length did not significantly influence mean group distance swam (GLM, $p$=0.1369). Furthermore, mean group distance was unaffected by the time spent as an individual (GLM, $p$=0.5828), a pair (GLM, $p$=0.9457) or a shoal (GLM, $p$=0.2434). In comparison to individual fish which covered an average distance of $230\pm217\,L_{fish}$, shoals swam significantly larger distances (GLM, estimate: 165.69, std error: 63.69, $p$=0.0136). This difference in distance swam was not associated with fish standard length (GLM, $p$=0.8715).

During the testing period, shoals remained an approximate mean distance of $8\pm2L_{fish}$ from the turbine which, however, significantly varied amongst group (ANOVA,
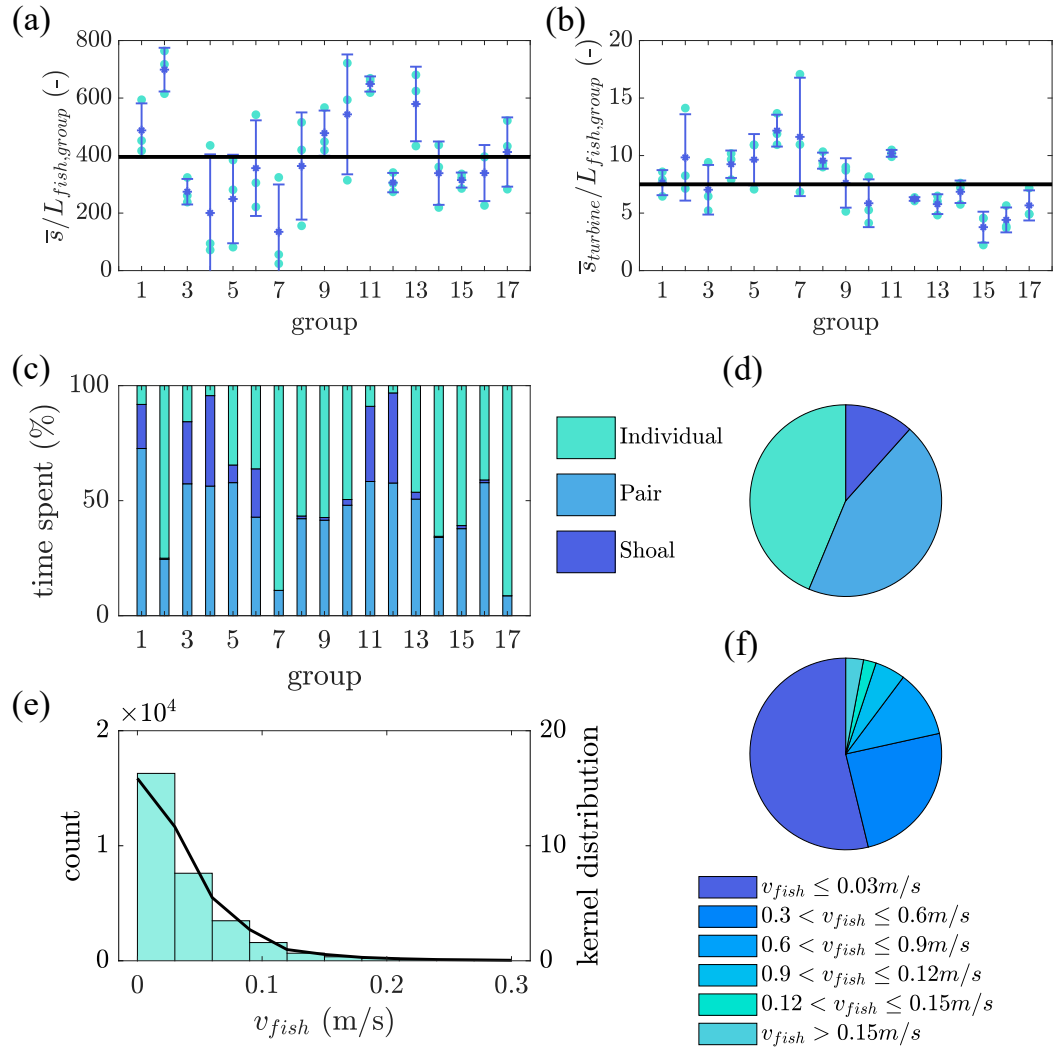
**Figure 3.27:** (a) Normalised distance covered ($\overline{s}/L_{fish,group}$) for each fish (light green dots) and mean $\pm$ s.d. (blue) for each group, with the black line marking the overall mean distance swam by all groups. (b) Estimated normalised distance maintained from the turbine ($\overline{s}_{turbine}/L_{fish,group}$) for each fish (light green dots) and mean $\pm$ s.d. (blue) for each group, with the black line marking the overall mean distance swam by all groups. (c) Percentage of time spent swimming as individuals (light green), as a pair (light blue) and as a shoal (blue), shown for each group analysed and (d) mean proportion of time for each category averaged over all groups. (e) Distribution of swimming speeds observed over time and associated kernel distribution visualised as black line. (f) Mean proportion of time spent at each velocity bin, ranging from 0 m/s to >0.15 m/s.

$p$=0.1080; Figure 3.27 (b)). As for the mean group distance covered, mean distance kept was not significantly influenced by mean group standard length (GLM, $p$=0.0745) or the time fish spent swimming as individual (GLM, $p$=0.6708), pair (GLM, $p$=0.7739) or shoal (GLM, $p$=0.4018). In contrast, individual fish kept approximately $14\pm3\,L_{fish}$ from the turbine which is a significantly greater distance compared to shoals (GLM, $p$=0.0169). Here, standard length was a significant impact factor when comparing shoals and individuals (GLM, $p$<0.001).

As in the individual fish experiment, the distribution of swimming velocities was analysed, with results presented in Figure 3.27 (e) and (f). Highest number of swimming velocities and density was found within the range of 0-0.3 m/s which was also reflected by fish swimming most time at these low velocities (54 %; Figure 3.27 (f)). The percentage of time spent swimming at velocities of 0-0.3 m/s and >0.15 m/s was not significantly influenced by the mean group standard length (GLM, $p$=0.848 and $p$=0.5796 for 0-0.3 m/s and >0.15 m/s, respectively). Comparing individual fish against shoals showed that shoals spent significantly less time swimming with velocities between 0-0.3 m/s (GLM, estimate: -25.720, std error: 7.094, $p$<0.001), unaffected by fish standard length (GLM, $p$=0.0557). In contrast, shoals, compared to individuals, swam significantly, especially at velocities greater than 0.15 m/s (GLM, $p$=0.0233).

## 3.4   Discussion

Globally, many people still lack access to affordable, reliable, sustainable energy, resulting in socio-economic inequality [149]. Hydropower offers a renewable energy source that is not yet fully used. Initially deemed environmentally friendly, the negative environmental impacts of traditional, large-scale hydropower plants [18] resulted in a greater focus on small-scale alternatives such as hydrokinetic vertical axis turbines. VAT harnesses energy from the free-flowing flow of rivers and estuaries without requiring hydraulic structures, large land areas, high rotational speeds, or complex turbine

designs, and are therefore presumed to reduce environmental impacts, particularly on the aquatic ecosystem. The main drawback, however, remains in their lower standalone performance, which can be overcome by deploying several VAT rotors in close proximity as an array [113, 227]. This chapter addresses the lack of empirical evidence on the wake alterations associated with twin-turbines and their impact on fish movement.

The wake of a single VAT was characterised by a low-momentum region immediately downstream of the rotor, which was asymmetric about its centreline. This wake asymmetry strongly influenced the wake of twin-VATs. Depending on the rotational direction of these turbines, their individual wakes either propagated alongside each other (SR), converged (CRB), or diverged (CRF). The lateral spacing between the turbines is an important parameter influencing wake recovery. The larger spacing tested allowed more flow through the bypass region, contributing to a faster wake recovery.

Fish behaviour response to a single VAT deployed under confined spatial conditions was unaffected by flow conditions and turbine operation state, with fish preferring to swim downstream outside the turbine wake. Under unconfined spatial conditions, fish remained at even greater distances from the turbine, further reducing fish-turbine interactions. In comparison to individual fish, shoals were more explorative, swimming closer to the turbine, and covered greater distances. In the following, hydrodynamic (Section 3.4.1) and fish behaviour results (Section 3.4.2) are discussed, and study limitations are outlined (Section 3.4.3). Furthermore, research gaps are highlighted (Section 3.4.4).

### 3.4.1 Impact of single and twin-vertical axis turbines on wake hydrodynamics

The turbine configurations tested comprised a single VAT (ST) and three twin-turbine setups with turbines rotating in the same rotational direction (SR) and in counter-clockwise forward (CRF) or backward (CRB) direction, laterally spaced by $S_y$=1.5$D$

and $S_y$=2$D$. The wake of a single VAT turbine (Section 3.3.1) was characterised by an area of large velocity deficit immediately downstream of the turbine. This low-momentum region was particularly pronounced on the upstroke side, where the blades moved against the flow and, therefore, generated the highest relative velocity. As a result, the wake was asymmetric about the turbine's centreline, which agrees with previous observations (e.g., [32, 173, 226]). Furthermore, the near wake of the turbine (i.e. $x/D$<2 [162]) was characterised by tip-vortices generated by the blade on the upstroke side, pockets of low mean streamwise velocity, high levels of tke, and positive and negative values in $\overline{u'v'}/U_0^2$ and $\overline{u'w'}/U_0^2$ at height of the bottom and top tip of the blades. These turbine-induced vortical structures, however, only prevailed in the near wake as they lost their coherence with increasing downstream distance due to mixing with the ambient flow. Similar energetic vortical structures were observed numerically [163] and experimentally, for instance, by using PIV to visualise the near wake of a VAT [186]. The downstroke side, in contrast, was described by higher mean streamwise velocities and lower values of tke. Following the near wake, the transitional wake (i.e., 2<$x/D$<5 [162]) was characterised by a lateral and vertical expansion of the wake. Overall, the wake evolution observed for the ST case is similar to the wake previously outlined in Figure 3.1, and those presented in [186] where Reynolds number was almost one order of magnitude higher.

The wake behind twin-VAT rotating in the same rotational direction was similar to the wake characteristics of the ST case, consisting of an individual, asymmetric low-momentum region downstream of each turbine. In the near wake, both wakes progressed alongside each other independent of the lateral turbine spacing. Only in the transition zone, both wakes began to interact and merge into a single wake forming a combined low-momentum region, characterised of high tke values [119]. With increasing downstream distance, the combined wake vertically and laterally expanded, particularly towards the upstroke side of $T_2$.

In the case of two counter-clockwise rotating turbines, rotational direction determined

whether the individual wakes generated by each turbine progressed towards or away from each other. As for the CRF case, similar wake characteristics were found as for the ST case [226]. In this scenario, both wakes propagated outwards in opposite directions [119, 173, 226, 225], with the bypass flow between turbines, amplified by the downstroke motion of the blades, further enhancing wake separation as indicated in Figure 3.2 (b). Hence, greater lateral turbine spacings further enhance the bypass flow and wake separation. In the case of CRF-1.5, both wakes remained separated by the bypass flow until $x/D \approx 1.5$ and mirrored each other relative to the centreline through the gap spacing $S_y$ before gradually merging into one combined wake at $x/D \geq 5$. In the case of CRF-2.0, this merging process was delayed, likely due to the increase in bypass flow. Similarly, an experimental study of CRF twin-wind turbines, laterally spaced by $S_y/D$=1.2 reported that both wakes remained separated until $x/D \approx 6$ [226], which is in agreement with the presented results for the CRF-1.5 case. For an inter-turbine spacing of $S_y/D$=2.0, Lam and Peng (2017) observed almost no interaction between both wakes by $x/D$=10 [119] as observed in this chapter.

In contrast, the individual wakes of two CRB twin-turbines were observed to propagate towards each other [119, 173, 226], already merging at $x/D$=1 and $x/D$=2 into a single low-momentum region characterised by high values in tke for the CRB-1.5 and CRB-2.0 case, respectively. The collapse into a single wake was a result of the weaker bypass flow between turbines, caused by the upstroke motion of the turbine blades in this region [119]. Similarly, in Lam and Peng (2017) wakes began to merge at $x/D$=3.0 and completely merged by $x/D$=7.0 for a similar CRB–2.0 case [119]. The combined wake showed a narrower lateral extent compared to the SR and CRF case [173] and extended notably in the vertical direction [225]. The vertical wake extension was observed to be a result of the lateral progression of the wakes towards each other, causing the wake to escape vertically [225].

Although all tested configurations showed a recovery of the cross-sectional mean velocity of at least 50%, turbine rotational direction and inter-turbine spacing influenced

wake recovery. Fastest initial wake recovery, for instance, was observed for the CRF case, with $\langle \overline{u} \rangle / U_0$ fully recovered to the bulk velocity value at $x/D$=5 and $x/D$=8 for the CRF-2.0 and CRF-1.5 case, respectively. In comparison, for an intra-turbine spacing of $S_y/D$=1.3, Vergaerde et al. (2020) reported a wake recovery of 75 % at $x/D$=5.2 [226]. In contrast, full wake recovery was attained at $x/D$=8 and $x/D$=10 in the case of CRB-2.0 and CRB-1.5, respectively. Similarly, Vergaerede et al. (2020) reported a slower wake recovery for CRB twin-turbines compared to a CRF setup [225]. The slowest wake recovery was found for both SR cases, which only achieved a wake recovery of 80 % by $x/D$=10. Hence, turbine rotational direction rather than inter-turbine spacing was the decisive factor influencing wake recovery.

## 3.4.2 Fish behaviour adaptations associated with vertical axis turbines

The observed changes in wake hydrodynamics associated with single and twin-VAT may influence the aquatic environment by altering the movement of aquatic organisms. Fish response to a single vertical axis turbine was investigated through a series of experiments, studying the influence of parameters such as discharge, turbine operation state and spatial confinement.

### 3.4.2.1   Impact of flow conditions and turbine operation state of fish movement

The impact of discharge and turbine operation state was examined under confined flow and spatial conditions, which may naturally arise when positioning turbines in arrays [52], or between rocks [87], and ducts [135, 12] to increase turbine performance.

Independent of the discharge and turbine operation state, fish spent most time within the downstream section, particularly along the sidewall and furthest downstream corners. Hence, only a few fish swam in the turbine wake. This observation was contrary to what was expected as fish were previously observed to accumulate in the wake of a marine

turbine support structure [74]. The low attraction to the turbine wake may be a result of a too low ambient flow. Fish exposed to an even higher environment (i.e., higher incoming flow) are anticipated to use the low-momentum region of the wake to seek refuge. Additional experiments investigating fish spatial behaviour under higher flow conditions will be required to verify this hypothesis. Moreover, the low attraction to the turbine wake may be a result of the three-dimensional turbulent structures shed by the turbine blades, creating pockets of high tke and Reynolds stress. Previous studies showed fish avoiding regions of high vorticity, Reynolds shear stress and tke [146, 93], and highlighted the ability of vortices to destabilise fish [134, 146].

Interestingly, although non-significant, a small number of fish swam immediately upstream of the turbine, hence, in the turbine's bow-wake. So far, this behaviour has only been reported for stationary obstacles such as D-shape cylinders [130, 177, 218]. The bow-wake of a D-shape cylinder is characterised by low streamwise velocities and high-pressure [130]. Rainbow trout swimming in this region swam with reduced tail-beat frequency, body wave speed, and body curvature, indicating a decrease in energy expenditure [130]. Although the bow-wake is characterised by a low Strouhal number, indicating suboptimal swimming efficiencies, the energy expenditure observed in this region suggests that "bow-waking" is a unique swimming mechanism to hold station, similar to Kármán gaiting [130].

Besides potential avoidance effects associated with the turbine's wake, fish were not attracted to the turbine structure, as shown by the large distance kept from the turbine and most time spent outside its vicinity. Similarly, a laboratory study investigating the impact of a small-scale HAT on *Oryzias latipes*, *Gnathopogon elongatus*, and *Rhodeus ocellatus ocellatus* reported that 71 % of the fish avoided the turbine area or swam away from the turbine [247].

Despite avoiding the turbine and its wake, fish swam the length of the test section, including both downstream and upstream regions. While exploring the test section, more than 50 % of the fish passed at least once from downstream into the upstream region,

unaffected by the treatment. Upstream passage was the most common behaviour, as also observed by Yoshida et al. (2020) [248]. Passage behaviour is species-specific but has so far only been studied for migratory fish species. Atlantic salmon (*Salmo salar*), for example, passed a model VAT more frequently than brown trout (*Salmo trutta*) [24], and American shad (*Alosa sapidissima*) [42]. Berry et al. (2019) also highlighted that fish preferred to pass around the turbine rather than through the rotor area [24], consistent with the results presented in Section 3.3.2.1. In contrast, Castro-Santos and Haro (2015) reported that 72 % of the downstream migrating Atlantic salmon smolts passed through, above, or underneath the VAT rotor while only 28 % passed around the turbine, potentially associated with smolts being actively entrained or even attracted to the turbine [42]. Passage behaviour has been associated with fish body shape, noting differences between compressiform (torpedo shape) and fusiform (tall and thin shape, small body width) fish, with compressiform fish passing through the gap furthest away from the turbine [87].

Another behaviour observed included fish entering the rotor area, which occurred during all treatments, except when the turbine rotated under high flow conditions. Similar observations were reported for a helical, marine VAT installed between reefs, showing that fish only entered the rotor area for low flow velocities and turbine rotational speeds [87]. Furthermore, the investigation of a ducted river turbine showed that 35 % less fish entered the rotor area when the turbine rotated compared to stationary conditions [229].

In the current study, collisions with the turbine and evasion movements to avoid a direct collision with the turbine blade were only observed when the turbine rotated. Evasion movement has been observed across a wide range of species, characterised by burst swimming away from the turbine and sudden moves near the turbine blade [87]. In contrast to the observations presented in this chapter, Hammar et al. (2013) and Berry et al. (2019) observed no collision or close contacts with a model VAT [87, 24]. Despite the observed strikes during the conducted experiments, no apparent external injuries were noted, consistent with previous laboratory studies investigating hydrokinetic turbines

[42, 248]. While strike risk is assumed to be influenced by wake alterations distracting fish from the turbine, under natural conditions, other environmental factors will also strongly influence strike risk (e.g., noise, turbidity) [248]. Proximity to the turbine may also depend on the fish's personality [87, 24], with bolder, more explorative fish being closer to the turbine or even entering the rotor area, and shyer individuals keeping greater distances. Fish-turbine interaction (e.g., entering, colliding, avoiding) has also been related to fish swimming capabilities [247]. A laboratory study examining the impact of a scaled HAT showed that *Gnathopogon elongates*, for instance, were more active near the turbine as their maximum swimming speed exceeded the turbine's tip speed. In contrast, fish with slower swimming speeds or preference to swimming near the bed such as *Oryzias latipes* and *Rhodeus ocellatus ocellatus* avoided swimming near the rotor, resulting in a reduced turbine interaction [247].

### 3.4.2.2 Impact of spatial confinement on fish movement

While most laboratory studies investigated the impact of hydrokinetic turbines under confined laboratory conditions [42, 24, 248, 247], only a few studies have examined the influence of space around the turbine on fish movement [87]. To investigate the impact of spatial confinement on fish movement, a replica test was conducted in a four times wider test section (Flume 1) under mild flow conditions for a stationary and rotating VAT.

Under unconfined flow conditions, fish spent more time upstream. In the downstream section, fish spent most time near the flume walls, characterised by free-stream velocities. As in the confined conditions, fish spent least time within the turbine wake. Hence, fish preferred the free-stream region rather than the low-momentum region. Likewise, fish spent less time within the turbine's vicinity under confined, compared to unconfined spatial conditions, further consolidating the assumption that fish avoid the near-turbine region. The difference in time spent within the turbine vicinity between the two confinement conditions likely arises from fish passing through this region to

move between downstream and upstream sections in Flume 3. The increased avoidance of the turbine region was also reflected by a greater distance maintained from the turbine under unconfined spatial conditions because of the increase in space.

Moreover, similar number of fish entering the rotor area, showing evasion movements, experiencing strikes, passing and attempting to pass upstream were recorded independent of the spatial confinement. Greater difference between confinement conditions were expected due to the increase in space between the turbine and flume walls allowing fish to swim within the free-stream region. Unlike under unconfined conditions, these regions were characterised by high-momentum flow due to the blockage provided by the turbine and the resulting flow confinement.

### 3.4.2.3   Impact of VAT on shoaling behaviour

Shoaling has several benefits regarding predation avoidance, increased foraging, and reduced energy expenditure [116]. Shoaling behaviour was investigated for a single, rotating VAT and compared to individual fish swimming under the same test conditions.

In comparison to individual fish, fish within the shoals covered, on average, longer distances during the test period and maintained a smaller distance to the turbine. Moreover, small groups of fish spent less time swimming at lower velocities than individual fish. Hence, small fish groups appeared to have a higher movement activity and were more explorative than individual fish. In contrast, a field study comparing individual fish and shoals in the vicinity of a ducted riverine turbine highlighted a 56 % lower probability of fish shoals entering the rotor and a higher probability of avoiding the turbine [229].

The increase in swimming activity of fish shoals, however, was not subject to the time spent as a shoal. In contrast, these fish spent most time swimming as pairs or individuals. The small proportion of time shoaling may be species-specific preference or caused by a too-short habituation period. As no literature exists defining the time required for rainbow trout to form a shoal, a similar time as used for guppies was applied [83]. The

short time shoaling may also be a response to the presence of the turbine. A tank study investigating shoaling behaviour of juvenile Atlantic striped bass (*Morone saxatilis*) in response to a single VAT showed that shoaling was influenced by the turbine operation state [137]. This study was conducted over several weeks, with the turbine being on, off, and on for weeks one, two, and three, respectively. While during week one 89 % of the fish shoaled and circled the tank, only 43% of the fish remained shoals, with 57 % engaged in other behaviours during week two when the turbine rotated. In week three, more fish were observed to shoal again (49 %).

### 3.4.3 Experimental limitations

Generalisation, transferability, and comparability of the fish behaviour experiments and the corresponding results to full-scale VAT deployed in riverine, estuarine, and marine environments are limited. Fish behaviour studies were conducted under simplified, laboratory conditions, comprising a straight flume with a fixed bed which may influence streamwise velocities near the bed. Furthermore, the interaction between flow alterations and sediment transport processes is neglected, which, in turn, may impact fish behaviour, particularly when investigating bottom-feeding species.

Also, experiments were conducted using clean, purified water, disregarding the natural turbidity, for example, of rivers and estuaries, potentially created through the suspension of particles. Water turbidity may be an important factor influencing fish vision and may therefore influence fish behaviour. In addition, experiments were conducted under strong lighting conditions. The light conditions within the lab also could not be adjusted to generate an even distribution of light inside the test section, despite the use of spotlights to minimise shaded areas. Studies investigating horizontal axis turbines under dark conditions reported an increase in avoidance behaviour, which was characterised by more fish avoiding the turbine, swimming away, and less frequently approaching the turbine [247]. This observed behaviour was assumed to be related to the inability to visually detect the blades [247].

Further limitations were caused by the experimental setup. To capture the whole of the test section, the camera was positioned at a height conflicting with other laboratory installation, resulting in skewed and distorted images as the camera could not be positioned directly above the test section's centre. Although the flume bed was covered with a white PVC sheet to enhance the contrast between fish and flume bed, fish blended in with the flow straightener and the flume walls which was exacerbated by the large difference between flume bed and camera, impeding their identification during the analysis process.

The experimental analysis was also limited using the open-source tracking software Kinovea 0.8.15. Due to the large susceptibility of errors in the tracking processes caused by the compromised image quality, images had to be manually corrected. Therefore, the number of images was reduced, causing a loss of information. Particularly when tracking multiple fish, a reduction in frame rate might have caused the mix-up of fish ids. A wide range of open-source tracking software are available [72], however, most software are only suitable for a small, idealised test section, struggling with obstacles within the test section (e.g., turbine, flow straighteners), floating particles, and uneven lighting conditions. Further research is required in identifying alternative methods to extract fish positions over time and swimming kinematics to efficiently generate more accurate results.

Methodical constraints regarding the hydrodynamic measurements arose from the physical limitations of the ADV, preventing velocity measurements over the upper part of the water column, near the bed, and within $x/D = 1$ downstream of the turbine. High-fidelity simulations or other advanced measurement techniques such as PIV may be advantageous to unveil the instantaneous flow and turbulent structures shed by the blades within the near wake of the turbine.

Despite the limitations listed, the results presented in Section 3.3 highlight flow alterations expected for a single VAT and different twin-turbine configurations, which are important to consider when designing larger turbine arrays. Furthermore, little

is known about fish behaviour response to hydrokinetic turbines. Hence, the results presented still provide new insights into how spatial confinement and turbine operation may impact individual fish and small groups of fish approaching a single VAT.

### 3.4.4 Scope for further research

Based on the findings discussed in Section 3.4.1 and 3.4.2 and the study limitations outlined in Section 3.4.3, the following research gaps were identified, providing scope for further research.

Firstly, a knowledge gap exists in quantifying the possible interaction between fish and high energetic vortices recorded within the near and transitional wake which might have cause the avoidance behaviour observed. This may be realised through the use of PIV to visualise the flow field around a fish swimming in the wake of a VAT or the use of numerical methods (e.g., LES, (inverse) reinforcement learning).

Secondly, to provide a comprehensive assessment of the impact of VAT on fish movement, further experimental conditions may be tested, including, for instance, variations in water turbidity and light [42, 24].

Thirdly, based on the behaviour changes observed by Molloy et al. (2017) [137] and the results obtained in the experiment (c) (Section 3.2.3.4.3), further research is required to quantify whether the little time shoaling was associated with the operation of the turbine. A control test, for example, consisting of a stationary turbine or a bare flume scenario should be conducted to understand the effect of turbine presence and turbine operation on fish.

A major research gap also exists in quantifying the impact of multiple turbines (e.g., twin-turbines and turbine arrays) on the movement of individual fish and fish shoals to better understand whether fish pass through the turbine arrangement or move around it, treating the multi-turbine arrangement as one large obstacle.

Further research, will also be required to identify the optimal lateral and streamwise distance between twin and multiple turbine arrangements to maximises installed power density per unit of land. Therefore, reduced wake effects should be considered, enhancing the performance of downstream turbines while allowing the twin-turbines to increase device energy yield due to synergistic blockage effects.

## 3.5 Conclusion

The impact of a single and six twin-vertical axis turbine configurations, varying in rotational direction and lateral spacing on wake hydrodynamics was investigated using small-scale, laboratory experiments. In addition, fish responses to a single VAT were investigated under a range of test conditions, varying in discharge, turbine operation state and spatial confinement.

The evolution and interaction between the wakes of adjacent VATs deployed in twin configurations has been experimentally studied by means of ADV measurements. A standalone and six twin-VAT setups were tested, including shaft-to-shaft spacings of $S_y$=1.5 and 2.0$D$ with the devices rotating in the same and in opposite directions. The wake of a single VAT was asymmetric about the turbine's centreline and shifted towards the upstroke side. In the case of the twin-turbine configurations, the wake evolution was more sensitive to the rotational direction of the VATs than their lateral spacing. When VATs rotated in the same direction (SR), both wakes evolve independently in the downstream direction, with a reduced interference in the near wake and a notably wake expansion in the lateral and vertical directions. In the counter-rotating forwards setups (CRF; i.e., turbine blades move along with the flow in the bypass region), the highest momentum deficit was found in the upstroke regions on the outskirts of the wake, preventing the wakes from merging and therefore, allowing larger velocities in the wake. In the counter-rotating backwards cases (CRB; i.e., blades move against the flow in the bypass region), the low-velocity regions merged immediately downstream

of the turbines, generating a single wake that was relatively narrow in the lateral direction but expanded through the whole water column. Cross-sectional averaged values of mean velocity and turbulence intensity showed that cases with turbines rotating in CRF direction achieved the highest momentum in the wake. This was especially noticeable for the CRF–2.0 configuration in which the cross-sectional mean velocity reached the bulk velocity value ($U_0$) at 5D downstream, a distance noticeably shorter than the 8D at which the single turbine attained full wake recovery. Hence, with increasing intra-turbine spacings (i.e., $S_y$=2$D$), momentum recovery was enhanced, and turbulence intensity decreased, suggesting that greater turbine spacings may be beneficial when designing multi-row twin-VAT arrays. Based on these results, lateral turbine spacing and turbine rotational direction should be considered when planning an array consisting of multiple turbine rows [199]. Results suggested that a lateral spacing of at least 2D, for instance, should be applied for counter-rotating forward (CRF) configurations to enhance wake recovery and minimise detrimental wake effects for downstream turbine rows. Wake characteristics suggest that such setups would allow adopting a streamwise spacing between rows of $5D$ so that secondary rows can harness kinetic energy efficiently. In contrast, counter-rotating backward (CRB) and co-rotating (SR) twin-turbines would require a wider streamwise inter-row spacing of, at least, $10D$, unless the lateral turbine spacing increases, which, however, would decrease the installed power density capacity. Moreover, twin-turbine setups with lateral spacing of $S_y$=2$D$ attained a faster wake recovery and lower turbulence intensities independent of their rotational direction, beneficial when designing multi-row twin-VAT arrays.

In total, three fish behaviour studies examining fish response to a single VAT were conducted. First, the impact of turbine operational state (stationary versus rotating) and two discharge (mild versus harsh) on individual fish movement was tested under confined spatial conditions. Here, fish spent more time downstream and least time upstream, with most time downstream being spent near the flume walls and least time spent within the downstream centre. Besides avoidance of the turbine wake, fish avoided the near region around the turbine. Neither discharge nor turbine operation

state influenced this avoidance behaviour. When increasing the lateral space of the test section, creating an unconfined spatial condition, fish further avoided the near turbine and wake region by spending more time outside this region and therefore, further reducing fish-turbine interaction. The additional space provided also led to an increase in upstream passage and a decrease in passage attempts. Hence, fish benefited from the unconfined spatial condition, as they could use the large free-stream regions on either side of the turbine. To investigate whether an increase in individuum number tested changes fish movement behaviour, shoals of three fish were tested under unconfined conditions. Results showed an increase in distance covered and a reduced distance maintained from the turbine. Exploration of the test section occurred predominantly by individuals or pairs of fish rather than shoals. Based on these results, turbine positioning and lateral spacing between multiple turbines should be carefully considered. Providing greater space around the turbine decreases fish-turbine interaction, suggesting a reduced impact of the VAT on fish movement. Turbine arrays comprising multiple turbines located in proximity may restrict fish movement and habitat connectivity [87]. Therefore, multi-turbine configurations should either provide sufficient space between turbines for fish to pass through the turbine arrangements or on either side of the turbine array allowing fish to pass around the array.

Both hydrodynamic and fish behaviour results expand the current state of knowledge on VAT and support their delivery as environmentally friendly alternatives to traditional small and large-scale hydropower plant. More specifically, the findings provide new insights into the wake characteristics behind twin-VAT arrays and informs the design of future multi-row arrays of VATs with minimised wake-turbine interactions. Furthermore, the fish behavioural studies confirmed low impact of VAT on fish movement. Turbine location and spatial confinement, however, are import factors which must be considered to ensure habitat connectivity and unhindered fish movement. Both, hydrodynamic and fish studies, together with further research, may play an important role in the arrangement and operation of single and twin-VAT configurations as sustainable energy solution, providing universal access to clean, reliable energy while conserving

the aquatic habitat.

## 3.6   Chapter acknowledgement and contributions

Prior to the submission of this thesis, parts of this chapter have been published. In the following, contributions of co-authors and persons involved in the presented experiments are highlighted.

Small Project SP111: A new technology of fish-friendly river turbines to provide renewable energy to impoverished isolated communities".

*Chapter 4*

# General discussion

Freshwater fish are subject to a wide range of current and emerging threats, with habitat degradation being one of the main reasons for their decline [60, 184]. Amongst other factors, habitat degradation is a result of the rapid expansion in infrastructure, residential and commercial development [55], causing the construction of numerous small-scale, zero-to-low head in-stream obstructions [100]. These obstructions may present physical, hydraulic, chemical, and or thermal barriers to aquatic organisms, blocking or delaying their movement between habitats [205]. Despite the well-known consequence of traditional in-stream structures, such as weirs, dams, water in- and out-takes, more obstructions are being added to riverine systems, often for flood mitigation or to harness the energy from free-flowing flow.

This thesis evaluated the impact of two emerging in-stream obstructions, namely leaky barriers used for flood management (Chapter 2) and vertical axis turbines used to generate hydrokinetic energy from the free-flowing flow of rivers and estuaries (Chapter 3), on channel hydrodynamics and fish movement using scaled laboratory experiments. In the following, the impact of these two potential barriers on primary impacts, such as fish movement and flow alterations, and potential secondary impacts on the aquatic ecosystem is discussed (Section 4.1). Furthermore, limitations and opportunities of using ecohydraulic flume studies to evaluate these impacts are explored (Section 4.2). Finally, considerations regarding installation, maintenance and monitoring of in-stream obstructions are highlighted with regards to maintaining longitudinal river connectivity (Section 4.4).

## 4.1   Importance of considering primary and secondary impacts of in-stream obstructions on the aquatic ecosystem

Fish are exposed to a wide range of riverine in-stream obstruction such as culverts and weirs, presenting physical as well as velocity barriers. Due to the consequences of these hydraulic structures on fish movement, physical design adaptations have been studied to improve fish movement across these structures [79, 11]. Yet, little is known about the physical design implications and their associated flow alterations of leaky barriers and VAT on fish movement behaviour.

Upstream and downstream flow alterations associated with leaky barriers were strongly dependent on the physical design of the barriers (Section 2.3.1). Due to the presence of a vertical gap ($b_0$) between river bed and the leaky barrier structure, upstream flow vertically diverted and formed a primary jet beneath all barriers. The high-momentum flow was preserved until $4b_0$ downstream of the leaky barriers, followed by a rapid decay. Although juvenile Atlantic salmon and juvenile rainbow trout were able to overcome this high-momentum flow (Section 2.3.2), this increase in mean streamwise velocity may, however, become a velocity barrier for weaker fish species or certain life stages. In contrast, the upper wake ($z/b_0 > 1$) was structure dependent, featuring weaker, secondary jets for all porous leaky barrier design with distinct flow paths (LB2-3, LB5-6). In contrast, the non-porous barrier (LB1) showed a rapid expansion of the primary jet. Along the shear layers between the primary jet and the upper wake, an increase in turbulence was observed in the case of the non-porous leaky barrier (LB1) and the short, porous barrier (LB5-6). As fish generally avoid regions of high turbulent kinetic energy and Reynolds shear stress [222, 93, 146], the upper wake region may have acted as a deterrent to fish. In contrast, the lower turbulence levels associated with the long, porous leaky barrier designs (LB2-4), potentially provided resting and foraging

areas for fish. Despite the detailed velocity measurements conducted, a research gap remains in quantifying the turbulent structures shed by the varying physical leaky barrier designs under high Reynolds numbers and whether these turbulent structures may be used to guide fish underneath the barrier into the upstream region. Vortices shed by single and multiple horizontal wooden cylinders in a row, like LB5-6, negatively impacted swimming stabilities of fish [222, 146]. Fish responses to more complex dowel arrangements resembling more natural structures, however, were not investigated. Further experimental studies using, for instance, particle image velocimetry and turbulent structure-resolving numerical modelling could be used to analyse these turbulent structures formed in the near wake of porous leaky barriers and more naturalized barrier designs, consisting of non-uniform branches and logs to outline potential impacts on fish swimming stability and habitat preference.

While the wake of leaky barriers strongly depended on their physical design, the wake of twin VAT was influenced by the lateral spacing and particularly the rotational direction of the individual turbines (Section 3.3.1). The wake of a single VAT (ST) was asymmetric about its centreline and shifted towards the upstroke side of the turbine. Twin-turbines rotating in the same rotational direct (SR), therefore created the widest wake, considering lateral and vertical wake expansion. In contrast, twin-VAT rotating in a counter-rotating back direction (CRB) created a single, narrow wake in the lateral direction, which expanded over the whole water column, while twin-turbines rotating in counter-rotating forward (CRF) direction generated two separate wakes diverting from each other. An increase in lateral turbine spacing enhanced the bypass flow between the turbines and therefore, wake recovery. Flow alterations associated with turbine positioning and rotational direction should be considered when planning turbine arrays, which consist of multiple rows of turbines, necessary to enhance power output. Studies investigating fish responses to the wake of a marine turbine support structure show an increase in fish shoaling, particularly within the structure's wake [74]. Aggregations of fish in the vicinity of turbine support structures may result in changing predator-prey relationships as predators identify these aggregations [74].

Preliminary fish studies (Section 3.3.2) undertaken under confined laboratory conditions, however, showed that fish spent least time within the turbine's wake and its vicinity. Yet, it remains unclear whether the turbine-induced flow structures generated in the near wake [32] may act as a deterrent to fish movement, safely guiding fish around the individual turbines and the array. An increase in lateral space, resulted in an even greater avoidance of the turbine and its wake. Furthermore, the unconfined test condition showed an even greater decrease in fish-turbine interaction, indicating the importance of providing suitable space in the lateral direction for fish to pass the turbine, thereby reducing impact on fish movement. Interestingly, investigating the response of shoals compared to individual fish under unconfined conditions showed an increase in movement activity and exploratory behaviour. Yet, a research gap remains in quantifying how the different wake structures observed for the twin-turbine setups (i.e., SR, CRF, CRB) influence fish movement of individual fish and shoals, and whether higher discharges may eventually attract fish by providing a resting area.

Physical design or operational alterations of in-stream structures and turbines, and their associated flow alterations may also be used specifically to create selective barriers, and hence, prevent certain species (e.g., INNS such as rainbow trout) from passing between adjacent habitats while maintaining habitat connectivity for desired species. Selective barriers, can be created through the application of ecological filters (e.g., physiological, biotic, anthropogenic barriers) [180]. Due to the channel-spanning nature and versatile design options of leaky barriers, these structures may be adapted as selective barriers. As INNS present a major threat to freshwater diversity [60, 180, 184, 101], using physical design alterations of leaky barriers and their associated flow alterations to prevent the spread of INNS may be worth exploring and has not been researched yet. Making use of the strength of the primary jet, which can be manipulated through barrier porosity, for instance, may prevent weaker species from moving upstream.

Secondary impact of these exemplary barriers on the riverine ecosystem may include changes in sediment transport as a result of flow alterations associated with in-stream

obstructions. The observed vertical flow diversion and resulting high-momentum flow beneath all leaky barriers (Section 2.3.1) is presumed to elevate bed shear stress, leading to an increased risk of downstream scour formation [70]. Similar scour formations are observed for flow underneath sluice gates [223] and accumulations of wooden pieces on vertical retention racks [194, 193]. Flow around vertical structures, such as the shaft of a VAT, has also been observed to create downstream scour formations if the turbine is installed at the river bed [215]. These scour formations are similar to those observed around bridge piers [30]. Furthermore, an increase in suspended sediment and fine particles is expected due to the mobilisation of these particles with increasing bed shear stress, increasing water turbidity. Changes in sediment transport may increase levels of dissolved oxygen, beneficial for oxygen-loving species (e.g., salmonids), but may also increase the suspension of contaminants within the water column, potentially affecting water quality. Excessive amounts of mobilised particles in the water column may, in turn, limit vegetation growth due to the increased water turbidity [91] and detrimentally impact fish by reducing spawning habitat by potentially leading to the exposure and or smothering of eggs at spawning grounds [59, 91, 44]. The impact on sediment transport and particle mobilisation, however, are assumed to only persist within the vicinity of these structures. Further research should be conducted to investigate changes in sediment transport associated with flow alteration of in-stream obstructions like leaky barriers and VAT to avoid these structures creating barriers to fish movement due to the creation unsuitable habitat.

Most flume or field studies assess the impact of a single in-stream structure on primary and secondary changes, but often disregard the potential cumulative impact when such structures are installed in greater number along a river or river reach. Leaky barriers, for instance, are installed in groups of 100 plus units in selected tributaries of a river network. Section 2.3.2 showed that the investigated leaky barrier designs did not prevent fish from passing between downstream and upstream section but their presence resulted in a reduction of the number of upstream passing fish and passes per fish. While these studies only considered a single structure, the installation of mul-

tiple leaky barriers may result in an even greater reduction of upstream passing fish. Weaker swimmers (e.g., cyprinids) or certain life stages may be particularly affected by barriers due to repeated exposure to the primary jet underneath the leaky barriers. This high-momentum region may cause fragmentation of the tributary if fish are not strong enough to overcome these flow velocities. Similarly, due to the low stand-along power of a single VAT, they are often clustered into turbine arrays to maximise power output. Clustering turbines into arrays requires the positioning of multiple turbines in close proximity. This would further reduce the unobstructed area remaining for the fish to pass around the array, potentially causing fish to enter the obstructed region. Furthermore, while the wake of a single and twin turbine recovered by less than 10D, the wake of larger turbine arrays may have a greater impact on the velocity distribution within a river. Hence, further research should be conducted, investigating the cumulative impact of multiple leaky barriers along a river stretch and multiple VAT clustered into turbine arrays to prevent the underestimation of the cumulative impact of such in-stream obstructions [100] and quantify the impact on fish movement and migration [87].

Alongside the wide range of concerns and habitat alterations associated with the installation of in-stream structures, they may also benefit the aquatic ecosystem. Wave and tidal energy converters as well as associated structures (e.g. anchors, foundation, buoys and lines), for instance, have been found to attract fish and to form artificial reefs, creating new habitats that can enhance fish productivity [115]. Similarly, the installation of leaky barriers not only serves the purpose of mitigating the impact of flooding but also contributes to the restoration of rivers. By partially blocking the flow, these structures cause the flow to spill out onto the floodplains, enhancing lateral river connectivity [189] and creating seasonal wetlands [249], which can be used as flow refuges [73], nursing and spawning areas [203]. Furthermore, leaky barriers created a complex flow field, comprising of a primary and multiple secondary jets, recirculation zones and overflow depending on the physical design of the leaky barrier (Section 2.3.1), which will alter the local geomorphology of the river channel by creating scour

pools, deposition mounds and undercut banks [67, 131]. In addition, leaky barriers create overhead cover [158] and refuge for fish [150]. In particular, smaller fish may be attracted to these complex, wooden structures to seek shelter from predators [192].

## 4.2 Opportunities and limitations of ecohydraulic flume studies

The experiments presented in Chapter 2 and Chapter 3 were conducted at the hydraulic laboratory of the Centre of the Hydro-Environmental Research Centre at the School of Engineering at Cardiff University using idealised, scaled model structures. Alongside field studies, large-scale ecohydraulic flume studies offer a promising alternative to investigate the aquatic flora and fauna under controlled conditions and to enhance the current state of knowledge on the interplay between flow and biota [106]. So far, such facilities were mostly used to quantify species-specific responses to in-stream structures and fish passages, identify mitigation strategies and practical applications [106]. The potential of such ecohydraulic flumes, however, is not fully exhausted yet, leaving room for further research, including, for instance, the analysis of movement behaviour, swimming abilities, passage performance of aquatic organisms and environmental flows (e.g., habitat requirements defined by ecosystem morphodynamics and flow regimes) [106]. Scaled ecohydraulic flume experiments can also be of great use when assessing preliminary geometric and physical modification of key design parameters of in-stream obstruction (e.g., leaky barrier length, porosity, dowel arrangement, and colour as shown in 2) on flow alterations and corresponding fish responses [11].

The experimental design of large-scale and particularly small-scale flume studies, however, is often accompanied by methodological limitations. Both, leaky barrier (Chapter 2.4.4) and vertical-axis turbine experiments (Chapter 3.4.3), for instance, were conducted in highly artificial and simplified environments, not reflecting the natural turbu-

lent flow, geomorphological conditions of the main river channel, variations in water quality (e.g., turbidity, dissolved oxygen levels), light conditions, predation risk, and interaction between flow, river bed (e.g., gravel, sediment) and instream vegetation. The large number of simplifications poses the question of whether results truly reflect behaviour observable under natural conditions and whether more effort should be undertaken to adapt laboratory setups towards more natural settings.

Another study limitation arises through the requirement of scaling of the experimental setup to the flume size available. While flow conditions and geometry of the investigated obstruction can be scaled using the Froude and Reynolds, and geometric scaling laws, respectively, determining the right fish size or scaling fish remains challenging and is typically not considered. Allometric scaling, for example, can be applied to scale the size or mass of a fish according to morphological, physiological, and ecological traits [151]. Moreover, geometric scaling was found to appropriately scale length to volume and surface to volume using $L = V^{1/3}$ and $S = V^{2/3}$, respectively, assuming mass $\sim$ volume [238]. These approximations only differed by 0.083 from biological observations for a wide range of animals [238]. Adapting the size of a fish to match the scale of the experimental setup may result in the use of different life stages which, in turn, may result in considerable variations in behaviour responses depending on, for example, past experiences, noise, predators, feeding and hydrodynamics [80]. When using certain life stages, the biological timing must be considered. For example, while anadromous juveniles migrate downstream, adult fish migrate upstream, approaching in-stream obstructions and fish passes from different sides with different swimming capabilities. Most flume studies are conducted only for a limited number of fish species, often concentrating on migratory fish species like salmonids but neglecting other migratory as well as non-migratory, resident species of varying swimming capabilities and locomotory patterns. Similarly, this thesis studied the passage and spatial behaviour of juvenile Atlantic salmon and rainbow trout due to the species dramatic decline and threat to native species, respectively. Furthermore, availability and accessibility of both species played another role in the choice of study species. Both species were

availability at local fish farms or the School of Biosciences at the time of the experiments. The close cooperation between the School of Engineering and Biosciences allowed the sharing of the study individuals, reducing the number of animals used for the experimental studies, supporting the ARRIVE guidelines and recommendations from the National Centre for the Replacement, Refinement and Reduction of Animals in Research [111].

## 4.3 Bridging the gap between laboratory and field

Based on the research gaps highlighted throughout the individual chapters and Sections 4.1 and 4.2, scope for future research exists to bridge the gap between scaled laboratory experiments and their installation in the field.

While scaled experiments may be beneficial to explore correlations under controlled laboratory conditions, such studies often entail a wide range of simplifications, discussed in Sections 2.4.4, 3.4.3, and 4.2. To drive the development of leaky barriers and VAT, further research may include a gradual increase in experimental complexity and structure scale until reaching the field scale. An increase in complexity may, for instance, be achieved through the use of more natural materials or 3D printed replicas [75] as well as the use of varying flow, turbidity, and light conditions. This step may help determine physical design and scale-depending effects on, for example, channel hydraulics or fish movement. In-depth hydrodynamic analyses may also be supported through numerical tools such as Reynolds-averaged and large-eddy simulations.

Once the spectrum of laboratory possibilities is exhausted (i.e., reaching maximum scale and/or complexity), both simplified and complex laboratory models may be transferred into the field. This step provides a "real world" test of the laboratory experiments, which typically only investigate a limited number of parameters at the time, against complex field conditions, allowing the identification of so far unconsidered parameters influencing fish behaviour or channel hydraulics.

While laboratory and field experiments are often bounded to single structures or locations within the river, 1D and 2D hydraulic simulations may be used to examine the reach, tributary, and catchment-based impacts on fish movement and channel hydrodynamics. Such numerical simulations may be of particular interest when investigating the cumulative impacts of leaky barriers, often installed in groups of 100 plus units, and VAT arrays.

## 4.4 Considerations when planning the construction of in-stream obstructions

When planning the installation of in-stream obstructions (e.g., leaky barriers and VAT), the current state of the aquatic environment should be carefully considered and assessed before the beginning of the construction. This assessment may then be used for comparison purposes with future river states. Characterisation of the current river state may include an assessment of river geomorphology, hydrodynamics, vegetation, invertebrate and fish species, and also their habitat preferences, swimming capabilities, and movement activities and motivations. In the presence of migratory fish species, for instance, flow requirements, migration time, and movement direction (i.e., source-to-sea or visa versa) present important factors, which need to be understood and taken into consideration to allow fish to complete their lifecycle [125]. Furthermore, the lateral location of in-stream obstructions should be considered to prevent them being positioned into migratory routes and thereby blocking the entire cross-section of the river. Hence, enough space should be provided for fish to move around these structures. Also, as leaky barriers are often installed in the upper catchments, their longitudinal positioning within the river should be examined to maintain access to spawning grounds and preserving suitable gravel beds for fish to spawn. Besides potential changes in sediment transport, other likely secondary effects may include shifts in invertebrate communities and predator-prey relationships as well as habitat availability (e.g., width and depth of

the main channel, access to floodplains).

The installation of multiple structures along a river may require consideration of the cumulative impacts on the aquatic environment and their organisms on a local and catchment-based scale. Also, the longitudinal extension of habitat and flow alterations of single in-stream structures must be clarified. For example, while flow alterations associated with the wake of a VAT diminished until approximately 10 turbine diameter $D$ downstream of the turbine (Section 3.3.1), downstream flow alterations generated by leaky barriers remained until approximately $35b_0$ (Section 2.3.1) and hence, changes in flow and sediment transport are expected only within the vicinity of these barriers. Small and large-scale ecohydraulic experiments, like those conducted in Chapter 2 and 3, and numerical simulations present suitable methods to assess potential primary and secondary alterations associated with in-stream structures without requiring installation in the field. These preliminary assessments may then be used to conclude physical design alterations, the ideal positioning of these structures within the river channel or reach, and further measures to mitigate their impact on the aquatic environment and create transparent barriers [39]. The holistic treatment of an in-stream obstruction requires experts from various disciplines to identify the best possible design solution [205], including, for instance, biologists, ecologists, hydraulic and environmental engineers.

Once the proposed location within the river system is characterised, the design and positioning of the in-stream structure are clarified, and the obstruction is installed in the field, the implementation of a monitoring program is important to assess changes in the aquatic habitat over time. Before-after installation monitoring is useful to highlight any habitat alterations. Physio-chemical and biological monitoring parameters may include river width, flow depth, water temperature and quality, bed substratum, hydrodynamic alterations, cover and shade availability, macrophytes, aquatic invertebrates as well as fish presence (including INNS), population, density, and movement. These monitoring results may then be used to conclude physical design adaptations and maintenance

requirements. For example, leaky barriers are prone to physical design changes due to the accumulation of leaf material, branches, sediment, and rubbish between the key log members of the structure. Hence, the porous leaky barriers (LB2-6) may become non-porous over time (like LB1). Furthermore, extreme flow conditions (e.g., major floods) may also alter the design and structural integrity of in-stream obstructions, as logs and sticks are displaced and accumulate downstream (e.g., at bridge piers [197, 157] or racks [194, 193]). Similarly, VAT may require occasional maintenance to ensure constant operations due to potential blockages caused by driftwood. The assessment of the impact of varying natural flow conditions (e.g., drought and floods) and flotsam on the operation, performance, and stability of such in-stream instruction provides scope for further research.

*Chapter 5*

# General conclusion

While pre-existing in-stream structures were often placed into rivers considering only direct human benefits without thought of potential environmental impacts, the removal or retrofitting of the barriers has now become a major focus to restore river connectivity. Due to increasing awareness of the impact of these structures on the riverine ecosystem, stricter regulations were enacted which require proof of environmental compatibility for any emerging, anthropogenic in-stream barrier planned to be installed into the river systems. Small and large-scale ecohydraulic flume experiments were identified as a suitable method to perform preliminary investigations of the impact of such emerging barriers on the aquatic ecosystem. Such experiments can be used, for instance, to conclude initial physical design alterations, operational requirements, and spatial arrangements, before transferring the knowledge across scale and into the field. In this thesis, two emerging barriers, namely leaky barriers used for natural flood management and vertical axis turbines used for the generation of hydrokinetic energy, were studied.

In the first part of this thesis, upstream and downstream flow alterations and associated fish movement responses were investigated to better understand whether leaky barriers may present a physical, behavioural, and/or flow barrier to fish movement. Results showed that a primary jet developed beneath all leaky barriers independent of their physical design, resembling a classic wall jet. This primary jet may, depending on life stage and swimming capabilities present a flow barrier to fish, especially when fish are repeatedly exposed to high-momentum flow. The upper wake, in contrast, strongly depended on the physical design of the leaky barriers. Barriers with clear through flow

paths, for instance, featured weaker secondary jets which were particularly pronounced for the short porous leaky barrier designs, resembling the flow around cylinders. While the tested physical leaky barrier designs did not prevent fish from moving between the downstream and upstream section, their presence and design reduced the time spent within the upstream section, the number of upstream passing fish and number of upstream passes per fish compared to the bare flume case. The non-porous and short porous leaky barrier design were found to influence fish movement the least. Potential reasons for the reduction in fish movement associated with the physical design of the leaky barriers may include the visual complexity of the structures, barrier colour, provision of overhead cover and shade, and flow alterations. Leaky barrier design should therefore be chosen depending on the needs of the fish community present (e.g., depending on preference of shade and cover, flow velocities). Besides the impact of the physical design of leaky barriers on channel hydrodynamics and fish movement, secondary impacts on the aquatic environment such as sediment transport, overbank flow and bank erosion, barrier positioning, and maintenance were identified as important parameters when considering the installation of these structures.

In the second part of this thesis, wake hydrodynamics and associated fish movement responses were assessed for a single VAT and six twin-VAT configurations to understand the impact of spatial confinement, rotational direction and lateral spacing of these turbines on wake hydrodynamics and fish movement. Hydrodynamic measurements of single VAT showed an asymmetric wake which was skewed towards the upstroke side of the turbine and regions of high-momentum flow on either side of the turbine under confined spatial conditions. Lateral turbine spacing and rotational direction of twin-VAT strongly influenced wake recovery and expansion. The wake of twin-turbines rotating in the same rotational direction, for instance, was characterised by individual wakes evolving almost independently in the downstream direction, showing a notably wake expansion in lateral and vertical direction. Moreover, the individual wakes of twin-turbines rotating in counter-clockwise forward direction progressively diverted outwards, causing a lateral expansion of the wake. In contrast, the individual wakes of

twin-turbines rotating in counter-clockwise backward direction progressively moved towards each other, creating a single combined wake which was relatively narrow in lateral direction but expanded over the whole water column. Hence, lateral spacing and rotational direction strongly influence wake recovery and therefore, the positioning of downstream turbines and the installed power density capacity of the entire turbine arrangement. A single VAT did not prevent fish from moving between the downstream and upstream section of the test area under confined and unconfined spatial conditions and independent of the turbine's operational state and discharge. Fish, however, were found to spend most time downstream and least time within the wake of the turbine and the turbine's vicinity, indicating avoidance behaviour when tested individually. In contrast, fish shoals increasingly explored the whole of the test section, keeping smaller distance to the turbine and covering greater swimming distances. Hence, when considering the deployment of such turbines, wake alterations as well as the positioning within the river channel should be considered to allow sufficient space for fish to pass to prevent single and multi-turbine arrangements from presenting behavioural and physical barriers to fish movement.

The presented results for both emerging in-stream barriers expand the current knowledge on the three-dimensional wake hydrodynamics and highlight anticipated changes to the aquatic environment. Moreover, the results presented contribute to a better understanding of the circumstances under which these structures may act as physical, flow, and/or behavioural barrier to fish movement. Therefore, the research conducted as part of this thesis supports their delivery as environmental-friendly anthropogenic in-stream obstruction while ensuring the mitigation of flooding, the generation of sustainable energy, and maintaining habitat connectivity for aquatic animals.

# Bibliography

[1] ABBASI, T., AND ABBASI, S. A. Small hydro and the environmental implications of its extensive utilization. *Renewable and Sustainable Energy Reviews 15* (2011), 2134–2143.

[2] ABBE, T. B., AND MONTGOMERY, D. R. Large woody debris jams, channel hydraulics and habitat formation in large rivers. *Regulated Rivers: Research and Management 12* (1996), 201–221.

[3] ABKAR, M., AND DABIRI, J. O. Self-similarity and flow characteristics of vertical-axis wind turbine wakes: an les study. *Journal of Turbulence 18* (2017), 373–389.

[4] ABRAMOVICH, G. N., AND SCHINDEL, L. *The theory of turbulent jets*. MIT Press, 1963.

[5] AGENCY, E. E. Mapping the impacts of natural hazards and technological accidents in europe, 2010.

[6] AKANYETI, O., AND LIAO, J. C. The effect of flow speed and body size on kármán gait kinematics in rainbow trout. *Journal of Experimental Biology 216* (2013), 3442–3449.

[7] AL-ZAWAIDAH, H., RAVAZZOLO, D., AND FRIEDRICH, H. Local geomorphic effects in the presence of accumulations of different densities. *Geomorphology 389* (2021).

[8] ALBAYRAK, I., HOPFINGER, E. J., AND LEMMIN, U. Near-field flow structure of a confined wall jet on flat and concave rough walls. *Journal of Fluid Mechanics 606* (2008), 27–49.

[9] ALFIERI, L., FEYEN, L., DOTTORI, F., AND BIANCHI, A. Ensemble flood risk assessment in europe under high end climate scenarios. *Global Environmental Change 35* (2015), 199–212.

[10] AMARAL, S. D., BRANCO, P., DA SILVA, A. T., KATOPODIS, C., VISEU, T., FERREIRA, M. T., PINHEIRO, A. N., AND SANTOS, J. M. Upstream passage of potamodromous cyprinids over small weirs: the influence of key-hydraulic parameters. *Journal of Ecohydraulics 1* (2016), 79–89.

[11] AMARAL, S. D., BRANCO, P., KATOPODIS, C., FERREIRA, M. T., PINHEIRO, A. N., AND SANTOS, J. M. Passage performance of potamodromous cyprinids over an experimental low-head ramped weir: The effect of ramp length and slope. *Sustainability 11* (2019).

[12] AMARAL, S. V., BEVELHIMER, M. S., ČADA, G. F., GIZA, D. J., JACOBSON, P. T., MCMAHON, B. J., AND PRACHEIL, B. M. Evaluation of behavior and survival of fish exposed to an axial-flow hydrokinetic turbine. *North American Journal of Fisheries Management 35* (2015), 97–113.

[13] ANDERSON, D., MOGGRIDGE, H., WARREN, P., AND SHUCKSMITH, J. The impacts of 'run-of-river' hydropower on the physical and ecological condition of rivers. *Water and Environment Journal 29* (2015), 268–276.

[14] ANDERSON, E. P., JENKINS, C. N., HEILPERN, S., MALDONADO-OCAMPO, J. A., CARVAJAL-VALLEJOS, F. M., ENCALADA, A. C., RIVADENEIRA, J. F., HIDALGO, M., CAÑAS, C. M., ORTEGA, H., SALCEDO, N., MALDONADO, M., AND TEDESCO, P. A. Fragmentation of andes-to-amazon connectivity by hydropower dams. *Science Advances 4* (2018), 1–8.

[15] APRIL, J., BARDARSON, H., AHLBACK BERGENDAHL, I., BOLSTAD, G. H., BREAU, C., BUORO, M., CAMARA, K., CHAPUT, G., COOPER, A., DAUPHIN, G., ENSING, D., ERKINARO, J., FISKE, P., FREESE, M., GILLSON, J., GREGORY, S., HANSON, N., JEPSEN, N., KELLY, N., MAXWELL, H., MEERBURG, D., MILLANE, M., NYGAARD, R., OUNSLEY, J., PATIN, R., PRUSOV, S., RAAB, D., RIVOT, E., ROBERTSON, M., SHEEHAN, T., TALLMAN, R., WALKER, A., WENNEVIK, V. Working group on North Atlantic salmon, International Council for the Exploration of the Sea, 2021.

[16] ARAYA, D. B., COLONIUS, T., AND DABIRI, J. O. Transition to bluff-body dynamics in the wake of vertical-axis wind turbines. *Journal of Fluid Mechanics 813* (2017), 346–381.

[17] ARCHER, M. W., PRACHEIL, B. M., OTTO, A. E., AND PEGG, M. A. Fish community response to in-channel woody debris in a channelized river system. *Journal of Freshwater Ecology 34* (2019), 351–362.

[18] BACHANT, P., AND WOSNIK, M. Performance measurements of cylindrical- and spherical-helical cross-flow marine hydrokinetic turbines, with estimates of exergy efficiency. *Renewable Energy 74* (2015), 318–325.

[19] BAKKEN, T. H., SUNDT, H., RUUD, A., AND HARBY, A. Development of small versus large hydropower in norway comparison of environmental impacts. *Energy Procedia 20* (2012), 185–199.

[20] BARDACH, H. E. Do fish have color vision? *Bios 21* (1950), 273–275.

[21] BARREDO, J. I. Major flood disasters in europe: 1950-2005. *Natural Hazards 42* (2007), 125–148.

[22] BEEBE, J. T. Flume studies of the effect of perpendicular log obstructions on flow patterns and bed topography. *Great Lakes Geographer 7* (2000), 9–25.

[23] BEJARANO, M. D., JANSSON, R., AND NILSSON, C. The effects of hydropeaking on riverine plants: a review. *Biological Reviews 93* (2018), 658–673.

[24] BENKE, A. C., AND WALLACE, J. B. Influence of wood on invertebrate communities in streams and rivers. *American Fisheries Society Symposium 2003* (2003), 149–177.

[25] BERRY, M., SUNDBERG, J., AND FRANCISCO, F. Salmonid response to a vertical axis hydrokinetic turbine in a stream aquarium. 1–10.

[26] BHUIYAN, F., HABIBZADEH, A., RAJARATNAM, N., AND ZHU, D. Z. Reattached turbulent submerged offset jets on rough beds with shallow tailwater. *Journal of Hydraulic Engineering 137* (2011), 1636–1648.

[27] BIRNIE-GAUVIN, K., TUMMERS, J. S., LUCAS, M. C., AND AARESTRUP, K. Adaptive management in the context of barriers in european freshwater ecosystems. *Journal of Environmental Management 204* (2017), 436–441.

[28] BISSON, P. A., WONDZELL, S. M., REEVES, G. H., AND GREGORY, S. V. Trends in using wood to restore aquatic habitats and fish communities in western north american rivers. *American Fisheries Society Symposium 37* (2003), 391–406.

[29] BORN, S. M., GENSKOW, K. D., FILBERT, T. L., HERNANDEZ-MORA, N., KEEFER, M. L., AND WHITE, K. A. Socioeconomic and institutional dimensions of dam removals: The wisconsin experience. *Environmental Management 22* (1998), 359–370.

[30] BOULTON, A. J. Hyporheic rehabilitation in rivers: restoring vertical connectivity. *Freshwater Biology 52* (2007), 632–650.

[31] BREUSERS, H. N., NICOLLET, G., AND SHEN, H. W. Erosion locale autour des piles cylindriques. *Journal of Hydraulic Research 15* (1977), 211–252.

[32] BROADHURST, M., BARR, S., AND ORME, C. D. L. In-situ ecological interactions with a deployed tidal energy device; an observational pilot study. *Ocean and Coastal Management 99* (2014), 31–38.

[33] BROCHIER, G., FRAUNIE, P., BEGUIER, C., AND PARASCHIVOIU, I. Water channel experiments of dynamic stall on darrieus wind turbine blades. *Journal of Propulsion and Power 2* (1986), 445–449.

[34] BRYANT, M. D., EDWARDS, R. T., AND WOODSMITH, R. D. An approach to effectiveness monitoring of floodplain channel aquatic habitat: Salmonid relationships. *Landscape and Urban Planning 72* (2005), 157–176.

[35] BUNN, S. E., AND ARTHINGTON, A. H. Basic principles and ecological consequences of altered flow regimes for aquatic biodiversity. *Environmental Management 30* (2002), 492–507.

[36] BURGESS-GAMBLE, L., NGAI, R., WILKINSON, M., NISBET, T., PONTEE, N., HARVEY, R., KIPLING, K., ADDY, S., ROSE, S., MASLEN, S., JAY, H., NICHOLSON, A., PAGE, T., JONCZYK, J., AND QUINN, P. Working with natural processes evidence directory (project number sc150005), 2018.

[37] BUTLER, R. L., AND HAWTHORNE, V. M. The reactions of dominant trout to changes in overhead artificial cover. *Transactions of the American Fisheries Society 97* (1968), 37–41.

[38] ČADA, G., AHLGRIMM, J., BAHLEDA, M., BIGFORD, T., STAVRAKAS, S. D., HALL, D., MOURSUND, R., AND SALE, M. Potential impacts of hydrokinetic and wave energy conversion technologies on aquatic environments. *Fisheries 32* (2007), 174–181.

[39] ČADA, G., AND ODEH, M. Turbulence at hydroelectric power plants and its potential effects on fish, report to bonneville power administration, contract no. 2000ai26531. 37.

[40] CASTRO-SANTOS, A. H. T. Fish guidance and passage at barriers, 2010.

[41] CASTRO-SANTOS, T. Optimal swim speeds for traversing velocity barriers: An analysis of volitional high-speed swimming behavior of migratory fishes. *Journal of Experimental Biology 208* (2005), 421–432.

[42] CASTRO-SANTOS, T., AND HARO, A. Quantifying migratory delay: A new application of survival analysis methods. *Canadian Journal of Fisheries and Aquatic Sciences 60* (2003), 986–996.

[43] CASTRO-SANTOS, T., AND HARO, A. Survival and behavioral effects of exposure to a hydrokinetic turbine on juvenile atlantic salmon and adult american shad. *Estuaries and Coasts 38* (2013), 203–214.

[44] CENTRE, N. S. How do i enhance correlation and snr?, 2019.

[45] CHAPMAN, J. M., PROULX, C. L., VEILLEUX, M. A., LEVERT, C., BLISS, S., ÈVE ANDRÉ, M., LAPOINTE, N. W., AND COOKE, S. J. Clear as mud: A meta-analysis on the effects of sedimentation on freshwater fish and the effectiveness of sediment-control measures. *Water Research 56* (2014), 190–202.

[46] CHARMANT, J. Kinovea 0.8.15.

[47] CHAUDHARI, S., BROWN, E., QUISPE-ABAD, R., MORAN, E., MÜLLER, N., AND POKHREL, Y. In-stream turbines for rethinking hydropower development in the amazon basin. *Nature Sustainability 4* (2021), 680–687.

[48] COCEAL, O., AND BELCHER, S. E. A canopy model of mean winds through urban areas. *Quarterly Journal of the Royal Meteorological Society 130* (2004), 1349–1372.

[49] COPPING, A., BATTEY, H., BROWN-SARACINO, J., MASSAUA, M., AND SMITH, C. An international assessment of the environmental effects of marine energy development. *Ocean and Coastal Management 99* (2014), 3–13.

[50] COPPING, A., GARAVELLI, L., HEMERY, L., FOX, J., MILLER, R., AND SEITZ, A. Collision risk to marine animals (fish) from tidal turbines: next steps towards understanding and retiring risk, 2021.

[51] COTEL, A. J., WEBB, P. W., AND TRITICO, H. Do brown trout choose locations with reduced turbulence? *Transactions of the American Fisheries Society 135* (2006), 610–619.

[52] CRAWFORD, S. S., AND MUIR, A. M. Global introductions of salmon and trout in the genus oncorhynchus: 1870-2007. *Reviews in Fish Biology and Fisheries 18* (2008), 313–344.

[53] DABIRI, J. O. Potential order-of-magnitude enhancement of wind farm power density via counter-rotating vertical-axis wind turbine arrays. *Journal of Renewable and Sustainable Energy 3* (2011).

[54] DADSON, S. J., HALL, J. W., MURGATROYD, A., ACREMAN, M., BATES, P., BEVEN, K., HEATHWAITE, L., HOLDEN, J., HOLMAN, I. P., LANE, S. N., O'CONNELL, E., PENNING-ROWSELL, E., REYNARD, N., SEAR, D., THORNE, C., AND WILBY, R. A restatement of the natural science evidence concerning catchment-based 'natural' flood management in the uk. *Proceedings of the Royal Society A: Mathematical, Physical and Engineering Sciences 473* (2017).

[55] DAUBNER, T., KIZHOFER, J., AND DINULESCU, M. Experimental investigation of five parallel plane jets with variation of reynolds number and outlet conditions. *EPJ Web of Conferences 180* (2018), 1–8.

[56] DEINET, S., SCOTT-GATTY, K., ROTTON, H., TWARDEK, W. M., MARCONI, V., MCRAE, L., BAUMGARTNER, L. J., BRINK, K., CLAUSSEN, J. E., COOK, S. J., DARWALL, W., ERIKSSON, B. K., DE LEANIZ, C. G., HOGAN, Z., ROYTE, J., SILVA, L. G. M., THIEME, M. L., TICKNER, D., WALDMAN,

J., WANNINGEN, H., AND BERKHUYSEN, A. The living planet index (lpi) for migratory freshwater fish, 2002.

[57] DENG, Z. D., LU, J., MYJAK, M. J., MARTINEZ, J. J., TIAN, C., MORRIS, S. J., CARLSON, T. J., ZHOU, D., AND HOU, H. Design and implementation of a new autonomous sensor fish to support advanced hydropower development. *Review of Scientific Instruments 85* (2014).

[58] DINGLE, H. *Migration : the biology of life on the move*, second edi ed. New York : Oxford University Press, 2014.

[59] DODD, J. A., NEWTON, M., AND ADAMS, C. E. The effect of natural flood management in-stream wood placements on fish movement in scotland. 43.

[60] DOLLOFF, C. A., AND JR., M. L. W. Fish relationships with large wood in large rivers. *American Fisheries Society Symposium 37* (2003), 179–193.

[61] DUDGEON, D., ARTHINGTON, A. H., GESSNER, M. O., KAWABATA, Z. I., KNOWLER, D. J., LÉVÊQUE, C., NAIMAN, R. J., PRIEUR-RICHARD, A. H., SOTO, D., STIASSNY, M. L., AND SULLIVAN, C. A. Freshwater biodiversity: Importance, threats, status and conservation challenges. *Biological Reviews of the Cambridge Philosophical Society 81* (2006), 163–182.

[62] EAD, S. A., AND RAJARATNAM, N. Plane turbulent surface jets in shallow tailwater. *Journal of Fluids Engineering, Transactions of the ASME 123* (2001), 121–127.

[63] ENDERS, E. C., BOISCLAIR, D., AND ROY, A. G. The effect of turbulence on the cost of swimming for juvenile atlantic salmon (salmo salar). *Canadian Journal of Fisheries and Aquatic Sciences 60* (2003), 1149–1160.

[64] ESTRELA, T., MENENDEZ, M., DIMAS, M., MARCUELLO, C., REES, G., COLE, G., WEBER, K., GRATH, J., LEONARD, J., OVENSEN, N. B., FE-

HER, J., AND CONSULT, V. Sustainable water use in europe part 3: Extreme hydrological events: floods and draughts. 1–84.

[65] DAM REMOVAL EUROPE About. `https://damremoval.eu/about/`

[66] FAO, AND DVWK. Fish passes design, dimensions and monitoring, 2002.

[67] FAUSCH, K. D. Introduction, establishment and effects of non-native salmonids: Considering the risk of rainbow trout invasion in the united kingdom. *Journal of Fish Biology 71* (2007), 1–32.

[68] FAUSCH, K. D., AND NORTHCOTE, T. G. Large woody debris and salmonid habitat in a small coastal british columbia stream. *Canadian Journal of Fisheries and Aquatic Sciences 49* (1992), 682–693.

[69] FOLLETT, E., SCHALKO, I., AND NEPF, H. Momentum and energy predict the backwater rise generated by a large wood jam. *Geophysical Research Letters 47* (2020).

[70] FOLLETT, E., SCHALKO, I., AND NEPF, H. Logjams with a lower gap: Backwater rise and flow distribution beneath and through logjam predicted by two-box momentum balance. *Geophysical Research Letters 48* (2021), 1–10.

[71] FOLLETT, E., AND WILSON, C. Bedload sediment transport induced by channel-spanning instream structures. *River Flow 2020* (2020), 735–742.

[72] FORBES, H., BALL, K., AND MCLAY, F. Natural flood management handbook, 2015.

[73] FRANCO-RESTREPO, J. E., FORERO, D. A., AND VARGAS, R. A. A review of freely available, open-source software for the automated analysis of the behavior of adult zebrafish. *Zebrafish 16* (2019), 223–232.

[74] FRANSSEN, N. R., GIDO, K. B., GUY, C. S., TRIPE, J. A., SHRANK, S. J., STRAKOSH, T. R., BERTRAND, K. N., FRANSSEN, C. M., PITTS, K. L., AND

PAUKERT, C. P. Effects of floods on fish assemblages in an intermittent prairie stream. *Freshwater Biology 51* (2006), 2072–2086.

[75] FRASER, S., WILLIAMSON, B. J., NIKORA, V., AND SCOTT, B. E. Fish distributions in a tidal channel indicate the behavioural impact of a marine renewable energy installation. *Energy Reports 4* (2018), 65–69.

[76] FRIEDRICH, H., RAVAZZOLO, D., RUIZ-VILLANUEVA, V., SCHALKO, I., SPREITZER, G., TUNNICLIFFE, J., AND WEITBRECHT, V. Physical modelling of large wood (lw) processes relevant for river management: Perspectives from new zealand and switzerland. *Earth Surface Processes and Landforms* (2021), 1–26.

[77] FUJISAWA, N., NAKAMURA, K., AND SRINIVAS, K. Interaction of two parallel plane jets of different velocities. *Journal of Visualization 7* (2004), 135–142.

[78] GHIMIRE, A., AND JONES, G. Restoration of a gauging weir to aid fish passage. *Journal of Hydro-environment Research 8* (2014), 43–49.

[79] GLADDEN, J. E., AND SMOCK, L. A. Macroinvertebrate distribution and production on the floodplains of two lowland headwater streams. *Freshwater Biology 24* (1990), 533–545.

[80] GOODRICH, H. R., WATSON, J. R., CRAMP, R. L., GORDOS, M. A., AND FRANKLIN, C. E. Making culverts great again. efficacy of a common culvert remediation strategy across sympatric fish species. *Ecological Engineering 116* (2018), 143–153.

[81] GOODWIN, R. A., POLITANO, M., GARVIN, J. W., NESTLER, J. M., HAY, D., ANDERSON, J. J., WEBER, L. J., DIMPERIO, E., SMITH, D. L., AND TIMKO, M. Fish navigation of large dams emerges from their modulation of flow field experience. *Proceedings of the National Academy of Sciences of the United States of America 111* (2014), 5277–5282.

[82] GORING, D. G., AND NIKORA, V. I. Despiking acoustic doppler velocimeter data. *Journal of Hydraulic Engineering 128* (2002), 117–126.

[83] GREGORY, S. V., BOYER, K. L., AND GURNELL, A. M. *The ecology and management of wood in world rivers*. American Fisheries Society.

[84] GRIFFITHS, S. W., AND MAGURRAN, A. E. Familiarity in schooling fish: How long does it take to acquire? *Animal Behaviour 53* (1997), 945–949.

[85] GRILL, G., LEHNER, B., LUMSDON, A. E., MACDONALD, G. K., ZARFL, C., AND LIERMANN, C. R. An index-based framework for assessing patterns and trends in river fragmentation and flow regulation by global dams at multiple scales. *Environmental Research Letters 10* (2015).

[86] GRILL, G., LEHNER, B., THIEME, M., GEENEN, B., TICKNER, D., ANTONELLI, F., BABU, S., BORRELLI, P., CHENG, L., CROCHETIERE, H., MACEDO, H. E., FILGUEIRAS, R., GOICHOT, M., HIGGINS, J., HOGAN, Z., LIP, B., MCCLAIN, M. E., MENG, J., MULLIGAN, M., NILSSON, C., OLDEN, J. D., OPPERMAN, J. J., PETRY, P., LIERMANN, C. R., SÃ¡ENZ, L., SALINAS-RODRÃGUEZ, S., SCHELLE, P., SCHMITT, R. J., SNIDER, J., TAN, F., TOCKNER, K., VALDUJO, P. H., VAN SOESBERGEN, A., AND ZARFL, C. Mapping the world's free-flowing rivers. *Nature 569* (2019), 215–221.

[87] GUILLERAULT, N., DELMOTTE, S., BOULÃªTREAU, S., LAUZERAL, C., POULET, N., AND SANTOUL, F. Does the non-native european catfish silurus glanis threaten french river fish populations? *Freshwater Biology 60* (2015), 922–928.

[88] HAMMAR, L., ANDERSSON, S., EGGERTSEN, L., HAGLUND, J., GULLSTRÖM, M., EHNBERG, J., AND MOLANDER, S. Hydrokinetic turbine effects on fish swimming behaviour. *PLoS ONE 8* (2013), 1–12.

[89] HAMMAR, L., EGGERTSEN, L., ANDERSSON, S., EHNBERG, J., ARVIDSSON, R., GULLSTRÖM, M., AND MOLANDER, S. A probabilistic model

for hydrokinetic turbine collision risks: Exploring impacts on fish. *PLoS ONE 10* (2015), 1–25.

[90] HAYES, D. S., MOREIRA, M., BOAVIDA, I., AND VIENNA, L. S. Establishing seasonal flow rules to mitigate adverse hydropeaking impacts on salmonid fish establishing seasonal flow rules to mitigate adverse hydropeaking impacts on salmonid fish. 19155.

[91] HEGGENES, J., AND TRAAEN, T. Daylight responses to overhead cover in stream channels for fry of four salmonid species. *Ecography 11* (1988), 194–201.

[92] HENLEY, W. F., PATTERSON, M. A., NEVES, R. J., AND LEMLY, A. D. Effects of sedimentation and turbidity on lotic food webs: A concise review for natural resource managers. *Reviews in Fisheries Science 8* (2000), 125–139.

[93] HERSKIN, J., AND STEFFENSEN, J. F. Energy savings in sea bass swimming in a school: Measurements of tail beat frequency and oxygen consumption at different swimming speeds. *Journal of Fish Biology 53* (1998), 366–376.

[94] HOCKLEY, F. Modification of fish behaviour by parasites under variable flow conditions.

[95] HOUSE, R. A., AND BOEHNE, P. L. Evaluation of instream enhancement structures for salmonid spawning and rearing in a coastal oregon stream. *North American Journal of Fisheries Management 5* (1985), 283–295.

[96] HUW, T. The robinwood robinflood report: Evaluation of large woody debris in watercourses, 2007.

[97] ELECTRIC POWER RESEARCH INSTITUTE Fish passage through turbines: application of conventional hydropower data to hydrokinetic technologies., 2011.

[98] JIA, G., SHEVLIAKOVA, E., AND AL., E. Chapter 2 : Land-climate interactions, 2019.

[99] JIANG, Y., ZHAO, P., STOESSER, T., WANG, K., AND ZOU, L. Experimental and numerical investigation of twin vertical axis wind turbines with a deflector. *Energy Conversion and Management 209* (2020), 112588.

[100] JONES, J., BÖRGER, L., TUMMERS, J., JONES, P., LUCAS, M., KERR, J., KEMP, P., BIZZI, S., CONSUEGRA, S., MARCELLO, L., VOWLES, A., BELLETTI, B., VERSPOOR, E., DE BUND, W. V., GOUGH, P., AND DE LEANIZ, C. G. A comprehensive assessment of stream fragmentation in great britain. *Science of the Total Environment 673* (2019), 756–762.

[101] JONES, P. E., TUMMERS, J. S., GALIB, S. M., WOODFORD, D. J., HUME, J. B., SILVA, L. G., BRAGA, R. R., DE LEANIZ, C. G., VITULE, J. R., HERDER, J. E., AND LUCAS, M. C. The use of barriers to limit the spread of aquatic invasive animal species: A global review. *Frontiers in Ecology and Evolution 9* (2021).

[102] HURST JR., P. M. Genes of the world's coolest fish. *The Progressive Fish-Culturist 15* (1953), 95–95.

[103] JULIEN, P. Y. *Erosion and Sedimentation*, 2 ed. Cambridge University Press, 2010.

[104] JUMP, S., COURTNEY, M. B., AND SEITZ, A. C. Vertical distribution of juvenile salmon in a large turbid river. *Journal of Fish and Wildlife Management 10* (2019), 575–581.

[105] KAHRAMAN, A., OZGÖREN, M., AND SAHIN, B. Flow structure from a horizontal cylinder coincident with a free surface in shallow water flow. *Thermal Science 16* (2012), 93–107.

[106] KATOPODIS, C., AND KEMP, P. S. Ecohydraulic flumes: are we taking full advantage of their potential for symmetrical interdisciplinary research? *Journal of Ecohydraulics 5* (2020), 1–2.

[107] KAWAMURA, G., MATSUSHITA, T., NISHITAI, M., AND MATSUOKA, T. Blue and green fish aggregation devices are more attractive to fish. *Fisheries Research 28* (1996), 99–108.

[108] KAY, A. L., OLD, G. H., BELL, V. A., DAVIES, H. N., AND TRILL, E. J. An assessment of the potential for natural flood management to offset climate change impacts. *Environmental Research Letters 14* (2019).

[109] KEEP, J. K., WATSON, J. R., CRAMP, R. L., JONES, M. J., GORDOS, M. A., WARD, P. J., AND FRANKLIN, C. E. Low light intensities increase avoidance behaviour of diurnal fish species: implications for use of road culverts by fish. *Journal of Fish Biology 98* (2021), 634–642.

[110] KHAN, M. J., BHUYAN, G., IQBAL, M. T., AND QUAICOE, J. E. Hydrokinetic energy conversion systems and assessment of horizontal and vertical axis turbines for river and tidal applications: A technology status review. *Applied Energy 86* (2009), 1823–1835.

[111] KILKENNY, C., BROWNE, W. J., CUTHILL, I. C., EMERSON, M., AND ALTMAN, D. G. Improving bioscience research reporting: The arrive guidelines for reporting animal research. *PLoS Biology 8* (2010), 6–10.

[112] KIM, J., AND MANDRAK, N. E. Effects of a vertical electric barrier on the behaviour of rainbow trout. *Aquatic Ecosystem Health and Management 22* (2019), 183–192.

[113] KINZEL, M., ARAYA, D. B., AND DABIRI, J. O. Turbulence in vertical axis wind turbine canopies. *Physics of Fluids 27* (2015), 115102.

[114] KINZEL, M., MULLIGAN, Q., AND DABIRI, J. O. Energy exchange in an array of vertical-axis wind turbines. *Journal of Turbulence 13* (2012), 1–13.

[115] KRAMER, H. S., HAMILTON, C., SPENCER, G., AND OGSTON, H. Evaluating the potential for marine and hydrokinetic devices to act as artificial reefs or fish aggregating devices. *OCS Study BOEM 2015-021* (2015), 90.

[116] KRAUSE, J., AND RUXTON, G. D. *Living in Groups*. Oxford University Press, 2002.

[117] LAGASSE, P. F., ZEVENBERGEN, L. W., AND CLOPPER, P. E. Impacts of debris on bridge pier scour. vol. ICSE-5, pp. 854–863.

[118] LAM, H. F., AND PENG, H. Y. Study of wake characteristics of a vertical axis wind turbine by two- and three-dimensional computational fluid dynamics simulations. *Renewable Energy 90* (2016), 386–398.

[119] LAM, H. F., AND PENG, H. Y. Measurements of the wake characteristics of co- and counter-rotating twin h-rotor vertical axis wind turbines. *Energy 131* (2017), 13–26.

[120] LAM, K., LI, J. Y., CHAN, K. T., AND SO, R. M. Flow pattern and velocity field distribution of cross-flow around four cylinders in a square configuration at a low reynolds number. *Journal of Fluids and Structures 17* (2003), 665–679.

[121] LAM, K., AND LO, S. C. A visualization study of cross-flow around four cylinders in a square configuration. *Journal of Fluids and Structures 6* (1992), 109–131.

[122] LAM, K., AND ZOU, L. Experimental study and large eddy simulation for the turbulent flow around four cylinders in an in-line square configuration. *International Journal of Heat and Fluid Flow 30* (2009), 276–285.

[123] LEHMANN, J., COUMOU, D., AND FRIELER, K. Increased record-breaking precipitation events under global warming. *Climatic Change 132* (2015), 501–515.

[124] LEHMKUHL, O., RODRÃGUEZ, I., BORRELL, R., AND OLIVA, A. Low-frequency unsteadiness in the vortex formation region of a circular cylinder. *Physics of Fluids 25* (2013).

[125] LENNOX, R. J., PAUKERT, C. P., AARESTRUP, K., AUGER-MÉTHÉ, M., BAUMGARTNER, L., BIRNIE-GAUVIN, K., BØE, K., BRINK, K., BROWNSCOMBE, J. W., CHEN, Y., DAVIDSEN, J. G., ELIASON, E. J., FILOUS, A., GILLANDERS, B. M., HELLAND, I. P., HORODYSKY, A. Z., JANUCHOWSKI-HARTLEY, S. R., LOWERRE-BARBIERI, S. K., LUCAS, M. C., MARTINS, E. G., MURCHIE, K. J., POMPEU, P. S., POWER, M., RAGHAVAN, R., RAHEL, F. J., SECOR, D., THIEM, J. D., THORSTAD, E. B., UEDA, H., WHORISKEY, F. G., AND COOKE, S. J. One hundred pressing questions on the future of global fish migration science, conservation, and policy. *Frontiers in Ecology and Evolution 7* (2019), 1–16.

[126] LEVINE, J. S., AND MACNICHOL, E. F. Color vision in fishes. *Scientific American 246* (1982), 140–149.

[127] LEWIS, S. L. Physical factors influencing fish populations in pools of a trout stream. *Transactions of the American Fisheries Society 98* (1969), 14–19.

[128] LIAO, J. C. A review of fish swimming mechanics and behaviour in altered flows. *Philosophical Transactions of the Royal Society B: Biological Sciences 362* (2007), 1973–1993.

[129] LIAO, J. C., BEAL, D. N., AND LAUDER, G. V. Fish exploiting vortices decrease. *Science 302* (2003), 1566–1569.

[130] LIAO, J. C., BEAL, D. N., LAUDER, G. V., AND TRIANTAFYLLOU, M. S. The kármán gait: Novel body kinematics of rainbow trout swimming in a vortex street. *Journal of Experimental Biology 206* (2003), 1059–1073.

[131] LINSTEAD, C., AND GURNELL, A. Large wood debris in british headwater rivers summary report. r& d technical report w185, 1998.

[132] LUCAS, K. N., LAUDER, G. V., AND TYTELL, E. D. Airfoil-like mechanics generate thrust on the anterior body of swimming fishes. *Proceedings of the National Academy of Sciences of the United States of America 117* (2020), 10585–10592.

[133] LUPANDIN, A. I. Effect of flow turbulence on swimming speed of fish. *Biology Bulletin 32* (2005), 461–466.

[134] MAIA, A., SHELTZER, A. P., AND TYTELL, E. D. Streamwise vortices destabilize swimming bluegill sunfish (lepomis macrochirus). *Journal of Experimental Biology 218* (2015), 786–792.

[135] MALIPEDDI, A. R., AND CHATTERJEE, D. Influence of duct geometry on the performance of darrieus hydroturbine. *Renewable Energy 43* (2012), 292–300.

[136] MALLEN-COOPER, M. Swimming ability of adult golden perch, macquaria ambigua (percichthyidae), and adult silver perch, bidyanus bidyanus (teraponidae), in an experimental vertical-slot fishway. *Marine and Freshwater Research 45* (1994), 191–198.

[137] MOLLOY, S., BATT, J., EDDINGTON, J., MAHON-HODGINS, L., MACNEIL, A. M., KREGTING, L., AND BIBEAU, E. Tidal turbine marine life interaction study: Fish. 24.

[138] MOREIRA, J. S. Color cue and movement attraction of bermuda bream diplodus-bermudensis. 61–66.

[139] MOREIRA, M., COSTA, M. J., VALBUENA-CASTRO, J., PINHEIRO, A. N., AND BOAVIDA, I. Cover or velocity: What triggers iberian barbel (luciobarbus bocagei) refuge selection under experimental hydropeaking conditions? *Water 12* (2020).

[140] MORI, N. Despiking, 2020.

[141] MORI, N., SUZUKI, T., AND KAKUNO, S. Noise of acoustic doppler veloci-meter data in bubbly flows. *Journal of Engineering Mechanics 133* (2007), 122–125.

[142] MOTT, N. Managing woody debris in rivers, streams & floodplains, 2006.

[143] MUELLER, M., PANDER, J., AND GEIST, J. Evaluation of external fish injury caused by hydropower plants based on a novel field-based protocol. *Fisheries Management and Ecology 24* (2017), 240–255.

[144] MUHAWENIMANA, V., WILSON, C. A., AND CABLE, J. Fish swimming kin-ematics in a turbulent wake: To spill or not to spill? *E3S Web of Conferences 40* (2018), 1–8.

[145] MUHAWENIMANA, V., WILSON, C. A., NEFJODOVA, J., AND CABLE, J. Flood attenuation hydraulics of channel-spanning leaky barriers. *Journal of Hydrology 596* (2021), 125731.

[146] MUHAWENIMANA, V., WILSON, C. A., OURO, P., AND CABLE, J. Spanwise cylinder wake hydrodynamics and fish behavior. *Water Resources Research 55* (2019), 8569–8582.

[147] MÜLLER, S., CLEYNEN, O., HOERNER, S., LICHTENBERG, N., AND THÉVENIN, D. Numerical analysis of the compromise between power output and fish-friendliness in a vortex power plant. *Journal of Ecohydraulics 3* (2019), 86–98.

[148] NAKANO, N., KAWABE, R., YAMASHITA, N., HIRAISHI, T., YAMAMOTO, K., AND NASHIMOTO, K. Color vision, spectral sensitivity, accommodation, and visual acuity in juvenile masu salmon oncorhynchus masou masou. *Fisheries Science 72* (2006), 239–249.

[149] NATION, U. Affordable and clean energy : people around the world lack access to electricity, 2020.

[150] NEACHELL, E. Large wood aids spawning chinook salmon (oncorhynchus tshawytscha) in marginal habitat on a regulated river in california). *River Research and Applications 27* (2011), 550–565.

[151] NIKORA, V. I., ABERLE, J., BIGGS, B. J., JOWETT, I. G., AND SYKES, J. R. Effects of fish size, time-to-fatigue and turbulence on swimming performance: A case study of galaxias maculatus. *Journal of Fish Biology 63* (2003), 1365–1382.

[152] NILSSON, C., REIDY, C. A., DYNESIUS, M., AND REVENGA, C. Fragmentation and flow regulation of the world's large river systems. *Science 308* (2005), 405–408.

[153] NISHINO, T., ROBERTS, G. T., AND ZHANG, X. Unsteady rans and detached-eddy simulations of flow around a circular cylinder in ground effect. *Journal of Fluids and Structures 24* (2008), 18–33.

[154] NORTEK. Vectrino velocimeter user guide. 42.

[155] ODEH, M. A summary of environmentally friendly turbine design concepts. *US Department of Energy, Idaho Operations Office* (1999).

[156] ODEH, M., NOREIKA, J. F., HARO, A., MAYNARD, A., CASTRO-SANTOS, T., AND CADA, G. F. Evaluation of the effects of turbulence on the behavior of migratory fish this is invisible text to keep vertical alignment this is invisible text to keep vertical alignment this is invisible text to keep vertical alignment this is invisible text to keep, 2002.

[157] OKAMOTO, T., TAKEBAYASHI, H., SANJOU, M., SUZUKI, R., AND TODA, K. Log jam formation at bridges and the effect on floodplain flow: A flume experiment. *Journal of Flood Risk Management 13* (2020), 1–13.

[158] OPPERMAN, J., MERENLENDER, A., AND LEWIS, D. Maintaining wood in streams: A vital action for fish conservation. *Maintaining Wood in Streams: A Vital Action for Fish Conservation* (2006), 1–11.

[159] OURO, P., HARROLD, M., STOESSER, T., AND BROMLEY, P. Hydrodynamic loadings on a horizontal axis tidal turbine prototype. *Journal of Fluids and Structures 71* (2017), 78–95.

[160] OURO, P., AND LAZENNEC, M. Theoretical modelling of the three-dimensional wake of vertical axis turbines. *Flow 1* (2021).

[161] OURO, P., MUHAWENIMANA, V., AND WILSON, C. A. Asymmetric wake of a horizontal cylinder in close proximity to a solid boundary for reynolds numbers in the subcritical turbulence regime. *Physical Review Fluids 4* (2019), 1–28.

[162] OURO, P., RUNGE, S., LUO, Q., AND STOESSER, T. Three-dimensionality of the wake recovery behind a vertical axis turbine. *Renewable Energy 133* (2019), 1066–1077.

[163] OURO, P., AND STOESSER, T. An immersed boundary-based large-eddy simulation approach to predict the performance of vertical axis tidal turbines. *Computers and Fluids 152* (2017), 74–87.

[164] OVIDIO, M., AND PHILIPPART, J.-C. The impact of small physical obstacles on upstream movements of six species of fish. synthesis of a 5-year telemetry study in the river meuse basin. *Hydrobiologia 483* (2002), 55–69.

[165] PALMER, M. Acoustic doppler velocimetry.

[166] PALSTRA, A. P., KALS, J., BÖHM, T., BASTIAANSEN, J. W., AND KOMEN, H. Swimming performance and oxygen consumption as non-lethal indicators of production traits in atlantic salmon and gilthead seabream. *Frontiers in Physiology 11* (2020), 1–14.

[167] PEETERS, A., HOUBRECHTS, G., HALLOT, E., CAMPENHOUT, J. V., GOB, F., AND PETIT, F. Can coarse bedload pass through weirs? *Geomorphology 359* (2020), 107131.

[168] PERRY, R. W., ROMINE, J. G., ADAMS, N. S., BLAKE, A. R., BURAU, J. R., JOHNSTON, S. V., AND LIEDTKE, T. L. Using a non-physical behavioural barrier to alter migration routing of juvenile chinook salmon in the sacramento-san joaquin river delta. *River Research and Applications 30* (2012), 192–203.

[169] PFLUGRATH, B. D., BOYS, C. A., CATHERS, B., AND DENG, Z. D. Over or under? autonomous sensor fish reveals why overshot weirs may be safer than undershot weirs for fish passage. *Ecological Engineering 132* (2019), 41–48.

[170] PIÉGAY, H. Interactions between floodplain forests and overbank flows: Data from three piedmont rivers of southeastern France *Global Ecology and Biogeography Letters 6* (1997), 187–196.

[171] PIPER, A. T., ROSEWARNE, P. J., WRIGHT, R. M., AND KEMP, P. S. The impact of an archimedes screw hydropower turbine on fish migration in a lowland river. *Ecological Engineering 118* (2018), 31–42.

[172] PLESIŃSKI, K., BYLAK, A., RADECKI-PAWLIK, A., MIKOŁAJCZYK, T., AND KUKUŁA, K. Possibilities of fish passage through the block ramp: Model-based estimation of permeability. *Science of the Total Environment 631-632* (2018), 1201–1211.

[173] POSA, A. Wake characterization of coupled configurations of vertical axis wind turbines using large eddy simulation. *International Journal of Heat and Fluid Flow 75* (2019), 27–43.

[174] POSA, A. Dependence of the wake recovery downstream of a vertical axis wind turbine on its dynamic solidity. *Journal of Wind Engineering and Industrial Aerodynamics 202* (2020), 104212.

[175] POSA, A., PARKER, C. M., LEFTWICH, M. C., AND BALARAS, E. Wake structure of a single vertical axis wind turbine. *International Journal of Heat and Fluid Flow 61* (2016), 75–84.

[176] PRACHEIL, B. M., DEROLPH, C. R., SCHRAMM, M. P., AND BEVELHIMER, M. S. A fish-eye view of riverine hydropower systems: the current understanding of the biological response to turbine passage. *Reviews in Fish Biology and Fisheries 26* (2016), 153–167.

[177] PRZYBILLA, A., KUNZE, S., RUDERT, A., BLECKMANN, H., AND BRÜCKER, C. Entraining in trout: A behavioural and hydrodynamic analysis. *Journal of Experimental Biology 213* (2010), 2976–2986.

[178] PULGAR, J., ZEBALLOS, D., VARGAS, J., ALDANA, M., MANRIQUEZ, P., MANRIQUEZ, K., QUIJÓN, P. A., WIDDICOMBE, S., ANGUITA, C., QUINTANILLA, D., AND DUARTE, C. Endogenous cycles, activity patterns and energy expenditure of an intertidal fish is modified by artificial light pollution at night (alan). *Environmental Pollution 244* (2019), 361–366.

[179] THOMAS, R., LELLO, J., MEDEIROS, R., POLLARD, A., ROBINSON, P., SEWARD, A., SMITH, J., VAFIDIS, J., VAUGHAN, I. *Data analysis with R statistical software A guidebook for scientists*, vol. 2. Eco-explore, 2017.

[180] RAHEL, F. J., AND MCLAUGHLIN, R. L. Selective fragmentation and the management of fish movement across anthropogenic barriers. *Ecological Applications 28* (2020), 2066–2081.

[181] RAJARATNAM, N. Turbulent jets. 153–161.

[182] RAUPACH, M. R. Conditional statistics of reynolds stress in rough-wall and smooth-wall turbulent boundary layers. *Journal of Fluid Mechanics 108* (1981), 363–382.

[183] REICH, M., KERSHNER, J. L., AND WILDMAN, R. C. Restoring streams with large wood : A synthesis. *American Fisheries Society Symposium 37: International Conference on Wood in World Rivers* (2003), 355–366.

[184] REID, A. J., CARLSON, A. K., CREED, I. F., ELIASON, E. J., GELL, P. A., JOHNSON, P. T., KIDD, K. A., MACCORMACK, T. J., OLDEN, J. D., ORMEROD, S. J., SMOL, J. P., TAYLOR, W. W., TOCKNER, K., VERMAIRE, J. C., DUDGEON, D., AND COOKE, S. J. Emerging threats and persistent conservation challenges for freshwater biodiversity. *Biological Reviews 94* (2019), 849–873.

[185] REN21. *Renewables 2020 Global Status Report*. 2020.

[186] ROLIN, V. F., AND PORTÉ-AGEL, F. Experimental investigation of vertical-axis wind-turbine wakes in boundary layer flow. *Renewable Energy 118* (2018), 1–13.

[187] ROMERO-GOMEZ, P., AND RICHMOND, M. C. Simulating blade-strike on fish passing through marine hydrokinetic turbines. *Renewable Energy 71* (2014), 401–413.

[188] ROMINGER, J. T., AND NEPF, H. M. Flow adjustment and interior flow associated with a rectangular porous obstruction. *Journal of Fluid Mechanics 680* (2011), 636–659.

[189] BURGESS, O. T., PINE III, W. E., WALSH, S. J. Importance of floodplain connectivity to fish populations in the apalachicola river, florida. *River Research and Applications 29* (2012), 718–733.

[190] SALANT, N. L., SCHMIDT, J. C., BUDY, P., AND WILCOCK, P. R. Unintended consequences of restoration: Loss of riffles and gravel substrates following weir installation. *Journal of Environmental Management 109* (2012), 154–163.

[191] SANTATO, S., BENDER, S., AND SCHALLER, M. The european floods direct-
      ive and opportunities offered by land use planning, 2013.

[192] SASS, G. G. Coarse woody debris in lakes and streams. *Encyclopedia of Inland
      Waters* (2009), 60–69.

[193] SCHALKO, I. Wood retention at inclined racks: Effects on flow and local bed-
      load processes. *Earth Surface Processes and Landforms 45* (2020), 2036–2047.

[194] SCHALKO, I., LAGEDER, C., SCHMOCKER, L., WEITBRECHT, V., AND
      BOES, R. M. Laboratory flume experiments on the formation of spanwise large
      wood accumulations: I. effect on backwater rise. *Water Resources Research 55*
      (2019), 4854–4870.

[195] SCHALKO, I., LAGEDER, C., SCHMOCKER, L., WEITBRECHT, V., AND
      BOES, R. M. Laboratory flume experiments on the formation of spanwise large
      wood accumulations: Part ii: effect on local scour. *Water Resources Research
      55* (2019), 4871–4885.

[196] SCHALKO, I., SCHMOCKER, L., WEITBRECHT, V., AND BOES, R. M. Back-
      water rise due to large wood accumulations. *Journal of Hydraulic Engineering
      144* (2018), 04018056.

[197] SCHALKO, I., SCHMOCKER, L., WEITBRECHT, V., AND BOES, R. M. Labor-
      atory study on wood accumulation probability at bridge piers. *Journal of Hy-
      draulic Research 58* (2020), 566–581.

[198] SCHALKO, I., WOHL, E., AND NEPF, H. M. Flow and wake characteristics
      associated with large wood to inform river restoration. *Scientific Reports 11*
      (2021), 1–12.

[199] SCHERL, I., STROM, B., BRUNTON, S. L., AND POLAGYE, B. L. Geometric
      and control optimization of a two cross-flow turbine array. *Journal of Renewable
      and Sustainable Energy 12* (2020), 1–14.

[200] SEITZ, A. C., MOERLEIN, K., EVANS, M. D., AND ROSENBERGER, A. E. Ecology of fishes in a high-latitude, turbid river with implications for the impacts of hydrokinetic devices. *Reviews in Fish Biology and Fisheries 21* (2011), 481–496.

[201] SELIGER, C., AND ZEIRINGER, B. River connectivity, habitat fragmentation and related restoration measures, 2018.

[202] SHAMSODDIN, S., AND PORTÃ©-AGE, F. A large-eddy simulation study of vertical axis wind turbine wakes in the atmospheric boundary layer. *Energies 9* (2016), 1–23.

[203] SHEAFFER, W. A., AND NICKUM, J. G. Backwater areas as nursery habitats for fishes in pool 13 of the upper mississippi river. *Hydrobiologia 136* (1986), 131–139.

[204] SHIELDS, F. D., AND ALONSO, C. V. Assessment of flow forces on large wood in rivers. *Water Resources Research 48* (2012), 1–16.

[205] SILVA, A. T., LUCAS, M. C., CASTRO-SANTOS, T., KATOPODIS, C., BAUMGARTNER, L. J., THIEM, J. D., AARESTRUP, K., POMPEU, P. S., O'BRIEN, G. C., BRAUN, D. C., BURNETT, N. J., ZHU, D. Z., FJELDSTAD, H. P., FORSETH, T., RAJARATNAM, N., WILLIAMS, J. G., AND COOKE, S. J. The future of fish passage science, engineering, and practice. *Fish and Fisheries 19* (2018), 340–362.

[206] SILVA, A. T., SANTOS, J. M., FERREIRA, M. T., PINHEIRO, A. N., AND KATOPODIS, C. Passage efficiency of offset and straight orifices for upstream movements of iberian barbel in a pool-type fishway. *River Research and Applications 28* (2012), 529–542.

[207] SMITH, D. L., GOODWIN, R. A., AND NESTLER, J. M. Relating turbulence and fish habitat: A new approach for management and research. *Reviews in Fisheries Science and Aquaculture 22* (2014), 123–130.

[208] STOESSER, T., MCSHERRY, R., AND FRAGA, B. Secondary currents and tur-
      bulence over a non-uniformly roughened open-channel bed. *Water (Switzerland)*
      *7* (2015), 4896–4913.

[209] STROM, B., BRUNTON, S. L., AND POLAGYE, B. Intracycle angular velocity
      control of cross-flow turbines. *Nature Energy 2* (2017), 1–9.

[210] STROSSER, P., DELACÁMARA, G., HANUS, A., WILLIAMS, H., AND JARITT,
      N. *Natural Water Retention Measures: A guide to support the selection, design*
      *and implementation of natural water retention measures in Europe*. 2014.

[211] STRUTHERS, D. P., GUTOWSKY, L. F., ENDERS, E., SMOKOROWSKI, K.,
      WATKINSON, D., BIBEAU, E., AND COOKE, S. J. Evaluating riverine hy-
      drokinetic turbine operations relative to the spatial ecology of wild fishes.
      *Journal of Ecohydraulics 2* (2017), 53–67.

[212] SU, G., LOGEZ, M., XU, J., TAO, S., VILLÃ©GER, S., AND BROSSE, S.
      Human impacts on global freshwater fish biodiversity. *Science 371* (2021), 835–
      838.

[213] SU, H., MENG, H., QU, T., AND LEI, L. Wind tunnel experiment on the
      influence of array configuration on the power performance of vertical axis wind
      turbines. *Energy Conversion and Management 241* (2021), 114299.

[214] SULLIVAN, B. G., TAYLOR, M. K., CARLI, C., WARD, T. D., LENNOX,
      R. J., AND COOKE, S. J. Partial dam removal restores passage for a threatened
      salmonid. *River Research and Applications 35* (2019), 669–679.

[215] SUN, C., LAM, W. H., LAM, S. S., DAI, M., AND HAMILL, G. Temporal
      evolution of seabed scour induced by darrieus-type tidal current turbine. *Water*
      *11* (2019), 1–21.

[216] SUN, J., GALIB, S. M., AND LUCAS, M. C. Rapid response of fish and aquatic habitat to removal of a tidal barrier. *Aquatic Conservation: Marine and Freshwater Ecosystems In press* (2021), 1–15.

[217] SZABO-MESZAROS, M., NAVARATNAM, C. U., ABERLE, J., SILVA, A. T., FORSETH, T., CALLES, O., FJELDSTAD, H. P., AND ALFREDSEN, K. Experimental hydraulics on fish-friendly trash-racks: an ecological approach. *Ecological Engineering 113* (2018), 11–20.

[218] TAGUCHI, M., AND LIAO, J. C. Rainbow trout consume less oxygen in turbulence: The energetics of swimming behaviors at different speeds. *Journal of Experimental Biology 214* (2011), 1428–1436.

[219] TESCIONE, G., RAGNI, D., HE, C., FERREIRA, C. J. S., AND VAN BUSSEL, G. J. Near wake flow analysis of a vertical axis wind turbine by stereoscopic particle image velocimetry. *Renewable Energy 70* (2014), 47–61.

[220] THORPE, J. E., AND MORGAN, R. I. Periodicity in atlantic salmon salmo salar l. smolt migration. *Journal of Fish Biology 12* (1978), 541–548.

[221] TICKNER, D., OPPERMAN, J. J., ABELL, R., ACREMAN, M., ARTHINGTON, A. H., BUNN, S. E., COOKE, S. J., DALTON, J., DARWALL, W., EDWARDS, G., HARRISON, I., HUGHES, K., JONES, T., LECLÃ¨RE, D., LYNCH, A. J., LEONARD, P., MCCLAIN, M. E., MURUVEN, D., OLDEN, J. D., ORMEROD, S. J., ROBINSON, J., THARME, R. E., THIEME, M., TOCKNER, K., WRIGHT, M., AND YOUNG, L. Bending the curve of global freshwater biodiversity loss: An emergency recovery plan. *BioScience 70* (2020), 330–342.

[222] TRITICO, H. M., AND COTEL, A. J. The effects of turbulent eddies on the stability and critical swimming speed of creek chub (semotilus atromaculatus). *Journal of Experimental Biology 213* (2010), 2284–2293.

[223] UYUMAZ, A. Scour downstream of vertical gate. *Journal of Hydraulic Engineering 114* (1988), 811–816.

[224] VANNOTE, R. L., MINSHALL, G. W., CUMMINS, K. W., SEDELL, J. R., AND CUSHING, C. E. The river continuum concept. *Canadian Journal of Fisheries and Aquatic Sciences 37* (1980), 130–137.

[225] VERGAERDE, A., TROYER, T. D., AND MUGGIASCA, S. Influence of the direction of rotation on the wake characteristics of closely spaced counter-rotating vertical-axis wind turbines influence of the direction of rotation on the wake characteristics of closely spaced counter-rotating vertical-axis wind turb. *Journal of Physics: Conference Series 1618* (2020).

[226] VERGAERDE, A., TROYER, T. D., MUGGIASCA, S., BAYATI, I., BELLOLI, M., KLUCZEWSKA-BORDIER, J., PARNEIX, N., SILVERT, F., AND RUNACRES, M. C. Experimental characterisation of the wake behind paired vertical-axis wind turbines. *Journal of Wind Engineering and Industrial Aerodynamics 206* (2020), 104353.

[227] VERGAERDE, A., TROYER, T. D., STANDAERT, L., KLUCZEWSKA-BORDIER, J., PITANCE, D., IMMAS, A., SILVERT, F., AND RUNACRES, M. C. Experimental validation of the power enhancement of a pair of vertical-axis wind turbines. *Renewable Energy 146* (2020), 181–187.

[228] VIDELER, B., HESS, F. Fast continuous swimming of two pelagic predators, saithe (pollachius virens) and mackerel (scomber scombrus): a kinematic analysis. *Journal of Experimental Biology 109* (1984), 209–228.

[229] VIEHMAN, H. A., AND ZYDLEWSKI, G. B. Fish interactions with a commercial-scale tidal energy device in the natural environment. *Estuaries and Coasts 38* (2014), 241–252.

[230] WAHL, T. L. Discussion of "despiking acoustic doppler velocimeter data" by derek g. goring and vladimir i. nikora. *Journal of Hydraulic Engineering 129* (2003), 484–487.

[231] WALLERSTEIN, N. P., AND THORNE, C. R. Influence of large woody debris on morphological evolution of incised, sand-bed channels. *Geomorphology 57* (2004), 53–73.

[232] WANG, H., CHANSON, H., KERN, P., AND FRANKLIN, C. Culvert hydrodynamics to enhance upstream fish passage: Fish response to turbulence. *Proceedings of the 20th Australasian Fluid Mechanics Conference, AFMC 2016* (2016).

[233] WANG, X. K., AND TAN, S. K. Experimental investigation of the interaction between a plane wall jet and a parallel offset jet. *Experiments in Fluids 42* (2007), 551–562.

[234] WANG, X. K., AND TAN, S. K. Environmental fluid dynamics-jet flow. *Journal of Hydrodynamics 22* (2010), 1009–1014.

[235] WANG, X. K., AND TAN, S. K. Flow around four circular cylinders in square configuration. *Proceedings of the 18th Australasian Fluid Mechanics Conference, AFMC 2012* (2012), 3–6.

[236] WEBB, P. W., AND COTEL, A. J. *buoyancy, locomotion, and movement in fishes | Stability and Turbulence*, vol. 1. Elsevier Inc., 2011.

[237] WEIHS, D. Hydromechanics of fish schooling. *Nature 241* (1973), 290–291.

[238] WEST, G. B., BROWN, J. H., AND ENQUIST, B. J. A general model for ontogenetic growth. *Nature 413* (2001), 628–631.

[239] WHEATER, H. S. Flood hazard and management: A uk perspective. *Philosophical Transactions of the Royal Society A: Mathematical, Physical and Engineering Sciences 364* (2006), 2135–2145.

[240] WILLIAMSON, B., FRASER, S., WILLIAMSON, L., NIKORA, V., AND SCOTT, B. Predictable changes in fish school characteristics due to a tidal turbine support structure. *Renewable Energy 141* (2019), 1092–1102.

[241] WILLIAMSON, C. H. Vortex dynamics in the cylinder wake. *Annual Review of Fluid Mechanics 28* (1996), 477–539.

[242] WOHL, E. A legacy of absence: Wood removal in us rivers. *Progress in Physical Geography 38* (2014), 637–663.

[243] WOHL, E. Bridging the gaps: An overview of wood across time and space in diverse rivers. *Geomorphology 279* (2017), 3–26.

[244] WOHL, E. Large wood in rivers. *Environmental Science* (2017).

[245] WU, S., AND RAJARATNAM, N. Ressauts libres, ressauts noyés et jets à la paroi. *Journal of Hydraulic Research 33* (1995), 197–212.

[246] WWF. Living planet report, 2018.

[247] YOSHIDA, T., FURUICHI, D., WILLIAMSON, B. J., ZHOU, J., DONG, S., LI, Q., AND KITAZAWA, D. Experimental study of fish behavior near a tidal turbine model under dark conditions. *Journal of Marine Science and Technology (Japan)* (2021).

[248] YOSHIDA, T., ZHOU, J., PARK, S., MUTO, H., AND KITAZAWA, D. Use of a model turbine to investigate the high striking risk of fish with tidal and oceanic current turbine blades under slow rotational speed. *Sustainable Energy Technologies and Assessments 37* (2020), 100634.

[249] ZALEWSKI, M., AND LAPINSKA, M. Fish relationships with wood in large rivers. *American Fisheries Society Symposium 37* (2003), 179–193.

[250] ZANFORLIN, S., AND NISHINO, T. Fluid dynamic mechanisms of enhanced power generation by closely spaced vertical axis wind turbines. *Renewable Energy 99* (2016), 1213–1226.

[251] ZHANG, N., RUTHERFURD, I., AND GHISALBERTI, M. Effect of instream logs on bank erosion potential: a flume study with a single log. *Journal of Ecohydraulics 5* (2020), 43–56.

[252] ZHANG, N., RUTHERFURD, I. D., AND GHISALBERTI, M. The effect of instream logs on bank erosion potential: a flume study with multiple logs. *Journal of Ecohydraulics 5* (2020), 57–70.

[253] ZONG, L., AND NEPF, H. Spatial distribution of deposition within a patch of vegetation. *Water Resources Research 47* (2011), 1–12.

[254] ZOU, L., FENG LIN, Y., AND LAM, K. Large-eddy simulation of flow around cylinder arrays at a subcritical reynolds number. *Journal of Hydrodynamics 20* (2008), 403–413.

[255] ZOU, L., LIN, Y. F., AND LU, H. Flow patterns and force characteristics of laminar flow past four cylinders in diamond arrangement. *Journal of Hydrodynamics 23* (2011), 55–64.